Report on

Geology and Metallogeny of the "Sierras de San Luis y Comechingones" 1:250 000 map sheet

Provinces of San Luis and Córdoba

John P. Sims, Roger G. Skirrow, Peter G. Stuart-Smith, and Patrick Lyons

GEOSCIENTIFIC MAPPING OF THE SIERRAS PAMPEANAS ARGENTINE-AUSTRALIAN COOPERATIVE PROJECT

AUSTRALIAN GEOLOGICAL SURVEY ORGANISATION

1997

CONTENTS

List of Figures

PREAMBLE

SECTION I: GEOLOGY

SECTION II: ECONOMIC GEOLOGY

List of Tables

SECTION I: GEOLOGY

SECTION II: ECONOMIC GEOLOGY

ABSTRACT

Geology

The *Sierras de San Luis y Comechingones* map area covers 12 000 km^2 extending from east of the Sierras de Comechingones to west of the Sierras de San Luis. The city of San Luis is located in the south west of the map area. The ranges form the southernmost part of the Sierras Pampeanas morphotectonic province of basement tilt blocks. Recent work, as part of the Geoscientific Mapping of the Sierras Pampeanas Argentine-Australian Cooperative Project, has shown that the basement is comprised of three lithostratigraphic domains, a Cambrian domain, a Cambro–Ordovician domain and a younger Ordovician domain. These three domains have shared a common tectonic history since the Early Devonian.

The Cambrain domain is comprised of the Monte Guazú, Conlara and Nogoli metamorphic complexes. These rocks consist of pelitic and psammitic gneiss and schist with subordinate orthogneiss. The meta-sedimentary protoliths are interpreted to have deposited on the a passive margin during the separation of Laurentia from Gondwana and the opening of the Iapetus Ocean at around 540 Ma. Deformation and upper amphibolite- to granulite-facies metamorphism of the Pampean cycle had commenced by about 530 Ma and occurred during convergence on the newly created margin of Gondwana. Widespread magmatism at the closing stages of the cycle produced granitoids within the Monte Guazú Metamorphic Complex and possibly the Nogoli Metamorphic Complex at around 515 Ma(?).

The Cambro–Ordovician domain consists of pelitic gneiss and schist of the Pringles Metamorphic Complex. The protoliths to these metasediments were probably deposited in a back-arc basin formed within the older basement, coincident with the commencement of subduction along the margin of Gondwana in the latest Cambrian. During the Early Ordovician widespread compressive deformation, metamorphism, and magmatism of the Famatinian cycle resulted in amalgamation of the back arc basin with the Cambrian basement. Mafic and ultramafic bodies of the Las Aguilas Group intruded the Pringles Metamorphic Complex at ~480 Ma and provided a significant heat source for high-grade metamorphism. Deformation at upper amphibolite- to granulite-facies

was accompanied by the development of kilometre-scale ductile shear zones. Towards the close of the Famatinian cycle, discrete belts of extensional tectonism developed at upper greenschist-facies conditions accompanied by emplacement of S-type granite and pegmatite. New U-Pb monazite data suggests that the Famatinian tectonism had ceased and the terrain was cooling by approximately 450 Ma.

The Ordovician domain comprises the San Luis Formation, which consists of phyllites, arenites and minor conglomerates. These low-grade metasediments were deposited during the Famatinian cycle and are intruded by granitoids that have been dated at about 470 Ma. The absence of Famatinian tectonic fabrics in these rocks suggests they were deposited in a basin formed during the late extensional phase.

The resumption of convergence on the Gondwana margin in the Early Devonian, resulted in compressive deformation of the San Luis Formation, and older basement rocks. This important tectonic episode is termed the Achalian cycle. Partial melting of crust during this tectonism produced voluminous felsic magmas which intruded during and after shearing. The magmatism had commenced by about 404 Ma and may have continued until the Early Carboniferous. Deformation was at greenschist facies and produced westerly directed thrusting and regionally extensive ductile to brittle-ductile, conjugate, strike-slip shear-zones. New ^{40}Ar-^{39}Ar data shows the shearing had ceased by approximately 350 Ma.

Subduction of the Nazca Plate resulted initially in Andesitic volcanism at the start of the Andean cycle in the Mid Miocene. The volcanism resulted in basement uplift with volcanic edifices and extensive pyroclastic aprons. Following cessation of volcanism in the Pliocene, continuing east-west compression has resulted in uplift of the basement along moderate to steeply dipping reverse faults.

Metallogeny

Three principal Paleozoic metallogenic cycles and one Neogene cycle are recognised in the southern Sierras Pampeanas, including the Sierras de San Luis and Comechingones. The first two metallogenic stages are closely related to the Early Ordovician Famatinian

tectonic and magmatic cycle, and the third major period of mineralisation occurred during the Devonian Achalian cycle.

The earliest metallogenic stage includes Ni-Cu-Co sulfide deposits with anomalous PGE-Au hosted by mafic/ultramafic intrusions, in the Las Aguilas district. Sulfide mineralisation formed initially in magmatic cumulate zones, with partial remobilisation during deformation. New U-Pb (zircon) age dating indicates that differentiates of the tholeiitic parent magma crystallised during the early Ordovician at 478±6 Ma, approximately coeval with Famatinian high grade metamorphism and compressive deformation. A resource of 2.2 Mt at 0.51% Ni and 0.50% Cu has previously been estimated. Regional mapping and metallogenic modelling indicates potential for Ni-Cu mineralisation in several exposed and concealed zones elsewhere in the Sierras de San Luis.

The second metallogenic phase is spatially and temporally related to extensional deformation of the final stages of the Famatinian cycle. Historically important deposits of Li, Be, Nb, Ta, Sn, and currently exploited industrial mineral resources (mica, feldspar, quartz), are associated with granites and voluminous pegmatites emplaced during this and the Achalian cycles.

The third phase of metallogenic evolution in the southern Sierras Pampeanas is broadly correlated with the Achalian cycle, and is characterised by diverse deposits of Au, W, Ag, Pb, Zn, Cu, and a second period of pegmatite-related mineralisation including Be, Li, Nb, Ta, U, REE, Th and F. New ^{40}Ar-^{39}Ar dating of white mica hydrothermal alteration associated with shear-related Au±Cu, W vein and Ag-Pb-Zn vein mineralisation in the southern Sierras Pampeanas suggests mineralisation occurred from about 390 to 360 Ma, including at least some of the W mineralisation in the Sierra de Los Morillos. This metallogenic phase commenced during the period of Devonian felsic magmatism, which includes granites yielding U-Pb (zircon) crystallisation ages of about 403 to 382 Ma. Oxygen and hydrogen isotope compositions of alteration and veins minerals are compatible with input of evolved meteoric fluids with or without a minor component of magmatic or metamorphic waters in the formation of these Au±Cu, W and Ag-Pb-Zn deposits.

Numerous tungsten deposits hosted in calc-silicate rocks in the Sierras del Morro, Yulto and Estanzuela are proposed to be epigenetic in origin and to have formed during the Devonian metallogenic phase. However, it is conceivable that minor tungsten accumulated in calc-silicate rocks prior to the Devonian and was remobilised during the Achalian cycle. Localisation of quartz-scheelite vein deposits and possibly some Au±W quartz vein deposits in the Sierras de San Luis in structures characteristic of the Achalian cycle suggests these deposits also formed during the Devonian metallogenic cycle. Structural studies and metallogenic modelling have been used to outline areas of potential for shear-related mesothermal Au in the Sierras de San Luis.

The Neogene metallogenic cycle is characterised by Au (-Ag-Pb-Zn) and Cu mineralisation formed in association with Miocene-Pliocene volcanism in the La Carolina - Sierra del Morro volcanic belt. Alteration, geochemical, and geological characteristics of the Au mineralisation indicate metal deposition in the upper levels of low sulfidation epithermal systems, controlled in part by Tertiary and pre-Tertiary structures. Quartz-chalcopyrite vein stockworks and alteration in andesite breccia at Diente Verde suggest the existence of porphyry Cu style mineralisation in the La Carolina - Sierra del Morro volcanic belt. Despite the extent of this belt, exploration for Au-Ag and Cu in this region has been relatively limited.

PREAMBLE

Funded by the Government of the Argentine Republic, the Geoscientific Mapping of the Sierras Pampeanas Argentine-Australian Cooperative Project is a collaborative program between the Australian Geological Survey Organisation and the Servicio Geológico Minero Argentino of the Subsecretaría de Minería de la Nación. The project aims to update the geoscientific knowledge base, provide a modern framework for resource assessment, and promote exploration and development in the region. Training of Argentinian geoscientists and technology transfer are key components of the project.

The pilot 'second generation' mapping program involved integrated geological, geophysical and metallogenic mapping totalling 27 000 km^2 in three selected areas of the southern Sierras Pampeanas, a Paleozoic basement terrane in central Argentina (Figures a and b). The three areas, in the provinces of La Rioja, Córdoba and San Luis, were selected to provide key sections of the major tectono-stratigraphic packages comprising the southern Sierras Pampeanas. The region is well known for its resources of industrial and construction materials. Additionally, a range of metallic mineral deposits containing Au, W, Ag, Be, Li, Ni, Cu, Pb, Zn, Nb and Ta, among other commodities, are represented in the region.

Mapping in the three survey areas, *Sierras de Las Minas, Chepes y Los Llanos* (Provincia de La Rioja); *Sierras Septentrionales de Córdoba* (Provincia de Córdoba), and the *Sierras de San Luis y Comechingones* (provincias de San Luis y Córdoba), was undertaken in 1995 to 1996 (Stuart-Smith and Lyons, 1995; Stuart-Smith and others, 1996b, 1996c). A major program of high resolution airborne magnetic and gamma-ray spectrometric surveys was carried out (Chambers, 1996; Figure b), and interpretation completed (see 1:250 000 scale *Interpretación Aeromagnetica* maps and accompanying reports: Hungerford and others, 1996a, 1996b, Hungerford and Pieters, 1996). Fieldwork and map compilation were supported by Landsat TM imagery, airborne geophysics, ground-based geophysical data, GPS located field sites, aerial photography, and geochronological, geochemical and stable isotopic studies. Airborne geophysical data and preliminary interpretations of the geology based on Landsat TM imagery were released to the public in mid-1996. Preliminary assessment of the regional geology and prospectivity of the La Rioja project area was documented by Pieters and Skirrow (1996). Analytical, petrological and geochronological results of the project were reported by Lyons and others (1996), Lyons and Skirrow (1996), Sims and others (1996), Camacho and Ireland (1997) and Camacho (1997).

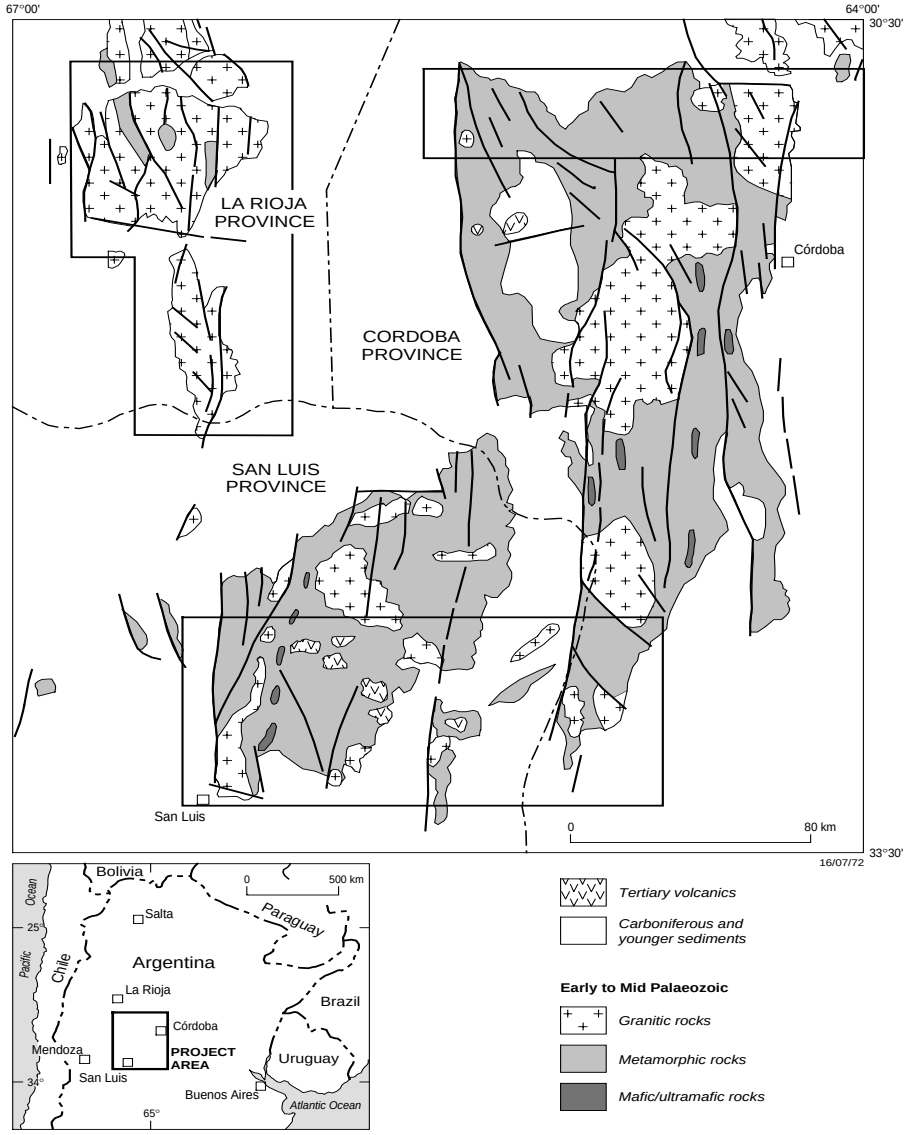

Figure a. Location of the three project areas and simplified regional geology of the southern Sierras Pampeanas

Over Page

Figure b. Total magnetic intenstity images of the three project areas

Syntheses of the geological, metallogenic and geophysical results of the project are presented in 1:250 000 scale *Hoja Geológica* and *Hoja Metalogenética* and accompanying reports for each of the three areas (Pieters and others, 1997; Lyons and others, 1997; Sims and others, 1997). A series of eighteen 1:100 000 scale geological and eighteen mineral occurrence maps constitute some of the principal datasets of the project. They are accompanied by reports on the geology and mineral deposits, including output datasheets from the ARGMIN mineral deposit database (Skirrow and Trudu, 1997). An Arcinfo-based Geographic Information System (GIS) of the Sierras Pampeanas project contains all major geoscientific map datasets (Butrovski, 1997). Selected datasets from the GIS along with metallogenic models of mineral potential have been compiled at 1:400 000 scale in the *Atlas Metalogenético* for the southern Sierras Pampeanas (Skirrow and Johnston, 1997).

This report covers the Geology and Metallogeny of the *Sierras de San Luis y Comechingones* 1:250 000 scale map sheet in the Provinces of San Luis and Córdoba. The report is divided into two sections*: (I) Geology, and (II) Economic Geology. The 1:250 000 scale *Hoja Geológica* and *Hoja Metalogenética* are contained in pockets at the back of the report.

***Recommended bibliographic citation:**

Report as a whole:

SIMS, J., SKIRROW, R.G., STUART-SMITH, P.G. and LYONS, P., 1997. Report on Geology and Metallogeny of the "Sierras de San Luis y Comechingones" 1:250 000 map sheet, Provinces of San Luis and Córdoba. Geoscientific Mapping of the Sierras Pampeanas Argentine-Australian Cooperative Project, Australian Geological Survey Organisation, unpublished report.

Individual sections:

SIMS, J., STUART-SMITH, P.G. and LYONS, P., 1997. Geology and Metallogeny of the Sierras de San Luis and Comechingones 1:250 000 map sheet. *In:* SIMS, J., SKIRROW, R.G., STUART-SMITH, P.G. and LYONS, P., 1997, Report on Geology and Metallogeny of the "Sierras de San Luis y Comechingones" 1:250 000 map sheet, Provinces of San Luis and Córdoba. Geoscientific Mapping of the Sierras Pampeanas Argentine-Australian Cooperative Project, Australian Geological Survey Organisation, unpublished report.

SKIRROW, R.G., 1997. Economic Geology of the Sierras de San Luis and Comechingones 1:250 000 map sheet. *In:* SIMS, J., SKIRROW, R.G., STUART-SMITH, P.G. and LYONS, P., 1997, Report on Geology and Metallogeny of the "Sierras de San Luis y Comechingones" 1:250 000 map sheet, Provinces of San Luis and Córdoba. Geoscientific Mapping of the Sierras Pampeanas Argentine-Australian Cooperative Project, Australian Geological Survey Organisation, unpublished report.

SECTION I: GEOLOGY

by John P. Sims, Peter G. Stuart-Smith & Patrick Lyons

1. INTRODUCTION

1.1 LOCATION AND ACCESS

The *Sierras de San Luis y Comechingones* map area forms an east-west transect within San Luis and Córdoba Provinces; 150km by 80km between 32° 40'-33° 20' S and 64° 30'-66° 30' W (Figure 1). The area includes parts of four 1:250 000 scale map sheets: 3366-I (San Francisco del Monte de Oro), 3366-II (Santa Rosa), 3366-III (San Luis), and 3366-IV (unnamed).

The main population centre is the city of San Luis and access is via national routes 7, 146 and 147. Additionally, the area covers the minor population centres of La Toma, Naschel, Tilisarao, Achiras, Saladillo, Trapiche and Villa de la Quebrada, and is traversed by national route 148 and provincial routes 1, 2, 9 and 20 (Figure 2). The main drainage is via Rio Conlara to the north-east, Rio Quinto to the south-east, Rio Nogoli to the west and Rio Chorillos to the south-west.

1.2 NATURE OF WORK AND PREVIOUS INVESTIGATIONS

The mapping of the sierras de San Luis and Comechingones was carried out in 1995 and 1996 under the Geoscientific Mapping of the Sierras Pampeanas Argentina - Australia Cooperative Project by geologists from the Australian Geological Survey Organisation and the Subsecretaria de Mineria, Argentina. The mapping employed a multidisciplinary approach using newly acquired high-resolution airborne magnetic and gamma-ray spectrometric data, Landsat TM imagery, and 1:20 000 scale (approximate) black and white air photography. All geological maps were compiled on either published 1:20 000 scale topographic maps where available, or topographic bases produced at photo-scale from rectified Landsat images controlled by field GPS sites.

Topography, including cultural, hydrography and relief data were derived from existing 1:20 000 coverages where available. In areas where existing coverage was not available, culture and hydrography was derived from the rectified Landsat images, and the relief data was derived from the digital terrane model (DTM).

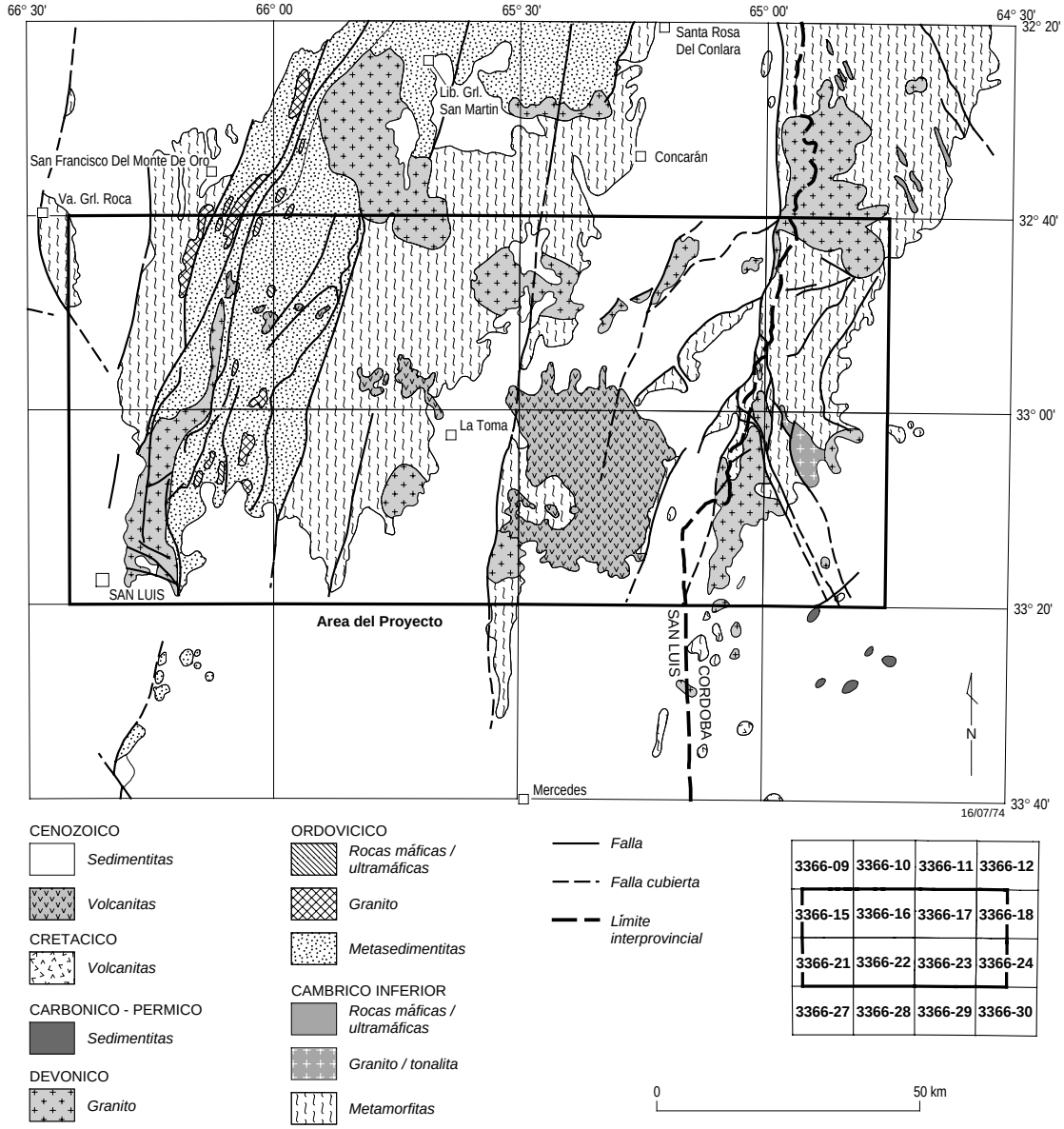

Figure 1. Location of the Sierras de San Luis y Comechingones 1:250,000 scale map area in San Luis and Córdoba Provinces with generalised geology. Locations of 1:100,000 scale map areas are indicated.

Over Page

Figure 2. Landsat-5 TM image of the map area showing main culture and location of known mineral occurrences.

Previous regional geological mapping of the *Sierras de San Luis y Comechingones* at a scale of 1:200 000 includes investigations by Pastore and Gonzalez (1954) of San Fransisco (Hoja 23g), Pastore and Huidobro (1952) of Saladillo (Hoja 24g), and Sosic (1964) of Sierra del Morro (Hoja 24h).

More recent geological investigations have been of greater detail and have concentrated on the stratigraphy (e.g., Prozzi & Ramos, 1988; Suarez and others, 1992) , regional structure (e.g., González Bonorino, 1961; Criado Roqué and others, 1981; von Gosen & Prozzi, 1996), the complex igneous intrusive history (e.g., Zardini, 1966; Brogioni & Ribot, 1994; Llambias and others, 1996; Sato and others, 1996; Otamendi and others, 1996; Pinotti and others, 1996), Tertiary volcanism (e.g., Brogioni, 1988; 1990), and extensive studies on the numerous mineral deposits (e.g., Sabalúa and others, 1981; Llambias & Malvicini, 1982).

1.3 GEOPHYSICS

As part of the cooperative project between AGSO and DNSG, a high resolution airborne geophysical survey was carried out over the map area. For this survey, magnetic and radiometric (U, K, Th) data were obtained by World Geoscience along flight lines spaced 500m apart, from a nominal height of 100m. To assist the aeromagnetic interpretation, magnetic susceptibilities of most exposed rock-types were measured during field work. Magnetic data from the airborne survey were processed by Hungerford Geophysical Consultants (HGC) and radiometric data were processed by AGSO. The data were interpreted by HGC and geoscientists from AGSO at 1:100 000 scale and have been reported separately (Hungerford and others, 1996).

In general, the magnetic data for Sierras de San Luis y Comechingones (Figure 3) may be separated into two distinct regions that are separated by a major NNE-SSW trending thrust fault (Rio Guzman Shear Zone). East of this fault there is a generally low magnetic background and a number of prominent and well defined circular granite intrusions. These granites have a magnetic metamorphic aureole which shows as a halo when unroofed, but which will simply be a large broad magnetic anomaly when not exposed, as is likely in the central part of the survey area. West of this fault the magnetic reponse is generally higher and marked by strong linear trends and moderate to highly magnetic, strike-parallel anomalies. Futhermore, granite intrusions in the

west generally form elongate belts and there is more diversity in the basement rock-types. In addition, a number of intense, isolated anomalies, which occur within both regions, are related to Tertiary volcanic plugs.

2. STRATIGRAPHY

2.1 GENERAL RELATIONS

The Sierras Pampeanas are a distinct morphotectonic province of early- to mid-Palaeozoic metamorphic, felsic and mafic rocks that form a series of block-tilted, north-south oriented ranges separated by intermontane basins. These ranges are bounded by escarpments developed on moderate to steeply dipping reverse faults developed during the Cainozoic Andean uplift (Jordan and Allmendinger, 1986).

Recent geological and geophysical surveys conducted during the Cooperative Argentine-Australia Project in the Sierras Pampeanas show that the Paleozoic basement of the southern Sierras Pampeanas contains of a number of distinct lithological, structural and metamorphic domains separated by major tectonic zones. There are two principal domains: an older, Cambrian domain, and a slightly younger, Ordovician domain. Both domains share a common geological history since early Devonian times.

Rocks of the Cambrian domain in the *Sierras de San Luis y Comechingones* include the Monte Guazú and Conlara metamorphic complexes, in the east, and the Nogoli Metamorphic Complex in the west. The Ordovician domain consists of Cambro-Ordovician rocks of the Pringles Metamorphic Complex and the Early Ordovician San Luis Formation. Several granitic, tonalitic, mafic and ultramafic bodies dominantly intrude the Ordovician domain. Both domains are intruded by voluminous Early Devonian granites and are partly covered by Neogene volcanics and Cainozoic continental deposits. A summary of the stratigraphy and age relations is shown in Table 1.

Previous page

Figure 3. Total magnetic intensity image of the map area, reduced to the pole, with location of known mineral occurences. The Rio Guzman Shear Zone that separates the dominantly Cambrian basement to the east from the belt of Ordovician basement to the west is marked by a major NNW-trending lineament at approximately 66˚ W.

Table 1. Summary of the stratigraphy and age relations of the *Sierras de San Luis y Comechingones*. Age data and discussion of the various tectonic cycles are presented within the text.

Tectonic Cycle	Age (Ma)	Deposition	Intrusion
Andean	present	Alluvial, aeolian and talus deposits.	
	1.9 – 9.5	Volcaniclastics	High-K, calc-alkaline to shoshinitic volcanism
Achalian	355 – 405		I- and S-type granite (e.g. Escalerilla, Renca, Achiras Igneous Complex)
Famatinian	470 – 490	San Luis Formation	Rio de Molle monzonite Bemberg suite tonalites Tamboreo granodiorite Undifferentiated granitoids Mafic & ultramafic rocks
		Pringles Metamorphic Complex sediments	
Pampean	515 – 530		Undifferentiated granitoids Undifferentiated mafics
		Sediments of: • Nogoli Metamorphic Complex • Conlara Metamorphic Complex • Monte Guazú Metamorphic Complex	?Intrusives

2.2 PALAEOZOIC METAMORPHIC BASEMENT

2.2.1 INTRODUCTION

The metamorphic basement of the *Sierras de San Luis y Comchingones* consists of four main subdivisions that relate directly to the geological ages of the units. The first subdivision represents basement rocks of at least Cambrian age that were deformed and metamorphosed during the late Cambrian, Pampean Tectonic-Cycle. These early

Palaeozoic metamorphic rocks have been further divided on the basis of composition into the Monte Guazú Metamorphic Complex in the east, the centrally located Conlara Metamorphic Complex and the Nogoli Metamorphic Complex in the West. The second subdivision represents Cambro-Ordovician rocks of the Pringles Metamorphic Complex that were deposited prior to the onset of collisional tectonics associated with the Famatinian Tectonic Cycle. The third subdivision are the low-grade rocks of the San Luis formation. These rocks were deposited very late in the Famatinian Cycle,

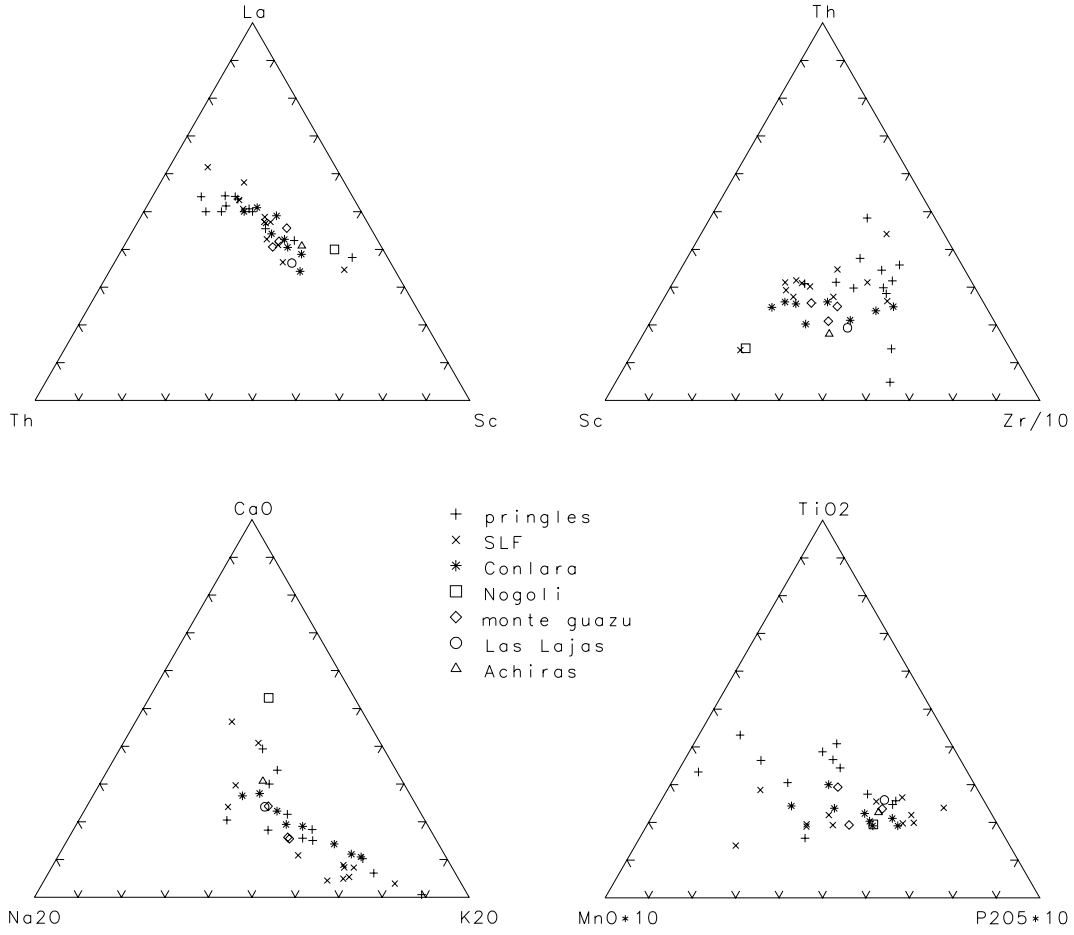

Figure 4. Ternary plots of Th-La-Sc, Sc-Th-Zr/10, Na_2O-CaO-K_2O and Mn*10-TiO_2-P_2O_5, showing distinct trends and fields of the different basement rock groups. The Pringles Metamorphic Complex rocks have distinct trends in all three plots, whereas the trends of the San Luis Formation analyses is close to those of the Cambrian, Conlara and Monte Guazu complexes. Samples from the Las Lajas Shear Zone and metasedimentary components from the Achiras Igneous Complex are included for comparison. Rollinson (1993) suggests that fields towards Sc indicate input from an island arc source, whereas fields towards La-Th and Th-Zr/10 indicate continental sourced material.

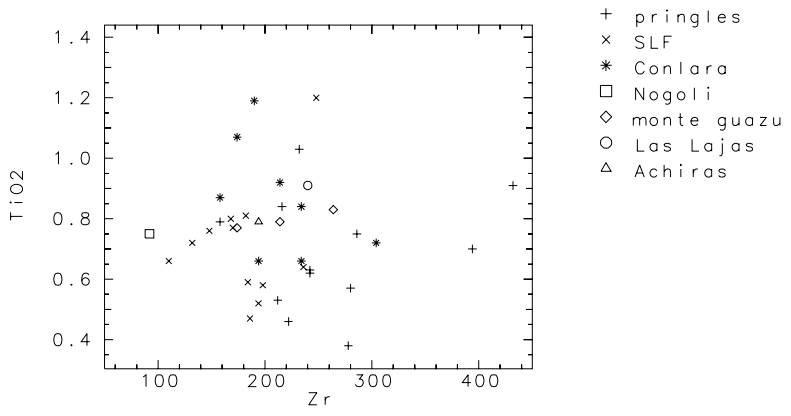

Figure 5. TiO2 vs Zr showing distinct fields for the different basement rock groups.

probably during a late extensional phase, and display little evidence of the intense effects of that tectonic event. They are, however, intruded by early Ordovician tonalites and granodiorites, and display contact metamorphic aureoles as a result of those intrusions. The fourth subdivision are represented by Devonian mylonite zones that formed during the Achalian Tectonic Cycle.Limited geochemical data suggests distinct differences in depositional sources and composition of the Cambrian, Cambro-Ordovician and Ordovician rocks (Figures 4, 5).

2.2.2 CAMBRIAN

Monte Guazú Metamorphic Complex (Ꞓggn, Ꞓga, Ꞓgt)
Pelitic gneiss, tonalitic orthogneiss, meta-mafic rocks, marble and calc-silicate rock

The Monte Guazú Metamorphic Complex is the main basement unit forming the southern Sierra de Comechingones. The area was mapped by Candiani and Maza (1982) as part of stream-sediment geochemical mapping program, and later, in the south, Otamendi and others, (1996) mapped and described the unit as "Metamorfitas Monte Guazú", including it in the Las Lajas Complex. The unit extends from south of Estancia Inti Huasi in the south to Cerro El Mogote in the north where it occupies the full width of the Sierra de Comechingones. Outcrop of the Complex is good to excellent in the sierras with gneiss forming low strike ridges. Meta-mafic rocks crop out as small isolated hills and also form the bulk of the magnetic anomalies within the unit.

The complex comprises interlayered metasedimentary and meta-intermediate and mafic rock, all of which were metamorphosed and deformed during the Early Cambrian Pampean Cycle. In the north, the unit is intruded by the Alpha Corral, Comechingones and Uspara Granites of the Cerro Aspero Batholith, and in the south, by the Inti Huasi

and Cerro Negro Granites. In the southwest, the unit is faulted against and thrust over the Conlara Metamorphic Complex. A thin veneer of unconsolidated Cainozoic continental sediments limits the easterly extent of the complex with remnants forming cappings along the higher parts of the Sierra de Comechingones south of Cerro Mogote.

The complex contains four main lithologies: pelitic gneiss; tonalitic orthogneiss; meta-mafic rocks; and minor marble and calc-silicate rocks. All are interlayered, and have the same medium-grade metamorphic and deformational history. Both the tonalitic orthogneiss and the meta-mafic rocks are interpreted as originally intrusive into the metasedimentary protoliths. Although having a similar composition and deformational/metamorphic history as the Conlara and Nogoli Metamorphic Complexes, these latter complexes are distinguished by the absence of tonalitic orthogneiss and the less feldspathic nature of the pelitic gneiss.

Banded, grey, garnet±sillimanite±muscovite-K-feldspar-biotite-plagioclase-quartz gneiss is the most abundant rock type, comprising about 80% of the Monte Guazú Metamorphic Complex. It is interlayered with minor calc-silicate rock, tonalitic orthogneiss and contains boudinaged pods of amphibolite, marble and pegmatite. Leucosome lenses and bands, a few cm's wide, are common and, in places, the texture is migmatitic. The medium-grade gneissic fabric is mostly rotated into parallelism with moderately-ENE dipping penetrative D3 shear planes. In zones of higher D3-strain, such as near Las Albahacas, this foliation has almost obliterated earlier fabrics and the gneiss is converted to mylonite with biotite replaced by chlorite and hematite, and sillimanite altered to fine muscovite aggregates.

Grey equigranular tonalitic orthogneiss is the second most abundant lithology within the Monte Guazú Metamorphic Complex. It is interlayered with the other rocks and is common, particulary in the south where it comprises over 50% of the unit and is faulted against the structurally underlying Conlara Metamorphic Complex. The rock consists essentially of granoblastic polygonal medium-grained plagioclase and quartz, with biotite ± hornblende. Acessories include zircon, apatite, allanite, magnetite and rare pyrite. Rare muscovite occurs as porphyroblasts and as microcrystalline secondary folia. The principal penetrative foliation (S1), is defined by aligned biotite, and a weak mineral lineation (L1) is defined by aligned biotite and quartz ribbons.

Weak chlorite, hematite, carbonate, sericite and epidote alteration is widespread, especially within D3 mylonitic zones, such as near Las Albahacas. Veins of tourmaline-muscovite pegmatite are present in the south, proximal to the Conalra Complex.

Geochemically the gneisses are oxidised and metaluminous to slightly peraluminous with ASI ratios of between 0.9 and 1.1, falling within the "I-type" field of Chappel and White (1974).

Meta-mafic rocks, are interlayered throughout the complex forming isolated pods or semi-continuous bands that are boundinaged within the penetrative, D1 metamorphic fabric. Individual bodies range from a few metres to more than one kilometre in length. Pegmatite commonly forms small fringes developed at boudin necking points. The rocks are mostly banded ortho-amphibolite comprising weakly aligned fine- to medium-grained subprismatic hornblende, with granoblastic polygonal plagioclase and quartz, and minor titanite. Minor diopside, carbonate, muscovite, K-feldspar and epidote may also be present. Minor meta-gabbro, comprising subprismatic anthophyllite, granoblastic polygonal plagioclase, biotite, minor micrographic K-feldspar-quartz, magnetite and zircon, occurs within tonalitic gneiss. The rocks preserve a differentiated medium-grade gneissic fabric formed during D1 which was little affected by later deformation. Similar meta-mafic rocks to those in the Monte Guazú Metamorphic Complex occur north of the Cerro Aspero Batholith. These have been interpreted as transitional tholeiites with within-plate affinities (Osvaldo and others, 1996; Demichelis and others, 1996), which were derived from a primary basic magma generated by low-degree partial-melting of an OIB-type asthenospheric mantle source (Demichelis and others, 1996). Marble and banded calc-silicate gneiss, are a minor consituents of the complex, forming isolated bodies, particularly in the west near Cerro Moro.

Several generations of pegmatite dykes intrude basement metamorphics and granitic rocks. The oldest are represented by zoned garnet-muscovite-rich types that form small deformed pods, within the gneiss of the Monte Guazú Metamorphic Complex. These pegmatites are probably the product of partial melting during M1 (Cambrian) metamorphism.

Conlara Metamorphic Complex (Ꞓcgn, Ꞓce)
Pelitic and psammitic schist and gneiss; orthogneiss, minor calc-silicate and marble; pegmatite.

The Conlara Metamorphic Complex, comprises the majority of the basement outcropping within the valley (Valle del río de Conlara) between the Sierras de San Luis and Sierra de Comechingones. The Conlara Metamorphic Complex also incorporates the metamorphic part (the "Metamorfitas y Anatexitas India Muerta") of a previously

defined metamorphic-intrusive complex, the Achiras Complex (Otamendi and others, 1996), in the extreme south of the Sierra de Comechingones. The igneous part of the Achiras Complex of Otamendi and others, (1996) has been redefined as the Achiras Igneous Complex.

The western margin of the Conlara Metamorphic Complex is defined by a major NNE trending magnetic lineament and mylonite zone (the Rio Guzman Shear Zone) in the eastern Sierras de San Luis, that seperates the Complex from the Ordovician San Luis Formation. A significant proportion of the Complex is covered by a thin mantle of unconsolidated Cainozoic deposits, however, good exposures occur within various rivers (Rio Quinto, Rio Rosario, Rio de la Cañada Honda, Rio Conlara) and sierras (eastern Sierras de San Luis, southern Sierra de Comechingones, sierras del Morro, de la Estanzuala, del Portezuelo, and de Yulto).

The Conlara Metamorphic Complex comprises dominantly late Neoproterozoic - early Cambrian sediments intruded by Cambrian and/or early Ordovician granite and polymetamorphosed in the early-mid Palaeozoic. The thickness of the sedimentary sequence is unknown due to the generally shallow orientation of the main transposition foliation. The Complex is intruded by a series of Devonian granites, which post-date the dominant structural and metamorphic episodes, and by Neogene calc-alkaline to shoshinitic volcanism. The Complex has a generally low magnetic signature and may be separated into regions that are comprised dominantly of gneiss, and areas comprised dominantly of schist.

Metapelitic and metapsammitic quartz-feldspar-biotite-muscovite-garnet-sillimanite ±tourmaline±chlorite schist is the most abundant rock type exposed in the Conlara Metamorphic Complex (approximately 50%). The schist contains a well-developed biotite-muscovite foliation that is openly folded at a meso- to macro-scopic scale with long, generally shallowly east-dipping limbs and short, shallowly west-dipping limbs. Strongly corroded sillimanite, biotite coronas on garnet, and coarse poikiloblasts of muscovite and quartz containing tightly crenulated inclusions of sillimanite, suggest that the dominant fabric is a low temperature overprint of an earlier higher-grade (amphibolite-facies) fabric. Biotite and muscovite define a generally east plunging mineral lineation while shear-sense indicators are well developed and show a dominantly east-up displacement that is consistent with the asymmetry of folding. An east-down shear-sense is locally preserved, however, particularly close to the western margin of the complex and where this fabric is associated with migmatitic shear bands and extensive pegmatites (Figure 6).

Figure 6. Pegmatitic veins contained in asymmetrical extensional shear bands formed late in the Famatinian Tectonic Cycle. The shear sense is east down (locality A95JS018).

Figure 7. Pegmatite intruding schists of the Conlara Metamorphic Complex (locality A96JS030). The pegmatite is offset along a discrete Devonian mylonite.

In places, the schist contains a metamorphic differentiated layering that consists of alternating leucosome and millimetre-scale quartz-rich layers, and in the southern Sierra

de Comechingones, contains minor interlayered tonalitic gneiss and banded ortho- and para-amphibolite. Within a kilometre of the Las Lajas Shear Zone in the southern Sierra de Comechingones, the schists are mylonitic and boudinaged, and chloritic alteration of biotite is common.

Metapelitic and metapsammitic quartz-feldspar-biotite±garnet±sillimanite gneiss is the next most abundant unit within the Conlara Metamorphic Complex (~40%). It is clearly distinguished from the schist by the paucity of muscovite in the foliation, and more massive outcrop style. Where secondary muscovite is developed, it is generally unoriented and a minor component of the mineral assemblage, or it is associated with discrete overprinting shear bands, where it is associated with biotite. Leucocratic and/or pegmatitic veins are common in this rock type and typically define the main foliation, which is tightly to isoclinally folded (and refolded) at a meso- to micro-scopic scale.

Felsic orthogneiss is interlayered with both the gneiss and schist and constitutes a relatively minor component of the Complex. The orthogneiss is strongly foliated and consists dominantly of equigranular quartz, feldspar and biotite with minor muscovite. The foliation in the orthogneiss appears to be contiguous with the earliest fabric in the enclosing rocks and suggests that the original granite was emplaced during either the early Cambrian Pampean orogeny or Cambro-Ordorvician Famatinian orogeny.

Calc-silicate and marble are intimately associated and are a minor constituent of the complex, they are restricted to a series of narrow layers and pods through Sierra de Yulto, Sierra Los Morillos, Sierra del Morro and Sierra de la Estenzuela. Marble is subordinate and is predominantly calcite with minor quartz and diopside, while the calc-silicate assemblage includes hornblende, plagioclase, garnet, sphene, calcite and magnetite, with thin diopside coronas locally developed on garnet. Additionally, secondary veins crosscut the marble and calc-silicate and are associated with tungsten mineralisation, these include wollastonite-flourite-scheelite veins in Sierra los Morillos, and pegmatitic epidote-feldspar-amphibole-biotite-pyrite-calcite-magnetite-quartz veins in Sierra de Yulto. The magnetic susceptibility of the marble is generally low ($<36 \times 10^{-5}$ SI) while the calc-silicate produced values up to 1231 ($\times 10^{-5}$) SI, and the late pegmatitic veins produced local values up to 3512 ($\times 10^{-5}$) SI.

Various generations of quartz-feldspar-biotite±muscovite±tourmaline±garnet pegmatite also occur within the Conlara Metamorphic Complex (e.g. Figure 7). Early generations are strongly deformed and are elongate and boudinaged in the schist and gneiss. Later generations are somewhat less deformed and are spatially associated with Devonian

granites. The magnetic susceptibility of the pegmatites is extremely low. Late-stage quartz-tourmaline dykes and veins that are generally stongly lineated, are also common within the Complex and are typically found in NW or SW trending sets. Additionally, late aplite dykes occur in the southern Sierra de Comechingones.

Nogoli Metamorphic Complex (Є̶n)
Felsic and mafic orthogneiss, paragneiss, monzonite and quartz-monzonite.

The Nogoli Metamorphic Complex represents the NW region of the Sierras de San Luis, in the region of the township of Nogoli, from which the name is derived. The complex is best exposed along the western escarpment of the Sierras de San Luis and within the deeply incised rios de la Quebrada, del Molle and Amieva. Additionally, a poorly outcropping region of basement rocks, largely defined from geophysical and satellite imagery, occurs to the northwest of the main San Luis Fault-escarpment and is tentatively included within the Nogoli Metamorphic Complex. The eastern boundary with the younger Pringles Metamorphic Complex is probably a tectonic contact but may represent an original terrane boundary, while the boundary with the Ordovician San Luis Formation is represented by a Tertiary thrust fault that may be a reactivated Devonian structure.

The Nogoli Metamorphic Complex comprises undifferentiated felsic and mafic orthogneiss of probable early Cambrian age, and pelitic gneiss of probable late Neoproterozoic to early Cambrian age, though an older Proterozoic age for the metasediments could not be discounted at this stage. Felsic orthogneiss dominates with subordinate lenses and pods of mafic gneiss (dominantly amphibolite) that preserve complex and discordant, high-grade, structural fabrics. The basement gneiss is intruded by numerous co-magmatic monzonite and quartz-monzonite bodies that occur as both discrete mappable plutons (e.g., Rio del Molle Monzonite; Figure 8) and as dykes at various scales. The aeromagnetic signature of the complex is relatively low with local anomalies probably related to amphibolite bodies or monzonite intrusions.

The strongly foliated felsic orthogneiss consists dominantly of recrystallised quartz, feldspar and biotite, with muscovite usually developed as a late retrograde phase. In some localities rare K-feldspar porphyroclasts are preserved within the felsic orthogneiss. Subordinate mafic gneiss occurs as layers and boudinaged pods within the felsic orthogneiss and pelitic gneiss, and consists of seriate hornblende, plagioclase, quartz and biotite, with retrograde epidote.

Minor outcrops (and extensive talus of very large boulders up to 15m diameter) consisting predominantly of high-grade pelitic gneiss occur within the Rio Amieva (e.g. Figure 9). The metapelite consists of a peak metamorphic assemblage of quartz-feldspar-cordierite-sillimanite-biotite with a well developed gneissic fabric, and local spectacular, discordant networks of cordierite bearing leucosome cross-cutting the gneissosity. Additionally, numerous boudinaged pods of amphibolite occur within the gneissic fabric.

The earliest pervasive (concordant) gneissic fabric within the complex trends in a west to northwesterly direction. This early fabric is folded and partially retrogressed through muscovite replacing sillimanite, and is overprinted by subvertical to steeply east-dipping shear zones up to tens of metres in width that trend in a northerly direction. These latter zones, which have recrystallised and retrogressed the early high-grade assemblages, display multiple reactivation with contrasting shear-sense and range in metamorphic grade from amphibolite- to greenschist-facies. Mafic orthogneiss in one of these mylonite zones is characterised by an intense foliation defined by biotite, quartz ribbons and lineated hornblende, with the hornblende partially replaced by biotite, zoisite, clinozoisite and epidote. The latest (low-grade) mylonitic reactivation of these zones, with east-up shear-sense, is correlated with the pervasive Devonian deformation that is associated with the Achalian Tectonic-Cycle.

The Nogoli Metamorphic Complex is clearly distinguished from the Pringles Metamorphic Complex by the significant pre-Ordovician orthogneiss component and lower magnetic response (Hungerford and others, 1996), and probably represents at least an Early Cambrian terrane equivalent to the Conlara and Monte Guazú Metamorphic Complexes further to the east.

2.2.3 CAMBRO–ORDOVICIAN

Pringles Metamorphic Complex (€Opgn, €Ope)
Pelitic and psammitic gneiss and schist, orthogneiss, amphibolite, minor calc-silicate

The Pringles Metamorphic Complex is exposed in the Sierras de San Luis, in three areas between the Conlara Metamorphic Complex in the east and the Nogoli Metamorphic Complex in the west. The easternmost and largest outcropping region occurs in a continuous north-south belt dissecting the sierras. This belt is fault bound to the east and to the west by the San Luis Formation and partly in the west by the Escalerilla Granite

and is well exposed in road cuttings beween Trapiche and La Carolina, and within various dissecting rivers and creeks (Rio Grande, Rio de la Cañada Honda, Arroyo los Manantiales, Arroya las Aguilas, Arroyo Virorco). The Pringles Metamorphic Complex is further exposed to the northwest of the Escalerilla Granite in two regions: the first of these is a small area in contact with the granite in the geographically high portion of the sierras, while the second region occurs further to the north in a deeply incised and poorly accessible area towards the township of San Fransisco del Monte de Oro.

Figure 8 (above). Contact between phases of the Rio del Molle Monzonite, which intrudes the Nogoli Metamorphic Complex (locality A95JS078). Darker phase is monzonite while lighter phase is quartz-monzonite.

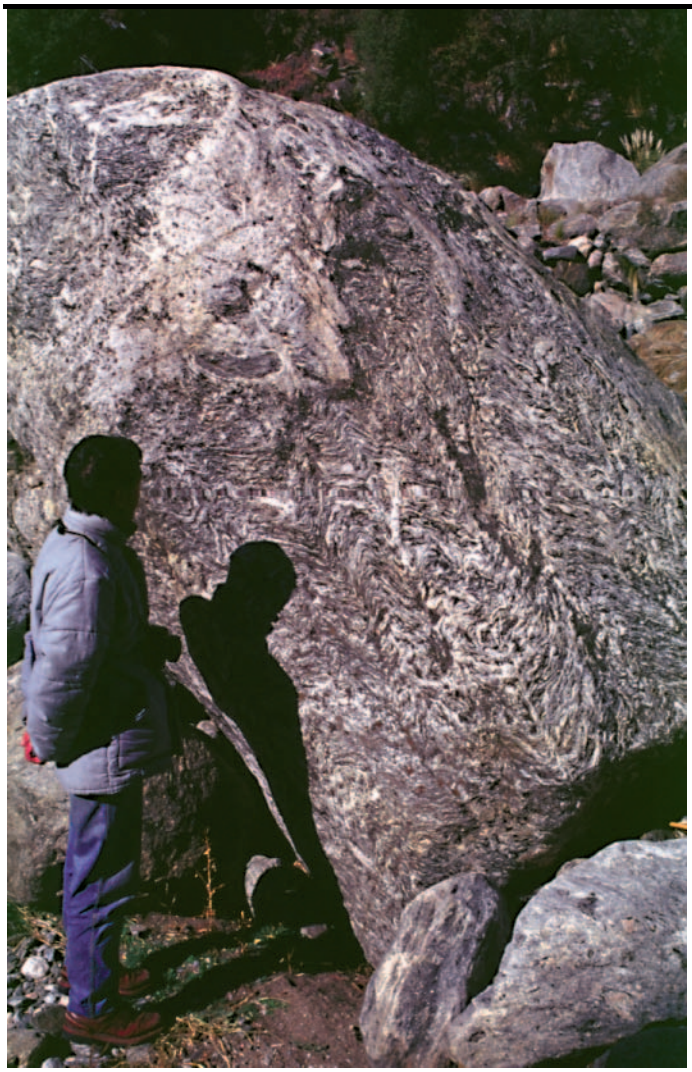

Figure 9 (left). Boulder of high-grade metapelitic gneiss of the Nogoli Metamorphic Complex exposed in Rio Amieva (Locality A96JS010). Note crenulation of the early gneissic fabric and the cross-cutting (cd-bearing) leucosomes.

The Pringles Metamorphic Complex comprises metasediments of probable late Cambrian - early Ordovician depositional age intruded by early Ordovician mafic and ultramafic rocks of the Las Aguilas Group (*c*. 480 Ma; see below), and by numerous granite and pegmatite bodies. Analysis of zircon separates from felsic orthogneiss (sample A95JS079e) and monazite separates from pelitic gneiss (sample A95JS129c) within the Pringles Metamorphic Complex suggest that the rocks reached a metamorphic peak at about the time of emplacement of the Las Aquilas Group, and had cooled to about 600 °C by about 450 Ma (Camacho & Ireland, 1997). The peak metamorphic grade in the rocks reached granulite facies, particularly in the region of the Las Aguilas Group intrusions. A close temporal relationship between the age of the Las Aguilas Suite and the peak metamorphism as well as the close spatial relationship, suggests that the ultramafic and mafic rocks may have been the heat source of the metamorphism.

The most abundant rock-types in the Pringles Metamorphic Complex are pelitic and semipelitic gneiss and pelitic and semipelitic schist. The gneiss represents domains

where peak (granulite-facies) metamorphic assemblages have been preserved, whereas the schist either represents domains of initially lower grade (amphibolite-facies) metamorphism or regions where subsequent deformation has been localised and resulted in a lower grade metamorphic overprint.

The gneiss contains quartz-feldspar-garnet-sillimanite-biotite-magnetite±cordierite ±spinel, is generally massive in outcrop and locally has a high magnetic susceptibility (maximum measured reading of 11371 x 10^{-5} SI). The gneiss generally contains a well developed mineral and compositional layering dipping steeply to the east with a near vertically plunging mineral lineation mostly defined by sillimanite ± biotite. Garnet is typically porphyritic, though locally it forms spectacular symplectic intergrowths with magnetite. Both cordierite and garnet are developed within leucosomes, intergrown with K-feldspar, that cross-cut the compositional layering but are generally flattened in the foliation plane and are elongate parallel to the extension lineation (Figures 10, 11). In addition, cordierite-bearing pegmatites truncate the mineral fabric and are interpreted to represent the melt product of the leucosome forming reactions.

Pods of hornblende-plagioclase±orthopyroxene±clinopyroxene mafic gneiss are abundant within the gneiss and are typically strongly elongated parallel to the mineral lineation. Some mafic pods are partly boudinaged through internal conjugate fracture sets containing veins of plagioclase-orthopyroxene-clinopyroxene, and veins of the same composition as the cordierite-bearing pegmatites.

Figure 10. Mylonitic fabric in high-grade gt-sill-cd-bi-mt gneiss of the Pringles Metamorphic Complex viewed towards north, parallel to the extension lineation (locality A95JS040; A˚ las Aguilas). Cordierite, which occurs in leucosomes, is stable, though recrystallised in the shear fabric, which suggests the shearing developed synchronously with peak metamorphism. Shear-sense is east up.

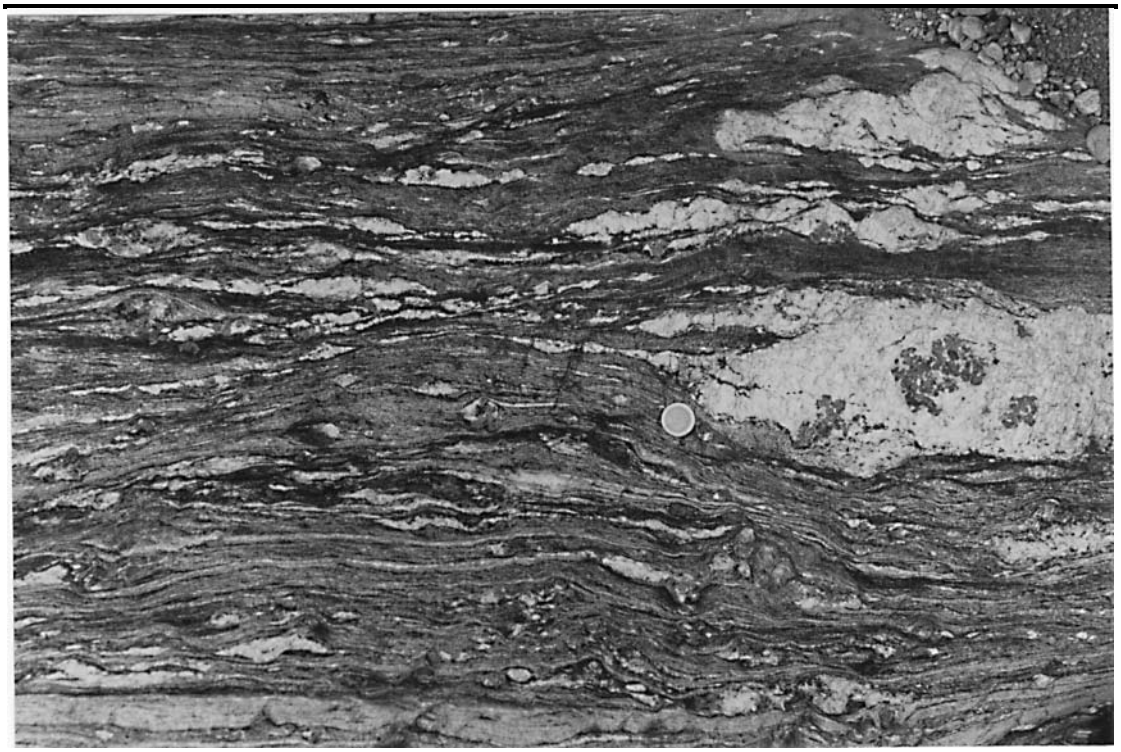

Figure 11. Garnet-bearing leucosomes in high-grade, mylonitic gneiss of the Pringles Metamorphic Complex, viewed perpendicular to the extension lineation (locality A96JS003; Rio Grande).

Within the gneiss, distinct belts of high-grade mylonite occur. These mylonites are of variable composition and locally contain cordierite- and sillimanite-stable assemblages and occasionally are overgrown by mm-scale, euhedral garnets with spiral inclusion trails. The mylonites are particularly well developed on the margins of the ultramafic bodies of the Las Aguilas Suite, which suggests that formation of the mylonites may be in part due to strain localisation along the contact between rheological contrasting rock-types. The mylonites contain a mineral and elongation lineation that is indistinguishable from that in the host gneiss, and generally have well developed shear-sense indicators such as S/C fabrics and winged porphyroclasts (Figure 12) that consistently show an east over west displacement sense.

The boundary between gneiss and schist is transitional and is marked by numerous, thin, k-feldspar rich pegmatites that form either thin discontinuous veins or occur as dykes. The schist consists of a peak metamorphic assemblage of quartz-feldspar-garnet-biotite-sillimanite, is generally well layered and has a low magnetic susceptibility. A primary compositional layering that consists of alternating pelitic and semi-pelitic units is apparent in many areas of the schist that is not apparent in the higher grade regions of the complex.

Extensive tourmaline-apatite-garnet±beryl-bearing pegmatites occur within the schist and are associated with a number of S-type granite and leucogranite intrusions. These

intrusions occur in distinct belts within which, a locally intense, moderate to shallow, dominantly east-dipping shear fabric is developed, with east-down shear sense on a moderately southeast plunging lineation. The shear fabric is mostly defined by muscovite-biotite±chlorite, while the lineation is locally defined by tourmaline. Many of the pegmatites are strongly folded and boudinaged in this shear fabric. Within the metasediments, the earlier, peak foliation was strongly folded and transposed, and texturally the peak sillimanite is largely replaced by coarse poikolitic muscovite+quartz, and fine folia of muscovite. In places, late radiating needles of tourmaline and coarse, unoriented porphyroblasts of muscoviteare grown on the secondary foliation plane.

Metre scale, elongate and zoned calc-silicate pods occur within both the gneiss and schist. An example of one of these pods from Arroyo Los Manantiales consists of an outer diopside-anorthite bearing rim with a core rich in calcite, garnet and diopside. These pods possibly represent boudins of originally thin and continuous, interlayered carbonate units, though the present lateral extent cannot be determined.

Figure 12. Sub-vertical, early Ordovician mylonite in the Pringles Metamorphic Complex (locality A95JS009; A° los Manantiales). Shear-sense is east up on a north-south trending zone (view to north). Note the winged garnet porphyroblast near the tip of the pencil.

Orthogneiss comprises a relative minor component of the Complex, is extensively recrystallised and contains quartz-feldspar-garnet±biotite. Garnet is subhedral and poikiloblastic and contains abundant granular inclusions of well-rounded quartz and minor plagioclase.

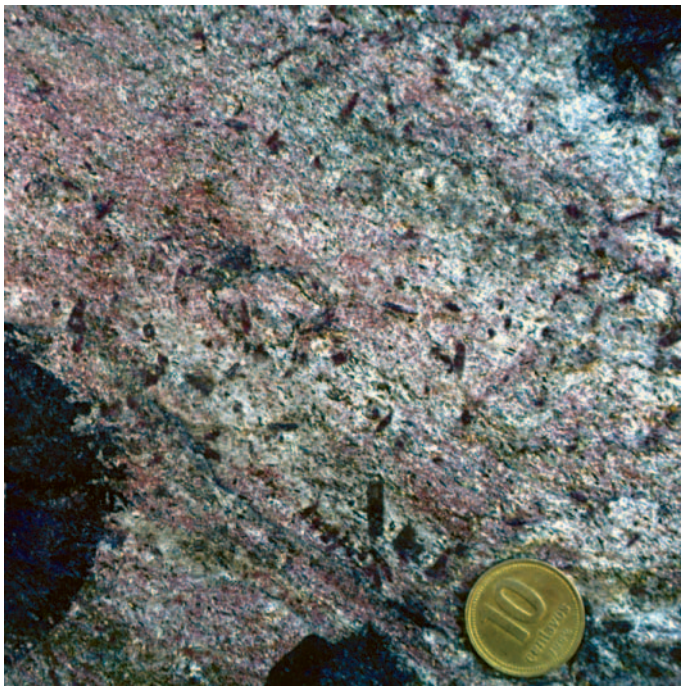

Figure 13. Radiating staurolite crystals in sheared contact zone between Pringles Metamorphic Complex and San Luis Formation (locality A95JS054; Dique La Florida). Staurolite overgrows crenulations in the muscovite-biotite-garnet-chlorite schist, suggesting it grew late in the development of the shear zone. Ar-Ar data shows this low-grade shearing occured during the Late Devonian.

2.2.4 ORDOVICIAN

San Luis Formation (Osl, Osls, Oslc)
Phyllite, schist, arenite, slate and metaconglomerate

The San Luis Formation (Prozzi & Ramos 1988) occurs in two elongate NNE trending belts in the Sierras de San Luis. The eastern belt is les than 5 km wide and bound to the east by the Rio Guzman Shear Zone and to the west by Embalse La Florida and Cerros Largos. It is truncated to the north by the Las Chacras batholith and passes under shallow cover to the south. The western belt is no more than 3 km wide and passes through La Carolina and extends discontinuosly southwards on both the eastern and western margins of Escalerilla Granite. A small exposure of this belt also occurs near El Volcan adjacent to the Escalerilla Granite. The San Luis Formation is well exposed in Rio de la Cañada Honda, in Rio Quinto below Embalse La Florida, Rio Grande adjacent to Escalerilla Granite and near La Carolina from the road to San Fransisco del Monte de Oro.

The age of the San Luis Formation (SLF) is tightly controlled by structural and stratigraphic constraints. The SLF unconformably overlies high-grade basement rocks of the Pringles Metamorphic Complex (metamorphosed at ~480 Ma) and is unaffected by the intense tectonism that has affected those rocks. However, the formation is intruded by the Tamboreo Granodiorite (472 ± 5 Ma), the Bemberg Suite tonalites (471 ± 5 Ma) and by a suite of aplitic to rhyolitic dykes that also cross-cut the Tamboreo Granodiorite. The contact of the SLF with the Pringles Metamorphic Complex and the Conlara Metamorphic Complex was strongly sheared during the Devonian, with kyanite, staurolite and garnet bearing assemblages (e.g. Figure 13) and minor quartz-feldspar-muscovite-kyanite-staurolite pegmatites locally developed within the SLF near the contacts.

The majority of the SLF consists of medium- to thinly-bedded quartz arenite and phyllite in varying proportion (e.g. Figure 14), and include areas dominated by either lithology. Black shales are locally associated with a dominantly fine-grained sequence southwest of Las Verbanas. Sedimentary structures, such as graded bedding, cross-bedding, channel and flame structures, are common in areas where there is a higher proportion of coarser grained beds. Most rock-types are quartz-rich, and significant carbonate occurs in the matrix of some coarser grained arenites.

Two main deformations affected the SLF during the Devonian compressional cycle. The first of these deformations (regional D3a) resulted in tight to isoclinal, upright to inclined folds with a well-developed, axial planar, slaty cleavage (e.g. Figure 15). The second deformation (regional D3b), resulted in the development of discrete shear zones, separated by domains of open refolding with a corresponding crenulation cleavage. Additionally, a very early foliation (?S2b) is also preserved in fine grained rocks in some areas. The regional metamorphic grade within the SLF is typically lower greenschist and the rocks are generally fine grained. In places though, a more schistose and coarser grained fabric is developed, which probably reflects slight variations in the metamorphic grade, during the Devonian compressional cycle. Local high-temperature metamorphic aureoles are also developed around Ordovician, granodioritic to tonalitic intrusives. The magnetic signature of the San Luis formation is generally low, however, local high magnetic responses are developed in the region of magnetite-bearing Devonian mylonites such as the Rio Guzman Shear Zone.

Where axial planes of the two main Devonian deformation phases are sub-parallel and occur in transposed fine-grained rocks, slate is developed. The slate is dark-grey to green and consists predominantly of thinly bedded phyllites with minor thin quartzites. The phyllite consists predominantly of quartz, chlorite and sericite with minor organic carbon (Prozzi and Rosso, 1990) and contain secondary euhedral crystals of calcite and

pyrite. The thin quartzites consist predominantly of quartz, chlorite and minor muscovite with abundant secondary euhedral calcite and minor epidote. Both rock-types are cross-cut by thin veins of quartz±pyrite. The slate has been extensively quarried for building stone.

A distinctive, poorly-sorted, polymictic, conglomerate unit, named the Metaconglomerado Cañada Honda by Saurez and others, (1992), occurs within the SLF. The conglomerate is up to 100 m thick and is well exposed in Rio de la Cañada Honda, in the eastern belt of the SLF. Additionally, Saurez and others, (1992) report the

Figure 14. Alternating units of thin, quartz- and phyllite-rich bedding within the San Luis formation (locality A96JS021; Rio Grande).

Figure 15. **A96JS4**: Hinge of mesoscopic isoclinal fold in alternating, thin phyllite and arenite beds of the San Luis Formation (locality A96JS043). The geologist on the left is pointing down the plunge of the fold-axis.

Figure 16. Alternating fine-grained bedding and strongly foliated conglomerate within the Conglomerado Cañada Honda of the San Luis Formation (locality A95JS123)

Figure 17. Moderately east-dipping mylonitic fabric in the Achiras Igneous Complex adjacent to the Las Lajas Shear Zone.

occurrence of a 100 m wide conglomerate unit that extends for about 2 km to the northwest of La Carolina within the western belt of the SLF. The conglomerate in the eastern belt consists predominantly of angular clasts of pebble- to cobble-sized, quartzite and phyllite, within a fine- to coarse-grained matrix. Some larger clasts preserve primary bedding features. Saurez and others, (1992) have also reported the occurrence of clasts of rhyolitic to dacitic metavolcanics. Interlayered with the conglomerate are discontinuos, thin to medium sandstone and mudstone beds (e.g. Figure 16) displaying channel structures and graded bedding. The top of the unit grades through alternating conglomerate and thinly bedded quartzite into thickly bedded massive quartzite units. An anastomosing mylonitic foliation is developed within the conglomerate parallel to bedding and most of the smaller quartzite clasts are recrystallised and display extensive sub-grain development. A sub-parallel cleavage is also developed on the mylonitic foliation and has resulted in a fine crenulation surface.

The combination of quartz-arenites, phyllites and conglomerates suggests the SLF was deposited in a mid-fan turbidite environment (e.g., Mutti and Ricci Lucchi, 1978). Thus, it would be unusual if the SLF contained felsic volcanics and associated syngenetic mineralisation as has been suggested by Brodtkorb and Brodtkorb (1979).

2.2.5 DEVONIAN

Las Lajas Shear Zone (Dlmi)
Mylonitic schist, granite, marble, orthoamphibolite, pegmatite and serpentinite

The Las Lajas Shear Zone is a linear northwest-trending high strain zone, traversing the southern Sierra Comechingones. The zone, from 1-2 km wide, can be traced on aeromagnetic images further to the southeast towards Sampacho, beneath a thin cover of Cainozoic sediments. The shear zone, named after Estancia Las Lajas, has been described by Otamendi and others, (1996) who differentiated two subunits, the "Unidad Metamorfitas Loma Blanca" and the "Unidad Metamorfitas Monte Guazú". The name Las Lajas Shear Zone is used here only for those rocks placed within the "Unidad Metamorfitas Loma Blanca". The "Unidad Metamorfitas Monte Guazú" has been renamed the Monte Guazú Metamorphic Complex. Rocks in the shear zone are mostly well exposed within the numerous quarries locatted in marble lenses.

The shear zone is a mylonitic melange of metamorphic and intrusive rocks, and is faulted-bounded within the Conlara Metamorphic Complex. The main penetrative greenschist-facies mylonitic fabric cross-cuts the Achiras Igneous Complex (382 ± 6 Ma) and hence must be no older than Early Devonian in age (Figure 17). Pelitic schist predominates with lesser granite, marble, amphibolite, pegmatite and rare serpentinite.

Sillimanite-bearing feldspar-muscovite-biotite-quartz schist is the predominant rock type in the shear zone. The schist is more quartz-rich than gneiss in the Monte Guazú Metamorphic Complex but is indistinguishable from that of the enclosing Conlara Metamorphic Complex. The schist is typically finely-banded with an early amphibolite grade foliation defined by sillimanite and differentiated mica-rich folia, leucosome and minor quartzitic bands. This fabric is cut by variably developed mylonitic shear planes associated with recrystallised quartz ribbons and a retrograde greenschist overprint of chlorite, hematite and geothite. Pegmatite veins within the schist are boudinaged and S-C fabrics are locally defined by asymmetry of deformed leucosome clasts.

Pink to buff medium-grained recrystallised equigranular leucogranite comprises about a third of the unit, forming concordant sheets interlayered with schist and other rocks within the shear zone. Foliated metamorphic muscovite and rare relict primary biotite together with bands of granoblastic polygonal quartz and feldspar define a well-developed moderate east-dipping mylonitic foliation with a quartz-muscovite mineral lineation. S-C fabrics are common. Rare idioblastic garnet is present in places, showing

sericitic alteration. The granite is indistinguishable to that in the Achiras Igneous Complex.

Lenses of white to grey banded marble, up to 500 m thick and 5500 m long, make up about 20% of the unit, and occur throughout the entire length of the exposed shear zone. The marble is typically strongly mylonitised with a prominent lineation.

Minor orthoamphibolite lenses (~5%) occur throughout the shear zone, interlayered with schist and marble. The amphibolite is a fine-grained, banded, dark green to black rock consisting mostly of prismatic hornblende, quartz and plagioclase. Bands of recrystallised quartz, carbonate, plagioclase and epidote define a penetrative greenschist facies mylonitic foliation with lineated quartz.

Semi-concordant pegmatite veins comprise up to 5% of the shear zone, forming boundinaged lenses or deformed veins intruding all other rock types. They are mostly white to buff in colour and contain up to 6% muscovite and trace amounts of biotite, garnet or tourmaline. A penetrative mylonitic foliation, defined by recrystallised granoblastic polygonal bands of quartz and deformed muscovite folia, contains a quartz-mica mineral elongation lineation.

Rare massive serpentinite crops out in a tectonised lense, about 50 m long, in the northernmost exposed portion of the shear zone. The rock consists of mesh-textured serpentine, carbonate, talc and magnetite with minor relict olivine and metamorphic prismatic tremolite. This is the only known occurrence of an ultramafic rock in the southern Sierra de Comechingones, however, these rocks are more common to the north of the Cerro-Aspero Batholith where they have been interpreted as dismembered ophiolites incorporated during the Pampean Cycle (Escayola and others, 1993; Martino and others, 1995).

Rio Guzman Shear Zone (Dzmi)
mylonite

The Rio Guzman Shear Zone is a linear north-northeast trending, high-strain zone, traversing the Sierras de San Luis from the Las Chacras batholith in the north, to near Saladillo in the south. The zone, which is up to 3 km wide, is a major lineament on aeromagnetic imagery (Figure 3) that can be traced further to the south, beneath a thin cover of Cainozoic sediments. The shear zone, named after the Rio Guzman, which follows the shear zone for several kilometres, has not previously been described. Rocks within the shear zone are mostly well exposed.

The shear zone consists predominantly of finely layered, steeply east-dipping mylonite that separates the high-grade, Cambrian Conlara Metamorphic Complex from the low-grade, Ordovician San Luis Formation. The shear zone and is largely contained within the low-grade rocks. The dominant assemblage in the mylonite consists of fine to very-fine grained quartz-chlorite-sericite±magnetite with a variably developed subvertical stretching and mineral lineation. Relict (retrogressed) kyanite? with staurolite and garnet, within Conlara Metamorphic Complex rocks on the eastern margin of the zone, near Cerros Largos, however, suggests the shear zone may have initiated at higher pressures and have a long-lived history. Shear-sense indicators in the form of S-C fabrics and assymetric extensional shear bands are well developed and give east up displacement. The similarities of the kinematic indicators and metamorphic grade suggests a close temporal relationship with the Las Lajas Shear Zone in the Sierra de Comechingones.

Ar-Ar data from sericite in the mylonitic fabric, indicates a growth age between 360 and 350 Ma (Camacho & Ireland, 1997), which therefore constrains the minimum age of the greenschist-facies shearing. This age also provides maximum age for the Las Chacras Batholith, which truncates the shear zone to the north of *Sierras de San Luis y Comechingones*. Additionally, the shear zone has been intruded by a number of undeformed lamprophyre dykes, and has been partly reactivated as an east dipping thrust during the presently active, Tertiary Andean compression.

2.3 PALAEOZOIC IGNEOUS ROCKS

2.3.1 INTRODUCTION

In the *Sierras de San Luis y Comechingones* Palaeozoic igneous rocks were emplaced during 3 main tectonic cycles (Table 1). The oldest igneous rocks were emplaced during the Cambrian (Pampean Cycle) and occur as highly deformed bodies within the Early Palaeozoic basement complexes. These are mostly represented by metagabbros, amphibolites and tonalitic orthogneisses within the Monte Guazú Metamorphic Complex. There are no geochronological data and very little geochemical data available for these rocks. The oldest dated rocks (Table 2) were emplaced during the Ordovician (Famatinian Cycle) and consist of ultramafic and mafic rocks, amphibolites, tonalites, granodiorites, and highly fractionated granites and pegmatites. These rocks are mostly strongly deformed. The most significant phase of intrusion, however, occurred during the Devonian-Carboniferous (Achalian Cycle) when a series of major granite batholiths were emplaced (Table3).

2.3.2 ORDOVICIAN INTRUSIVES

Las Aguilas Group (Ola)
Dunite, pyroxenite, hornblendite, amphibolite.

Mafic, ultramafic rocks and amphibolite are exposed in a series of discrete elongate bodies up to 3.5 km in outcrop length and up to 500 metres in outcrop width, in two NNE-SSW trending belts, within the Pringles Metamorphic Complex. Mappable ultramafic and mafic units appear to be restricted to a number of intrusions within a belt approximately 5 km wide and approximately 50 km long, to the west of Trapiche,

Table 2. Geochronology of early Palaeozoic intrusives. Data from: 1 = Camacho & Ireland (1997); 2 = Llambias and others, (1991) 3 = Linares (1959); 4 = Rinaldi and Linares (1973). WR = whole rock, # indicates minimum age, * indicates may be a Devonian intrusive

Intrusive	Age	Ref	Method	Comment
Orthogneiss	484 ± 7	1	U-Pb Zircon	Pringles Metamorphic Complex
Las Aguilas	478 ± 6	1	U-Pb Zircon	Felsic segregation in ultramafic rock of Las Aguilas Group
Tamboreo	470 ± 5	1	U-Pb Zircon	Tamboreo granodiorite
Bemberg	468 ± 6	1	U-Pb Zircon	Bemberg Suite tonalite
Pegmatite	466 ± 20#	4	K/Ar Muscovite	Yac. Los Duraznos - west of Tilisarao
Pegmatite	466 ± 20#	4	K/Ar Muscovite	Yac. Flamingo - 7 km west of Tilisarao
Pegmatite	460 ± 1#	3	U-Pb uraninite (isot.)	Santa Ana - Paso del Rey.
Pegmatite	455 ± 25#	3	U-Pb uraninite (chem.)	Santa Ana - Paso del Rey
Various	454 ± 21#	2	Rb/Sr WR	11 sample isochron from undifferentiated granitoids
Pegmatite	438 ± 15#	4	K/Ar Muscovite	Yac. Cholita - Sa. de La Estenzuela
Pegmatite	430 ± 15#	4	K/Ar Muscovite	Yac. Don Paco, S.d.l. Estenzuela
Pegmatite	415 ± 20#*	4	K/Ar Muscovite	Yac. Maria, Sa. de La Estenzuela

within a region of granulite-facies gneiss, and to a small body just west of Escalerilla granite. Although the ultramafic rocks have a high magnetic reponse, individual bodies within the main belt are not readily distinguished in the aeromagnetics due to the high magnetic response of the enclosing pelitic gneiss. Additionally, numerous metre- to 100 metre-scale, moderately to highly magnetic, amphibolite bodies, representing either differentiated or metamorphosed equivalents of the ultramafic rocks, also occur within the Pringles Metamorphic Complex. These bodies are apparent in the aeromagnetics, particularly away from the region of granulite-facies gneiss, however, due to the small scale or lack of exposure they are not generally differentiated from the Pringles Metamorphic Complex.

Figure 18. **No 79** Primary cumulate layering at the Virorco mafic/ultramafic body

The mafic and ultramafic rocks intruded into the Pringles Metamorphic Complex and are spatially and texturally associated with granulite-facies rocks. The margins of the larger bodies, and many of the smaller bodies, are extensively recrystallised with high-grade hornblende-pyroxene-bearing metamorphic assemblages. The recrystallised metabasic rocks are extensively boudinaged and contain a foliation parallel to that in the enclosing pelitic gneiss. Conversely, the cores of a number of the larger mafic bodies preserve relict igneous textures. For example, at Virorco, subhorizontal igneous layering is preserved (e.g. Figure 18) while at Las Aguilas sub-vertical contacts occur between various intrusive phases. Furthermore, it is apparent that individual bodies are strongly elongate parallel to the stretching lineation in the enclosing gneiss. The implication being that the mafic, ultramafic and amphibolite rocks intruded synchronously with regional deformation.

The age of the Las Aguilas Suite has been constrained by U/Pb dating of zircon seperates from a felsic segregation in the ultramafic rocks at Las Aguilas. The zircons from this late crystallising phase provide an Early Ordovician age of 478 ± 6 Ma (Camacho & Ireland, 1997). Zircon rims from a spatially associated felsic orthogneiss at Las Aguilas produced a similar age of 484 ± 7 Ma (Camacho & Ireland, 1997).

The mafic and ultramafic rocks are composed of dunite, pyroxenite and hornblendite. Orthopyroxene is typically the most abundant primary mineral phase with subordinate olivine, plagioclase, clinopyroxene, spinel (chromite) and sulphide phases (pyrrhotite,

pentlandite and chalcopyrite). Olivine is partially altered to serpentine, clinopyroxene is extensively replaced by clinoamphibole, and phlogopite is locally extensively developed associated with late deformation surfaces. Secondary sulphides include marcasite, covellite and pyrite.

The numerous bodies of amphibolite consist dominantly of hornblende and plagioclase with or without orthopyroxene and contain minor quartz and accessory phases (apatite, sphene, ilmenite and magnetite). Primary hornblende is variably replaced by biotite and secondary hornblende replaces orthopyroxene. Other secondary phases include epidote, zoisite, clinozoisite and calcite.

Whole rock geochemistry indicates that the mafic, ultramafic and amphibolite rocks are low-K gabbroic tholeiites (Figures 19, 20). Trace element discrimination after Mullen (1983) using Ti-Mn-P (Figure 19), suggests that the more mafic magmas may have been derived via partial melting of the mantle in a back-arc setting while the amphibolites may have affinities with island arc tholeiites.

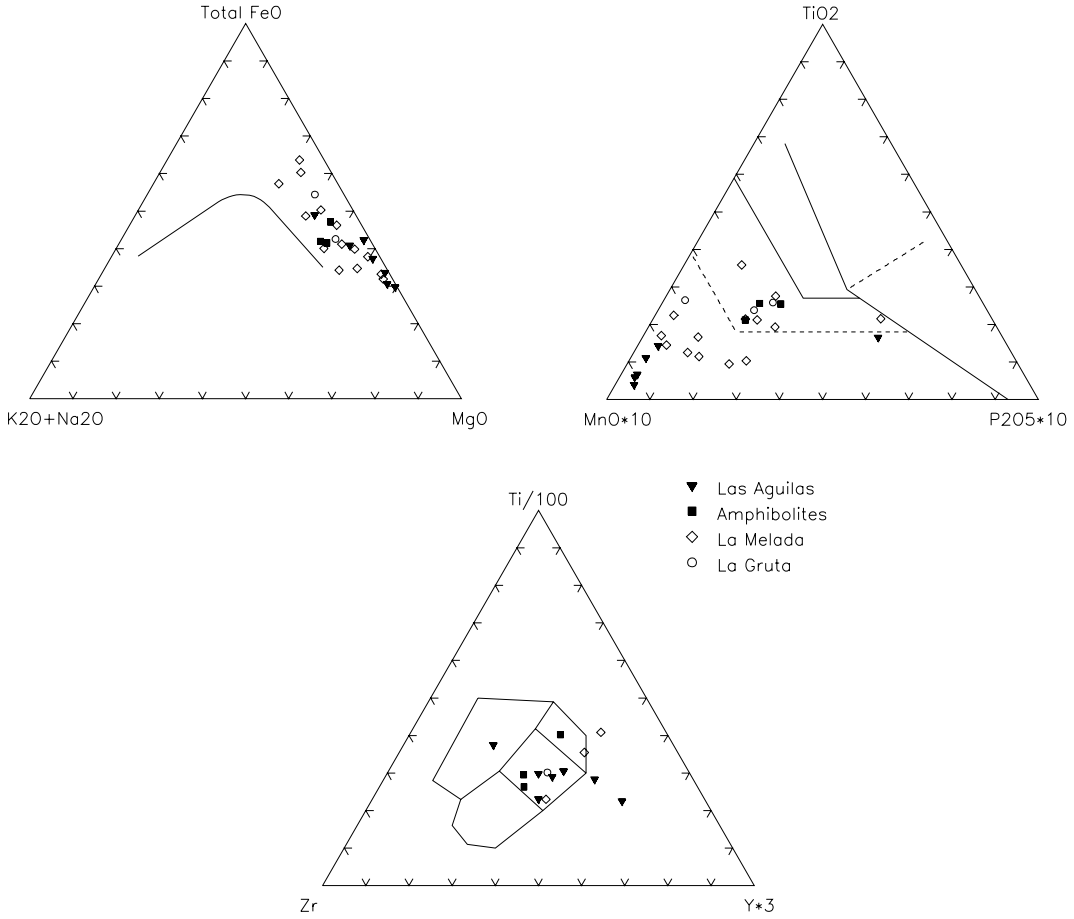

Figure 19. Ternary plots of analyses from rocks of the Las Aguilas Group. The plots towards MnO in MnO*10-TiO_2-$P2O_5$ space may indicate a back arc setting while the La Gruta and amphibolite analysis plot in the region of island-arc tholeiites (e.g. Rollinson, 1993). Data for La Gruta and La Melada from Brogioni & Ribot, (1994)

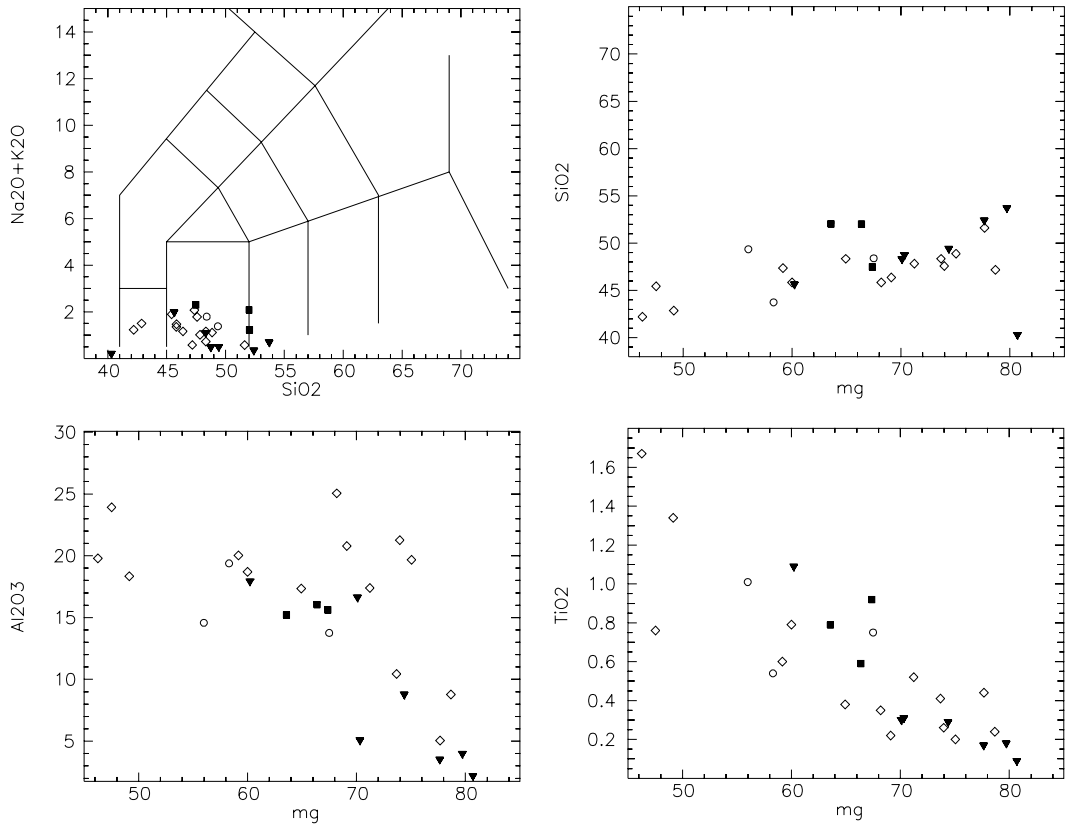

Figure 20. Discrimination diagrams of SiO2 vs (K2O + Na2O) and mg# vs SiO2, Al2O3 and TiO2.

Undifferentiated granitoids and pegmatite (Ogu, Opeg)
S-type leucogranite, granite, granodiorite, tonalite and pegmatite

This unit includes a distinctive suite of S-type granite, leucogranite and pegmatite that occur in an elongate NNE trending belt that passes through Embalse La Florida to the east of Trapiche. This group of rocks, which has previously been described as "granitoids sin-cinematicos" by Saurez and others, (1992) and Llambias and others, (1996a), is well exposed from Embalse La Florida through Paso del Rey and within Rio Grande east of Siete Cajoles.

Structural constraints on the "granitoids sin-cinematicos" suggest that the granites and pegmatites intruded a high-grade (amphibolite facies) basement. Previous geochronology by Linares (1959) and Llambias and others, (1991) indicates that the pegmatites associated with these rocks were emplaced prior to the 460 Ma (Table 2).

The undifferentiated granitoids comprise various phases of leucogranite, granite (including La Florida, Paso del Rey, Cruz de Caña and Cerros Largos granites) granodiorite and pegmatite. The granite is typically leucocratic and equigranular,

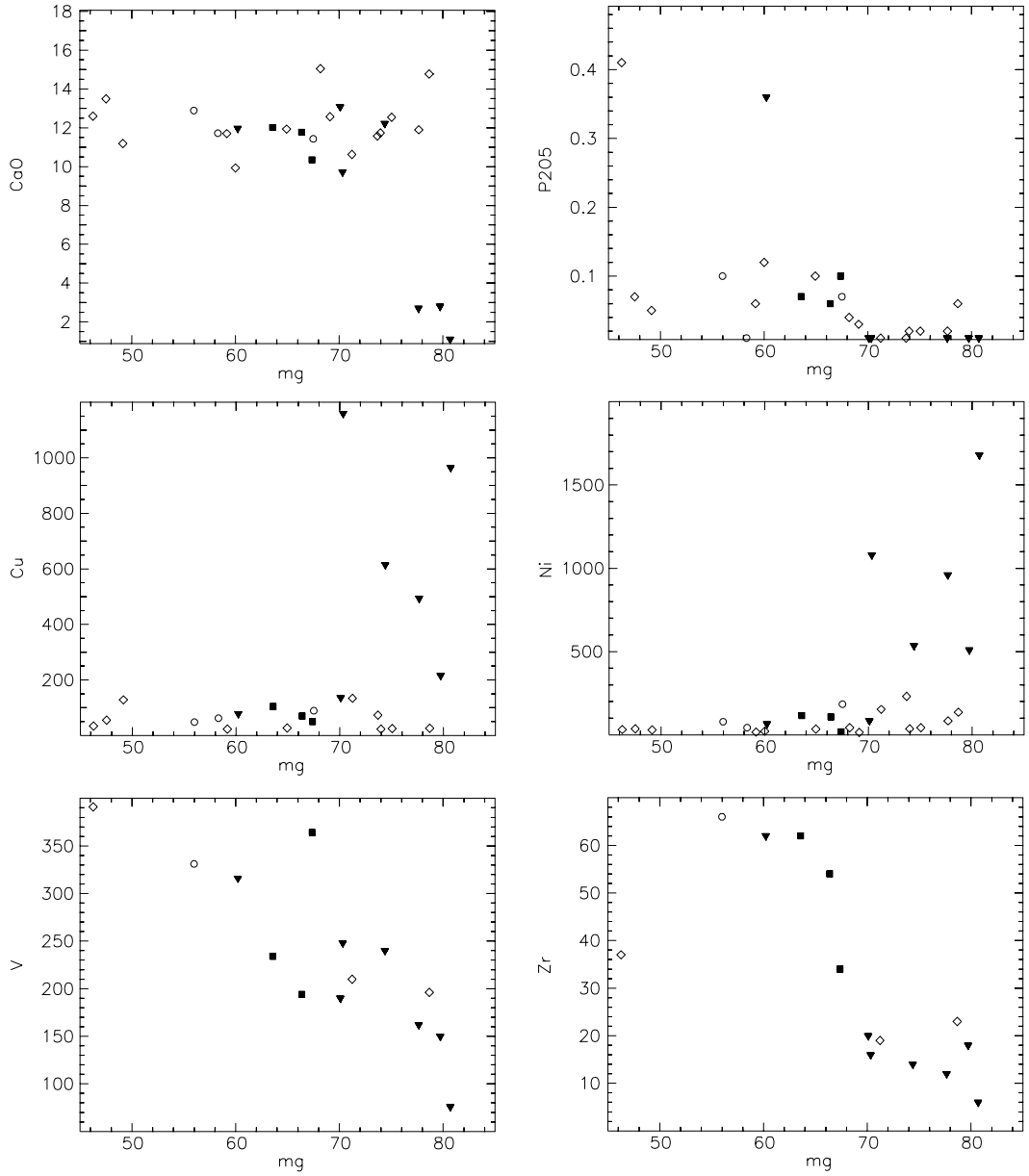

Figure 21. Discrimination diagrams of mg# vs CaO, P2O5, Cu, Ni, V and Zr. Trends are generally similar apart from the Las Aguilas ultramafic/mafic body, which is enriched in Cu and Ni relative to La Melada, La Gruta and the amphibolite bodies.

containing quartz-feldspar-biotite-muscovite±garnet. The associated pegmatites are extremely coarse grained, feldspar-quartz-muscovite-tourmaline-garnet-apatite bearing varieties that are typically compositionally zoned. Limited geochemistry of granites from the "granitoids sin-cinematicos" group (Figures 22, 23, 24) suggests that these granites are highly fractionated.

The "granitoids sin-cinematicos" are spatially associated with zones of extensional deformation developed late in the Famatinian tectonic cycle. They are spatially

associated with pervasive retrogression of the high-grade assemblages within the Pringles Metamorphic Complex and development of a muscovite-tourmaline-bearing assemblages at the expense of sillimanite-biotite-bearing assemblages. Complex interference folds defined by pegmatites of this suite suggests multiple deformation episodes. Llambias and others, (1996) have estimated that the initial deformation within the granites developed under amphibolite-facies conditions, whilst open refolding is consistent with the initial upright folding of the San Luis formation under greenshist-facies conditions.

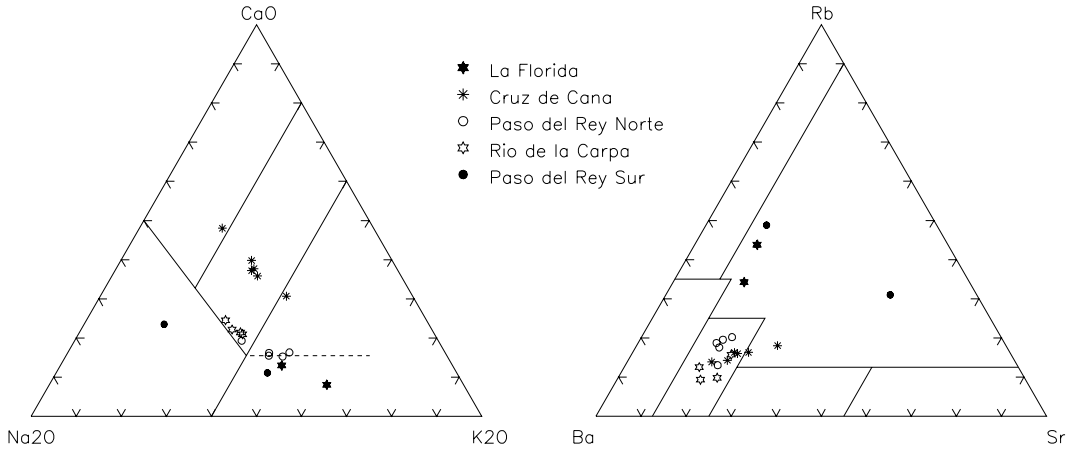

Figure 22. Ternary plots of the Undifferentiated Ordovician Granitoids. Cruz de Caña is enriched in CaO with respect to the other bodies. Data for Cruz de Caña, Paso del Rey Norte, Paso del Rey Sur and Rio de la Carpa from Llambias and others, (1996).

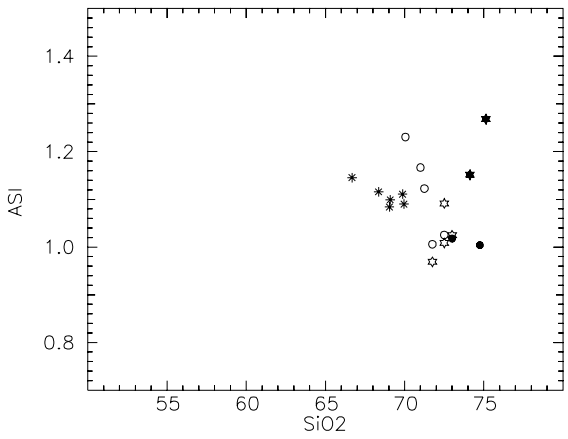

Figure 23. Discrimination diagram of SiO2 vs ASI for the undifferentiated Ordovician granitoids. Labels as per figure 22.

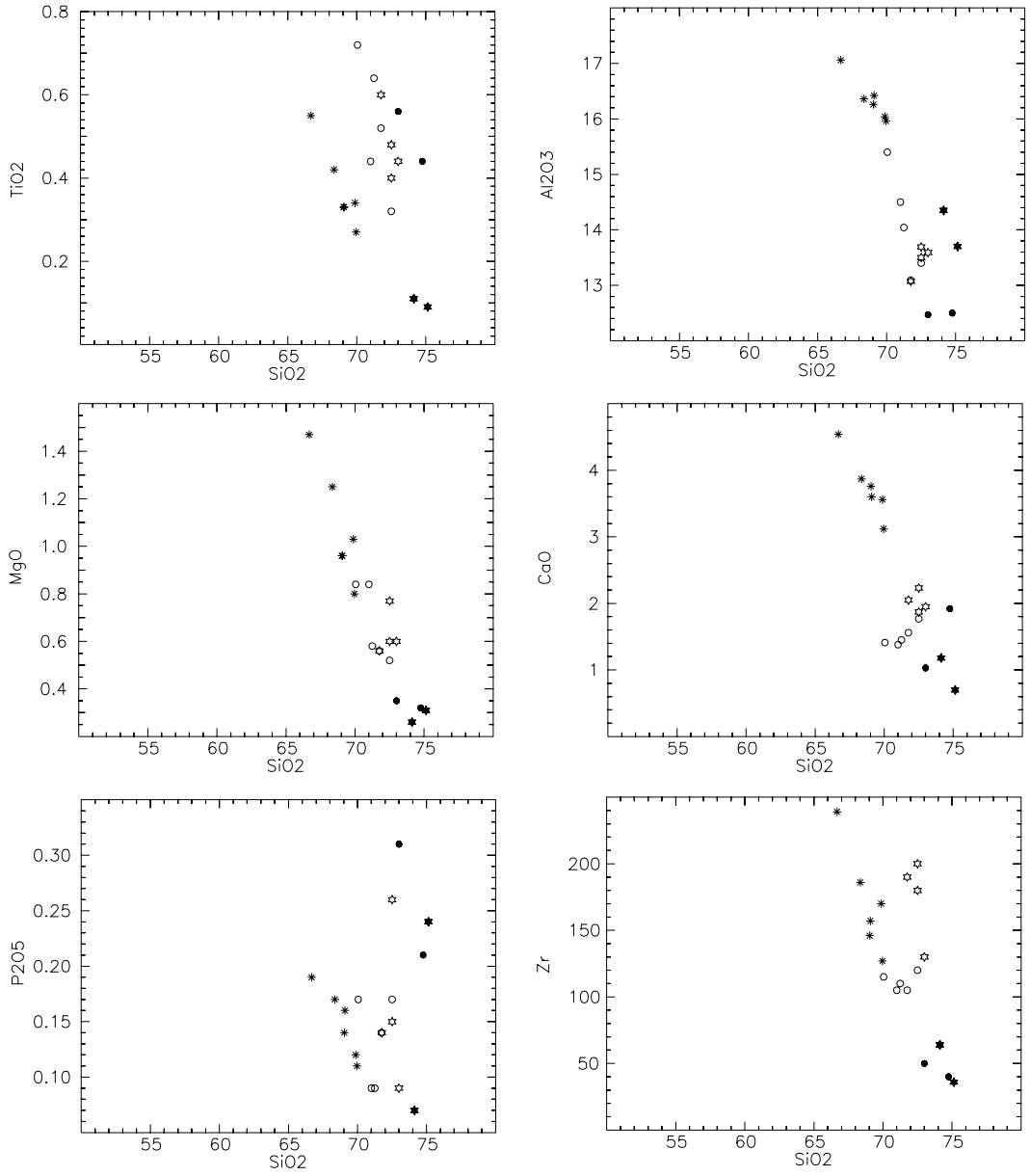

Figure 24. Harker diagrams of SiO2 vs TiO2, Al2O3, MgO, CaO, P2O5 and Zr. Labels as per figure 22. Cruz de Caña appears to be depleted in TiO2 and P2O5 with respect to the other bodies.

Tamboreo Granodiorite (Ogdt)

The Tamboreo Granodiorite forms a slightly elevated plateau ~3 km wide by ~6km long, called Pampa del Tamboreo, which is ~5km to the northeast of Embalse La Florida. Detailed studies of the pluton have been carried out by Zardini (1966) and Sato and others, (1996). These previous studies referred to this pluton as the Tamboreo Tonalite.

The granodiorite intrudes the San Luis Formation and has a distinct metamorphic aureole on the eastern margin. The western margin, however, is strongly sheared and in contact with schist of the Pringles Metamorphic Complex. The granodiorite is intruded by north-south trending aplitic to rhyolitic dykes. U/Pb geochronology of zircon separates has produced an early Ordovician age of 470 ± 5 Ma (Camacho & Ireland, 1997).

The granodiorite is grey to pink in outcrop, and contains a low proportion of mafic xenoliths, which are elongate parallel to a locally well-developed foliation (Sato and others, 1996) defined by biotite. K-feldspar proportions range from 1.5% (Sato and others, 1996) to 25% (Sims and others, 1996), which suggests that there is either a strong compositional zonation within the pluton or multiple phases with a range of compositions. Biotite (up to 25%) is the main mafic mineral along with minor epidote. Minor phases include calcite, chlorite, titanite, apatite, allanite and zircon. Recrystallised feldspars and secondary phases including zoisite and muscovite, suggests that deformation of the pluton occurred under upper-greenschist facies metamorphic conditions. The maximum recorded magnetic susceptibility was 25 x 10^{-5} SI. The composition, geochemical characteristics (Figures 25, 26) and age of the pluton suggest it is closely related to the Bemberg suite tonalites.

Bemberg suite (Otb)
Granodiorite, Tonalite, Gabbro

A suite of intermediate to mafic intrusives, which are exposed in the Sierras de San Luis to the southwest of Carolina, is called here the Bemberg suite. The suite is wholey contained within the Ordovician San Luis Formation and consists of three main plutons, the Gasparillo, Las Verbanas and Bemberg tonalites, and a number of dykes and smaller unnamed plutons. Previous studies on these intrusives have been carried out by Sato and Llambias (1994), Sato and others (1996), Sanchez and others (1996) and Llambias and others (1996). Sato and Llambias (1994) classified these plutons as "granitoids precinematicos".

The Bemberg suite intrudes low-grade rocks of the San Luis Formation and have produced a contact aureole within those rocks defined by cordierite (von Gosen & Prozzi, 1996). Llambias and others, (1996b) have described pendants of early high-grade gneiss within the western margin of the Gasparillo Tonalite, while the Las Verbanas Tonalite is cross-cut by the early Devonian Escalerilla Granite. U/Pb geochronology of zircon separates from the Bemberg Tonalite has produced an early Ordovician age of 468 ± 6 Ma (Camacho & Ireland, 1997).

The Bemberg suite are dominantly tonalites but consist of multiple intrusive phases that range from granodiorite to gabbro in composition and include minor dykes of granitic composition (Sanchez and others, 1996; Sato and others, 1996). The tonalites are comprised dominantly of plagioclase, quartz, biotite and hornblende, and subordinate epidote (Sanchez and others, 1996). K-feldspar comprises less than 2% and accessory phases include titanite, apatite, allanite and magnetite (Sato and others, 1996; Llambias and others, 1996). The average magnetic susceptibility of the tonalites is 28 x 10^{-5} SI. Various geochemical plots comparing the Bemberg suite to the Tamboreo granodiorite are shown in Figures 25 and 26.

The Bemberg suite are affected by regional tectonism in the Devonian (Achalian Tectonic Cycle), and Sato and others (1996) report an irregularly developed metamorphic foliation as well as brittle and ductile shear zones developed within the intrusives.

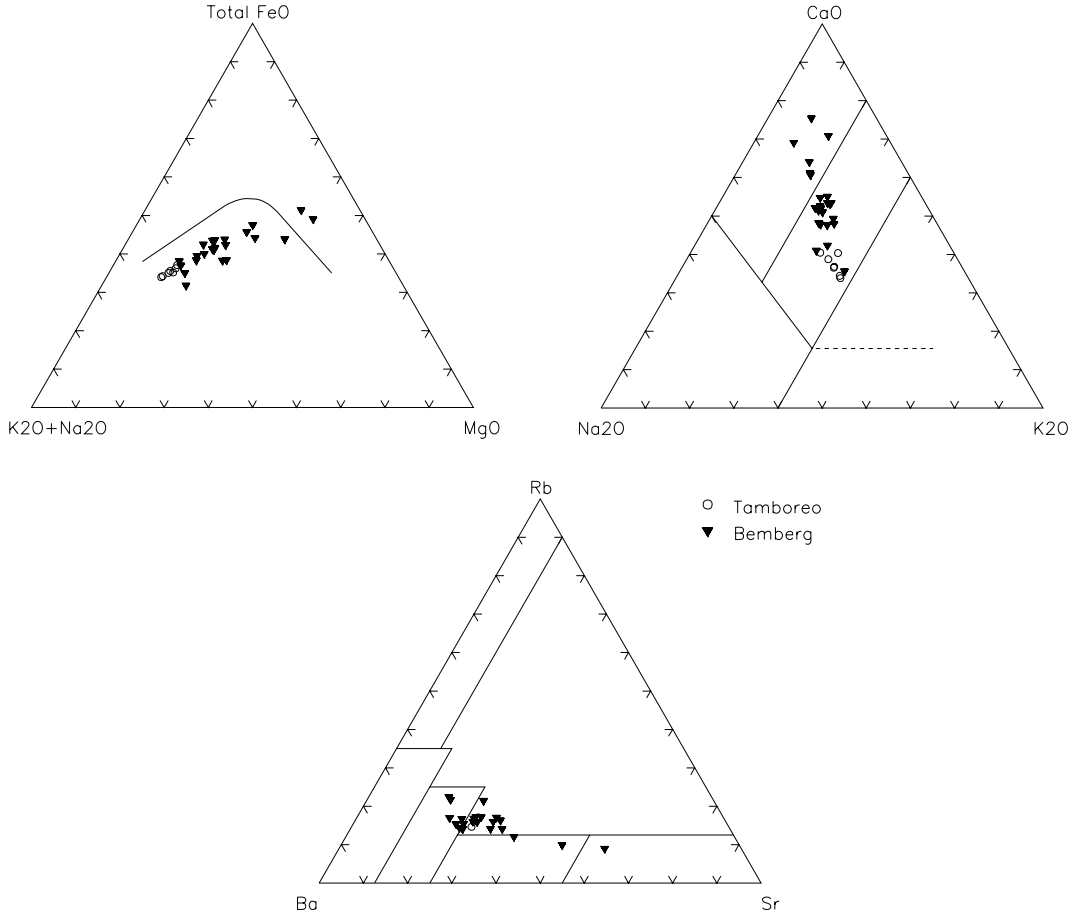

Figure 25. Ternary plots of analysis of the Bemberg Suite and Tamboreo Granodiorite. Additional data from Sato and others, (1996).

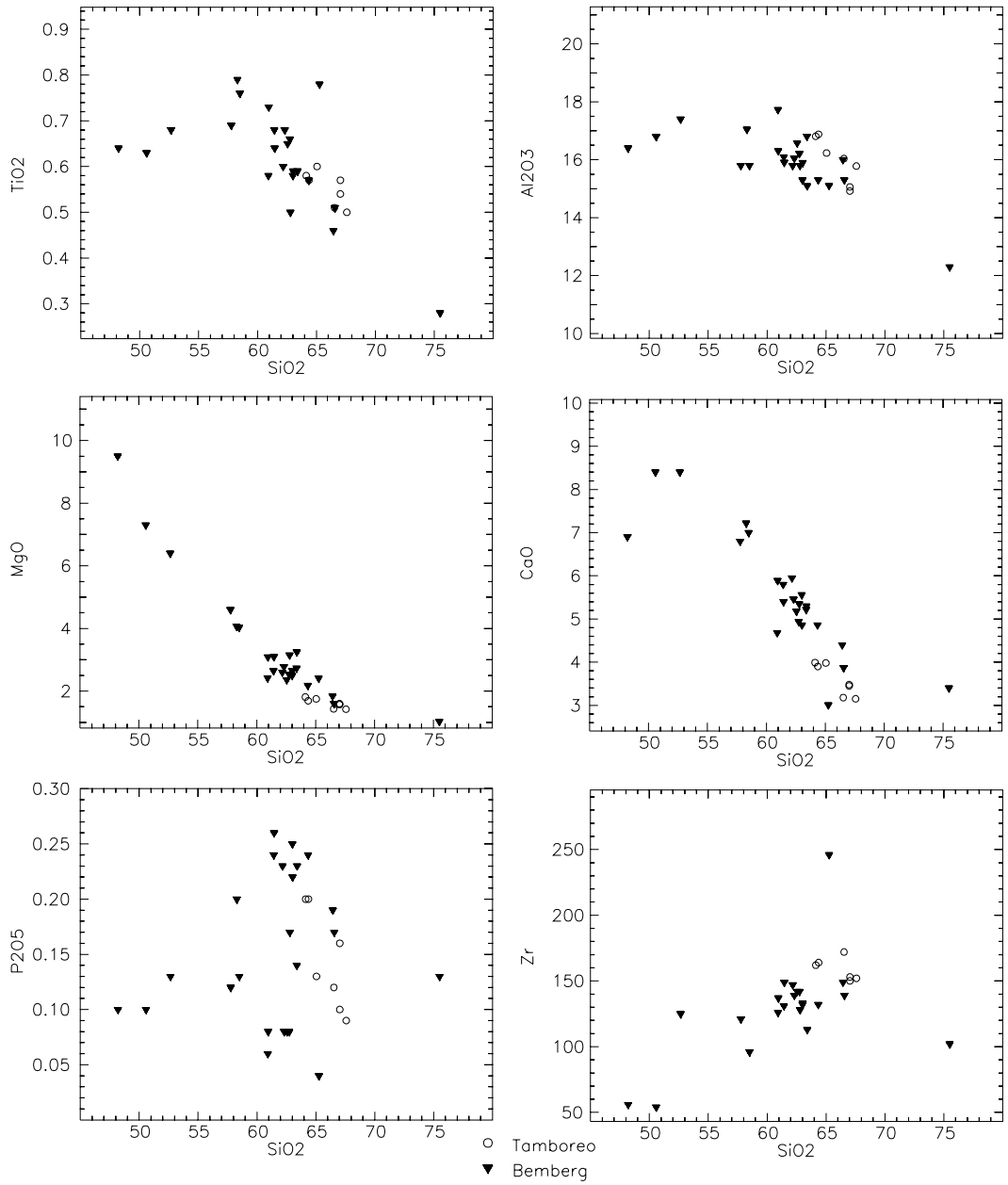

Figure 26. Harker diagrams of the Bemberg Suite and Tamboreo Granodiorite analysis showing SiO2 vs TiO2, Al2O3, MgO, CaO, P2O5 and Zr.

Rio del Molle Monzonite (Omzm)

The Rio del Molle Monzonite is an elongate, composite body approximately 3km long and 1.5km in width that is exposed in Rio del Molle in the Sierras de San Luis, east of the township of Nogoli. The intrusion consists of various comagmatic phases of monzonite and quartz-monzonite (Figure 8).

This body contain numerous discordant xenoliths and rafts of the basement gneiss. Although there are no isotopic constraints for the monzonite, the regional structural relations and apparent continuity of this belt with the Sierra de las Minas, in La Rioja province, where early Ordovician ages have been derived for various granitic to tonalitic intrusives (Pankhurst and others, 1996; Pieters and others, 1997; Camacho & Ireland, 1997), suggests an early Ordovician emplacement age.

Outcrops of the monzonite and quartz-monzonite are typically rich in porphyritic K-feldspar (up to 50% in quartz-monzonite) and plagioclase. Quartz comprises less than 10% of modal abundance and the major mafic phases are biotite (10-30%) and hornblende (2-25%). Accessory phases include primary epidote, aegirine-augite, zoisite, sphene and allanite. The more mafic phases of the suite contain minor sulphides (dominantly chalcopyrite). Magnetic susceptibilty is generally low, being less than 91 x 10^{-5} SI in monzonite and less than 22 x 10^{-5} SI in quartz-monzonite, though local anomalous readings do occur adjacent to visible sulphides. Geochemically, the Nogoli Suite are in the range of ~50-60% SiO_2 and are oxidised. Trace elements Ba, Sr, Zr, Ce, La are particularly high and Rb is low (see Appendix). Deformation and metamorphosism under amphibolite-facies conditions has heterogeneously recrystallised these intrusions and folded and crenulated the earlier fabrics within the xenoliths.

2.3.3 DEVONIAN INTRUSIVES

Numerous Devonian granites and related pegmatites occur in *Sierras de San Luis y Comechingones*. The granites are generally distinct plutons with a marked aeromagnetic signature (see for example large ring pluton – Renca Granite – in Figure 3). The granites can be divided into two separate groups, concordant granites and discordant granites. The concordant granites include the Escalerilla granite and the Achiras Igneous Complex, while the majority of the remaining plutons could be considered as discordant. The concordant granites are intruded as sheets or as highly elongated bodies and generally contain a well developed mineral fabric either due to subsequent deformation or flow banding. The discordant granites are sub-circular, zoned plutons that show little evidence of tectonic overprint (e.g. Renca Granite).

U-Pb zircon analysis shows that ages of the concordant and discordant granites are within error (Table 3), which suggests that the intrusion of the concordant granites may be controlled by some form of a large-scale, crustal structure. Escalerilla granite has produced the oldest age of those analysed by U-Pb in zircon at 403 ± 6 Ma, while ages as young as mid-Carboniferous have been produced through K/Ar techniques

(Table 3). These young ages may be interpreted as cooling ages. Geochemical data from a number of these granites is presented in Figures 27, 28 and 29, and descriptions of the individual plutons follows below.

Table 3. Geochronology of mid Palaeozoic intrusives Data from 1 = Camacho and Ireland, (1997); 2. Linares and Gonzales (1990); 3 = Lema, (1980).

Intrusive	Age	Ref.	Method	Comment
Tilisarao	415 ± 25	**2**	Rb/Sr Whole Rock	Cantera Pena Pintada
Renca	415 ± 25	**2**	Rb/Sr Whole Rock	1 km west of Renca
Escalerilla	404 ± 5	**1**	U-Pb Zircon	
Renca	394 ± 5	**1**	U-Pb Zircon	
Los Nogales	384 ± 6	**1**	U-Pb Zircon	Achiras Igneous Complex
S.J. del Morro	380 ± 20	**3**	K-Ar Biotite	
S.J. del Morro	380 ± 15	**3**	K-Ar Biotite	
Pegmatite	375 ± 16	**2**	K/Ar Muscovite	Sierra de Yulto
Pegmatite	371 ± 20	**2**	K/Ar Biotite	Yac. Don Paco, Sa. de La Estenzuela
Pegmatite	368 ± 15	**2**	K/Ar Biotite	Yac. Renquina - Sa. de Tilisarao
S.J. del Morro	365 ± 15	**3**	K-Ar Biotite	
S.J. del Morro	360 ± 20	**3**	K-Ar Amphibole	
Pegmatite	360 ± 15	**2**	K/Ar Muscovite	Yac. Renquina - Sa. de Tilisarao
Pegmatite	347 ± 15	**2**	K/Ar Muscovite	Yac. Don Paco, Sa. de La Estenzuela
Pegmatite	343 ± 20	**2**	K/Ar K-feldspar	Yac. Los Duraznos - west of Tilisarao
Pegmatite	343 ± 10	**2**	K/Ar Biotite	Sierra de Tilisarao
Pegmatite	340 ± 10	**2**	K/Ar K-feldspar	Yac. Cholita - Sa. de La Estenzuela
Las Chacras	336 ± 17	**2**	K-Ar Amphibole	
Potrerillos	335 ± 17	**2**	K-Ar Biotite	
Pegmatite	328 ± 15	**2**	K/Ar K-feldspar	Yac. Maria - Sa. de La Estenzuela
Pegmatite	325 ± 20	**2**	K/Ar K-feldspar	Yac. Don Paco - Sa. de La Estenzuela
Las Chacras	320 ± 16	**2**	K-Ar Biotite	
Las Chacras	320 ± 15	**2**	K-Ar Biotite	
Pegmatite	310 ± 20	**2**	K/Ar K-feldspar	Yac. Rona - Sa. de La Estenzuela
Pegmatite	305 ± 20	**2**	K/Ar K-feldspar	Yac. Cholita - Sa. de La Estenzuela

Escalerilla Granite (Dge)

The Escalerilla granite is a large elongate granite with positive relief that forms the main range of the Sierras de San Luis. The granite varies from less than 1 km, to around 8 km in width along an outcrop length of approximately 55 km. The granite is well exposed along the entire length of outcrop, including the southern half of the main western escarpment of the Sierras de San Luis, from near Villa de la Quebrada to the city of San Luis. The northernmost extent of the granite is exposed at Carolina. Numerous roads, rios and arroyos cross the granite along its entire length.

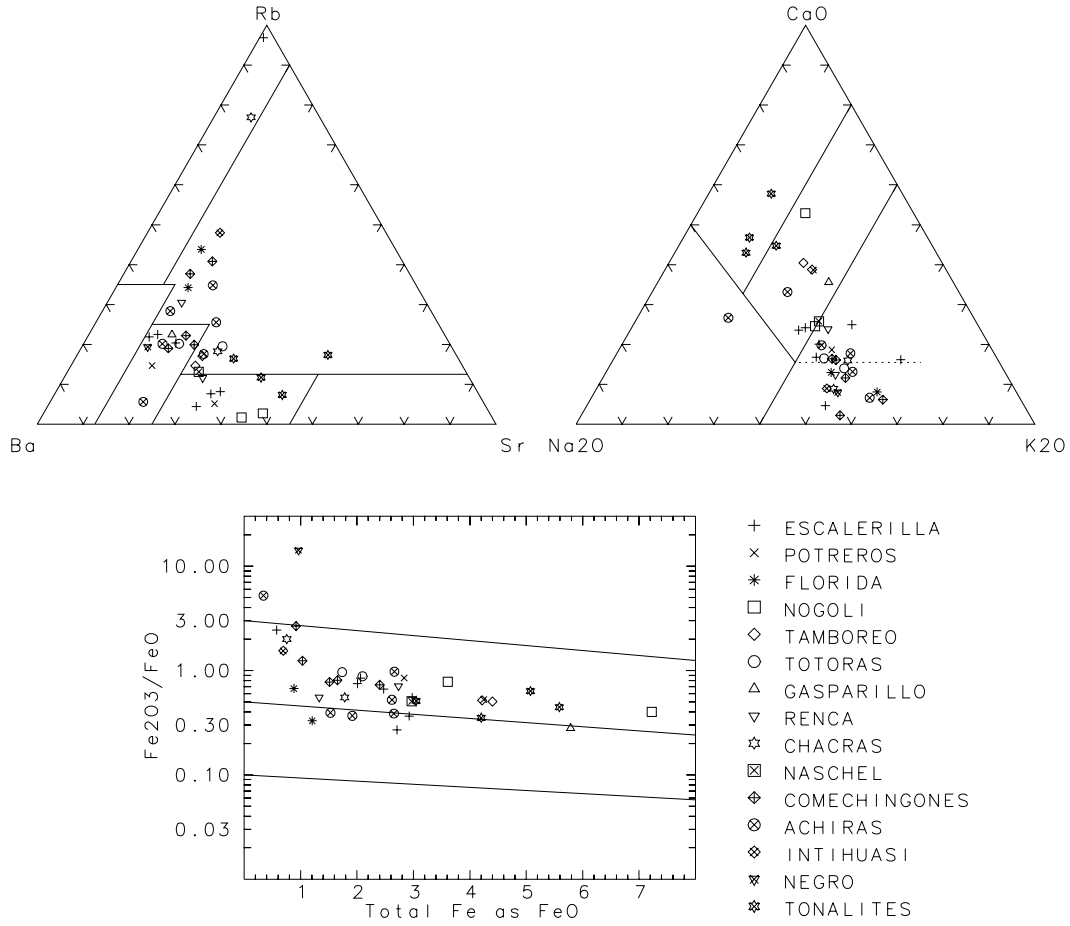

Figure 27. Ternary plots and oxidation state of selected Devonian granites. Analyses of Florida (La Florida granite), Nogoli (Rio del Molle Monzonite), Tamboreo (Tamboreo Granodiorite), Gasparillo (Gasparillo Tonalite) granites and tonalites from Sierra de Comechingones are included for comparison.

The granite intrudes basement rocks of the Pringles Metamorphic Complex and the San Luis Formation as well as the Las Verbanas tonalite, and contains xenoliths and rafts of all three rock-types. The granite truncates the main structural fabric within the Pringles Metamorphic Complex and is cross-cut by numerous veins and dykes of pegmatite and granite. U/Pb zircon geochronology of zircon separates indicates the Escalerilla granite crystallised at 403 ± 6 Ma (Camacho & Ireland, 1997).

The granite is grey to pink and contains up to 30% porphyritic K-feldspar and 25% plagioclase. Biotite comprises up to 10% and muscovite up to 5% of the total rock and accesory phases include sphene, epidote, apatite, clinozoisite and ilmenite. The pluton is non-magnetic, and the geochemistry of the pluton is quite variable, which is

probably a reflection of the degree of mylonisation. It is oxidised to slightly reduced and peraluminous (Figures 27, 28).

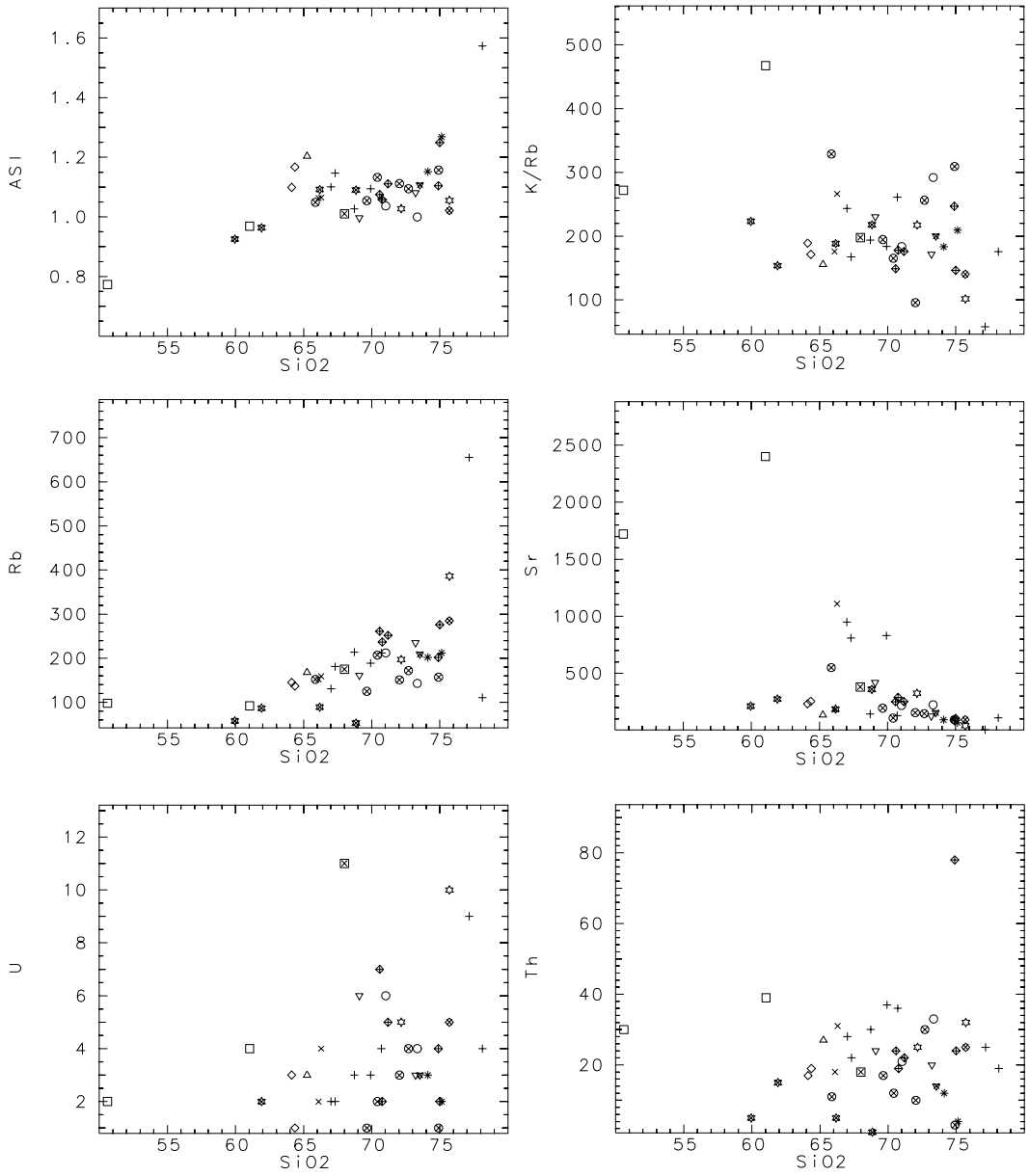

Figure 28. Harker variation diagrams of SiO2 versus ASI, K/Rb, Rb, Sr, U and Th for the Devonian granites. Legend as per Figure 27.

Quartz (<30%) and biotite are extensively recrystallised and define a mylonitic foliation that is associated with a least two different styles of deformation. The dominant and pervasive fabric is steeply east dipping with a steeply plunging mineral lineation defined by biotite and muscovite with a shear-sense of east over west. K-feldspar porphyroclasts are mechanically rotated in the foliation and are weakly

aligned with the lineation (Figure 30) The sub-ordinate mylonitic foliation is generally north trending and is strongly partitioned within the granite, it is sub-vertical in orientation with a sub-horizontal mineral lineation defined by biotite. K-feldspar is partially recrystallised within these shear zones. Various shear-sense indicators show a sinistral displacement sense.

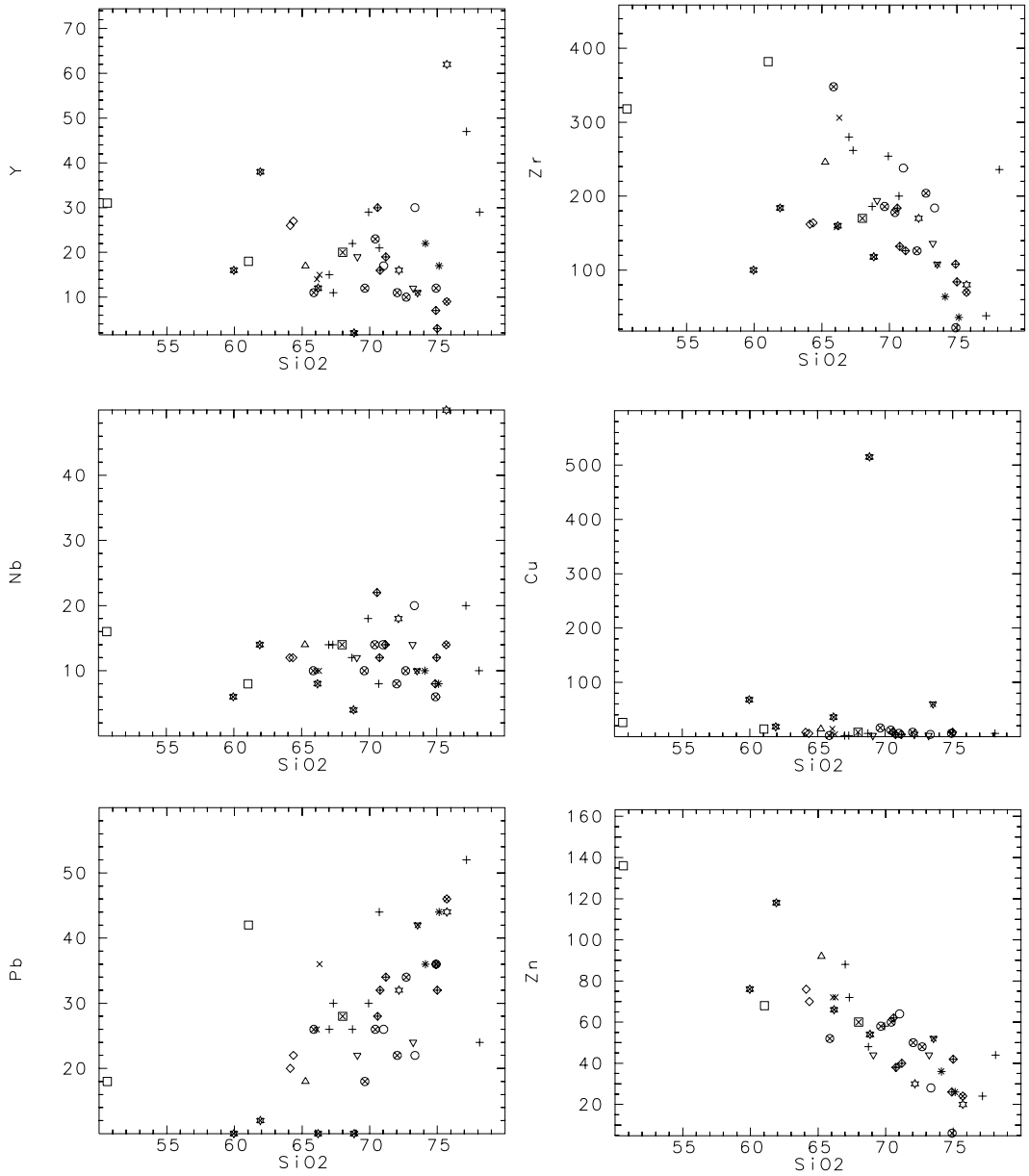

Figure 29. Harker variation diagrams of SiO2 versus Y, Zr, Nb, Cu, Pb and Zn for the Devonian granites. Legend as per Figure 27.

Inti Huasi Granite (Dgi)

Small hills and isolated outcrops of granite on the eastern flank of the Sierra de Comechingones, north of La Barranquita, about 35 km northeast of Achiras, were named the Inti Huasi Granite. The granite crops out as low rocky pavements and bouldery hills around Cerro Inti Huasi, and Estancias Los Cerros and La Piedra.

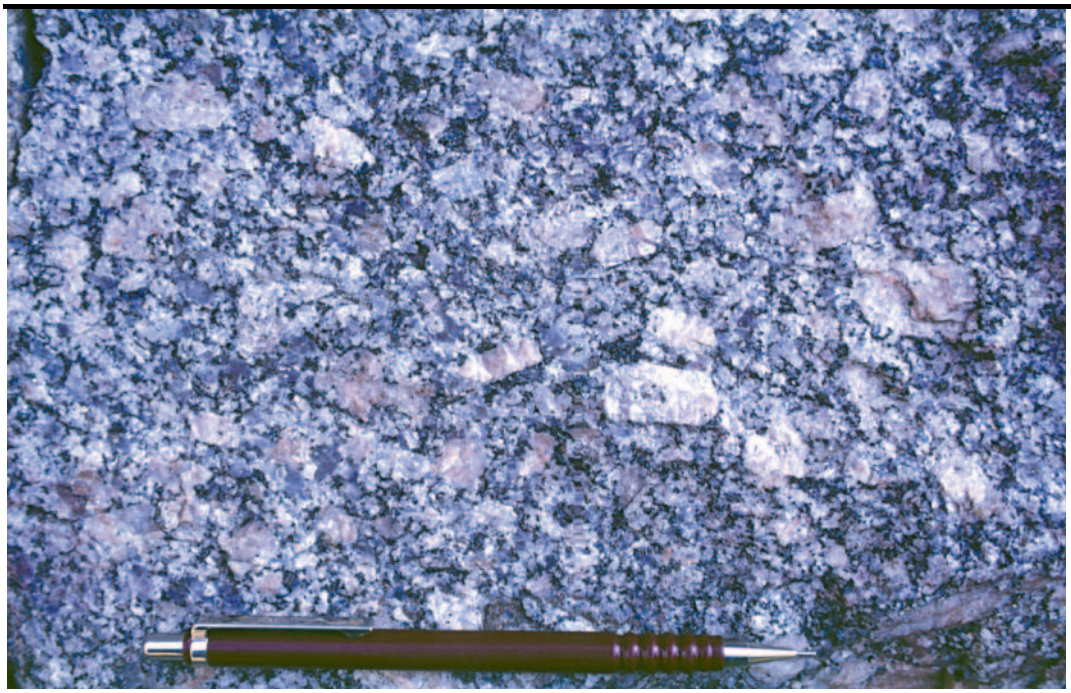

Figure 30. Porphyritic Escalerilla granite. Note the strong crystal alignment formed through low-grade shearing during the Devonian, Achalian Tectonic Cycle. U-Pb dating of zircon separates from this locality (A95JS033) give a crystallisation age of 403 ± 6 Ma (Camacho & Ireland, 1996).

Magnetic anomalies indicate that the granite exposures form part of the western border of an elliptical-shaped zoned pluton about 12.5 km across, comprising a non-magnetic core and a magnetic border facies about 4 km wide. The bulk of the pluton, including the entire non-magnetic zone, extends to the east beneath Cainozoic and Quaternary sediments at shallow depth (<200 m). Contacts between the granite and surrounding basement rocks of the Complejo Monte Guazú to the northwest are not exposed. However, the magnetic anomalies indicate that the pluton truncates early Devonian structures in the complejo, consistent with the massive nature and lack of penetrative structures in granite outcrops. Although there are no isotopic age data for the granite, the shape and zoned form of the pluton suggests it may be part of the Early Devonian suite of granites.

Outcrops of the pluton are typically coarse grained pale pink equigranular leucogranite. Biotite forms less than 2% of the rock and is partly altered to chlorite. Up to 3% muscovite is present, both as primary interstitial grains and as a secondary alteration of oligoclase, together with trace carbonate and epidote. The leucogranite forms the outer magnetic phase of the pluton with an average magnetic susceptibility

of 258 x 10^{-5} SI. Trace magnetite is present in unaltered specimens, however, it is replaced by hematite

Magnetic anomalies indicate that the granite exposures form part of the western border of an elliptical-shaped zoned pluton about 12.5 km across, comprising a non-magnetic core and a magnetic border facies about 4 km wide. The bulk of the pluton, including the entire non-magnetic zone, extends to the east beneath Cainozoic and Quaternary sediments at shallow depth (<200 m). Contacts between the granite and surrounding basement rocks of the Complejo Monte Guazú to the northwest are not exposed. However, the magnetic anomalies indicate that the pluton truncates early Devonian structures in the complejo, consistent with the massive nature and lack of penetrative structures in granite outcrops. Although there are no isotopic age data for the granite, the shape and zoned form of the pluton suggests it may be part of the Early Devonian suite of granites.

Outcrops of the pluton are typically coarse grained pale pink equigranular leucogranite. Biotite forms less than 2% of the rock and is partly altered to chlorite. Up to 3% muscovite is present, both as primary interstitial grains and as a secondary alteration of oligoclase, together with trace carbonate and epidote. The leucogranite forms the outer magnetic phase of the pluton with an average magnetic susceptibility of 258 x 10^{-5} SI. Trace magnetite is present in unaltered specimens, however, it is replaced by hematite where the granite is intensely jointed. Relative to other basement rocks in the region the leucogranite has a high total count (123 cps) with high uranium (8.5 cps).

Limited geochemical data indicates that the Inti Huasi Granite is an oxidised peraluminous granite indistinguishable from other Achalian Granites (Figures 27, 28, 29).

Alpa Corral Granite (Cerro Aspero Batolith) (Dgae, Dgas)

The Alpa Corral Granite is a circular concentrically zoned pluton about 8 km across and covering an area of about 50 km^2, forming the southeastern part of the Cerro

Aspero Batholith, in the Sierra Comechingones in the northeast of the area. Detailed geological mapping and petrographic studies of the pluton have been carried out by Coniglio and Esparza (1988), Pinotti and others, (1992 & 1996) and Esparza and Fagiano (1995). The area was also mapped by Candiani and Maza (1982) as part of an exploration program in the Sierra Comechingones.

Exposure of the granite is good, particularly of the border facies which forms a prominent discontinuos ridge circling much of the pluton. The main central porphyritic phase is less well exposed, cropping out as low pavements and boulders, separated by active alluvial plains which drain mostly into the Rio San Bartolome.

The granite is an earlier phase of the Cerro Aspero Batholith and is intruded by the Comechingones Granite to the north and by numerous late stage aplite and fluorite-bearing pegmatite dykes. The pluton intrudes interlayered gneiss and amphibolite of the Monte Guazú Metamorphic Complex with marked discordance in most places, interdigitating locally. Within 500 m of the granite, along the eastern margin a penetrative greenschist facies mylonitic foliation in the metamorphic rocks, normally dipping shallowly to east (30˚), steepens progressively towards the contact where it is subvertical, indicating at least some forceful diapiric emplacement of the pluton. Contact metamorphic effects are typically extensive recrystallisation with the development of cordierite at the expense of biotite in gneisses, epidotisation of amphibolite and areas of greisenisation and silicification (Pinotti and others, 1996).

The pluton comprises two main phases: a central seriate phase and an outer equigranular border facies. The main phase is a pink coarse-grained seriate, biotite monzogranite, with minor perthitic microcline phenocrysts up to 5 cm across and numerous biotite-rich schlieren (Coniglio and Esparza, 1988) and microgranular mafic enclaves up to 30 cm (Coniglio and Esparza, 1988; Pinotti and others, 1996). Accessory minerals include zircon, fluorite, apatite, xenotime, monazite, titanite, ilmenite, rutile, beryl, molybdenite and anatase (Pinotti and others, 1992, 1996). The granite is weakly sericitised and chloritised. The main phase grades locally into a strongly porphyritic phase and into a border phase of the same composition which is equigranular in texture. This latter phase crops out mainly along the southern and

northeast borders and in the centre of the pluton where it forms a shallow dipping cap overlying the main phase (Pinotti and others, 1992).

The granite is well-jointed and veined by quartz in places. Minor steeply dipping SE-trending cataclasite zones, up to 2 m wide, with chalcedony, hematite and fluorite cut the pluton and the outer phase of the adjacent Comechingones Granite. Neodyminium and strontium isotope studies indicate an age of 117±26 Ma for a fluorite occurrence in the Alpa Corral Granite and an unconformity-related origin associated with mixed ascending and "descending" hydrothermal fluids of low-to moderate temperatures (Galindo and others, 1996).

Whole rock geochemistry of the pluton confirms that both the Alpa Corral granite and Comechingones Granite together form a fractionated suite. The granites fall within the anomalous granite field and are slightly peraluminous with ASI indexes of around or above 1.1 (Figures 27, 28, 29). The granites are oxidised, however, magnetite is not common in the Alpa Corral Granite with mean magnetic susceptibilities less than 100 x 10^{-5} SI.

Previous authors have have placed the granite in the G2 group of Rapela and others, (1990) and infered an Ordovician age (eg. Pinotti and others, 1992, 1996). However, the granite truncates Early Devonian greenschist shear zone fabrics within the Monte Guazú Metamorphic Complex indicating a maximum age for the unit.

Uspara Granite (Cerro Aspero Batolith) (Dgu)

Previously unmapped granite crops out semi-continuously along the base of the Comechingones range for about 12 km south of Papagayos. The granite also forms low exposures along route 1 in the San Luis Province in the vicinty of A°. Uspara, after which the granite is named. The granite is non-magnetic (magnetic susceptibility <10 x 10^{-5} SI), and aeromagnetic anomalies indicate that it is considerably more extensive in the shallow subsurface over much of the plain, as far south as La Estanzuela and to about 10 km west of Papagayos.

The pluton is a grey to pale pink, medium-grained, equigranular to weakly seriate leucogranite. Primary muscovite and biotite are equally abundant and comprise together about 5% of the rock. Anhedral quartz forms scattered phenocrysts up to 1 cm across. Patches and veins of muscovite-tourmaline-feldspar quartz pegmatite are common. There is no chemical or isotopic data available.

The relationship with adjacent units is not known. Along the base of the Comechingones the granite is highly altered (kaolinised and chloritised), brecciated and cut by numerous moderately east-dipping faults. Kaolinite has been extracted from several quarries located in the area. These faults form part of the 1-2 km wide Cainozoic reverse fault zone along which the present ranges have been uplifted. Towards the top of the fault scarp, the granite contact with the overlying Monte Guazú Metamorphic Complex dips shallowly to the east and is inferred to be intrusive. At Papagayos the Comechingones Granite truncates the northern extent of the Uspara Granite. The contact, not exposed between the two plutons, is interpreted to be either faulted or intrusive. The lack of any high grade deformation fabrics (primary biotite is undeformed and shows only very weak hematite alteration) and the spatial relationship of the granite to the Cerro Aspero Batholith, suggests it may be part of the Devonian batholithic suite, possibly an earlier peraluminous phase which is intruded by the later Comechingones Granite.

Comechingones Granite (Cerro Aspero Batolith) (Dgol, Dgog, Dgoa)

The Gomechingones Granite, referred to as the El Talita pluton by Pinotti and others, (1996), is the main pluton of the Cerro Aspero Batholith, forming the central part of the Sierra de Comechingones. Detailed studies of aspects of the granite has been made by Coniglio and Esparza (1988), and Pinotti and others, (1992 & 1996). Only the southern part of the pluton is exposed in the extreme northeast of the study area where it extends the full width of the Sierras. The granite is well-exposed in rugged rock mountains, deeply dissected by watercourses which follow the main fracture pattern in the granite.

An unbroken, curvlinear southern contact margin suggests that the pluton is probably the youngest in the Cerro Aspero Batholith, intruding, both the Alpa Corral Granite and probably the Uspara Granite. Both contacts are either not exposed or are difficult to locate in the field. However, they can be readily defined by coincident boundaries on aeromagnetic, spectrometric and Landsat TM imagery. The pluton intrudes the Monte Guazú Metamorphic Complex with a medium-to high grade contact metamorphic aureole extending up to 500 m from the granite. Within the aureole the rocks are intensely recrystallised with the development of cordierite at the expense of biotite and areas of greisenisation, silicification and epidotisation (Pinotti and others, 1996). The contact is well exposed east of Papagayos, where an intricate intrusive contact with tonalitic gneiss is preserved and, in places, is strongly sheared parallel to the subvertical ESE-trending intrusive contact. Intrusion appears to be syntectonic with respect to the shearing as pegmatite, aplite and granite veins both crosscut and form boudinaged stringers within the zone. The pluton is intruded by numerous aplite and pegmatite dykes, interpreted as late stage fractionated phases which intruded along structurally controlled concentric and radial fractures within the cooling pluton. Minor steeply dipping SE-trending and fluorite-bearing cataclasite zones are also present in the outer phase, but are more common in the adjacent Alpa Corral Granite.

The pluton inthe area comprises two main granitic phases, the outer comprising a border facies 6 to 8 km wide. The zones probably represent separate pulses of fractionated magma during batholith emplacement. The contact between the two phases is well-defined on Landsat TM and aeromagnetic imagery and is possibly gradational.

The inner phase consists of pink coarse-grained porphyritic biotite granite to monzogranite with up to 5% biotite. Accessory phases include titanite, apatite, zircon and allanite. K-feldspar megacrysts up to 5 cm across are also present and are weakly aligned parallel to the contact with the outer phase. Pinotti and others, (1992) suggested that that orientation of the megacrysts was a product of simple shear generated during emplacement. Xenoliths of biotite microgranite are rare. The outer phase is more felsic and less altered and comprises pink, coarse-grained, porphyritic

biotite-leucogranite with K-feldpar phenocrysts up to 3 cm across. Most biotite is chloritised, and sericitic and hematitic alteration is common.

Whole rock geochemistry of the pluton confirms that both phases and the phases of the Alpa Corral granite together form a fractionated suite. The granites fall within the Anomalous granite field and are slightly peraluminous with ASI indexes of around or above 1.1 (Figures 27, 28, 29). The granites are oxidised with magnetite a common accessory phase and mean magnetic susceptibilities above 816 x 10^{-5} SI for the inner phase and 200-300 x 10^{-5} SI for the outer phase.

Previous authors have have placed the granite in the G2 group of Rapela and others, (1990) and infered an Ordovician age (eg. Pinotti and others, 1992, 1996). However, the granite truncates Early Devonian greenschist shear zone fabrics within the Monte Guazú Metamorphic Complex indicating a maximum age for the unit. Not isotopic age determinations are available for the unit. Similar, intrusive relations and whole rock and trace element chemistry are consistent with the batholith being part of the Early Devonian Achalian Cycle, rather than the older Ordovician Famatinian Cycle.

San Jose del Morro Granite (Dgm)

The San Jose del Morro Granite is exposed over approximately 60 km^2 in the north of the Sierra de Yulto near the town from which the name is derived. Aeromagnetic images show the pluton is semi-ovoid in shape and more extensive than is outcropping. To the east of the exposed area, approximately 80 km^2 of the granite is covered by neogene volaniclastics, while to the west, approximately 40 km^2 is covered by fault bounded Cainozoic sediments.

The granite intrudes the Conlara Metamorphic Complex and K/Ar ages indicate that the granite was emplaced between 390-360 Ma (Lema, 1980). The granite is strongly foliated on the NW margin and generally has a moderately well developed mineral alignment.

The granite is moderately magnetic, pink to red, strongly jointed and consists of equigranular and porphyritic phases. Compositionally the granite ranges from monzogranite to syenogranite and has a metaluminous character (Quenardelle, 199?) The granite consists of predominantly porphyritic K-felspar (microcline), plagioclase, quartz, with abundant biotite and minor titanite. Quenardelle (199?) also reports trace apatite, magnetite, ilmenite and zircon. Locally, the granite contains numerous mafic enclaves and xenoliths of the the country rock. A number of large rafts of basement rock, suggest the pluton may be only shallowly exposed. Numerous pegmatites and aplite dykes intrude the country rock on the margin of the granite and cross-cut the large basement rafts. Additionally, minor, shallowly worked, skarn mineralisation occurs in calc-silicate and marble units adjacent to the pluton.

Renca Granite (Dgre, Dgrp)

The Renca Granite is a generally well exposed pluton that is nearly elliptical in plan, with a long axis of about 25 km oriented WNW-ESE, and a short axis about 13 km long. The village of Renca lies just on its eastern margin. This batholith has been well studied. See López de Luchi (1996) for references.

It is a dual phase 'ring' granite which intruded the metasedimentary Conlara Metamorphic Complex. The ring structure of the Renca Granite is clearly seen on the magnetic and, to a lesser extent, radiometric images. López de Luchi (1996) inferred a late Devonian to Carboniferous age based on Rb-Sr data obtained from the Las Chacras-Piedras Coloradas batholith (Brogioni, 1993). However, Halpern and others, (1970**R**) obtained a Rb-Sr date of 415 ± 25 Ma for the Renca Granite and recent U-Pb zircon data (Camacho and Ireland, 1997) give a crystallisation age of 393 ± 5 Ma.

The outer ring, about 2 km to 5 km thick, is a coarse-grained, K-feldspar phyric, biotite granite/monzogranite and the core is an equigranular, medium-grained, two-mica granite. About the north end of the Dique San Félipe the equigranular phase has been partially haematised during later alteration. The phyric outer phase contains K-feldspar phenocrysts about 5 cm to 10 cm long in a groundmass of grains up to 1 cm.

It contains about 40% K-feldspar, 30% quartz, 15% biotite, and 10% muscovite. Accessory phases include titanite, apatite, magnetite, zircon, and allanite as well as secondary chlorite and epidote. The equigranular core phase contains about 30% quartz, 25% K-feldspar, 15% plagioclase, 10% muscovite, and 10% biotite and accessory zircon, and apatite as well as chlorite replacing biotite.

Geochemical analyses are presented in Figures 27, 28 and 29. Both phases are peraluminous with ASIs around 1.1. Magnetic susceptibilities vary from about 100 x 10^{-5} to 1000 x 10^{-5} SI for the ring phase, and are less than 10 x 10^{-5} SI for the core phase.

Tilisarao Granite (Dgsi, Dgse)

The Tilisarao Granite is a large foot-shaped body, 25 km long and 5 - 10 km wide, that is discernible on magnetic images and is only partially exposed in the westernmost part of the Sierra de Tilisarao. From magnetic imagery, the granite consists of a large non-magnetic core surrounded by a narrow, moderately magnetic, rim that is 1 - 2 km wide. The core facies is a of a peraluminous granodiorite containing about 30% quartz, 25% plagioclase, 20% K-feldspar, 15% biotite, 5% hornblende and minor titanite, allanite and garnet. Accessory minerals are zircon, apatite, magnetite, with secondary chlorite and epidote. The granite has a seriate texture with grains ranging between 1 mm and 10 mm. The rim facies has not been examined. Limited geochemical data suggest the Tilisarao Granite is related to the suite of Devonian grantites.

Los Cerrillos Granite (Dgl)

The exposed portion of the Los Cerrillos Granite forms most of the Sierra de Tilisarao. It is a medium grained, equigranular, quartz, K-feldspar, biotite, minor muscovite granite with abundant K-feldspar-quartz- muscovite pegmatite dykes. In general, it is well exposed except for small area near its centre where it is predominantly subcrop

with more resistant pegmatite veins well eminent and clearly visible on aerial photographs. Pegmatite veins are vertical to sub-vertical with dominant NW and NE strikes. No geochemical or age data are available but stratigraphic relationships and K-Ar dates obtained from pegmatites intruding the granite (Rinaldi and Linares, 1973; reported in Fernandez Lima and others, 1981) suggest it is older than mid Devonian.

Totora Granite (Dgtl, Dgte, Dgti)

The Totora Granite is a semi circular pluton, approximately 10 km in diameter that crops out in the southeastern Sierras de San Luis between the townships of Saladillo and La Toma. The granite forms a slightly elevated plateau with a well exposed margin and is also well exposed in low platforms along provincial route 20. The name of the granite derives from the small town of La Totora which is located on the pluton.

The granite intrudes the basement rocks of the Conlara Metamorphic Complex and truncates the main structural fabric in those rocks. Aeromagnetic data suggests that the granite continues under shallow cover to the southeast. Though there is no isotopic data for this pluton, the shape and magnetic zonation of the pluton and the absence of a marked tectonic overprint suggests that this granite is Devonian in age.

The pluton is grey to pink in outcrop and consists predominantly of K-feldspar, quartz and plagioclase, with minor mafic enclaves. Photographic and magnetic imagery as well as petrography, suggests the granite consists of three phases: a main, coarse- to very coarse-grained, sub-equigranular phase that is moderately magnetic (average magnetic susceptibility of 972 x 10^{-5} SI) and strongly jointed in outcrop, a thin leucocratic border phase that occurs on the western margin and is not jointed, and an inner porphyritic and slightly-less-magnetic phase (average magnetic susceptibility of 721 x 10^{-5} SI). Biotite comprises approximately 5% of the total rock in the main and inner phase and is partially replaced by chlorite, while accesory phases include magnetite, sphene and garnet. The K-feldspar is microcline and is partially replaced by muscovite, while plagioclase displays myrmekitic grain boundaries. The inner

phase of the pluton contains significantly more plagioclase than the main phase (20% c.f. 10%) and is also weakly foliated.

Limited geochemical data suggests that Totora Granite is an oxidised peraluminous granite (Figures 27, 28, 29). The Totora Granite has been extensively quarried for building stone in La Speñas Cantera and Cantera Yugo.

Las Chacras Granite (Batolito de Las Chacras-Piedras Coloradas) (Dgc)

The Las Chacras Batholith consists of multiple phases of circular granite that are exposed over an area greater than 500 km^2, in the central north of the Sierras de San Luis. However, less than 5 km^2 of the southern most pluton is exposed on *Sierras de San Luis y Comechingones*. The Batholith derives its name from the township of Las Chacras which is located on the batholith. Detailed studies of the batholith have been made by by Brogioni (1987 & 1991), who incorporates the Potrerillos granite and the Las Chacras batholith as the Batolito de Las Chacras-Piedras Coloradas. The granite has positive relief is well exposed in platforms and low bouldery hills.

The Las Chacras granite on *Sierras de San Luis y Comechingones* is undeformed and intrudes the Conlara Metamorphic Complex. Isotopic ages for the batholith range from 336 ± 17 Ma (K/Ar amphibole) to 320 ± 16 Ma (K/Ar biotite) (Table 3), and must be considered as minimum ages. A maximum age for the batholith is provided by an Argon-Argon age of 350-360 Ma (Camacho & Ireland, 1997) for the Rio Guzman Shear Zone that the batholith truncates. Similarities with Devonian plutons such as Renca Granite, suggest the batholith must have been emplaced in the Devonian or early Carboniferous. Geochemical data for the granite is shown in Figures 27, 28 and 29.

Portrerillos Granite (Batolito de Las Chacras-Piedras Coloradas) (Dgpi, Dgpe)

The Potrerillos granite is an ovoid pluton with a maximum diameter of approximately 12 km exposed between the townships of Renca and Las Chacras in the central north of *Sierras de San Luis y Comechingones*. The name of the pluton is derived from the small community of Potrerillos, which is situated on the exposed pluton. The pluton has positive relief compared to the country rock (Conlara Metamorphic Complex) and is hence very well exposed in low bouldery hills that form the Sierrita de las Piedras Coloradas. It has previously been described as the Potrerillos Stock of the Batolito de Las Chacras-Piedras Coloradas by Brogioni (1987, 1991).

The Potrerillos granite is undeformed and intrudes the Conlara Metamorphic Complex and the outer phases of the Las Chacras Batholith. An isotopic (K/Ar biotite) age of 335 ± 17 Ma has been reported (Table 3), which must be considered as a minimum age. The marked similarity of the aeromagnetic signature of this pluton to that of the Renca granite, strongly suggests that the Potrerillos granite is no older than Devonian in age and assocated with the Achalian tectonic cycle.

Aeromagnetic data, suggests the Potrerillos granite is either strongly zoned or consists of a non-magnetic core-phase and a moderately magnetic rim phase that is approximately 2.5 km wide. Measured magnetic susceptibilities of the central phase are low, and average 8 x 10^{-5} SI. The Potrerillos granite has a high radiometric signature.

This coarse grained, porphyritic and strongly jointed granite is deep pink to red in outcrop. It consists of approximately 40% very coarse, porphyritic k-feldspar, with up to 30% quartz, 10-15% plagioclase and up to 15 % biotite. K-feldspar contains inclusions of biotite, plagioclase and quartz, and matrix plagioclase displays myrmekitic textures. Quartz is slightly recrystallised. Accessory phases include allanite, zircon, apatite and magnetite, while secondary phases include muscovite replacing plagioclase and chlorite replacing biotite.

The Potrerillos granite is quarried for building stone in the Cantera Los Aquilchuchos "Granito Rojo Dragon".

Achiras Igneous Complex (Dag, Dagl)
Interlayered granite, leucogranite

An intrusive complex, defined as the Achiras Igneous Complex, forms the extreme south of the Sierras Commechingones centred on the town of Achiras. This complex comprises the intrusive part (the "Granito Los Nogales") of what was previously termed the Achiras Complex by Otamendi & others (1996). Outcrop of the the complex is good but becomes poorer south of Provincial Route 1 where elevation is lower and topography more undulating. Aeromagnetic anomalies, however, indicate that the complex extends under thin unconsolidated Cainozoic sediments, to the south and southwest.

The intrusive complex comprises a stratified, subconcordant granite suite. The unit consists mainly of two different granite types, a coarse seriate strongly magnetic granite and a non magnetic equigranular leucogranite-granite. Late-stage aplite and tourmaline-garnet-muscovite-bearing pegmatite dykes are common. The granites form sheet-like bodies which display mostly concordant but intrusive contacts, postdating earlier, differentiated, high-grade metamorphic fabrics within the metamorphic basement (Figure 31). U-Pb zircon age determinations of the magnetic granite yield a crystallisation age of 382 ± 6 Ma (Camacho & Ireland, 1997). This contrasts with previous authors (eg. Fagiano and others, 1992; Nullo and others, 1992) who interpreted an Early Ordovician age for the granite, correlating it with the syn D2 granitic group of Rapela & others (1970).

The complex is structurally stratified from dominatly magnetic, seriate granite at the base, through to dominantly leucogranite/granite at the top. These two informal subunits are entirely gradational and represent only a change in proportion of the constituent rock types. The lower subunit was previously mapped as "Granito Los

Nogales" (Fagiano and others, 1992; Nullo and others, 1992), while Otamendi and others, (1966) used the term "Granito Los Nogales" for granites in both the subunits.

Pink, coarse-grained, seriate biotite-granite is the predominant rock (90%) in the southernmost and structurally lowest of the subunits, forming only a minor component of the overlying granite-leucogranite dominated subunit. The granite is distinguished by its strongly magnetic character (magnetic susceptibilities about 500-1500 x 10^{-5} SI) and the presence of rare hornblende and common, pink, perthitic microcline crystals, which are up to 5 cm across. Apatite, magnetite and lesser pyrite are accessories. In places, weakly aligned biotite and pegmatite bands define flow banding. Xenoliths of pelitic gneiss, amphibolite and tonalite are common as concordant enclaves parallel to flow banding.

Flow-banded, pink to grey, medium- to coarse-grained, equigranular biotite-granite to leucogranite forms about 70% of the upper subunit and is a minor constituent in the remainder of the complex. The granite is equigranular with a ubiquitous flow-banded fabric evident by aligned biotite, concordant pegmatitic bands and patches, and schlieren and lenses of pelitic gneiss. Zircon, apatite, and rare garnet are accessory phases. Muscovite is a minor primary consituent but is more abundant as a secondary mineral in zones adjacent to the Las Lajas Shear Zone where the granite has a mylonitic fabric. In these areas biotite is replaced by chlorite and quartz and muscovite form a ENE-dipping mineral lineation on a muscovite-rich mylonitic foliation. Very weak carbonate, epidote, sericitic and hematitic alteration is widespread. Small fibrous aggregates of sillimanite with muscovite reaction rims are present near contacts with gneiss and possibly represent minor contamination of intrusive margins with host pelitic gneiss.

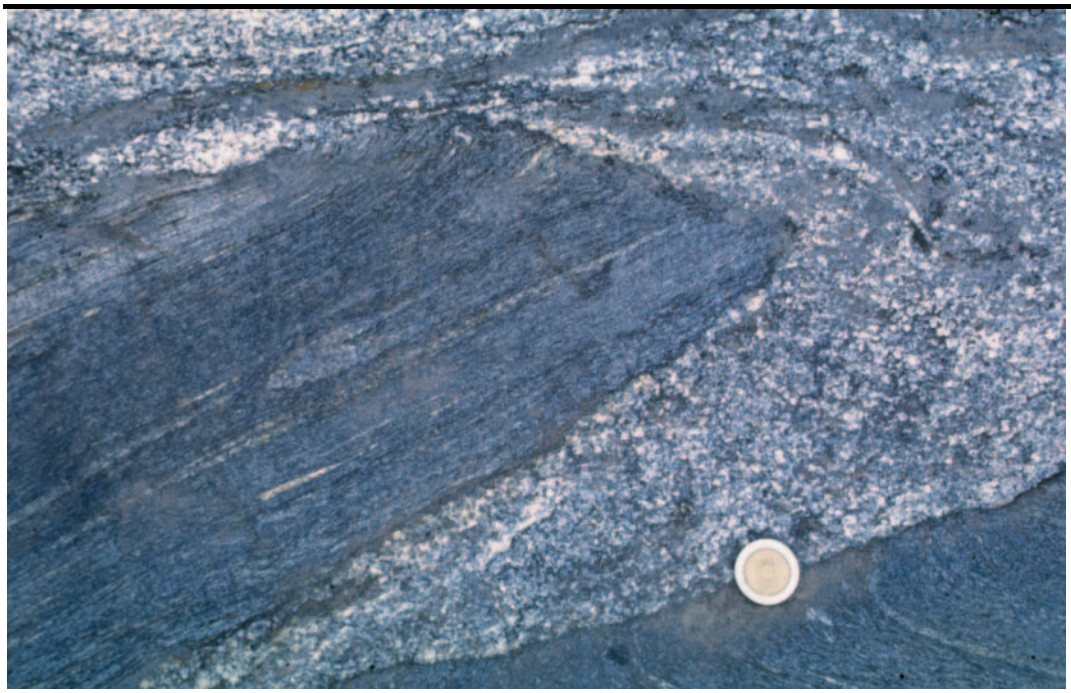

Figure 31. Devonian granite intrusions post-date S1 & S2 metamorphic fabrics (locality A95PS166)

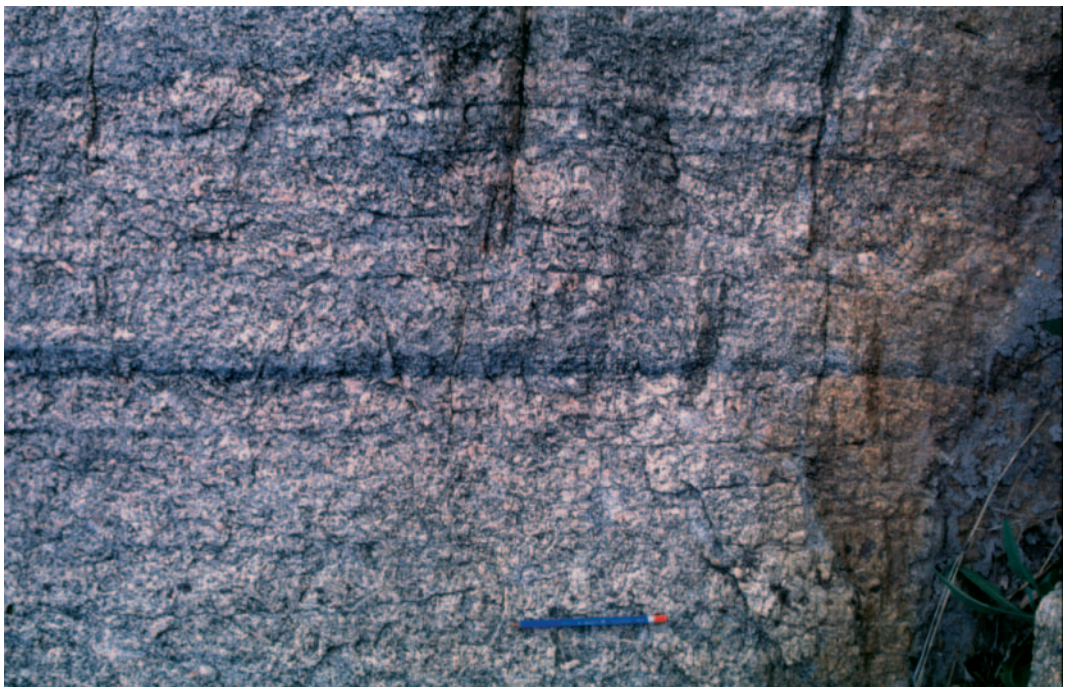

Figure 32. Strongly developed compositional banding in the Achiras Igneous Complex. This is interpreted as primary flow banding (locality A95PS165).

Interlayered grey banded, feldspar-biotite-quartz (±garnet±muscovite) gneiss and (±garnet±sillimanite±feldspar) muscovite-biotite-quartz schist occur throughout the

complex as concordant enclaves and xenoliths within the layered seriate granite and granite-leucogranite intrusions.

Geochemically both the seriate granite and equigranular granite-leucogranite form a fractionated suite, the latter the most fractionated (Figures 27, 28, 29). They have similar major and trace element trends to other Devonian granites, and are peraluminous with an ASI of about 1.1. However, they differ in that they show little enrichment in Rb, Y, U with fractionation compared to other granites of the same age and are mostly less oxidised.

The granites have been interpreted as products of local anatexisis (Fagiano and others, 1992; Nullo and others, 1992; Otamendi and others, 1996) with emplacement conditions estimated at 700+˚C and 3Kb (Fagiano and others, 1992). This interpretation has been largely based on the interpretation of a tectonic origin for biotite alignment in the granites and a correlation with the principal second deformation phase (D2) of Dalla Salda (1984).

It is clear from this study that the alignment of biotite is a product of magma flow and that the granite truncates both D1 and D2 fabrics and is only affected by greenschist facies deformation. The granites probably represent products of a fractionated granitic magma, derived from metasedimentary sources, which intruded the Early Cambrian metamorphic rocks at mid/upper crustal levels during the Early Devonian as a series of multiple injections during progressive mylonitisation and eventual truncation by a greenschist facies high-strain zone, differentiated as the Las Lajas Shear Zone.

A major swarm of pegmatites is spatially associated with the Achiras Igneous Complex. The pegmatites occur as either semiconcordant veins intruding both granitic and gneissic rocks, or as discordant, mostly NW- and NNW-trending tourmaline-bearing veins. The concordant variety form part of the layered granite complex and represent highly fractionated melts injected during multiple granite intrusion. The discordant variety are more common and more widely distributed than the earlier pegmatites. They are spatially associated with the Las Lajas Shear Zone and concentrated within the basement hanging-wall. In places, they crosscut folds formed

during the mylonite formation, and in others, they are strongly mylonitised. These relationships indicate that the discordant pegmatites intruded during thrusting on the Las Lajas Shear Zone and represent the final products of felsic magmatism in this region.

Undifferentiated granite (Dg)

A number of small granite (sensu latu) bodies (e.g., Potrero de Los Funes; Figures 27, 28, 29) occur within *Sierras de San Luis y Comechingones*. These granites range in composition and texture and are essentially undeformed. Proximity to intrusions of known Devonian age, or intrusive relation with Devonian granites, suggest that these small undifferentiated granites are of similar age.

2.3.4 MINOR DYKE ROCKS

Pegmatite (peg)

Numerous pegmatite dykes intrude the basement of *Sierras de San Luis y Comechingones*. There are essentially four mainsubdivisions:

1. Pegmatites emplaced during M1 metamorphic peaking the Middle Cambrian, at around 530-515 Ma. These are restricted to within the Nogoli, Conlara and Monte Guazú metamorphic complexes.

2. Pegmatites emplaced during the M2 metamorphic peak in the early Ordovician at around 480 Ma. These are largely restricted to within the Pringles Metamorphic Complex.

3. Pegmatites emplaced post-M2 in the mid Ordovician at around 460Ma, and spatially associated with the undifferentiated Ordovician granites. These voluminous pegmatites are widespread within distinct belts in the Pringles, Nogoli, Conlara and Monte Guazú metamorphic complexes.

4. Pegmatites emplaced during the Devonian,and associated with the extensive granite bodies.

Aplite

Sierra de Comechingones

In the far northeast of the Sierra de Comechingones, a swarm of aplite dykes, up to 200 m wide and 5 km long, intrudes the Cerro Aspero batholith and the Monte Guazú Metamorphic Complex. The dykes, concentrated near the contact of the Comechingones and Alpha Coral Granites, intrude along a well-developed ring fracture system, paralleling the contact of the Comechingones Granite. The dykes comprise pink fine- to medium-grained equigranular biotite-muscovite-bearing aplite, commonly with minor quartz veinlets. Chloritic, hematitic and sericitic alteration is also common. A high total count (180 cps) reflects high potassic and thorium contents. The dykes are probably late fractionates associated with the Comechingones Granite.

Sierras de San Luis

A group of thin aplite dykes that are wholly contained within the San Luis Formation and intrusives within those rocks, occur in the Sierras de San Luis. These dykes are up to 5 km in length and no more than 3 m in width. They cross-cut the Tamboreo granodiorite, which has been dated at 472 ± 5 Ma (Camacho & Ireland, 1997), and are folded and recrystallised. A minimum age for for the dykes is provided by Devonian ages for the deformation of the San Luis formation. The dykes consist of medium-grained phenocrysts of quartz, feldspar, garnet and muscovite, in a fine grained recrystallised matrix, with minor secondary zoisite. Limited geochemistry from Sato and others, (1996) indicates that the dykes are granitic in composition. Brodtkorb and others, (1984) have interpreted some of these dykes, that occur within the San Luis Formation as metavolcanics.

Lamprophyre

Sierra de Comechingones

A swarm of long linear lamprophyre (minette) dykes intrudes the Monte Guazú Metamorphic Complex in the southern part of the Sierra de Comechingones. Individual dykes, may be up to 10 m wide, and extend discontinuously for up to 10 km. Typically, the dykes are negative topographic features and poorly exposed as small, spheroidally-weathered boulders, lying between resistant outcrops of the basement rocks. A chilled margin is commonly developed in the lamprophyres. The dykes trend northwesterly, parallel to faults developed at the close of the Devonian Achalian deformation.

Sierras de San Luis

A number of thin lamprophyre (minette) dykes have also been observed within and adjacent to the Rio Guzman Shear Zone in the Sierras de San Luis. These dykes are no more than 1 m in width and consist almost entirely of medium-grained biotite. Within the shear zone, the dykes have intruded parallel to the mylonitic foliation but are not deformed.

The precise age of the dykes is not known from either region, however, they clearly postdate Late Devonian thrusts and therefore must be late Paleozoic or Mesozoic in age. Toselli and others, (1996) interpret similar lamprophyre dykes, intruding the Granito Ñuñorco in the western Sierras Pampeanas, to be related to the late Devonian/upper Carboniferous "Chánica Orogeny".

2.4 TERTIARY VOLCANICS

San Luis Volcanic Group (Tva, Tvp, Tvb, Tt)

Intrusive plugs, domes, breccia pipes and dykes, lava, pyroclastic deposits, epiclastic volcanic deposits and hydrothermal deposits

A series of volcanic centres occur in a northwest-southeast trending belt of approximately 90 km length through central and western *Sierras de San Luis y Comechingones*. The volcanic centres include Sierra del Morro in the southeast, cerros Rosario and Tiporco, Cerros Largos, Cañada Honda, and La Carolina in the northwest. The geology, petrography and geochemistry of the volcanics have been examined by Brogioni (1987b, 1990). A general description of the volcanic centres is presented in Table 4.

The volcanic rocks, called here the San Luis Volcanic Group, range from late Miocene (~9.5 Ma) to Pliocene (~1.9 Ma) in age and are intrusive into the Conlara and Pringles metamorphic complexes and the San Luis Formation. Associated pyroclastic and epiclastic deposits form aprons around the volcanic centres and have been variously reworked or eroded. The intrusive volcanic rocks have a high reversely magnetised signature and highly potassic radiometric signature. Magnetic susceptibilities of the intrusive volcanics are generally in the range of 1000 – 3000 x 10^{-5} SI, while the pyroclastics are generally in the range of 400 – 800 x 10^{-5} SI. The volcanic rocks fall within the calc-alkaline to shosonitic series and geochemical data is presented in Figures 33, 34, and 35.

Table 4. Volcanic centres, age and general descriptions. References for age determinations: [1] Ramos and others, (1991); [2] Urbina and others, (1995); [3] Sruoga and others, (1996).

Volcanic centre *(dating location)*	**Age (Ma)** (K/Ar)	**Rock-types and general description**
La Carolina *(Tres Cerritos)* *(C• Tomolasta)* *(C• Pan de Azucar)* *(not specified)*	 8.2 ± 0.4[3] 7.5 ± 0.4[2] 7.3 ± 0.4[2] 6.3 ± 0.3[3]	Range of volcanic plugs and domes, minor pyroclastic deposits and subvolcanic breccias. Extensive alteration of host rocks. Basement deeply eroded (~300m?). NW trending faults
Cañada Honda *(Diente Verde)* Cerros Largos	 9.5 ± 0.5[2]	Range of volcanic plugs and domes. Extensive alteration of host rocks. Basement deeply eroded (~200m?) Volcanic domes. Tuff mostly preserved in topographic low (?diatreme) to SW of volcanic domes. Basement eroded (~100m?)
Tiporco		Single isolated volcanic dome in raised (~50m) basement ring. Travertine and subsurface veins of calcareous onyx encircle the volcanic centre. Paleao landsurface readily apparent, however, much of the pyroclastic material has been removed
Cerros del Rosario	2.6 ± 0.6[1]	Range of volcanic plugs and domes partly centred in raised (~200m) basement ring. Paleao landsurface readily apparent, however, much of the pyroclastic material has been removed. Ring faults around basement dome
Sierra del Morro *(not specified)* *(not specified)* *(not specified)*	 6.4 ± 0.6[1] 2.6 ± 0.6[1] 1.9 ± 0.2[1]	Range of volcanic plugs and domes, breccia pipes and dykes mostly contained within domed (~700m) basement rocks with a central collapsed(?) caldera. Palaeo landsurface readily apparent with thick cover of pyroclastic and epiclastic material preserved on the north, east and south flanks. Western flank deeply dissected (~200m) adjacent to Los Morillos fault escarpment. 'Box' faults around basement dome.

The volcanic rocks (labelled Tva) include plugs, domes (e.g. Figure 36), dykes, sills and minor lavas and range in composition from basaltic andesite to dacite. Brogioni (1987) also reports rocks of latitic to trachytic composition. Sub-volcanic breccia pipes and dykes (labelled Tvb) are well exposed within the central caldera of Sierra del Morro (e.g. Figure 37) and on the southern flanks of Cerro Rosario. The breccia pipes form hard resistant topography and consist of unoriented, welded, angular fragments of both volcanic and country rock, ranging in size from microscopic to metre scale. The breccia dykes are poorly outcropping and consist dominantly of well layered, poorly welded, fragmental volcanic-material.

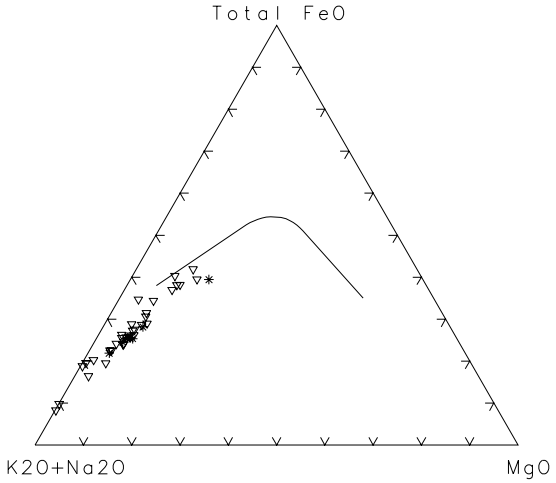

Figure 33. AFM diagram showing trend of analysis for the San Luis Volcanic Group. Asterisk represent data from this study, open triangles are data from Brogioni (1987b).

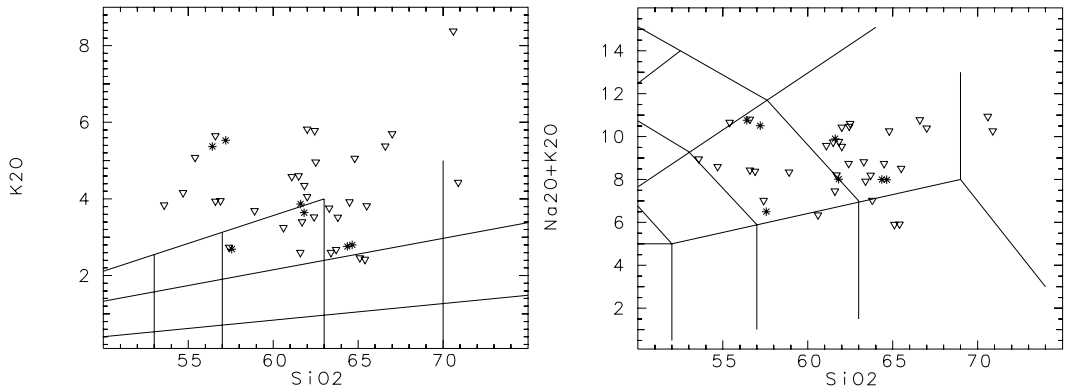

Figure 34. Discrimination diagrams of SiO2 vs K2O and (Na2O + K2O) for the San Luis Volcanic Group. Legend as per Figure 33.

Pyroclastic and epiclastic deposits (labelled Tvp) are well preserved, particularly in the region of Sierra del Morro and Cerros del Rosario. The pyroclastic deposits are generally cream to grey, well bedded, and are hard to friable. The beds may range from centimetres to metres in thickness and consist of a combination of pumice, ash and lithic fragments. The beds include ground surge deposits, ash fall tuff and fragmental tuff. Welded pyroclastic breccia was also observed adjacent to Cerro Tiporco. Bombs of both basement and volcanic material are common in the pyroclastics. Epiclastic deposits are well developed in the region of Sierra del Morro, where they form resistant radial fans with inverted relief around the main basement dome.

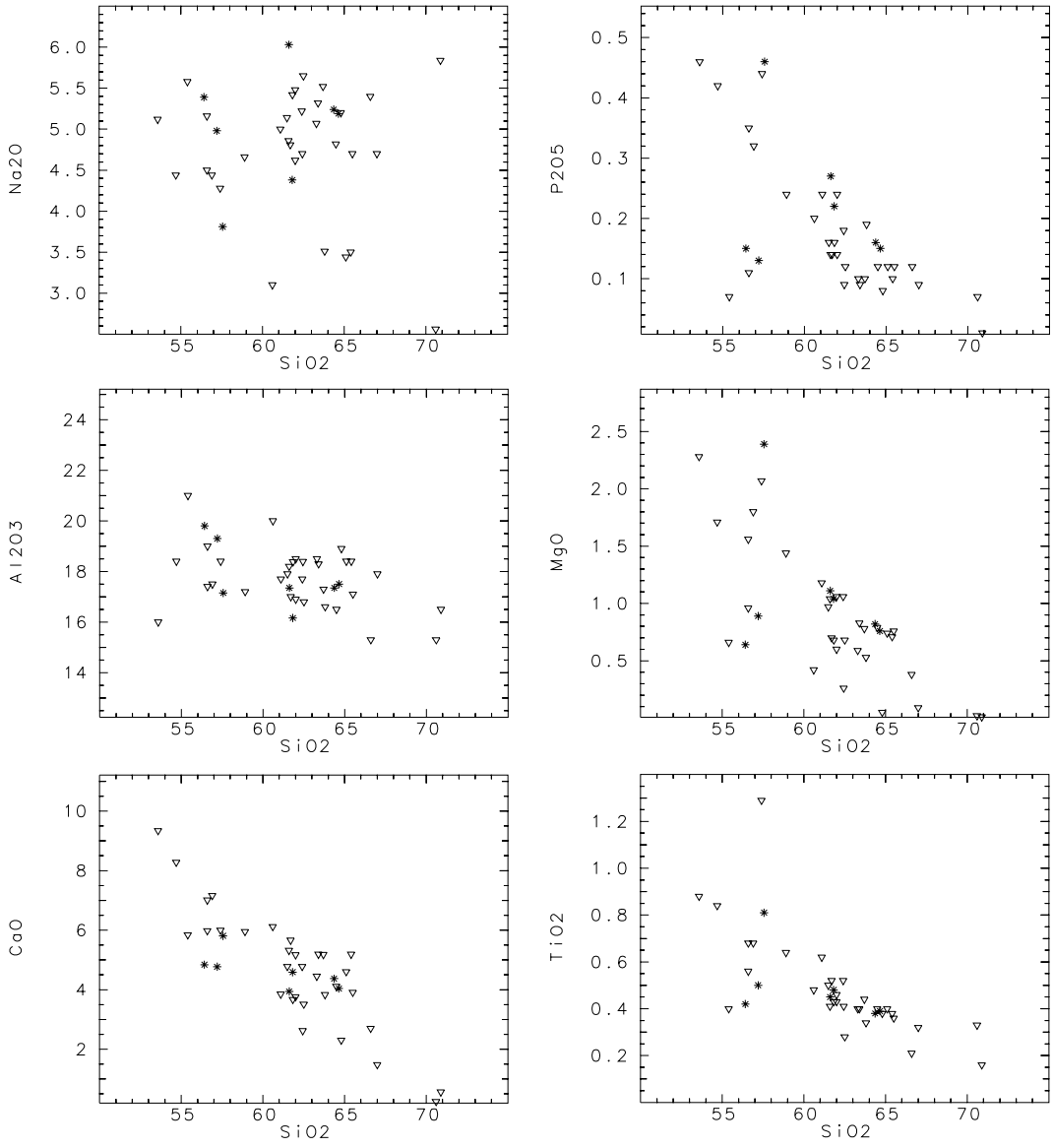

Figure 35. Harker variation diagrams of SiO_2 versus Na_2O, P_2O_5, Al_2O_3, CaO, MgO and TiO_2 for the San Luis Volcanic Group. Absence of distinct trends suggests extensive crustal contamination. Legend as per Figure 33.

Hydrothermal deposits including calcareous onyx and travertine (labelled Tt) occur distributed about Cerro Tiporco. The calcareous onyx, which is exposed within quarries such as *Santa Isabela*, forms veins of various thickness (generally < 2m) that intrude basement schist (Figure 38) and are interlayered in places with pyroclastic deposits. The veins consist of green to brown carbonate with local, vuggy porosity and late aragonite and flourite crystallisation. The travertine generally forms a rigid cap rock (probably a palaeo-landsurface) that is well presesrved to the NW of Cerro

Tiporco where it is deeply dissected and now form the caps of hills. The travertine seems to be in part, basal to the volcaniclastics.

The more deeply eroded volcanic centres in the northwest, are associated with significant epithermal alteration and minor (to date) precious metal (Au-Ag) mineralisation. These deposits are covered in more detail in the Economic Geology section.

2.5 CAINOZOIC

unconsolidated cover (Czu, Czg, Czc, Czd)
loess, alluvial deposits, fans, gravels, caliche,channel deposits etc.

Unconsolidated alluvial, colluvial and aeolian deposits, as well as palaeosols, overly the basement rocks in Sierras de San Luis y Comechingones and are interspersed with some of the volcaniclastic deposits. The most extensive Cainozoic unit (labelled Czu) is an intercalted sequence of undifferentiated Tertiary to Quaternary fluvial and aeolian deposits and paleosols that cover a large part of the Pampean region. In areas of low lying relief, these deposits cover all older units and forms a mantle or rarely dune fields between the main Pampean ranges. The undifferentiated Cainoizoic deposits comprise mostly friable illite and silt, with material derived from both the metamorphic-igneous basement rocks and a volcanic-pyroclastic source (Strasser and others, 1996). Strasser and others, (1996) have correlated the stratigraphically younger deposits in the San Luis region with Late Pleistocene and Holocene units in the Buenos Aires Province.

At the southern end of the Sierras de San Luis, unconsolidated sediments (labelled Czd) preserve evidence of Tertiary basin formation in the region of Potrero de los Funes and San Luis. The sediments consist of poorly sorted, sand and mud dominated beds with a distinctive red colouration. The deposits range from fine-sand to cobbles in grainsize. The unit is unconformably overlain by Cainozoic conglomerates, and both units are dissected by Quaternary alluvial systems.

In places, paleosols (labelled Czc), typically with a hardpan of calcrete, form thin (a few metres thick) remnant cappings over basement rocks. They are best exposed along the gently sloping eastern flanks of the Sierras de Comechingones and in the easternmost Sierras de San Luis where they are overlain by intercalated Tertiary to Quaternary fluvial and aeolian deposits (Figure 39). The age of the deposits is not known. Their formation predates the last significant uplift which probably took place during the Late Pliocene-Pleistocene (Costa,1996).

Figure 36. Andesitic volcanic plugs (~200m in height) within the collapsed caldera(?) of Sierra del Morro.

Figure 37. Large boulder from breccia pipe exposed within the collapsed caldera(?) of Sierra del Morro.

Figure 38. Vuggy, calcareous-onyx (green-brown, sub-horizontal) veins cross-cutting steeply dipping schist of the Conlara Metamorphic Complex with overlying tuff. Calcareous onyx forms the upper portion of an epithermal system associated with the nearby volcanic center of Cerro Tiporco (locality A95JS088; Santa Isabel).

Figure 39. Tertiary palaeosol consisting of calcrete overlain by Quarternary fluvial and aeolian sediments. This sequence is exposed in block uplifted duing Recent Andean Tectonism (locality A96JS045; Dique de Paso de Las Carretas).

Raised fluvial and colluvial fan deposits of unconsolidated gravels (labelled Czg) form low, wooded, dissected hills at the base of many of the main Cainozoic fault scarps. The most extensive of these occur along the western scarp of the Sierras de San Luis. These deposits are correlated with similar Pleistocene (Quaternary level 1 subdivision of Massabie, 1982) deposits in the Capilla del Monte area of Córdoba. Increased erosion and exposure of Miocene-Pliocene volcanic plugs from east to west places a lower age constraint on the earliest uplift and hence the maximum age of the fans at mid-Pliocene.

2.6 QUATERNARY

Unconsolidated deposits (Qa, Qg, Qs, Qt)

active alluvial deposits, fans, gravels, talus.

Holocene (Santa Cruz, 1978) to Recent alluvial deposits of clay, sand and gravel along active river courses and adjacent terraces and overbank deposits (labelled Qa) dissect the undifferentiated Cainoizoic units**.** The most extensive of these deposits are associated with the Rio Rosario in the south, several rivers draining east from the Sierra Comechingones and west from the Sierras de San Luis, and are also common in numerous minor drainages within the Sierras de San Luis. Bodies of fluvial channel deposits of mainly sand and minor gravel within the presently active channels (labelled Qs) are best developed within the Rio Rosario. Active fan deposits (labelled Qg) occur along the base of the fault scarps bordering the Sierra de Comechingones and San Luis. And minor Recent talus deposits (labelled Qt) occur along the exhumed, steeply dipping contacts of the Comechingones and Alpa Corral granites in the northeast, and also occur around many of the highly resistant volcanic plugs of the San Luis Volcanic Group.

3. TECTONICS

Three major deformation, metamorphic and magmatic events have affected the basement rocks of *Sierras de San Luis y Comechingones* (Table 1). Rocks of the Monte Guazú, Conlara and Nogoli metamorphic complexes preserve evidence of the earliest event, while the latter two are present within the rocks of the Pringles Metamorphic Complex. The San Luis Formation only shows effects of the latest event. The three tectonic events are termed here the (Early Cambrian) Pampean Cycle, the (early Ordovician) Famatinian Cycle, and the (Devonian) Achalian Cycle. All regions were also affected by reverse faulting and block-tilting during the Cainozoic Andean Cycle.

3.1 PAMPEAN CYCLE: EARLY CAMBRIAN DEFORMATION AND METAMORPHISM

The oldest preserved structural feature in *Sierras de San Luis y Comechingones* is a medium- to high-grade metamorphic differentiated foliation which is well-preserved in pelitic gneiss and amphibolite of the Monte Guazú, Conlara and Nogoli metamorphic complexes. The foliation (S1), which is variably developed, is typically a penetrative gneissic foliation in pelitic gneiss, defined by leucosome lenses (Figure 40) and a mineralogical layering defined by biotite, quartz and sillimanite with a lineation (L1) defined by sillimanite and quartz. In tonalitic orthogneiss, aligned biotite forms S1 folia, with a weak biotite and quartz lineation. In amphibolite and calcsilicate rocks the foliation forms strongly differentiated mineralogical bands with aligned hornblende. Throughout most of the Monte Guazú Metamorphic Complex the S1 foliation, trends NNW and dips ~45° to the east. The trend of the S1 foliation in the Conlara and Nogoli metamorphic complexes is generally similar, however, the dip of the foliation is more variable due to locally intense reworking during subsequent events. No kinematic indicators where observed.

Sillimanite-garnet assemblages in pelitic gneiss indicate M1 metamorphism was at least amphibolite facies and abundant muscovite-pegmatites, and leucosome (forming subconcordant lenses with S1) suggest limited partial melting took place. Pressure-temperature (*P–T*) estimates of peak metamorphic conditions for rocks of the Monte Guazú Metamorphic Complex in the Sierra de Comechingones range from 6.1 to 9.5 Kb, at 700 to 800 °C (Cordillo, 1984; Martino and others, 1994; Cerredo, 1996). No *P–T* estimates exist for the Conlara or Nogoli metamorphic complexes, however, peak metamorphic assemblages in the Nogoli Metamorphic Complex of cordierite-garnet-sillimanite in pelitic rocks, and an apparent scarcity of orthopyroxene in metamafic rocks, suggests pressures of <~7 Kbars at temperatures of no more than ~750 ˚C (e.g. Grant, 1985; Spear, 1981, 1993).

No isotopic data exist from *Sierras de San Luis y Comechingones* to constrain the age of the Pampean Cycle. However, uranium-lead dating of zircon and monazite from Córdoba (*Sierras de Septentrionales*), which grew during M1 (Lyons & Stuart-Smith, 1997), give an age of ~530Ma (Camacho & Ireland, 1997). Late Pampean granites in

Córdoba give ages of ~515-520 Ma (Camacho & Ireland, 1997; Rapella & Pankhurst, 1996; AGSO-Subsectretaría de Minería Argentina, unpublished data).

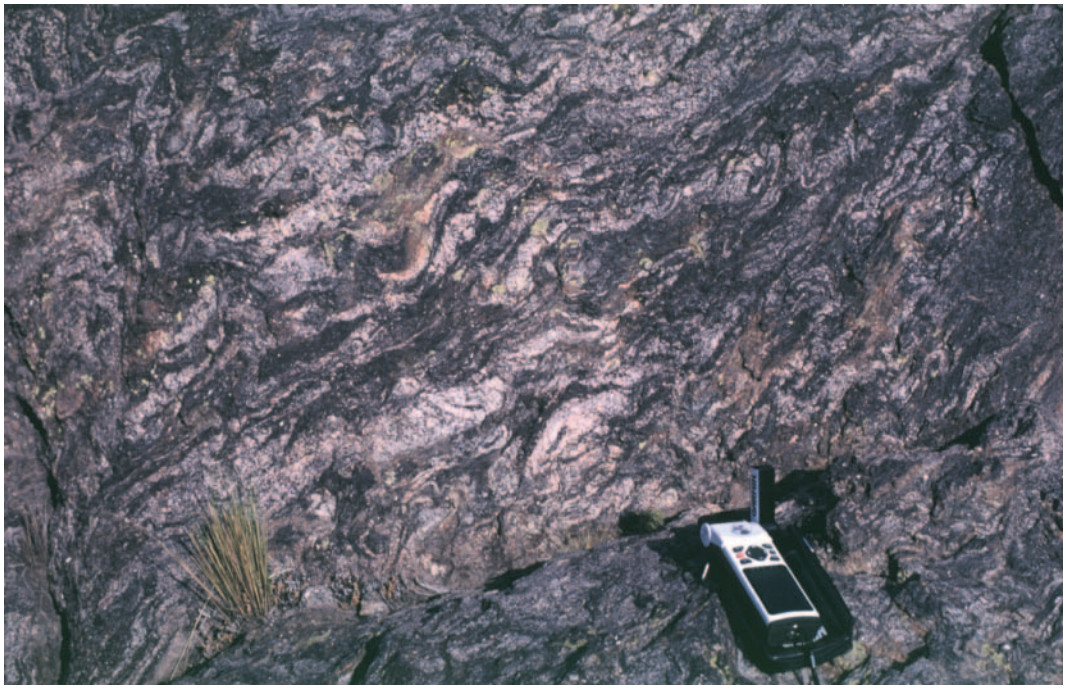

Figure 40. Sub-stromatic migmatic gneiss of the Conalra Metamorphic Complex (locality A95JS106). Melting probably developed during M1 (Pampean Tectonic Cycle) and open to isoclinal folding during D2 (Famatinian tectonic cyle). Outcrop is cross-cut by low-grade upright shear-zones of Devonian age.

Figure 41. Migmatic gneiss of the Conalra Metamorphic Complex (locality A95JS106). Not that there appears to be multiple generations of pegmatite veins, including an early one that is strongly deformed and a later, more massive, one that cross-cuts the gneissic fabric.

3.2 FAMATINIAN CYCLE: ORDOVICIAN DEFORMATION AND METAMORPHISM

Formation of a basin, in which the sedimentary protolith to the Pringles Metamorphic Complex was deposited, possibly marks the initiation of a subduction complex to the west of the Sierras de San Luis in the late Cambrian. Numerous intrusives within the La Rioja area that were emplaced around 490-480 Ma (Camacho & Ireland, 1997) probably represent the core of the associated volcanic arc. Correlatives of these intrusive within *Sierras de San Luis y Comechingones*, are represented by monzonites and quartz-monzonites (e.g., the Rio del Molle Monzonite) emplaced into the Nogoli Metamorphic Complex. The back-arc basin had closed, however, by the early Ordovician, when the Cambro-Ordovician rocks were strongly deformed and intruded by syn-kinematic mafic and ultramafic rocks of the Las Aguilas Group (LAG) at ~480 Ma (Camacho & Ireland, 1997).

Compressional phase

The peak metamorphic assemblages in the Pringles Metamorphic Complex, which formed under granulite facies conditions during the Famatinian Cycle, are spatially located in an elongate belt around the LAG. The pelitic rocks contain a gneissic fabric defined by sillimanite and biotite (S1 in the Pringles Metamorphic Complex but regional S2), with lenses and pods of cordierite- and garnet-bearing leucosomes. The gneissic layering trends N-NNE and dips mostly steeply to the east, and sillimanite and biotite laths define a steeply plunging mineral lineation. A number of discrete mylonite zones are formed within the complex, these are generally less than 20-30 m wide and parallel the gneissic layering. High-grade assemblages involving sillimanite and locally cordierite in the mylonites and a stretching lineation parallel to that in the gneiss suggest they formed synchronously. The mylonites are particularly well developed along the margins of the ultramafic bodies. Shear sense indicators both in the gneissic layering and in the mylonites and give an east-up displacement sense.

In gneiss and schist of the Conlara Metamorphic Complex, in particular those structurally beneath the Las Lajas Shear Zone, a schistosity parallel to S1 forms the main penetrative structure. All S1 fabrics are rotated into parallelism forming a new S2 foliation with a pronounced mineral lineation (L2) of biotite, muscovite and quartz. Lower amphibolite/upper greenschist facies metamorphism (M2) is indicated. Quartz-feldspar leucosome, formed during M1, are deformed into asymmetrical clasts indicating westward-directed thrusting. In places, the schistosity is axial plane to relict isoclinal folds (F2) which plunge parallel to the lineation. These folds are also present in Monte Guazú Metamorphic Complex gneiss, however, S2 development was limited in those rocks.

Extensional phase

By ~470 Ma, however, the compressional regime had ceased and the terrane was in extension, resulting in deposition of the San Luis Formation (SLF). This was followed subsequently by intrusion of the Tamboreo Granodiorite and tonalites of the Bemberg Suite, which produced metamorphic aureoles in the cover rocks.

The extensional structures developed under greenschist-facies conditions, and deformation was partitioned into domains of shearing with a shallow to steep, east to southeasterly dipping lineation and domains of open to tight folding of the older structural surfaces in the basement rocks. Shear fabrics defined by muscovite ± biotite predominate, with a lineation locally defined by tourmaline. Shear sense indicators give an east-down displacement sense. Numerous pegmatites and (fractionated) granites intruded synchronously with the deformation and show varying degress of folding and dynamic recrystallisation (Figure 41). A U-Pb uraninite age of ~460 Ma has been derived from one of these pegmatites (Linares, 1959). Although this age is is younger than that derived from either the Tamboreo Granodiorite or the Bemberg tonalite (Table 2), the intense deformation of the pegmatites, which does not affect the SLF (nor the granodiorite or tonalites), and a distinct absence of similar pegmatites in the SLF suggests that the uraninite age is reset, or is a cooling age. This age, however, is consistent with a Th-Pb monazite age of 451 ± 10 Ma (Camacho & Ireland, 1997) derived from a high-grade compressional fabric within the Pringles Metamorphic Complex. These younger ages may be interpreted to indicate a delayed

thermal relaxation of the exhumed high-grade basement rocks, or be indicative of a late fluid pulse in the Famatinian cycle. Alternatively, the discrepancy in the ages may suggest that the cover sequence is parautochthonous, in that the cover may have been separated from the basement (a core complex) during extension but was rejuxtaposed during subsequent compression in the Devonian.

3.3 ACHALIAN CYCLE: DEVONIAN DEFORMATION AND RETROGRESSION

Throughout much of the region, the medium- to high-grade Pampean(D1) and Famatinian (D2) fabric elements are mostly rotated into parallelism by a shallowly- to moderately-dipping, penetrative shear fabric associated with a prologed collisional episode, termed here the Achalian Cycle. This episode is marked by the development of mylonite in high-strain zones and pervasive, retrogressive greenschist-facies metamorphism and the emplacement of voluminous granite plutons. To varying degrees, the deformation affects all basement rocks, and is probably the the most significant single tectonic episode in the region.

Deformation in the Achalian Cycle involved repeated partitioning of strain between zones of thrusting and zones of strike slip displacement, with repeated overprinting relationships. Domains between shearing were folded and refolded; in some places producing basin and dome interference folds. Strain was focussed in a number of major mylonite zones, in particular, in the northwest-trending Las Lajas Shear Zone, which truncates the Conlara Metamorphic Complex, north of Achiras; and in the north-northeast trending Rio Guzman Shear Zone, which separates the Conlara Metamorphic Complex from the San Luis Formation. Additionally, a number of significant mylonite zones developed, including one along the eastern flank of the Sierra de Comechingones, passing through Las Albahacas, and a complex zone that follows the eastern contact of the Escalerilla Granite in the Sierras de San Luis. These deformations have been previously incorporated within the Famatinian Cycle (e.g. von Gosen & Prozzi, 1996)

At least 4 distinct styles of deformation are recognised within the Achalian Cycle. These styles are in part an effect of the partitioning of strain but also an effect of changing stress or metamorphic conditions in the terrane through the tectonic cycle.

1. Pervasive mylonitic foliation and tight to isoclinal folding

The earliest structural element is a pervasive mylonitic foliation associated with thrusting under upper greenschist-facies conditions. In the Conlara Metamorphic Complex, this forms a pervasive fabric defined by biotite that rotates the earlier Pampean and Famatinian fabrics into parallelism. Interference with flat-lying folds in both the Pringles and Conlara metamorphic complexes produced open basin and dome fold-interference patterns. In the early Ordovician San Luis Formation, tight to isoclinal folds are developed in bedding with an axial planar slaty cleavage (S1 in the SLF but regional S3) developed between major shear zones (e.g. Figure 42). A maximum age for this early fabric forming event is provided by a 403 ± 6 Ma age (U/Pb zircon; Camacho & Ireland, 1997) for the Escalerilla granite which is affected by the early tectonism.

Within the mylonite fabric, quartz is recrystallised to ribbons, biotite is deformed and locally replaced by chlorite, hematite and geothite, and M1 sillimanite is altered to fine muscovite aggregates. A mineral lineation (L3) or slickenline plunges down-dip to the ENE and is defined by aligned muscovite, chlorite, quartz and rotated relict biotite.

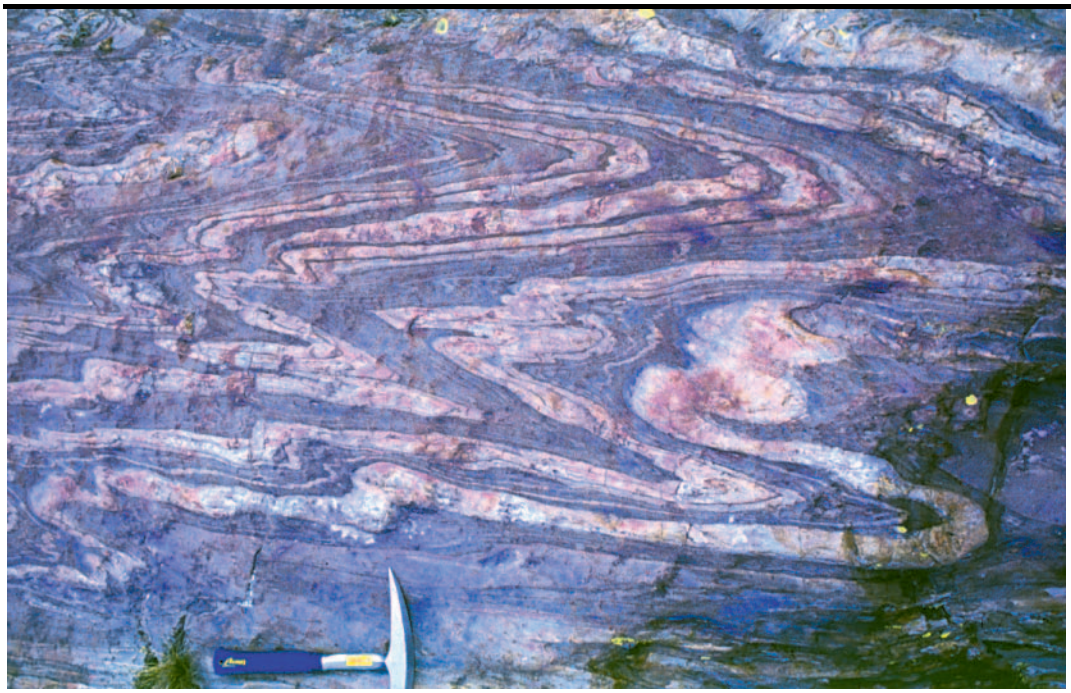

Figure 42. Tight folding within alternating, thin phyllite and quartzite beds of the San Luis Formation. The folding is developed adjacent to a major Devonian shear-zone on the margin of the Escalerilla Granite. (locality A95JS025; A˚ los Manantiales).

Figure 43. Asymmetric extensional shear band in Devonian strike-slip shear zone on the margin of Escalerilla Granite. Plan view, top of photo to east (locality A95JS039; A˚ de los Molles).

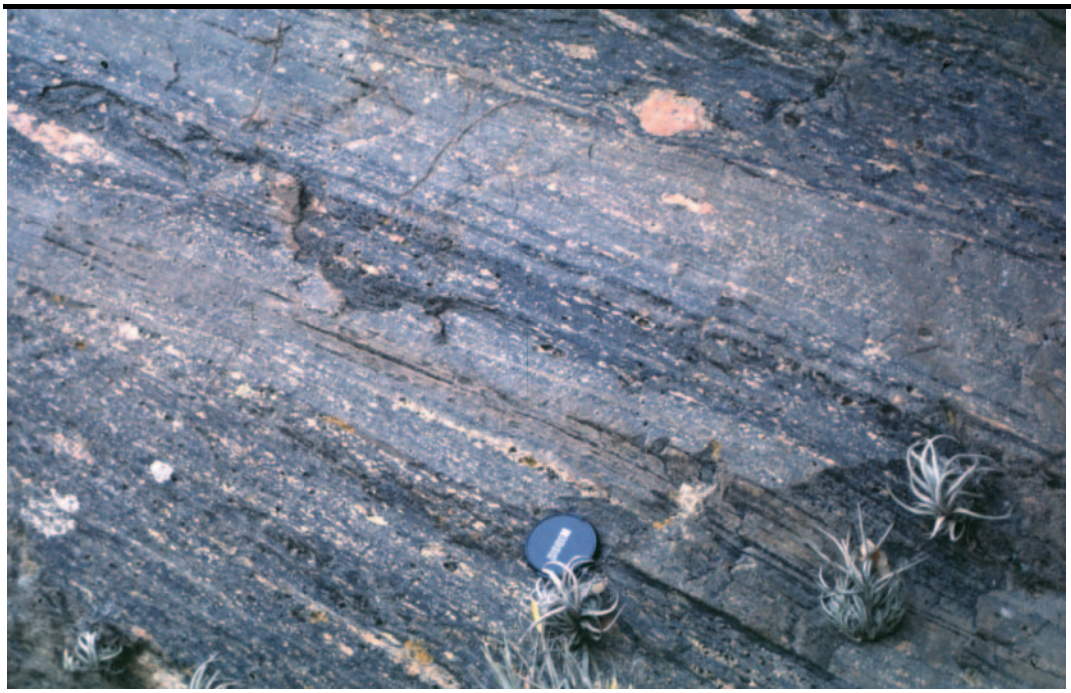

Figure 44. **A95PS128**: Greenschist-facies mylonite, Las Albahacas Fault Zone.

Sheath folds are also present, in places, plunging parallel to L3. Kinematic indicators including, asymmetric mantled porphyroclasts and S-C fabrics all indicate westward-directed thrusting.

2. Ductile strike-slip shearing

Discrete sinistral shear-zones up to 50m wide are developed in a number of areas within the Sierras de San Luis. The most prominent example is located along the eastern margin of the Escalerilla Granite. The shear zones contain a mylonitic fabric with a sub-horizontal mineral and elongation lineation and well developed shear sense indicators (e.g. Figure 43).

A strongly sheared pegmatite, located east of El Volcan, with a sub-horizontal stretching and mineral lineation and sinistral shear sense indicators was dated by Ar/Ar as part of the project. The pegmatite is interpreted to be part of the extensive pegmatite swarms that were emplaced in the early Ordovician. Two phases of muscovite were present in the mylonitised pegmatite, an early coarse-grained muscovite that is strongly deformed and is interpreted as part of the primary igneous assemblage, while the second muscovite is fine grained and grew parallel to the

stretching lineation in the shear fabric. The earlier muscovite produced a total fusion age of 384 ± 1 Ma (Camacho, 1997), which is interpreted as a reset age, while the fine-grained muscovite produced a stepped heating age of 374.7 ± 0.5 Ma (Camacho, 1997), which is interpreted as the age of the sinistral shearing in the pegmatite. This age suggests that a change in the regional stress field may have occurred in the Middle Devonian.

3. *Thrusting at low-grade in discrete shear zones with contemporaeous folding and crenulation of the earlier mylonitic fabric*

Overprinting the strike-slip shear-zones are a number of major low-grade shear-zones that traverse both the Sierras de San Luis (Rio Guzman Shear Zone) and the Sierras de Comechingones (Las Lajas Shear Zone and Las Albahacas Shear Zone; Figure 44). These shear zones are up to several kilometres in width, and contain greenschist-facies mineral fabrics that show east-up shear-sense on an easterly plunging lineation, parallel to the early L3 fabric. A regional crenulation cleavage associated with north-south trending open folding is considered to be have developed contemporaneously between the main shear-zones.

In leucogranite within the Las Lajas Shear Zone, foliated metamorphic muscovite, rare relict primary biotite, and bands of granoblastic polygonal quartz and feldspar define the mylonitic foliation. S-C fabrics are also common with a quartz-muscovite mineral lineation. Idioblastic garnet where present is altered to sericite.. In ortho-amphibolite, bands of recrystallised quartz, carbonate, plagioclase and epidote define a penetrative greenschist facies mylonitic foliation, and in pegmatite, S3 is present as recrystallised granoblastic polygonal bands of quartz and deformed muscovite folia.

The mylonitic fabric of the Las Lajas Shear Zone extends up to 1 km into the structurally underlying parts of the Conlara Metamorphic Complex. In areas further south (and structurally deeper), the main penetrative fabric is the medium-grade S2 foliation along which the Early Devonian subcordant granite sheets of the Achiras Igneous Complex were intruded. These layered granites are essentially undeformed, containing no penetrative tectonic foliations, and together with the metamorphics are

folded about shallow N- to E-plunging regional open inclined to overturned macroscopic folds and mesoscopic chevron folding (F3). A weak axial plane crenulation (S3b) dips moderately to steeply (40-85) to ENE. The same folds also occur throughout the Monte Guazú Metamorphic Complex and Las Lajas Shear Zone, where they rotate the greenschist mylonitic fabric elements. As the folds are also truncated in part by the Las Lajas Complex the folds most likely developed during the later stages of progressive westward-thrusting and mylonite formation.

4. Brittle-ductile strike-slip faulting typically in conjugate sets trending NW and SW

A complex system of rectilinear brittle vertical WNW- and ENE-trending strike-slip faults, breccia zones and fractures (von Gosen & Prozzi, 1996) affect all the basement units in the Sierras de San Luis and the Sierra de Comechingones, in places displacing the S3 mylonitic foliations and related folds. The faults are rarely exposed, but are prominent on aerial photographs and Landsat images. Some of the faults are also delineated on magnetic images as low magnetic zones owing to magnetite destruction. One such fault is exposed in the extreme south of the Sierra de Comechingones (65.0644 °S, 33.3223 °W) where it cuts the Achiras Igneous Complex. Here the fault forms a silicified geothite breccia zone up to 5 m wide that is subvertical and trends toward 033°. Other exposures of the faults include a cataclastic fault zone over 20 m wide, which separates the Conlara Metamorphic Complex from the structurally overlying Monte Guazú Metamorphic Complex near Cerro Moro (64.95113 °S, 33.01399 °W). At this locality, inliers of the Achiras Igneous Complex are broken and highly altered by epidote, sericite, hematite and chlorite with rare geothite psuedomorphs after pyrite. Within the Sierras de San Luis, where exposed, these faults typically consist of narrow zones (<1 m wide) of brittle-ductile mylonite and minor ultramylonite.

The orientation and conjugate relationship of the WNW- and NE-trending strike-slip faults, breccia zones and fractures indicates possible continuation of the east-west compressive regime that accompanied S3 and S4 development. This fracture system is developed throughout the Sierras Pampeanas and in Córdoba and La Rioja Provinces where muscovite Ar-Ar ages of micas from quartz veins indicate that this stage began about 385 Ma, peaked at 370 Ma and continued until 355 Ma (ref).

3.4 ANDEAN CYCLE: REVERSE FAULTING

Tectonism associated with the collision of the Nazca and South American plates resulted in a period of extensional deformation in the Sierras Pampeanas region during the Neogene, followed by compression from the late Neogene through to the present. The extensional phase resulted in the development of a number of small southeast – northwest trending basins. The best examples of these occur in the southernmost Sierras de San Luis in the area of Potrero de los Funes and San Luis, where small segments of the uplifted basin sediments are preserved. Also during this period, high-K calc-alkaline to shoshonitic volcanics were emplaced in a ~80 km belt, parallel to the extensional basins, from Sierra del Morro to La Carolina,.

A marked change in the regional stress field occurred after the mid-Pliocene, coincident with the cessation of volcanism. Since that time, the Sierras Pampeanas region has been in a compressional regime and the Sierras de San Luis and Sierra de Comechingones are examples of the uplift on basement thrusts that have formed during this period (e.g., Costa and Vita-Frinzi, 1996). The ranges slope gently to the east and are bounded to the west by escarpments developed on low to moderate angle, east dipping, reverse faults. In the Sierra Comechingones, a major north-south fault zone, the Comechingones Fault (Costa and others, 1994), extends along the base of the western escarpment, and can be traced on aeromagnetic images to the south of La Punilla, beneath a veneer of Cainozoic sediments. ^{14}C ages suggest the fault was active as recently as c. 1000 years ago (Costa and Vita-Frinzi, 1996). Immediately south of Papagayos, the main fault zone, which is possibly up to 2 km wide, is exposed in kaolinite quarries within the Uspara Granite. Exposures of the granite are intensely brecciated, altered to chlorite and kaolin and cut by gouge zones dipping 45˚ to the southeast. The vertical component of displacement decreases to the south and is probably taken up by a number of fault splays such as that which borders the Sierra de la Estanzeula.

4. GEOMORPHOLOGY

The uplift during the Late Cainozoic of peneplanated crystalline basement on reverse faults, generally trending north-south, produced a series of tilt blocks through out the Sierras Pampeanas (Jordan and Allemendinger, 1986). The asymmetry of the basement blocks is produced by the formation of steep escarpments on the bounding fault side and gentle slopes, the dissected peneplanated surface, on the other. Broad flat valleys between major blocks are depositional centres filled with a variety of Cainozoic and Quaternary sediments including aeolian, fluvial, and lacustrine material.

The sheet area is comprised of three main physiographic regions, the Sierras de San Luis in the west, the Sierra de Comechingones in the east, and the Conlara Valley in the centre which includes a number of minor ranges and the uplifted basement around the volcanic centre of Sierra del Morro. The principal faults along which uplift occurred are the San Luis and Comechingones Faults which dip to the east. The fault scarps are on the western side of the main sierras and the dissected peneplanated surfaces slope to the east. The broad depositional basin of the Conlara Valley contains the smaller tilt blocks of the Sierras de La Estanzuela, de Tilisarao, del Portezuelo, San Félipe, and del Yulto. Fault scarps on the minor sierras occur on the western or north western side except for the Sierra de Portezuelo which is fault bound on its eastern side by a west dipping fault. A narrow valley dissecting the Sierra de La Estanzuela is a possible Mesozoic graben similar to those which occur in the sheet areas in Córdoba and La Rioja. The Sierra del Morro is a broad cone of uplifted basement resulting from the intrusion of the volcanic centre.

The Conlara Valley is filled with Cainozoic alluvial, aeolian, and volcanogenic deposits which preserve an earlier Cainozoic surface evidenced by the presence of palaeo-channels found away from present day watercourses. The intermontane deposits in the west of the sheet area are characterised by Quaternary gravels shed from the Sierras de San Luis.

The main drainage from the Sierras de San Luis is via the Río Quinto to the south east, which flows in to the Conlara Valley, and the Río Chorillos to the south west. The Sierras de Comechingones are drained by the east-south east flowing Río Cuarto. The

Conlara Valley is drained by the north-north east flowing Río Conlara and the southward flowing Río Rosario.

5. GEOLOGICAL HISTORY

The *Sierras de San Luis y Comechingones* area forms part of the southern Sierras Pampeanas, comprising basement ranges of Neoproterozoic to early Palaeozoic metamorphic rocks and Palaeozoic granitoids, separated by intermontane Cainozoic sediments. The basement rocks form a series of north-trending lithological and structural domains separated by major mid-crustal shear zones. These domains have been variously interpreted to form originally part of an ensialic mobile belt (eg. Dalla Salda, 1987) or as terranes that either accreted, or developed on a western convergent margin of the Rio Plata craton (e.g., Ramos, 1988; Demange and others, 1993; Escayola and others, 1996, Kraemer and others, 1995, 1996). Recent geochronological studies (e.g. Camacho & Ireland, 1997) and the geological relationships, indicate that there are two principal domains in the southern Sierras Pampeanas: an older Cambrian domain, and a younger Cambro–Ordovician domain. Both domains share a common tectonic history since early Devonian times.

5.1 EARLY CAMBRIAN SEDIMENTATION

The oldest rocks in the region form a structurally thick sequence of pelitic and lesser psammitic gniesses which comprise the Valle de la Rio Conlara and the Sierra de Comechigones (Conlara and Monte Guazú metamorphic complexes), as well as an orthogneiss dominated terrane with minor pelitic gneiss (the Nogoli Metamorphic Complex) in the western Sierras de San Luis. No original sedimentary structures, such as bedding, can be recognised in these metamorphic rocks. Minor marbles are common in the eastern complexes of the *Sierras de San Luis y Comechingones* but are less extensive than in interpreted extensions of the same domains in northern Cordoba (Lyons and Stuart-Smith, 1997), where they form semicontinuous belts. These metasediments are interpreted as being deposited on a passive margin, developed during intracontinental rifting and breakup of Laurentia from Gondwana in

Eocambrian times at about 540Ma (Dalziel & others, 1994). Uranium-lead dating of detrital zircons in paragneisses from Córdoba (Quilpo Formation and Pichanas Metamorphic Complex; Lyons & Stuart-Smith, 1997) show a 500–600 Ma Gondwana signature common to Cambro-Ordovician sediments previously described from Australia, New Zealand and west Antarctica (Camacho and Ireland, 1997). Lithological similarities and comparable ages indicate that the metasediments may be correlatives of the Early Cambrian (Aceñolaza & Toselli, 1981) Puncoviscana Formation in the northern Sierras Pampeanas as postulated by Willner and Miller (1986). This formation was interpreted by Dallas Salda and others, (1992) to be related to the rift-drift transition during postcollisional G ondwana-Laurentia breakup.

5.2 PAMPEAN CYCLE

Early Cambrian Deformation, metamorphism, mafic and felsic intrusion

Following intrusion of tholeititic mafic dykes, the sediments were deformed at mid-crustal levels by a compressive event (D1) and metamorphosed at mostly upper amphibolite facies and locally, granulite-facies. Uranium-lead dating of zircon rims and monazite formed during this metamorphic event (M1) in Córdoba give an age of ~530 Ma **(**Lyons and Stuart-Smith, 1997; Camacho and Ireland, 1997). This event includes both the D1 and D2 domains of Dalla Salda (1987) and has been previously termed the "Ciclo orogénico Pampeano" (Aceñolaza and Toselli, 1976) or "Ciclo Pampeano" (Dalla Salda, 1987, Toselli and others, 1992). The deformation is interpreted as the first in a series of deformation events associated with convergence on the newly created Pacific Gondwana margin formed after final amalgamation of the supercontinent (eg. Dalzeil and others, 1994).

At the closing stages of the Pampean Cycle, an extensive phase of felsic magmatism is evident by widespread subconcordant intrusion of tonalite, granodiorite and granite within the Monte Guazú Metamorphic Complex. There are no radiometric dates on these intrusions, however, in the Sierra Norte - Ascoghinga area in Córdoba, similar intrusions, dated at ~515 Ma (AGSO-Subsecretaria de Mineria Argentina, unpublished data), form a complex with minor xenoliths and enclaves of dioritic rocks.

5.3 EARLY PALAEOZOIC TUBIDITE SEDIMENTATION

Continental and arc derived pelitic turbidites were deposited in a probable back arc basin setting along the Pampean margin in the early Palaeozoic. Remnants of this back arc basin form the protoliths to the Pringles Metamorphic Complex in the Sierras de San Luis.

5.4 FAMATINIAN CYCLE

Early Ordovician Deformation, metamorphism, mafic and felsic intrusion

During the Ordovician, closure of the Iapetus Ocean and collision of the Precordillera with the Pampean margin of the Gondwana craton (Dalla Salda and others, 1992, 1996, Dalziel and others, 1996) resulted in amalgamation of the Cambro-Ordovician back arc (Pringles Metamorphic Complex) and the Cambrain basement during a widespread deformational, metamorphic and magmatic event known as the "Ciclo orogénico Famatiniano" (Aceñolaza & Toselli, 1976), Famatinian Orogen (eg. Dalla Salda and others, 1992) or "Ciclo Famatiniano" (Dalla Salda, 1987). A compressive deformation (D1 in the Cambro-Ordovician rocks, D2 in the Cambrian rocks) at mostly upper amphibolite facies, though locally, granulite-facies was accompanied by the development of kilometre-scale east-dipping ductile shear-zones with, orthogonal westerly-directed thrust movement. Dalla Salda (1987) and Toselli and others, (1992) ascribed this deformation (in the Córdoba region) to the D2 domain. Primary structures were mostly overprinted, although original graded beds and turbidite sequences are still recognisable in places within the Cambro-Ordovician, Pringle Metamorphic Complex. A number of mafic/ultramafic bodies (the Las Aguilas Group) which intruded the sediments were involved in the deformation and represent a significant mantle-derived heat source contributing to the high temperature metamorphic conditions. In the Cambrian basement, the earlier D1 fabrics were openly to tightly folded and locally recrystallised to form a new foliation (S2).

The high-grade metamorphic episode during the Famatinian cycle was closely followed by extensional tectonism under upper-greenschist-facies conditions accompanied by emplacement of S-type granite and pegmatite (undifferentiated

granitoids and pegmatite). Extensional tectonism and granite emplacement was restriced to discrete belts and resulted in pervasive retrogression within those belts of the high-grade metamorphic assemblages. The low-grade San Luis Formation was probably deposited during this extensional phase. Igneous activity culminated at ~ 470 Ma in the emplacement of granodioritic to tonalitic intrusives (Tamboreo Granodiorite & Bemberg Suite) that are spatially restricted to within the San Luis Formation. U-Pb monazite data (Camacho and Ireland, 1997) from the Pringles Metamorphic Complex and U-Pb urananite data (Linares, 1959) from pegmatites suggest the terrain had cooled through 600 ˚C by ~450-460 Ma.

5.5 ACHALIAN CYCLE

Early Devonian deformation, metamorphism and granite intrusion

resumption of convergence on the western margin of Gondwana in the mid Palaeozoic is evidenced by a widespread compressive deformation of the Ordovician cover sequence (San Luis Formation) and older crystalline basement, and the development of an Early Devonian magmatic arc. The deformation was dominated by orthogonal westerly-directed thrusting, with a component of sinistral shearing, both at greenschist facies, and the development of regionally extensive ductile and brittle-ductile, conjugate shear-zones. Locally, outside the principal shear zones, the basement and cover rocks were open to isoclinally folded and refolded with an axial planar crenulation surface developed in places. Dalla Salda (1987) defined this deformation as D3, placing it in the "Ciclo Famatiniano", however, U-Pb and Ar-Ar data (Camacho and Ireland, 1997; Camacho, 1997) indicate this is a discrete event separated from the Famatinian cycle by at least 60 Ma.

Peraluminous to slightly peralkaline felsic melts, generated from partial melting of MgO depleted crustal rocks (Dalla Salda and others, 1995) intruded into the metamorphics discontinuously during and after shear zone development. Some of the shear zones (eg the La Lajas Complex) were the locus of multiply injected subconcordant granite and later pegmatite intrusion. In other areas, circular, zoned, and fractionated plutons, commonly coalesced forming batholiths, and crosscut early,

greenschist-facies shear-zones. Uranium-lead zircon dating of the granites suggests that initial plutonism was around 404 Ma (Camacho and Ireland, 1997). Ar-Ar ages from greenschist-facies mylonite zones and brittle-ductile strike-slip faults and fractures suggests that deformation continued through till ~355 Ma (Camacho, 1997), however, granite intrusion mayhave continued into the Caboniferous. The Achalian Cycle derives its name from the Achala Batholith, the largest of the Devonian Batholiths in the southern Sierras Pampeanas, which is exposed north of the Sierra de Comechingones in the Sierras Grandes. The cycle probably corresponds to the "Fase Precordilleránica" (Astini, 1996) in the precordillera west of the Sierras Pampeanas where it is related to the amalgamation of the Chilena terrane.

5.6 CARBONIFEROUS - PERMIAN SEDIMENTATION

Following peneplanation, and later marine transgression, fluvio-lacustrine and shallow-marine sediments of the Paganzo Group (Gonzále & Aceñolaza, 1972) were deposited during the Carboniferous and Permian times. These sediments, which are not represented in *Sierras de San Luis y Comechingones* may have covered much of the crystalline basement, however, only remnant outcrops of the group are now preserved in narrow (<2 km wide) grabens. These grabens, possibly initiated during syn-sedimentary extensional faulting, were active after the cessation of sedimentation and prior to the Andean Cycle deformation. It is possible that these late-Palaeozoic sediments were first deposited in basins controlled by a regional wrench tectonic regime late in the Achalian cycle.

5.7 MESOZOIC SEDIMENTATION AND MAGMATISM

During the Early Cretaceous, extensional faulting, including probable reactivation of some basement faults along the eastern margin of the southern Sierras Pampeanas, accompanied local deposition of continental clastics in half grabens. Mafic magmas, generated by partial melting (<2%) of garnet-bearing OIB-like mantle (Kay & Ramos, 1996), formed minor dykes or extruded as basalt flows intercalated with the sediments. These extrusive occur to the north of *Sierras de San Luis y Comechingones* in both the Sierras de San Luis and the Sierras de Córdoba. Age

determinations on the mafic rocks range from 150 Ma to 56 Ma (Linares & González, 1990).

5.8 ANDEAN CYCLE

During the Cainozoic, in the Sierras de San Luis and Valle de Rio Conlara dominantly andesitic lavas extruded, doming basement rocks and forming volcanic edifices with extensive pyroclastic aprons. This magmatism, which is dated between 9.5 Ma and 1.9 Ma (Table 4) was probably related to an extensional phase following the development of flat subduction of the Nazca plate (Smalley and others, 1993) in the mid-Miocene. The cessation of magmatism is marked by the commensement of east-west compression that resulted in inversion of the Cretaceous basins (Schmidt, 1993) and block thrusting of the basement rocks, forming north-south oriented ranges, separated by intermontane basins. The ranges are bounded by escarpments developed on moderate to steeply-dipping reverse faults (Jordan and Allmendinger, 1986; Martino and others, 1995; Costa, 1996), many of which show a reactivated and long-lived history. Costa interpreted most significant movement in the region to have occurred during the Late Pliocene-Pleistocene with further movement continuing during the Quaternary.

SECTION II: ECONOMIC GEOLOGY

by Roger Skirrow

1. INTRODUCTION

The San Luis map area contains a wide range of metallic and industrial mineral occurrences, including Au (Ag, Pb, Zn) in the La Carolina and Santo Domingo districts, Ni-Cu-Co (PGE, Au) at Las Aguilas and Virorco, and W, Be, Li, Nb and Ta in a large number of districts (see Figure 2 in previous Section). Minor occurrences of Cu, Sb, Sn and U are also present, and the region is well known for its production of muscovite, feldspar, quartz, onyx and high quality building stones (marble, granite, etc.).

Geological and resource data on mineral occurrences have been compiled in a database (ARGMIN, in MicroSoft Access; Skirrow & Trudu, 1997) using a

combination of data from the literature and field data. The principal deposits in most mining districts of the map area were investigated in the field, with observations subsequently entered into the ARGROC and ARGMIN databases. Petrography of ore and host rock samples (thin sections and polished thin sections) was recorded in a petrographic database (Sims and others, 1996), and selected samples for ore genesis studies were analysed for whole rock geochemistry (Lyons and others, 1996; Lyons & Skirrow, 1996), stable isotopes of oxygen, hydrogen and sulfur (Lyons & Skirrow, 1996), as well as $^{40}Ar/^{39}Ar$ radiometric age dating (Camacho, 1997). Geographic coordinates were measured by GPS (locational accuracy ±50m), whereas those occurrences not visited in the field were generally located on airphotographs and their geographic coordinates digitised. The locational accuracy for photo-located occurrences is ±200 m. The locations of remaining occurrences are taken from the original data sources, which in some cases allow only very approximate geographic coordinates to be estimated (up to ±3000m). Locational and commodity data for a number of mineral deposits in Departamento Pringles were derived from the CREA (1996) mineral deposit database. The positional accuracy of occurrences from this data source is estimated as ±400m.

Mineral occcurrence data as well as non-metallic mineral and dimension stone occurrences are shown on the 1:100 000 scale metallogenic map accompanying this report. Output data sheets from the ARGMIN database are appended to the report. Details of the geology and grade-tonnage data, where available, for individual metallic mineral occurrences may be found in the database. The 1:250 000 scale Metallogenic Map for the Sierras Septentrionales de Córdoba shows the mineral occurrences in relation to 'prospectivity domains' or areas of mineral potential. These domains are defined on the basis of 'metallogenic models' for each mineral deposit style, which were developed from the observations and interpretations presented in the following sections. For further datasets of mineral potential, the reader is referred to the *Atlas Metalogenético* (1:400 000 scale) for the Sierras Pampeanas mapping project (Skirrow and Johnston, 1997) and project GIS (Butrovski, 1997) in which metallogenetic models for the principal styles of metallic mineralisation are presented as separate coverages.

2. METALLIC MINERAL OCCURRENCES

2.1 NI-CU-CO (PGE-AU) DEPOSITS

2.1.1 LAS AGUILAS - VIRORCO NI-CU-CO DISTRICT

Regional setting: Mafic and ultramafic plutonic bodies up to 5 km in length crop out in an 80 km NNE trending belt in the Sierras de San Luis. The Las Aguilas and Virorco Ni-Cu prospects, located 40-45 km NE of the city of San Luis, are the best known deposits in the belt. The petrology of the mafic-ultramafic rocks and/or associated mineralisation have been described by numerous workers, including González Bonorino (1952), Pastore and Ruíz Huidobro (1952), Brodtkorb and others (1976), Sabalua and others (1981), Sabalua (1986), Brogioni (1992), Malvicini and Brogioni (1993), Brogioni and Ribot (1994) and Gervilla and others (1995).

The mafic-ultramafic bodies in the Las Aguilas - Virorco district occur within a belt of Cambro-Ordovician high grade metasedimentary gneisses and schists, orthogneiss, amphibolite and pegmatite of the Pringles Metamorphic Complex (Sims, these Notes). An orthogneiss dated by U-Pb zircon methods at 484±7 Ma (Camacho & Ireland, 1997) suggests that metamorphism peaked at high grade in the early Ordovician. Magnetite is locally abundant in the high grade rocks, and together with the high magnetic susceptibility of the mafic-ultramafic bodies, has resulted in a broad regional magnetic domain of high amplitude within the Pringles Metamorphic Complex. The Las Aguilas deposit occurs towards the northwest margin of this magnetic domain.

U-Pb dating of zircons from a plagioclase-orthopyroxene magmatic segregation from the Las Aguilas Este mafic-ultramafic body indicates a crystallisation age of 478±6 Ma (Figure 1; Camacho & Ireland, 1997), which is the inferred age of high-grade metamorphism. The close temporal and spatial relationship between emplacement of the mafic-ultramafic complex and high-grade metamorphism suggests these intrusive rocks may have been the heat source for the metamorphism (Sims and others, this Report).

Gneisses enclosing the Las Aguilas mafic-ultramafic rocks are mylonitic, with subvertical stretching lineations on a steeply dipping N-S foliation. Margins of the larger mafic-ultramafic bodies, and the centres as well as margins of the numerous lenticular smaller bodies, are recrystallised with high grade metamorphic textures and are foliated in places. The deformed margins led González Bonorino (1961) to suggest that emplacement of the intrusions commenced during deformation, an interpretation supported in the current studies (Sims and others, this Report). The smaller bodies are generally hornblende amphibolites, whereas the larger bodies at Las Aguilas consist of mainly norite (or melanorite) and pyroxenite with minor melagabbronorites,

leuconorite, peridotite and dunite (Sabalua, 1986; Brogioni, 1992; Malvicini and Brogioni, 1993). Contacts are generally subvertical at Las Aguilas. Compositional layering is well exposed in subhorizontal 'strata' of mainly hornblende norite in the Virorco igneous body (González Bonorino, 1961).

Geology: Diamond drilling and surface mapping at the Las Aguilas Este body (Sabalua, 1986), which contains the most significant Ni-Cu-Co mineralisation discovered to date, indicates that the igneous rocks are zoned horizontally from east to west as follows (Figure 2): a thin pyroxenite margin; dunite; alternating pyroxenite and dunite units; pyroxenite; norite (or melanorite) with minor pyroxenite. Pyroxenite and melanorite exhibit cumulate textures involving orthopyroxene, plagioclase, hornblende and phlogopite (Malvicini & Brogioni, 1993). As part of our petrological investigations of the Las Aguilas Este deposit, textural studies of dunite and pyroxenite in drill hole 6/4 have revealed that fresh to partially serpentinised euhedral olivine, orthopyroxene and chromian spinel formed cumulates with interstitial net-textured, semi-massive or disseminated sulfides (Figure 3). The preserved primary magmatic cumulate textures and gross compositional zonation westwards from ultramafic to mafic rocks within the Las Aguilas Este body suggest, by comparison with mafic-ultramafic intrusions elsewhere (Naldrett, 1989), that the

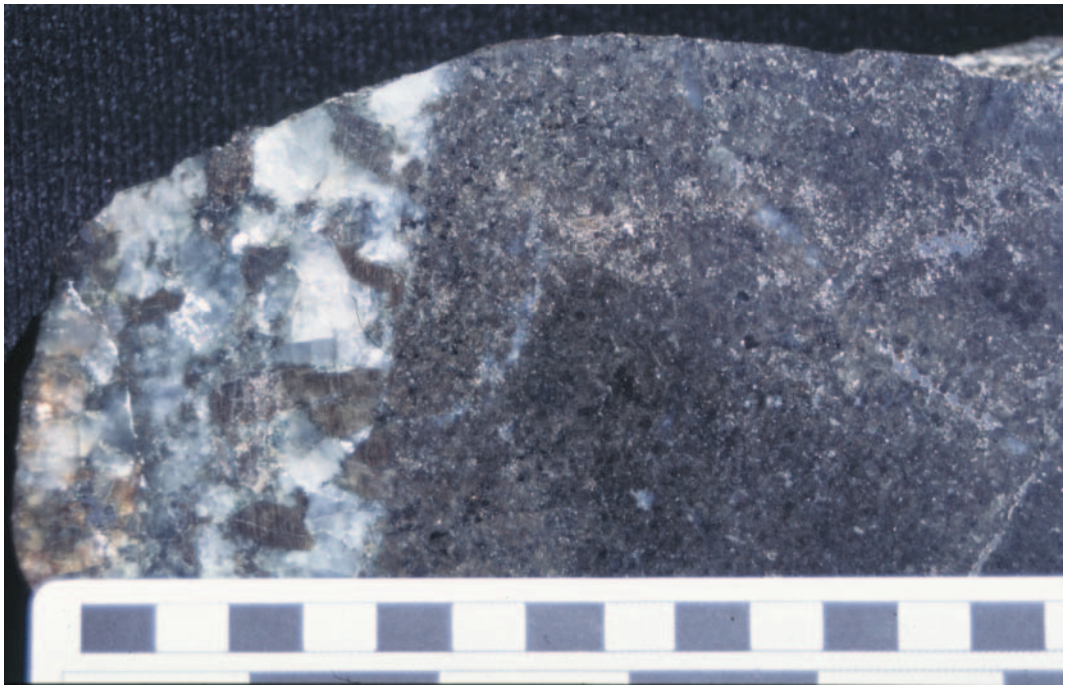

Figure 1. Plagioclase-orthopyroxene differentiate or segregation (light colour, left side of sample), within sulfidic pyroxenite, Las Aguilas igneous body. Euhedral,

magmatic zircons separated from the felsic rock were dated at 478±6 Ma (Camacho & Ireland, 1997). Sample A95JS080F, scale bar divisions 1cm.

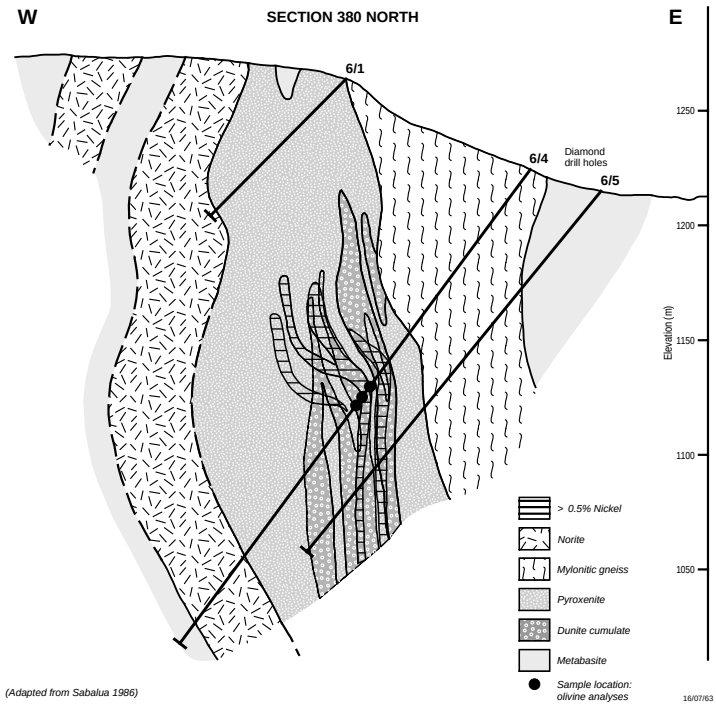

Figure 2. Cross section of the Las Aguilas Ni-Cu-Co deposit (Section 380 North) showing Ni distribution (>0.5% contour) in relation to dunite cumulate and pyroxenite. Selected samples from drill hole 6/4 with olivine (locations indicated) were analysed by electron microprobe at the Research School of Earth Sciences, Australian National University (see text and Fig. 5).

eastern contact may be close to the original base of the intrusion. Subsequent (and/or synchronous) deformation resulted in rotation of contacts to subvertical orientations as well as boudinage, shearing and possibly transposition of parts of the intrusion(s).

A resource of 2 220 000 tonnes @ 0.51% Ni, 0.50% Cu and 0.035% Co has been outlined in the Las Aguilas deposits (Sabalua, 1986). Zones of highest grade Ni (>0.5% to ~1.5%) correspond with those of Cu and Co in the Las Aguilas Este deposit, and occur predominantly in pyroxenite and dunite units towards the eastern contact (Figure 2; Sabalua, 1986). Grade contours of Ni closely follow dunite and pyroxenite contacts in the lower portions of the explored deposit, but the contours evidently are discordant to these contacts in the upper levels where pyroxenite is the principal host to sulfide mineralisation. Based on observations in drill hole 5/2 which

intersects the upper parts of the Las Aguilas Este deposit, Malvicini and Brogioni (1994) suggested the ore sulfides replaced silicates, and occur only in sheared igneous rocks. However, in deeper parts of the deposit (e.g drill holes 6/4, 6/W2) pyrrhotite, pentlandite and chalcopyrite are interstitial to well preserved cumulate olivine, orthopyroxene and chromian spinel in unfoliated dunite and pyroxenite, and show no evidence of replacement of the silicates (Figure 3). In these deeper zones veinlets of pyrrhotite and chalcopyrite cutting the silicates are volumetrically very minor, and represent local, limited, remobilisation of sulfides during post-crystallisation brittle deformation (Figure 4). It is possible that larger scale remobilisation of sulfides occurred in the upper parts of the deposit during deformation, although Sabalua (1986) described sulfides in the upper zones (e.g. drill hole 5/2) as massive and disseminated with only minor veins.

Minor tabular phlogopite occurs within the interstitial sulfides and at contacts of sulfides with olivine or orthopyroxene; in some cases it also occurs with clino-amphibole replacing pyroxenite (Malvicini & Brogioni, 1993). Other minerals occurring in the igneous rocks are: rare clinopyroxene, biotite, magnetite, ilmenite, and graphite which is conspicuous in some of the mylonitic gneisses close to the igneous bodies and within some leucocratic and sulfide mineralised igneous rocks. Late carbonate-pyrite-amphibole(?) veins and chlorite cut the igneous rocks.

In addition to the ore minerals mentioned, the following phases have been reported (Sabalua and others, 1981; Malvicini & Brogioni, 1993; Gervilla and others, 1995): gold, electrum, platinum-group minerals (PGM; tellurides and arsenic sulfides), cobaltite, cubanite, molybdenite, tellurobismutite, altaite, mackinawite. Pyrite,

Figure 3. Photomicrograph of cumulate olivine (clear, subhedral to ovoid, fractured crystals) and interstitial pyrrhotite-chalcopyrite-pentlandite (opaque). Black ink circle in centre of photomicrograph marks an olivine crystal analysed by electron microprobe (see text and Fig. 5). Las Aguilas diamond drill hole 6/4, 139.2m. Plane polarised light, scale bar 2mm.

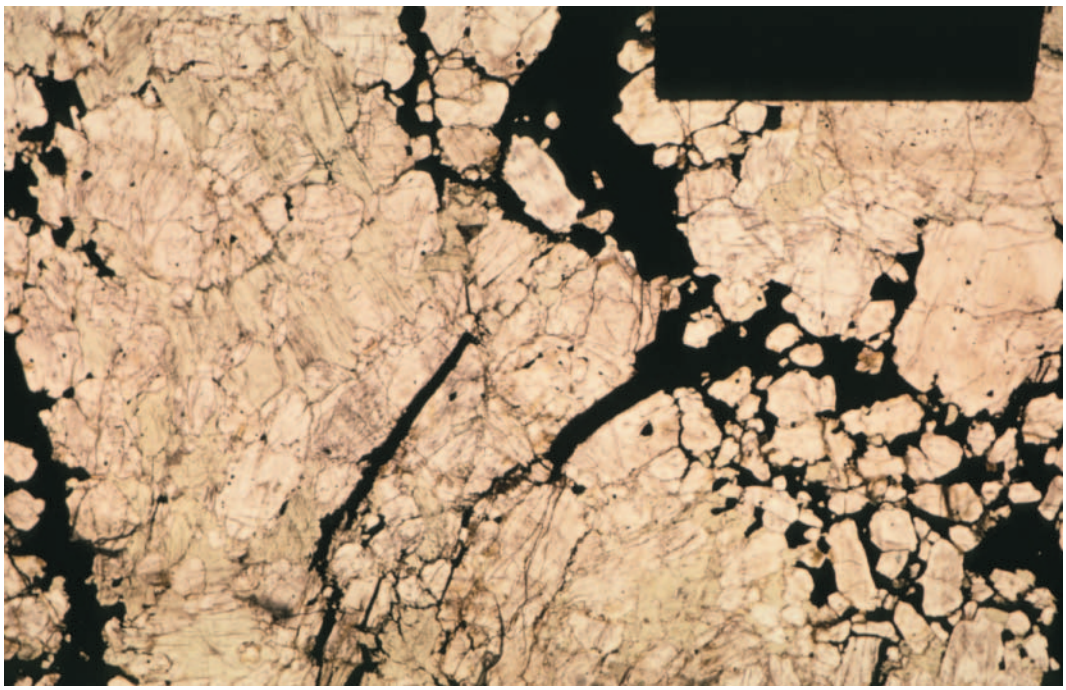

Figure 4. Photomicrograph of pyroxenite (orthopyroxene and clinopyroxene) with veinlets of pyrrhotite-chalcopyrite cutting pyroxene crystals. Pyrrhotite, chalcopyrite and pentlandite also occur in irregular patches interstitial to pyroxene cumulate crystals. The cross cutting sulfide veinlets are interpreted to have formed by local remobilisation during deformation of pre-existing magmatic sulfides (see text). Las Aguilas, sample A95RS082A. Plane polarised light, scale bar 2mm.

marcasite, goethite, hematite, greigite, violarite, bravoite, covellite and digenite are supergene alteration products. Native platinum and/or PGM occur in chromite (Sabalua and others, 1981; Malvicini & Brogioni, 1993) and in pyrrhotite, pentlandite and chalcopyrite (Gervilla and others, 1995). At least some PGM appear to postdate crystallisation of the mafic-ultramafic rocks (Gervilla and others, 1995), although PGM inclusions in chromite may be magmatic. Analyses of up to 2.8 ppm Pt, 0.5 ppm Pd and 0.3 ppm Au have been reported (Sabalua and others, 1981; Malvicini & Brogioni, 1993), but precious metals have not been analysed systematically in drill holes.

Genesis: The results of electron microprobe analyses of olivines from high grade dunite and peridotite from Las Aguilas Este (Figure 5) indicate Mg/(Mg+Fe) ratios of 80.2-82.6%, which correspond to crystallisation from a magma with Mg/(Mg+Fe) ratio 56-59% (assuming $K_{D,\ olivine\text{-}liquid} = 0.3$; Roeder & Emslie, 1970). These Mg-numbers are typical of mafic magmas, with SiO_2 contents of ~52%; e.g. Hoatson and others, 1992). Whole rock geochemistry of the igneous rocks at Las Aguilas indicate the parent magma was tholeiitic (Sims and others, this Report), corroborating the suggestion of Sabalua and others (1981). A similar conclusion was reached by Brogioni and Ribot (1994) for the La Malada and La Gruta gabbroic bodies to the north of Las Aguilas. Furthermore, the Ni contents of olivines at Las Aguilas Este suggest this magma was somewhat Ni-depleted as compared to layered mafic intrusions elsewhere (Figure 5; Simkin & Smith, 1970). Following Naldrett (1989), this observation is consistent with a model in which sulfide liquid was present as segregations in the mafic parent magma, and Ni partitioned preferentially into the sulfide liquid leaving a Ni-depleted magma from which olivine crystallised. In this model, the sulfide liquid settled gravitationally into zones of cumulate olivine, orthopyroxene and chromian spinel, and cystallised to form disseminated, net-textured and massive Fe, Ni and Cu sulfides interstitial to silicates and oxides.

Chromian spinel compositions were reported by Malvicini and Brogioni (1993) and, based on comparison with chromian spinels from the Bushveld Complex, were suggested to have formed hydrothermally. While it is possible the chromite compositions were modified during subsolidus reactions, the cumulate textures and concentration in dunites and peridotites in the Las Aguilas Este deposit supports the proposal of their initial magmatic cystallisation in association with olivine, orthopyroxene and Fe, Ni and Cu sulfides.

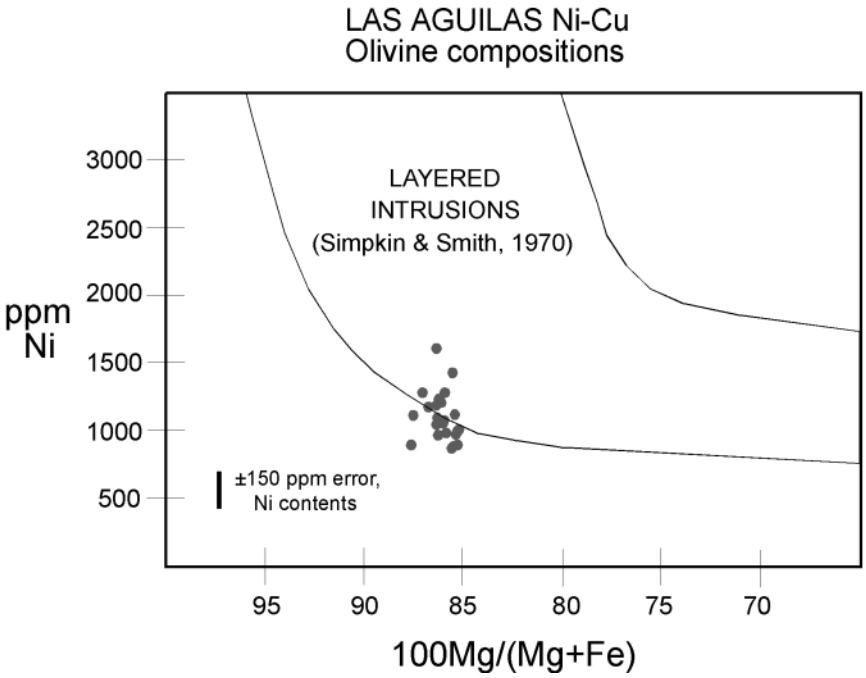

Figure 5. Olivine Mg/(Mg+Fe) versus Ni contents, Las Aguilas Ni-Cu deposit, analysed by electron microprobe (wavelength dispersive spectrometry) at the Research School of Earth Sciences, Australian National University. The field for layered mafic intrusions elsewhere in the world is from Simkin and Smith (1970). Diamond drill hole 6/4.

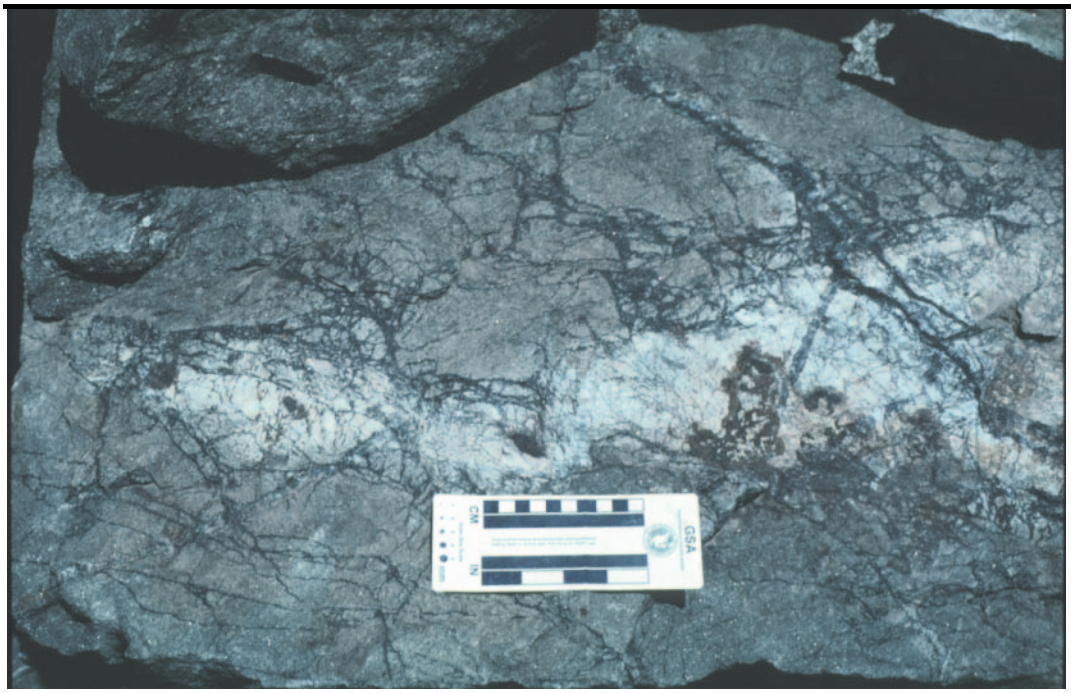

Figure 6. Tourmaline-quartz-epidote-scheelite vein network (black) and associated(?) quartz-sericite alteration patch (cream) in biotite schist, La Florida. Site A95RS092, scale bar 10cm.

The inferred mafic (tholeiitic) parent magma composition, in conjuction with olivine and chromite compositions and bulk rock Pt/(Pt+Pd) vs. Cu/(Cu+Ni) relationships (Naldrett, 1989), strongly argue against the intrusions being of ophiolite (alpine) type. Differentiates of the mafic parent magma crystallised during the early Ordovician, approximately coeval with Famatinian high grade metamorphism and compressive deformation (Malvicini and others, 1991). The whole rock geochemistry of the mafic-ultramafic rocks and metasediments from the Sierras de San Luis is similar to those of rocks emplaced in back-arc basin tectonic settings (Brogioni & Ribot, 1994; Sims and others, this Report). It is proposed that the mafic-ultramafic rocks were emplaced within a back-arc basin as it underwent compression in a collisional tectonic setting.

These observations and the textures, host rocks and mineralogy described above invite comparison with Ni-Cu deposits in synorogenic mafic intrusions (Naldrett, 1989). In particular, there are geological and geochemical similarities with the Devonian gabbroic plutons of northern Maine, USA, which were emplaced syn-tectonically during the Acadian Orogeny, and contain sub-economic Ni-Cu mineralisation (Thompson & Naldrett, 1984). By contrast many of the larger layered mafic

intrusions such as the Bushveld Complex, Great Dyke of Zimbabwe, and Stillwater Complex, were emplaced in cratonic areas.

The presence of graphite in some sulfide mineralised zones and in mylonitic gneiss at Las Aguilas raises the possibility that the mafic parent magma was contaminated by siliceous carbonaceous metasedimentary rocks. González Bonorino (1961) recognised the unusual hybrid compositions of 'basic granulites' at the contacts of the mafic igneous and metasedimentary gneisses. One effect of such contamination may have been to reduce the solubility of sulfide in the magma and, depending on the timing of contamination, could have caused saturation of sulfide earlier in the crystallisation history than otherwise would have occurred (Naldrett, 1989). The significance of such contamination is that it is a potentially favourable process for generation of relatively high grades of Ni sulfides. Whether the sulfides discovered to date at Las Aguilas represent the full extent and highest grades of Ni-Cu-Co (PGE-Au) mineralisation remains unknown. Further work is required to test this hypothetical depositional mechanism, and to investigate the exploration implications for Ni-Cu-Co (PGE-Au) mineralisation in the Las Aguilas district.

2.2 W DEPOSITS

More than 250 named W occurrences have been identified in the San Luis map area, ranging from mines with extensive surficial and underground workings to small pits and shafts. Although some of the principal deposits have been located by GPS and many others have been located on airphotographs and their geographical coordinates measured, a large number of occurrences necessarily have been grouped because of lack of accurate locational data. Groupings are based on those given in the data source (e.g. Ricci, 1971); such groups of occurrences have been assigned the coordinates of principal deposits in the group that have been located on airphotographs or by GPS (if any).

Three main styles of W mineralisation are present: (i) scheelite associated with quartz veinlets in generally low grade metasedimentary sequences, (ii) wolframite with minor sulfides in large quartz veins, and (iii) scheelite associated with calcsilicate rocks. Minor wolframite and scheelite also occur in pegmatites. Style (i) includes deposits in the La Florida - Paso del Rey - Santo Domingo belt of the eastern Sierras de San Luis, and deposits in the Pancanta district south of La Carolina. Wolframite-quartz veins of style (ii) are evidently restricted to the La Carolina - San Román district. Both styles (i) and (ii) are distributed preferentially in the San Luis Formation, a sequence of early

Ordovician metapelites, metapsammites and metaconglomerates that were deposited during and after Famatinian extensional deformation, and that were intruded by felsic dykes. The two belts of San Luis Formation occur to the west of the Rio Guzman Shear Zone, and represent thrust slices that developed during compressive deformation in the Devonian (Sims and others, this Report). Type (iii) calcsilicate-associated scheelite occurrences are confined to mainly the Conlara Metamorphic Complex to the east of the Rio Guzman Shear Zone where calcsilicate rocks, metacarbonates and amphibolites are intercalated with metapelitic rocks. The major districts of style (iii) W mineralisation within the map area are situated in the sierras del Morro, Los Morillos, Yulto and La Estanzuela.

2.2.1 LA FLORIDA - PAMPA DEL TAMBOREO - SANTO DOMINGO W BELT

The geology and genesis of W deposits in this belt have been discussed by numerous workers, including Monchablon (1956), Stoll (1963), Ambrosini and others (1981), Leveratto and Malvicini (1982), Carotti and others (1985), Brodtkorb and others (1984, 1985), Hack and others (1991), Fernandez and others (1991) and Ramos (1990, 1992). The W occurrences are distributed in a belt approximately 25 km long and tend to form clusters of deposits in areas of a few kilometres diameter.

Regional setting: The regional geology and structure of the La Florida - Pampa del Tamboreo - Santo Domingo region is complex (Sims and others, this Report). The Rio Guzman Shear Zone marks the boundary between the Ordovician San Luis Formation to the west and the Cambrian Conlara Metamorphic Complex to the east. A zone of D_3 shears separate the San Luis Formation from metapsammites and metapelites of the Pringles Metamorphic Complex to the west, whose tectonic and metamorphic history differs from that of the younger San Luis Formation. These quartzo-feldspathic metasediments were initially metamorphosed to medium grade during D_1 in the early Ordovician, then intruded by extensive granitoids and tourmaline-bearing pegmatites during D_2 extension. Regional low grade retrogression accompanied D_2, resulting in widespread muscovite±tourmaline development in schists. Following deposition of the San Luis Formation late- to post-D_2, the Pampa del Tamboreo granodiorite was emplaced at 470±5 Ma (Camacho & Ireland, 1997), producing a contact metamorphic aureole in the San Luis Formation. This granodiorite and the San Luis Formation were subsequently intruded by numerous plagioclase-quartz porphyritic rhyolite dykes. The metasedimentary and igneous rocks were intensely deformed and metamorphosed to low grade during the Devonian D_{3-4} compressive events, with strain generally localised in and near shear zones. Although no Devonian granites are known to crop out in the

La Florida - Santo Domingo region, a broad zone of low aeromagnetic response occurs near La Florida and may represent a Devonian granite in the subsurface.

Geology: The principal features that are shared by many of the W deposits in the La Florida - Santo Domingo belt are as follows.

- Scheelite is the primary ore mineral
- The W mineralisation is associated with quartz veinlet networks or is disseminated
- Host rocks are part of the low grade metamorphic rocks of the San Luis Formation, except for some of the westernmost deposits in the belt (Los Cocos district)
- Deposits occur within or in proximity (<1 km) to zones of intense D_3 deformation
- Scheelite commonly occurs in feldspathic rock types such as plagioclase-quartz porphyry to aplitic bodies and meta-arkosic rocks
- Quartz veinlet networks are most intensely developed in relatively competant units where they are in contact with less competant rocks, for example metapsammite, quartzite or felsic porphyry/aplite within phyllite or metapelitic schist
- The mined zones are broadly confined to particular compositional layers but locally transgress layering
- Veins and veinlet networks are deformed and vein minerals are recystallised
- Sulfides and oxides are very low in abundance; pyrite, arsenopyrite, and ilmenite altered to rutile, occur at La Teodolina (Ramos, 1992; Brodtkorb and others, 1985), and pyrite is widespread (e.g. Carotti and others, 1985)
- Tourmaline and white mica commonly are very abundant in proximity to the quartz veinlet systems with scheelite mineralisation; calcsilicates such as epidote and titanite as well as apatite, fluorite and carbonate occur in veins and wall rocks with scheelite in some deposits (Figure 6; see also Brodtkorb and others, 1985; Carotti and others, 1985; Hack and others, 1991), and scapolite, hornblende and garnet were reported in scheelite-bearing quartzite host rocks in the Los Cocos district (Stoll, 1963; Brodtkorb and others, 1985)
- Biotite is very abundant in mineralised zones of some but not all deposits (e.g. La Teodolina), and is partially chloritised

Other critical observations of relevance in understanding the timing and depositional controls of the W deposits are as follows.

1. Felsic dykes (some previously interpreted as felsic volcanics, Brodtkorb and others, 1984) cutting the compositional layering in the San Luis Formation (e.g. at El Araucano) are mineralised with quartz-scheelite veins; these dykes are of identical texture and mineralogy to a dyke that intrudes the Pampa del Tamboreo

granodiorite at Puesto Tito. A maximum age of 470±5 Ma is therefore suggested for the formation of quartz-scheelite veinlets.

2. Relatively thin, fine to medium grained, feldspathic bands are present in the San Luis Formation (e.g. at La Riojita), and although they could represent metavolcanics, they are texturally distinct from the prominant porphyritic felsic bodies which at least in some cases are certainly dykes.
3. Quartz veins containing scheelite at Fortuna cross cut the Pampa del Tamboreo granodiorite, but xenoliths of biotite schist in the granodiorite are mineralised at Donosa (Brodtkorb and others, 1985).
4. Intense D_{3-4} deformation has resulted in transposition of compositional layering in large parts of the San Luis Formation, so that many of the porphyritic felsic bands are parallel to both the main foliation and to compositional layering in the metasediments.
5. Mineralised zones in some deposits are confined to structures interpreted to have formed during D_{3-4}, such as F_{3-4} fold hinges and F_{3-4} axial planes (e.g. Los Cocos, Figure 7).
6. Scheelite porphyroblasts in biotite schist at La Teodolina are wrapped by the main foliation which is a crenulation cleavage (Figure 8). Ramos (1992) suggested the scheelite porphyroblasts predated the crenulation cleavage; our observations concur with this conclusion, but we propose that the scheelite overgrew the earlier slatey cleavage. La Teodolina is situated within the D_{3-4} shear zone at the western contact of the San Luis Formation. Both foliations in this area are believed to have formed during D_{3-4} progressive deformation and low grade metamorphism, in the Devonian (Sims and others, this Report), implying a Devonian age of scheelite growth at La Teodolina.
7. Scheelite occurs in tourmaline-bearing pegmatites (e.g. La Teodolina, Ramos, 1992; and in mylonitic quartz-feldspar-tourmaline pegmatite at General Joffre), but the timing of pegmatite emplacement and of the scheelite in the pegmatites is not known.

Genesis: Previous interpretations of the timing and origin of W mineralisation in the La Florida - Pampa del Tamboreo - Santo Domingo belt may be grouped into two main hypotheses. (a) The W was syngenetic, associated with felsic volcanism, and was remobilised during deformation and metamorphism (Brodtkorb & Brodtkorb, 1975, 1979; Brodtkorb and others, 1985; Fernandez and others, 1991; Hack and others, 1991). (b) The W was epigenetic-syndeformational and formed from pneumatolitic or hydrothermal fluids related to granites (Stoll, 1963a,b; Carotti and others, 1985).

Smith and González (1947) noted that scheelite postdated aplite dykes at the Santo Domingo deposit.

An alternative hypothesis is that W was introduced by hydrothermal fluids into the San Luis Formation and schists immediately to the west no earlier than ~470 Ma and most likely during the early Devonian, synchronous with D_3 compressive deformation. The major controls on localisation of scheelite were the presence of D_3 structures such as shear zones and folds, particularly where there were significant competancy contrasts between compositional layers. In the resultant dilational sites (felsic porphyry bodies, quartzites, granitoid contacts, etc), quartz ±tourmaline ±calc-silicate ±fluorite vein networks developed. Scheelite precipitated preferentially in

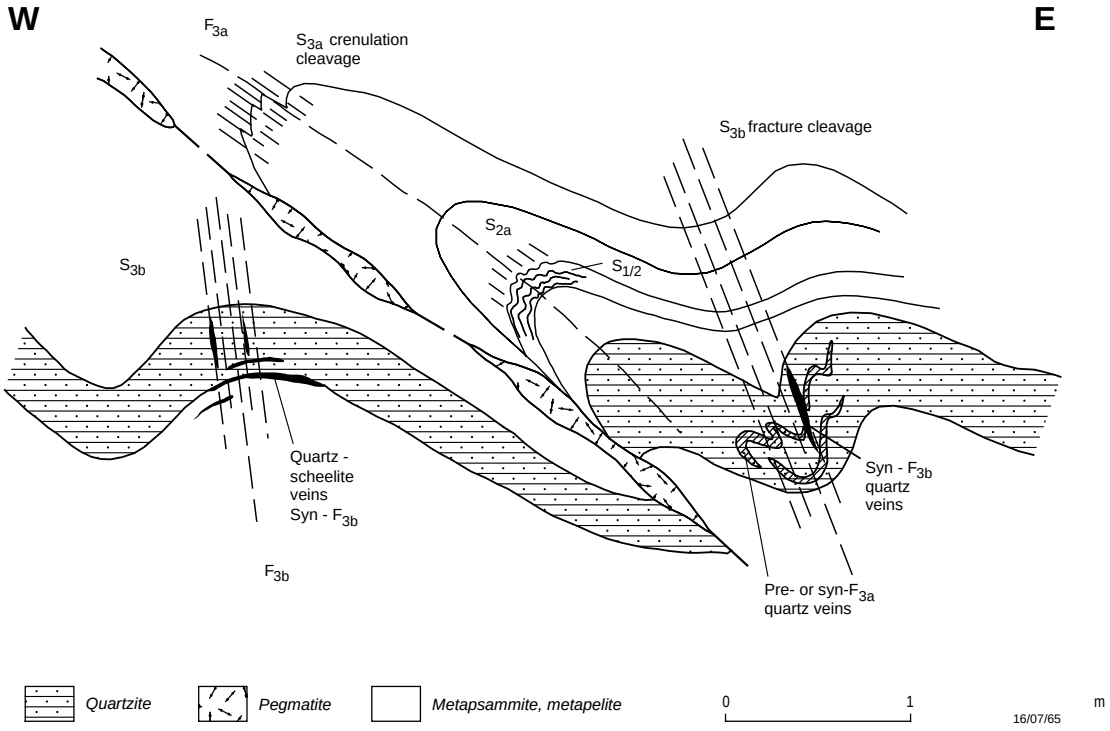

Figure 7. Schematic vertical section of mine workings, Los Cocos W (scheelite) deposit, Pampa del Tamboreo region, drawn from a photograph. Both generations of folds (F_{3a}, F_{3b}) and associated axial planar surfaces (S_{3a}, S_{3b}) are interpreted to correlate with regional D_{3a} and D_{3b} structures which formed in the Achalian tectonic cycle (Devonian). Quartz-scheelite veins occur in D_{3b} structures.

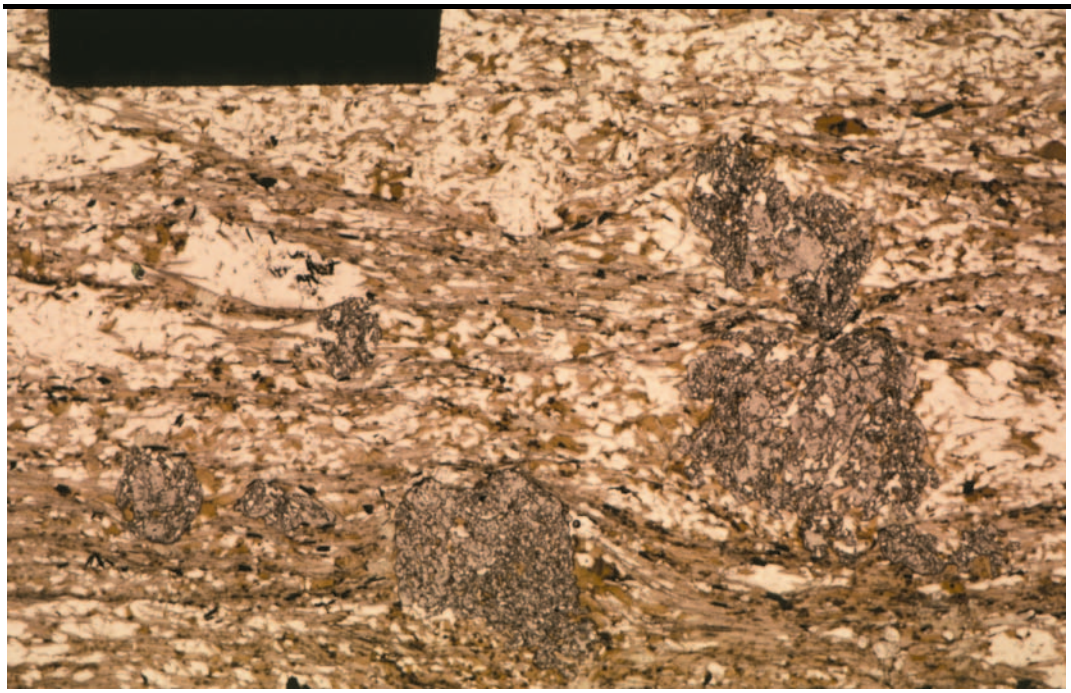

Figure 8. Photomicrograph of scheelite porphyroblasts in biotite-quartz-plagioclase schist, La Teodolina. Biotite and ilmenite define a strong foliation that wraps the scheelite porphyroblasts. This foliation is interpreted to have formed during compressive deformation in the Achalian (Devonian) tectonic cycle. This scheelite predated or grew early in development of this fabric. An earlier, relict foliation defined by biotite inclusions in some scheelite porphyroblasts is oblique to the main biotite foliation (see text). Sample A95RS090B, scale bar 2mm, plane polarised light.

'chemical traps': these consisted of calcic host rocks such as feldspar porphyry bodies, meta-arkosic layers and amphibole-bearing contact metamorphic zones (e.g. at the Pampa del Tamboreo granodiorite).

The hydrothermal fluids transporting W were B±F-rich and probably were moderately acid to neutral (producing white mica or carbonate or biotite alteration) and locally reduced, as indicated by the assemblage biotite-pyrite-arsenopyrite-ilmenite at La Teodolina. Biotite stability in some alteration assemblages suggests temperatures of >350°C for scheelite deposition in these deposits. The source(s) of hydrothermal fluids is not known but if, as proposed, the W was introduced mainly during D_3 deformation then there is potential for fluids to have been contributed by Devonian granitoids, which were partly synchronous with D_3 (Sims and others, this Report).

This hypothesis is consistent with the early Devonian ages obtained for muscovite associated with W mineralisation in the Sierra del Morro district (see below) and at Agua de Ramón in Provincia de Córdoba (Skirrow, Cordoba Notes). A magmatic fluid input was likely in these areas, as indicated from oxygen isotope results.

The possibility that some W was introduced during D_2 extensional deformation in association with pegmatites cannot be ruled out given the presence of scheelite in some tourmaline-bearing pegmatites (e.g. La Teodolina, General Joffre). However, the general lack of W deposits in the broad regional zone of pegmatite-granite-schist to the west of the San Luis Formation argues against a major phase of W introduction at this time.

2.2.2 SAN ROMÁN - PANCANTA W BELT

Regional setting: The San Román - Pancanta W belt is located in the western of the two thrust slices of San Luis Formation, which is separated from the early Devonian Escalerilla granite by a major D_3 shear zone (Sims and others, this Report).

Geology: W mineralisation of the Pancanta district consists of quartz-scheelite veins up to 0.6 m wide hosted by granitoid (Angelelli, 1984) and metasedimentary schists of the San Luis Formation. Some quartz-scheelite veins occur near lamprophyre dykes that intrude the granitoid, and are associated with tourmaline and epidote alteration (Angelelli, 1984). Descriptions in the literature suggest the W in the Pancanta district is of style (i).

W mineralisation in the San Román district 2 km south of La Carolina comprises large tabular to lens shaped quartz veins up to 2 m wide with wolframite and scheelite (style (ii)). The veins are hosted by sheared metapelitic and metapsammitic rocks of the San Luis Formation, within ~300 m of the Escalerilla granite. Intense shearing of host rocks and quartz veins along the western contact zone of the granite has resulted in transposition of compositional layering in the metasediments into parallelism with the veins and with the main shear foliation. Boudinaged quartz veins and granite blocks with quartz pressure shadows near Galeria A (see Figure 130, Angelelli, 1984) indicate shearing was synchronous or postdated granite and vein emplacement. Reverse movement on the shear zone here was west-over-east, as indicated by assymetric shear bands in the metasediments. Minor quartz veins within the margin of the granite are of unknown genetic relationship to the W-bearing veins but probably formed during shearing.

In addition to wolframite and scheelite, the recrystallised saccharoidal quartz veins contain minor white mica, tourmaline, pyrite, chalcopyrite, native bismuth and other bismuth(?) minerals. Hydrothermal alteration of the host rocks within 1-2 m of veins consists of tourmaline and white mica. Tourmaline forms a lineation which pitches in the same orientation as biotite in the sheared metasediments, suggesting hydrothermal alteration was pre- or more likely syn-shearing.

Genesis: Given the early Devonian age of the Escalerilla granite (Sims and others, this Report), and spatial and possible temporal association of the veins in the San Román and Pancanta districts with D_3 shearing (Sims and others, this Report), it is likely that the W veins were emplaced in the early Devonian D_3 compressive deformation, and may be genetically related to the Achalian Escalerilla granite. The association with granites was recognised by Malvicini and others (1991) but the Escalerilla granite was believed to have been Famatinian.

2.2.3 SIERRAS DEL MORRO, LOS MORILLOS AND YULTO W BELTS

The geology of W deposits of the sierras del Morro, Los Morillos and Yulto have been discussed in numerous unpublished reports and publications. Some of the relatively recent publications include: review/synthesis papers by Brodtkorb and Brodtkorb (1975, 1977, 1979); summary by by Angelelli (1984); regional geology, petrography and genesis of the deposits by Llambías and Malvicini (1982) and Delakowitz and others (1991); and a review/synthesis by Brodtkorb and Pezzutti (1991). References to the older literature including studies of individual deposits may be found in these publications. Geochemistry of the host rocks was presented by Delakowitz and others (1991), while K-Ar dating results for minerals from five samples of the host rocks were given by Llambías and Malvicini (1982).

Regional setting: The W deposits of the south-eastern San Luis map area are distributed in three main districts: the Sierra de Los Morillos (or 'Faja Los Morillos', Llambías & Malvicini, 1982), which includes the most important mines; the Sierra del Morro and the Sierra de Yulto (constituting the 'Faja Oriental'). The region forms part of the late Neoproterozoic to early Cambrian Conlara Metamorphic Complex and comprises mainly metapelitic, metapsammitic and met acarbonate rocks and associated amphibolitic rocks that were polymetamophosed and deformed in the early Paleozoic (Sims and others, this Report). Biotite-muscovite±sillimanite±garnet banded gneiss

and schist, foliated migmatite and massive migmatite are the principal metamorphic rock types in the W districts (Llambías & Malvinini, 1982). Leucotonalitic pegmatites and aplite occur subparallel to parallel with the foliation in the medium grade metamorphic rocks. Mylonite and other shear fabrics are common, and generally trend N-S. Zones of dolomitic and calcitic marble up to 5 m thick and amphibolite up to 4 m thick occur in the three abovementioned W districts where, in association with calcsilicate rocks ('tactites'), they host scheelite mineralisation. Intense multiphase deformation has resulted in complex distributions of the marble-amphibolite zones (e.g. at El Morro No. 1, Smith & González, 1947; also Delakowitz and others, 1991).

The San José del Morro granite was emplaced in the central part of the region, and has a K-Ar radiometric age of 365±15 to 380±20 Ma (for biotite; Lema, 1980). Numerous granitic pegmatites containing K-feldspar, plagioclase, quartz and muscovite cut the earlier foliation-parallel tonalitic pegmatites, and are themselves cut by the San José del Morro granite (Llambías & Malvinini, 1982). Some of the granitic pegmatites contain accessory beryl, apatite, fluorite and tourmaline. Aplite is associated with the San José del Morro granite.

Geology: Three types of W mineralisation have been defined: (i) disseminated scheelite hosted by calcsilicate rocks; (ii) wolframite and scheelite in quartz veins; and (iii) non-economic scheelite and minor wolframite in granitic pegmatites where they cross cut calcsilicate zones (Llambías & Malvicini, 1982).

(i) Disseminated scheelite in calcsilicate rocks. Calsilicate rocks ('tactites') occur as zones within and at the contacts of marble or amphibolitic rocks with gneiss. Contacts with the enclosing rocks are commonly gradational. The calcsilicate rocks contain assemblages typical of skarns (Meinert, 1993) and consist of combinations of tremolite-actinolite, biotite/phlogopite, hornblende, epidote, clinozoisite, feldspar, calcite, dolomite, muscovite, and accessory quartz, titanite, magnetite, pyrite, pyrrhotite, fluorite, apatite, chlorite, ilmenite and beryl (Llambías & Malvicini, 1982; Delakowitz and others, 1991). Chalcopyrite, sphalerite, molybdenite, aikinite, bismuthinite and sulfosalts are present in some areas. In the Loma Blanca deposit minor garnet occurs with epidote in alteration patches that overprint banded amphibole-phlogopite/biotite rock (Figure 9). Minor to trace disseminated diopside and vesuvianite and veins of wollastonite occur in marble at Loma Blanca, and at Don José veins containing wollastonite, fluorite and scheelite cross cut marble (J. Sims & M. Marcoux, pers. comm., 1996). Paragenetically later, unoriented, talc, tremolite (replacing diopside), epidote-clinozoisite and chlorite (replacing wollastonite) suggest

the presence of a retrograde hydration stage that post-dated both the amphibolite facies regional metamorphism and later high temperature metamorphism at Loma Blanca.

(ii) Wolframite and scheelite in quartz veins. Although quartz vein hosted W mineralisation represents only 5-7% of total W production for the region, it is widespread in the sierras del Los Morillos and Yulto, and is significant from a genetic viewpoint. The veins consist of quartz, muscovite, tourmaline, fluorite, apatite, epidote, beryl, and accessory titanite, scheelite, wolframite, pyrite, chalcopyrite, sphalerite, bismuthinite, cassiterite, magnetite, hematite, rutile and ilmenite (Llambías & Malvicini, 1982). Tourmaline is ubiquitous in the veins except at the large Loma Blanca deposit, where quartz veins cutting marble contain abundant coarse muscovite, fluorite, apatite and scheelite. In another exposure at Loma Blanca quartz-feldspar pegmatite dykes have offshoot veins of quartz-feldspar that follow the relict banding in the biotite/phlogopite-amphibole rock. Further from the main dykes these thin pegmatites grade into quartz-only veins, and an aureole of unoriented tremolite/actinolite-epidote alteration is developed adjacent to these veins/pegmatites, overprinting unoriented biotite/phlogopite and amphibole in the host rock. The calcsilicate alteration is identical to that in scheelite-mineralised zones. These relationships and vein mineralogy suggest the veins and associated calcsilicate alteration formed at temperatures transitional between pegmatitic and hydrothermal conditions. The veins and associated hydrous alteration postdate the regional deformation and overprint the banding in biotite/phlogopite-amphibole rock.

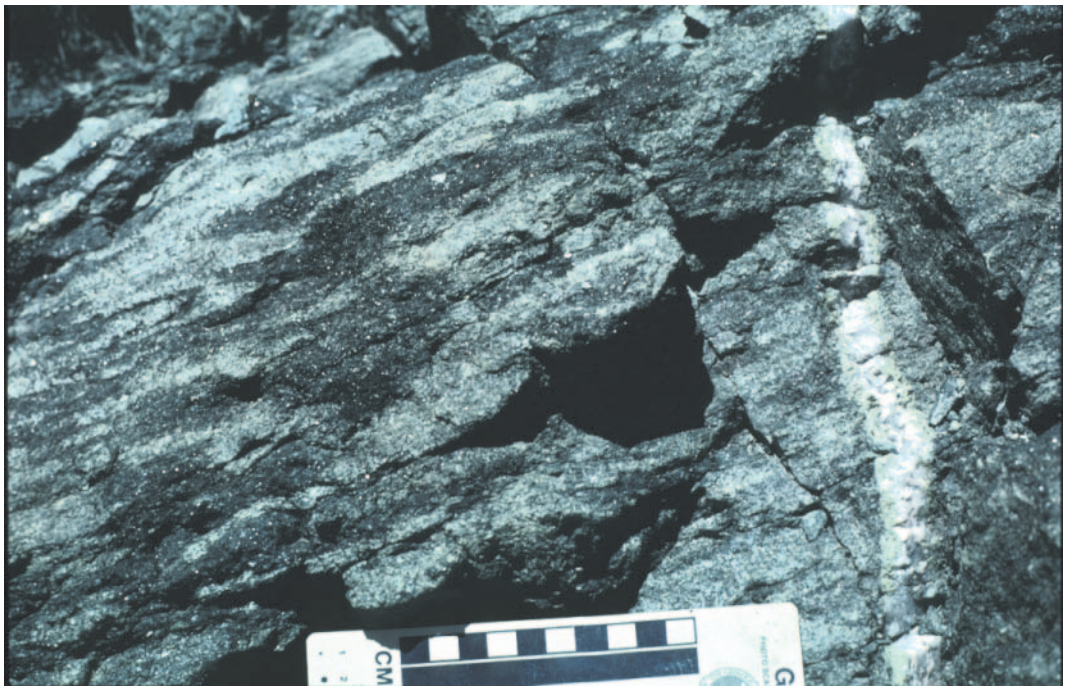

Figure 9. Vein of quartz–K-feldspar with epidote-altered margin cutting amphibole-phlogopite/biotite rock (dark green-grey), Loma Blanca, Sierra de Los Morrillos district. Alteration phases are interpreted to have formed during a progressive metasomatic hydrothermal event during which some tungsten was introduced. Site A95RS101, scale bar 10cm.

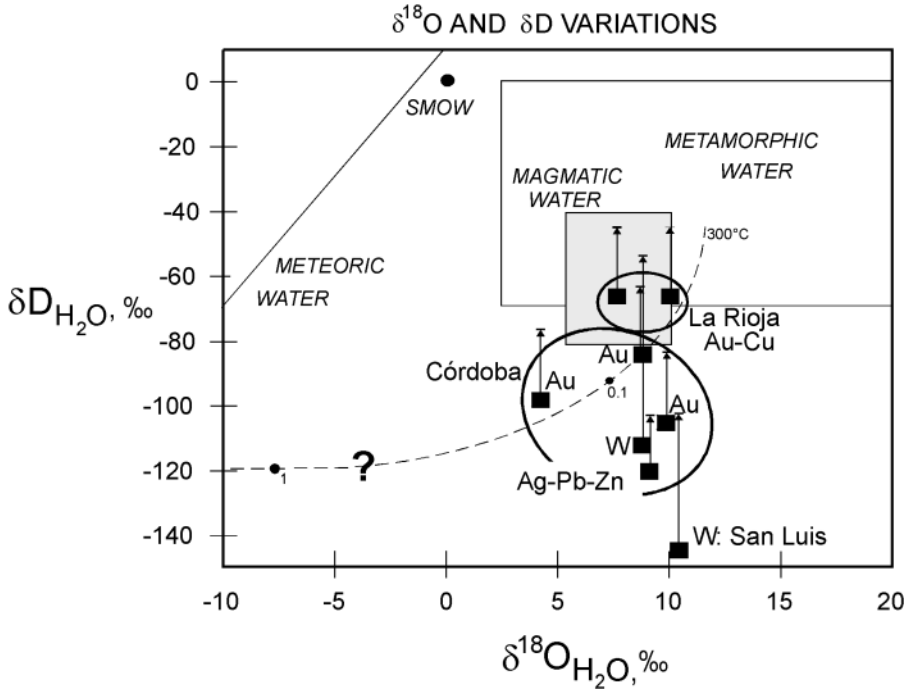

Figure 10. Calculated oxygen and hydrogen isotope compositions of hydrothermal fluids in Au±Cu, Ag-Pb-Zn and W deposits of the southern Sierras Pampeanas, derived from $\delta^{18}O$ and δD values of hydrothermal white mica at the assumed temperatures given in the figure (see text for discussion). SMOW = standard mean ocean water; magmatic water field from Taylor (1979); meteoric water line after Craig (1961); metamorphic water field from Sheppard (1986). Trend of possible reaction of deuterium-depleted meteoric water with sedimentary (or metasedimentary) rocks at low water-rock ratios (1 to 0.1) at 300°C, from Field and Fifarek (1985). Muscovite-water $\delta^{18}O$ fractionation factor from O'Neil & Taylor (1969); muscovite-water δD fractionation factor from Suzuoki & Epstein (1976; lower limit of bars) compared to that of Vennemann & O'Neil (1996; upper limit of bars).

(iii) Non-economic scheelite and minor wolframite in granitic pegmatites where they cross cut calcsilicate zones. This association of W with pegmatites, along with the common presence of apatite, beryl and fluorite in pegmatites, calcsilicate rocks and quartz veins, was cited by Llambías and Malvicini (1982) as evidence for a genetic association of W with pegmatitic fluids.

Genesis: Wollastonite and diopside indicate attainment of relatively high temperatures (>500°C; Winkler, 1979) during either regional metamorphism or during later local thermal metamorphism. The relatively planar, undeformed, veins of wollastonite-fluorite-scheelite, and scheelite with weakly undulose extinction at Loma Blanca, argue in favour of formation of wollastonite and at least some scheelite after regional amphibolite facies metamorphism and accompanying intense deformation. Further evidence for a relatively high temperature thermal event postdating regional amphibolite facies metamorphism is provided by the apparently partially re-set K-Ar age of 428±15 Ma for amphibole in amphibolite at Don José (Llambías & Malvicini, 1982). This age does not correspond to any known thermal event in the San Luis map area, but is between the Famatinian and Achalian deformational-metamorphic-intrusive cycles (Sims and others, this Report). Since the blocking temperature for Ar diffusion for hornblende is 530±30°C (McDougall & Harrison, 1988), it is likely that the amphibolites at Don José were subjected to temperatures exceeding this blocking temperature after the Famatinian cycle, and probably during the Achalian cycle.

Scheelite in wollastonite veins at Don José and in pegmatites suggests introduction of W at temperatures of >500°C, and possibly at lower temperatures where scheelite occurs in quartz-muscovite-fluorite veins. Scheelite may have continued to precipitate through the retrograde stage, for example where it replaced epidote group minerals (Llambías & Malvicini, 1982).

Hydrothermal muscovite within the quartz-fluorite-scheelite veins at Loma Blanca has been dated by the $^{40}Ar/^{39}Ar$ method at 363±1 Ma (early Devonian; Camacho, 1997). This age range is considered to closely represent the time of introduction of W in the vein structures and, by implication, into the calcsilicate zones where textures indicate post-deformational formation of hydrothermal alteration assemblages.

Our studies corroborate the epigenetic timing of W deposition suggested by Llambías and Malvicini (1982) and Malvicini and others (1991) although they proposed a Famatinian (Ordovician-Silurian) age of W mineralisation. The apparent stratabound nature of the W mineralisation associated with calcsilicate rocks in the El Morro

region was cited by Brodtkorb and Brodtkorb (1975, 1977, 1979), Delakowitz and others (1991), and Brodtkorb and Pezzutti (1991) as evidence for a syngenetic volcanic-exhalative origin of the tungsten. Delakowitz and others (1991) described disseminated scheelite oriented in the plane of the regional metamorphic foliation, and suggested pre-tectonic crystallisation of this scheelite, with syntectonic remobilisati on. Given the very intense nature of the regional deformation accompanying medium grade metamorphism, it is clear that the unoriented biotite/phlogopite, tremolite/actinolite, talc and associated minerals such as epidote and scheelite in calcsilicate rocks and marbles crystallised after the amphibolite facies metamorphism. Although it is conceivable that some tungsten accumulated in calcsilicate rocks prior to this metamorphism, all of the textural features of scheelite and calcsilicates described in the literature and observed in the present study can be explained by metasomatic replacement of calcareous and amphibolitic rocks during an early Devonian hydrothermal event. Bulk compositional variations, particularly in carbonate and Ca content, within the carbonate and amphibolitic rocks probably controlled the depositional locations of scheelite. Muscovite in quartz-scheelite veins indicates the hydrothermal fluids were relatively acid, and reaction with calcium carbonate bearing rocks may have caused an increase in fluid pH and increase in activity of dissolved Ca. Both these changes would have favoured scheelite precipitation from the fluid.

The newly determined oxygen and hydrogen isotopic composition of muscovite in a quartz-scheelite vein at Loma Blanca (Figure 10) is consistent with derivation of W-bearing fluids from either magmatic or meteoric fluids that have reacted with wall rocks, or a mixture of both (assuming a temperature of 400°C for muscovite formation). The $^{40}Ar/^{39}Ar$ age of the vein muscovite (363±1 Ma) is significantly younger than the youngest crystallisation age of Devonian granites dated by the U-Pb zircon method in the present project (382±6 Ma, Los Nogales granite), but is within the range of K-Ar (biotite) ages for the San José del Morro granite (365±15 to 380±20 Ma; Lema, 1980). Although the $^{40}Ar/^{39}Ar$ and stable isotopic data are few, both the age and oxygen-hydrogen compositions are similar to our findings for quartz-wolframite veins at Aguas de Ramón (Prov. de Córdoba), and some Au deposits in Córdoba (Figure 11). Consideration of the textural and geological timing relationships discussed above, and the isotopic data, leads us to suggest that the W deposits of the sierras del Morro, Los Morrillos and Yulto may form part of a regional metallogenic event that is spatially and temporally associated with Devonian magmatism and resulted in formation of Au±Cu, W and Ag-Pb-Zn deposits.

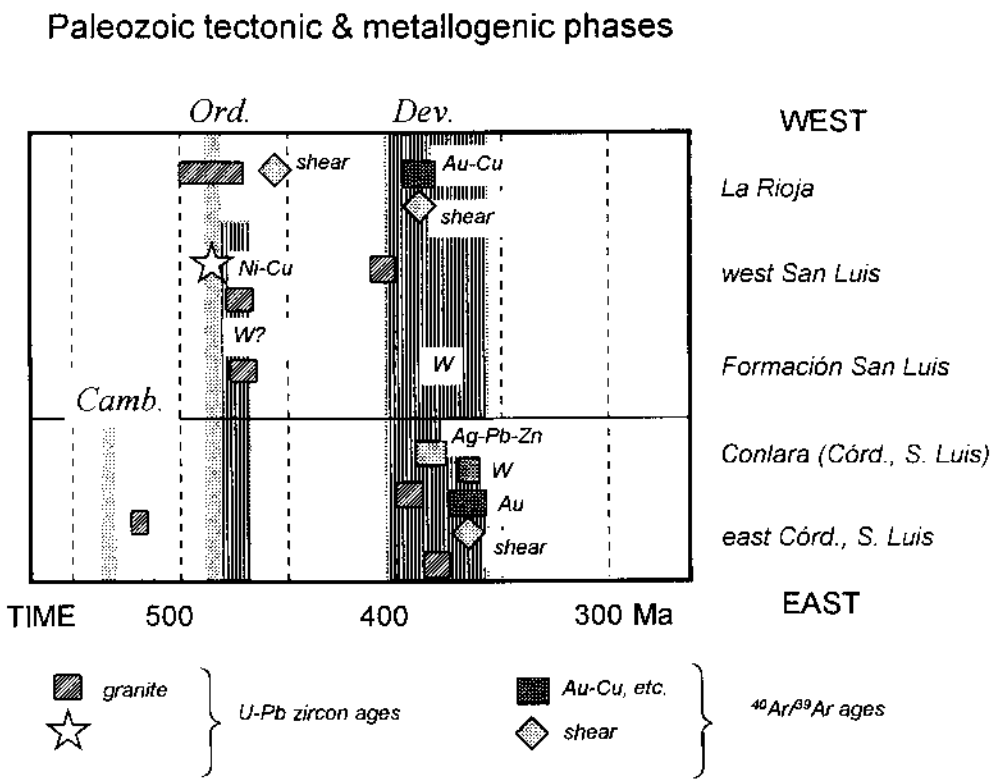

Figure 11. Summary of $^{40}Ar/^{39}Ar$ and U-Pb (zircon) dating in the southern Sierras Pampeanas, in relation to the Pampean (early Cambrian), Famatinian (Ordovician) and Achalian (Devonian) tectonic cycles. Age ranges for metallic mineralisation are based on $^{40}Ar/^{39}Ar$ dating of hydrothermal white mica alteration associated with mineralisation. Shaded vertical bars represent main periods of medium-high grade metamorphism, and ruled vertical pattern represents main periods of low grade metamorphism. Geochronology data from Camacho and Ireland (1996, 1997) and Camacho (1997).

Although the San José del Morro granite which occupies the centre of the region of W mineralisation may be older than the W mineralisation, recent aeromagnetic imagery shows several other possible Devonian granitoids at depths of 300 m to >2 km within the basement rocks of the El Morro region (see Carta Aeromagnetica, Hungerford and others 1996c). All of the documented W deposits of the region occur within ~4 km horizontal distance of the contacts of the outcropping and inferred granites, projected to surface. These intrusions may have provided heat energy and/or the W and associated metals for the deposits of the El Morro region. Whether or not the pegmatites that appear to be associated with W mineralisation were derived from these plutons or form another Devonian magmatic event is not known.

The major controls on location of calcsilicate-associated W mineralisation are interpreted to be as follows:

- Carbonate- and Ca-rich lithologies (marble and amphibole-rich rocks); these have been partially to wholly replaced by calcsilicate assemblages
- Zones of abundant pegmatites and/or quartz veins that postdated the regional high grade metamorphism and deformation
- Proximity to Devonian granitoids; the W deposits occur within ~4 km of outcropping and inferred granite contacts, projected to surface.

The calcsilicate-associated W mineralisation of the El Morro region shares several key characteristics of tungsten skarn deposits (Meinert, 1993), including: (a) an association of scheelite with carbonate rocks, and (b) metasomatic replacement of carbonate and silicate rocks by calcsilicate assemblages including epidote, amphibole, phlogopite/biotite, fluorite, apatite, garnet and sphene. However, the deposits of the El Morro region differ from 'classical' W-skarns in the apparent lack of adjacent plutons. Nevertheless, the association of W with pegmatites and quartz-tourmaline±muscovite±fluorite veins in some deposits suggests that W was transported in high temperature volatile-rich fluids of magmatic affinity. These magmatic-hydrothermal fluids evidently transported pegmatite- and vein-forming components distances of up to several kilometres from any 'causative' plutons. By implication they also may have carried W and other metals for considerable distances from the plutons (cf. Brodtkorb & Brodtkorb, 1979). In calcsilicate-associated W deposits where no pegmatites or quartz veins are present, the hydrothermal fluids may have gained access to the chemical 'trap' rocks via faults and shears that were active during the early Devonian.

2.2.4 SIERRA DE LA ESTANZUELA W DISTRICT AND OTHER W OCCURRENCES OF THE CONLARA METAMORPHIC COMPLEX

Tungsten deposits of the Sierra de La Estanzuela were described by Monchablon (1956) and Angelelli (1984), and the regional geology has been discussed by Fernandez Lima and others (1981) and in the present project (Sims and others, this Report). Other W mineralisation in the Conlara Metamorphic Complex include the Sierra San Felipe district and isolated deposits between Paso Grande and Villa Praga. The geological settings, association of scheelite with carbonate±amphibolitic host rock types and presence of pegmatites described by Monchablon (1956), Brodtkorb and Brodtkorb (1977) and Angelelli (1984) in the sierras de La Estanzuela and San Felipe (e.g. at 'La Chiquita') districts are similar to those of the sierras del Morro, Los Morrillos and Yulto (see above). It is therefore likely they formed by similar magmatic-hydrothermal processes to those suggested for the El Morro W deposits.

Some of the W deposits in the Paso Grande - Villa Praga area, however, are hosted by the Devonian Las Chacras granite, and consist of quartz-wolframite veins (Angelelli, 1984). This relationship indicates either syn- or post-Devonian W vein formation.

2.3 AU±AG DEPOSITS

Three principal syles of Au deposits occur within the San Luis map area: (a) Au and W-Au quartz veins in high strain zones, (b) epithermal Au-Ag associated with Miocene-Pliocene volcanic rocks, and (c) alluvial Au.

2.3.1 SHEAR-ASSOCIATED AU AND W-AU QUARTZ VEIN DEPOSITS OF THE SANTO DOMINGO AND EL DURAZNITO DISTRICTS

Several small Au±W deposits are known from the Santo Domingo and El Duraznito districts in the Paso del Rey region. The geological setting of this region was summarised in section 1.2.1, and the geology of the deposits was described by Angelelli (1984), Leveratto and Malvicini (1982) and Fernandez and others (1991).

Geology: The El Duraznito W (-Au) deposit occurs within a few hundred metres of the terrane boundary between the Conlara Metamorphic Complex to the east and San Luis Formation in the west. Leveratto and Malvicini (1982) described the host rocks to the vein system as fine grained quartz-muscovite schists and mylonitic. The veins are commonly 30-50 cm wide and form a zone ~150 m in width. The main paragenetic and structural stages are as follows.

Tourmaline veins trending 005-015° and dipping steeply east, and alteration of host rock

Quartz veining with similar orientation to tourmaline veins, accompanied by minor tourmaline, muscovite, rutile, pyrite and chalcopyrite

Brecciation of earlier veins, and infilling by quartz±scheelite

Quartz veining trending 015-030° and inclined 55-75° west, and containing wolframite, scheelite, native gold, bismuthinite, chalcopyrite, native bismuth, sphalerite, bismuth sulfosalts, pyrite, pyrrhotite, beryl, rutile and siderite

Cataclastic deformation

Hydrothermal alteration consists of carbonate, pyrite, quartz and feldspar? replacement of schist adjacent to veins. Leveratto and Malvicini (1982) interpreted both alteration and cataclastic deformation to have postdated the vein systems.

Alternatively, the hydrothermal alteration may have been synchronous with quartz-W-Au-Bi vein formation, occurring during ductile deformation which produced boudinage of veins and mylonitic fabrics in host rocks.

The small Santo Domingo Au deposit occurs within a belt of quartz-scheelite vein deposits in a high strain zone in the San Luis Formation. Quartz veins between 0.2 and 1.2 m wide and vein networks are hosted by metapsammite and phyllite, and are subparallel to the mylonitic foliation. Veins show pinch-and-swell and gash shaped morphologies, and are interpreted to have formed synchronously with the mylonite. Zones of bleached and ferruginous (after pyrite?), argillic and/or sericitic altered wall rock in the vicinity of the quartz-pyrite-gold veins may be related to vein formation, or alternatively may have postdated vein formation. Relatively late, brittle, hematitic fault zones occur within the mylonitic metasediments. Gold has been reported in a number of other quartz-scheelite vein deposits in the Santo Domingo district (Fernandez and others, 1991), and antimony occurs in economic quantities in some of the Au-W occurrences (Rossello, 1987).

Genesis: The structural history of the Santo Domingo - El Duraznito area is complex, and the terrane boundary shear zone may have been reactivated many times between the early Ordovician and the Tertiary. Nevertheless, the principal mylonite fabrics in the San Luis Formation of the Santo Domingo district are interpreted to have formed during the Devonian D_3 compressive deformation (Sims and others, this Report). Scheelite at El Duraznito was suggested by Leveratto and Malvicini (1982) to have formed during regional metamorphism. We infer this metamorphism to have been the low grade event that accompanied D_3 deformation in the early Devonian. The structural style is similar to those of Au-quartz vein deposits in the Sierra de Las Minas (La Rioja) and the Candelaria district (Córdoba). It is therefore proposed that Au±W±Sb mineralisation associated with quartz veins in the Santo Domingo - El Duraznito formed syn-D_3, possibly during the early Devonian metallogenic event. The association of Au with W, B, Be, Bi and Sb is suggestive of a magmatic component in the ore fluids. Remobilisation of syngenetic volcanic-related Au, Sb and W during subsequent deformation events has also been suggested (Malvicini and others, 1991). Further studies are required to test the hypothesis of Devonian Au introduction and spatial association with shear zones, as there are important implications for gold prospectivity in the region.

2.3.2 EPITHERMAL AU-AG (-PB-ZN) MINERALISATION OF THE LA CAROLINA DISTRICT

The La Carolina district in the Sierra de San Luis has been mined intermittently for Au, Pb and Zn since the 1880's, from primary hydrothermal mineralisation hosted mainly by Tertiary volcanic rocks and from alluvial deposits. The principal exploited primary precious and base metal mineralisation occurs at the La Carolina (Esperanza), La Estancia and La Rica mines. More recently, numerous prospects were delineated in a ~20 square kilometre area in the La Carolina district during exploration by the Dirección Nacional de Fabricaciones Militares between 1986 and 1988. Subsequent exploration until 1990 was carried out by Carolina SAM, an association of Dirección Nacional de Fabricaciones Militares with Minera Mincorp (Anglo American and Perez Compang) (Beninato and others, 1994). During this period 65 diamond drill holes, 570 percussion holes, trench and soil geochemical sampling and geological mapping were completed. Diamond drill hole intersections included 9m @ 4g/t Au (La Ilusión) and 6m @ 2.5 g/t Au, 122 g/t Ag, 0.3% Pb, 0.5% Zn (Cerro Mogote).

Regional setting: Regional geology of the basement in the La Carolina district has been previously discussed by numerous workers (see Sims and others, this Report), including Pastore and Gonzalez (1954), Kilmurray and Villar (1981), Ortiz Suarez and others, (1992), Bassi (1992) and von Gosen and Prozzi (1996). A regional zone of mylonitic shears trending NNE through the vicinity of La Carolina separate greenschist facies metasediments of the San Luis Formation in the west from older amphibolite facies metasedimentary biotite±muscovite±garnet±graphite schists, gneisses and migmatites in the east. Intense penetrative deformation fabrics in metapsammites and metapelites of the San Luis Formation were generated during the Devonian D_3 and D_4 compressive events (Achalian cycle), whereas fabrics in the amphibolite facies rocks developed initially in the early Ordovician during D_1 and D_2 (Famatinian cycle), and were overprinted by the Devonian deformation (Sims and others, this Report). Pegmatites and minor amphibolite zones occur within the schist, gneiss and migmatite. The Escalerilla granite extends from La Carolina southwards for >45 km, and near La Carolina occurs partly within the regional mylonite zone. U-Pb zircon dating has revealed an early Devonian crystallisation age of 403±6 Ma (Camacho & Ireland, 1997).

Calcalkaline to shoshonitic, intermediate to felsic, volcanic rocks of the La Carolina district form the northwestern part of an ~80 km linear Miocene-Pliocene volcanic belt that extends southeastwards to the Sierra del Morro (Llambías & Brogioni, 1981;

Brogioni, 1987, 1988, 1990; Ramos and others, 1991). Nine K-Ar radiometric dates ranging from 9.5±0.5 Ma to 1.9±0.2 Ma were reported by Ramos and others (1991), Urbina and others (1995) and Sruoga and others (1996). The available dates indicate that between ~9.5-6.3 Ma andesite to trachyte were erupted in the northwestern (La Carolina - Cañada Honda) and southeastern (El Morro) parts of the belt, while andesitic volcanism occurred in the central Cerros de Rosaria area. Younger andesitic to trachyandesitic volcanism (2.6-1.9 Ma) occurred in the central and southeastern parts of the belt. Tertiary andesites of the Sierra de Pocho in Provincia de Córdoba show a similar age distribution of older volcanism in the west, although the compositional variations differ in that shoshonitic rocks are restricted to the eastern part of the Pocho area (Gordillo & Linares, 1981; Kay & Gordillo, 1985; Kay and others, 1988). Together with the Farallón Negro volcanic-plutonic rocks in Provincia de Catamarca, the Miocene-Pliocene volcanics of provincias del San Luis and Córdoba represent the easternmost manifestations of Tertiary magmatism in this region of South America. They are interpreted to have formed above a shallowly dipping ('flat slab') portion of the subducting Nazca plate, erupting over a deep segment of the seismic zone (Kay and others, 1988).

Geology: Volcanic rocks of the La Carolina to Sierra del Morro belt comprise domes, lava flows, dykes, and volcaniclastic rocks including breccias, lapillistones and tuffs (Brogioni, 1987, 1990; Urbina and others, 1995; Sruoga and others, 1996). Several volcaniclastic breccia facies have been described: autoclastic, hydrothermal, 'explosion' and pyroclastic. The 'explosion' breccias are believed to have resulted from phreatomagmatic activity that preceded dome emplacement (Sruoga and others, 1996). The presence of possible base-surge deposits (Brogioni, 1990; Sruoga and others, 1996) together with 'explosion' breccias led Sruoga and others (1996) to suggest a maar-diatreme environment of volcanism in the La Carolina area. Hydrothermal breccias are spatially associated with both the domes and 'explosion' breccias, and they commonly occur in arc-shaped lenses (Sruoga and others, 1996). The arcs may represent segments of subcircular fracture systems. A diatreme model had previously been applied to gold exploration in the district by the Dirección Nacional de Fabricaciones Militares, and at least three diatremes up to 2 km diameter were identified (Beninato and others, 1994). However, some of the diagnostic features of a maar-diatreme environment such as intra-maar deposits and well defined annular fracture systems are not clearly evident, and may have been removed or obscured by erosion.

In the Sierra del Morro a 4 km diameter summit crater was interpreted by Brogioni (1990) as a caldera. Lacreu (1990) inferred the presence of a 2.5 km diameter caldera structure in the northwest part of the Cerros del Rosario area, and a series of subcircular ring fractures encompass volcanics of the Cerros del Rosario (see 1:100,000 scale geology map). Travertine in this district (Lacreu, 1990, 1992, 1995; Brogioni, 1990) together with preservation of volcanic cones suggests that the present erosional level in the Cerros del Rosario may not be as deep as in the La Carolina area. A 3.5 km diameter subcircular topographic depression filled with tuff occurs to the south of the Cerros Largos volcanics; its origin is unknown.

Alteration and mineralisation: Currently known primary precious and base metal mineralisation and hydrothermal alteration zones are restricted to the La Carolina - Cañada Honda area. Hydrothermal alteration of volcanics and to a lesser extent metamorphic basement rocks in an area totalling at least 9 km^2 was mapped by Bassi (1992), the Dirección Nacional de Fabricaciones Militares (Beninato and others, 1994), Urbina and others (1995) and Sruoga and others (1996). Alteration types reported in these studies, and confirmed in the present work, include: argillic, sericite-pyrite, silicification, and propylitic (chlorite-carbonate-hematite±epidote±pyrite). In addition, sericite-adularia was reported by Urbina and others (1995), and minor alunite occurs the La Rica deposit (Malvicini & Urbina, 1995). Alteration assemblages appear to be zoned around precious-base metal mineralisation in the La Carolina district, as follows (see Table 1):

- Distal, propylitic, chlorite-carbonate-hematite±montmorillonite±mixed layer clay zones (e.g. alteration of latite, Cerro Tomalasta, A95RS088), which may or may not be directly related to mineralisation.
- Argillic (illitic±mixed layer clay) and sericite±pyrite zones up to several hundred metres wide (e.g. alteration zone south of historical La Luisa mine, A95RS110).
- Core zones up to a few metres wide consisting of silica-pyrite±illite±sericite±calcite± adularia±pyrophyllite±alunite±jarosite, and containing Au, Ag, Pb and Zn mineralisation (e.g La Estancia, A95RS105; Cerro Mogote, A95RS113).

Metamorphic muscovite, garnet and graphite are partially preserved in these alteration assemblages (e.g. La Estancia, La Rica).

Zones of intense argillic and sericitic alteration occur in the following settings:

1. In association with ‘explosion’ and hydrothermal breccias, within inferred diatreme structures (Dirección Nacional de Fabricaciones Militares, Beninato and others, 1994; Urbina and others, 1995; Sruoga and others, 1996);
2. At the intersections of NW- and NNE-trending fracture zones in metamorphic basement(Bassi, 1992), for example at La Estancia the mineralisation occurs in a WNW trending Tertiary(?) fault zone cutting a NNE-trending silicified pre-Tertiary mylonite zone;
3. In annular zones encompassing volcanic centres (e.g. Diente Verde, Sruoga and others, 1996);
4. spatially associated with breccia dykes in volcanics and basement metamorphics (e.g. La Carolina, La Rica, La Luisa).

Table 1. X-ray diffraction (XRD) results for hydrothermally altered samples from the La Carolina district, Sierras de San Luis.

Occurrence	Sample number	Alteration & mineralisation	Diagnostic minerals detected by XRD
La Carolina Au	A95RS084B, 099B	Argillic; disseminated pyrite & Cu minerals	illite (*whph 0.3, #I=250); sericite or muscovite (whph 0.13); chalcanthite; possible jarosite; feldspar
La Estancia Au-Ag-Pb-Zn	A95RS105B	Silicification; argillic; disseminated pyrite, sphalerite, galena;	illite (whph 0.38 & 0.52, I=200); possible feldspar; possible pyrophyllite; possible jarosite; calcite
Cerro Mogote Au	A95RS113	Silicification with disseminated sphalerite, galena	illite-sericite/muscovite (whph 0.27, I=500); alunite; pyrophyllite
Cerro Tomolasta	A95RS088B	Propylitic and argillic; no mineralisation	illite (whph 0.29, I=60); mixed layer clay; kaolinite; calcite; hematite; chlorite
La Luisa	A95RS110	Argillic	sericite or muscovite (whph 0.17 & 0.12, I=350); mixed layer clay (whph 0.53, I=110); K-feldspar; possible jarosite

*whph: width at half peak height; together with peak intensity (I), the whph is related to crystallinity of the mica and hence to its temperature of formation - broader peaks representing lower temperatures

#I: peak intensity

At the La Carolina, La Rica and La Luisa Au-Ag-Pb-Zn workings, the intense argillic and sericitic alteration with pyrite is centred on heterolithic breccia dykes (10's of cm to >5m wide) that are composed of angular, unsorted, metamorphic wall rock and unvesiculated volcanic clasts in a comminuted rock matrix (Figure 12). The breccia

Figure 12. Breccia dyke, approximately 10m wide and steeply dipping, emplaced in sheared metasediments of the San Luis Formation, La Carolina Au Mine. The dyke contains fragments of metasedimentary host rock and sparse clasts of porphyritic volcanic rock in a matrix of the same composition, all intensely altered to illite-sericite-pyrite-quartz. Copper sulphate and anomalous Au occur in the breccia dyke. Hydrothermal alteration of host rocks is most intense adjacent to the breccia dyke. View to the north, site A95RS084.

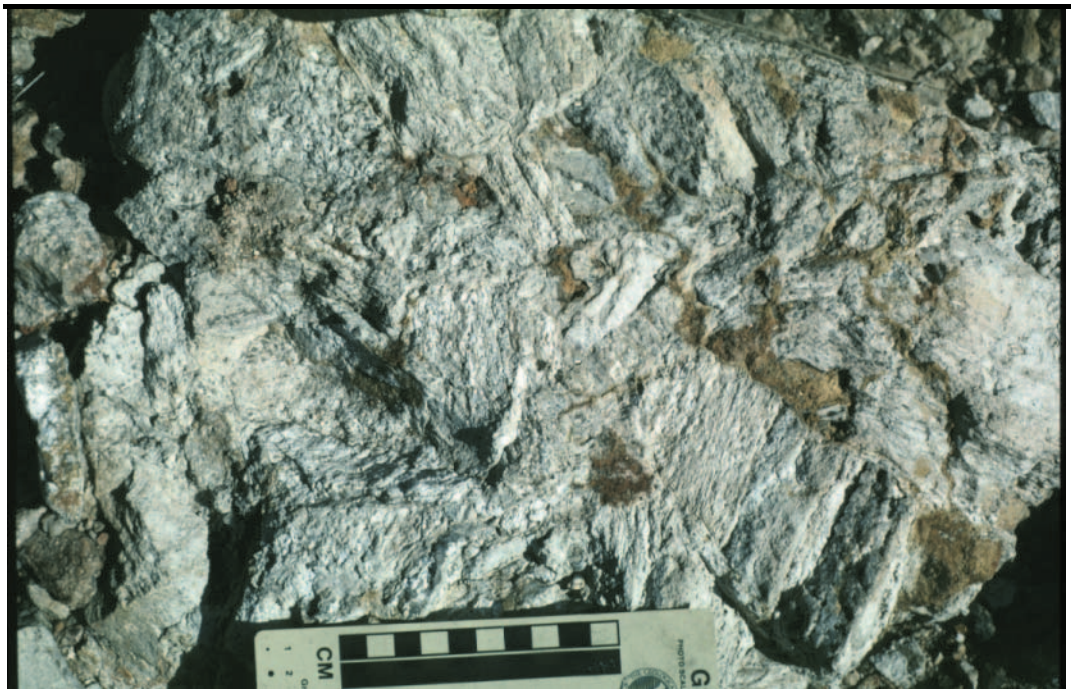

Figure 13. Breccia of silicified, argillic altered, banded metasedimentary wall rock fragments in quartz-rich matrix, Cerro Mogote. Disseminated fine-grained sulfides occur in the breccia matrix, and very anomalous Au values were intersected in drilling in this area (Beninato et al., 1994). The breccia forms part of an arcuate zone at the contact between unbrecciated host metasediments and various volcanic rocks of the La Estancia area. Site A95RS113, scale total 10cm

Figure 14. Sample of volcanic breccia in the La Luisa area, La Carolina district. Clasts comprise argillic and sericitic altered host metasediments, and porphyritic volcanic rock, in an argillic-sericitic altered matrix. Trenching and drilling in the area have revealed strongly anomalous Au, Ag, Pb and Zn values (Beninato et al., 1994). Site A95RS110, scale subdivisions 1cm.

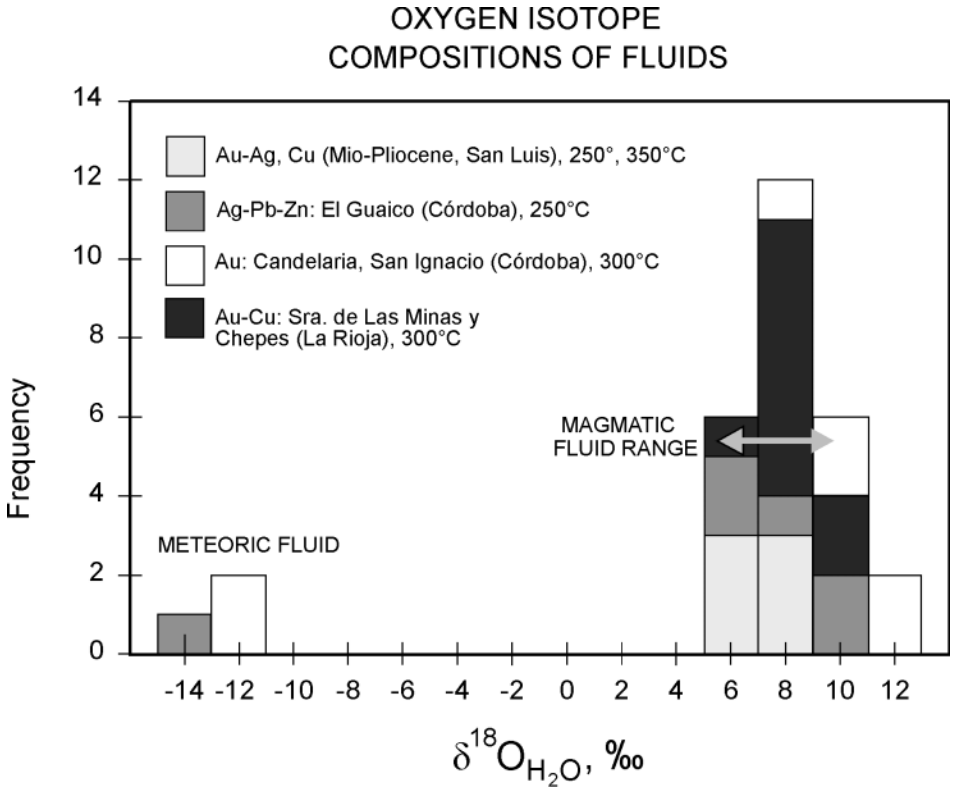

Figure 15. Calculated oxygen isotope compositions of hydrothermal fluids in Au±Cu, Ag-Pb-Zn and W deposits of the southern Sierras Pampeanas, derived from $\delta^{18}O$ values of quartz and chalcedony (Lyons & Skirrow, 1996) at the assumed temperatures given in the figure (see text for discussion). Quartz-water $\delta^{18}O$ fractionation factor from Matsuhisa et al. (1979).

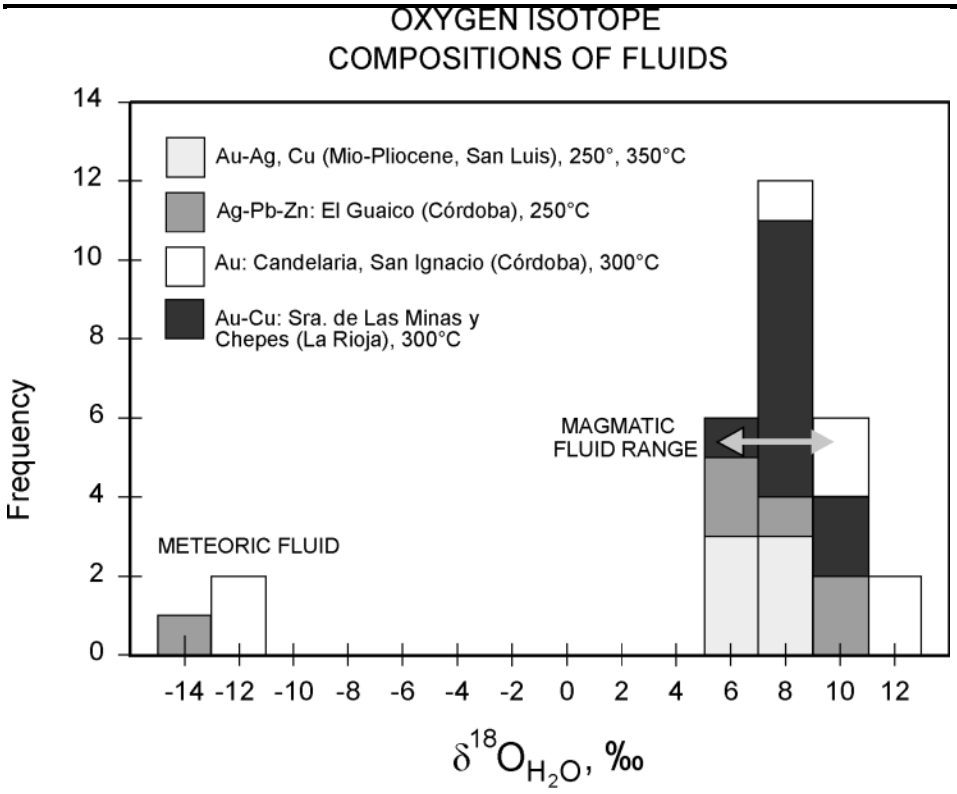

Figure 15. Calculated oxygen isotope compositions of hydrothermal fluids in Au±Cu, Ag-Pb-Zn and W deposits of the southern Sierras Pampeanas, derived from $\delta^{18}O$ values of quartz and chalcedony (Lyons & Skirrow, 1996) at the assumed temperatures given in the figure (see text for discussion). Quartz-water $\delta^{18}O$ fractionation factor from Matsuhisa et al. (1979).

dykes and spatially associated alteration follow pre-existing foliation and compositional layering orientation in metamorphic wall rocks (e.g. La Carolina, A95RS084, 099), or cross cut this orientation (e.g. La Rica, A95RS108). The dykes are interpreted to have formed by phreatomagmatic processes, and may have been permeable zones through which hydrothermal fluids were focussed. The dykes are overprinted by the argillic, sericitic, pyritic and silicic alteration. The 'hydrothermal' breccias described by Urbina and others (1995) and Sruoga and others (1996) have similar clast makeup and fabrics (e.g. Cerro Mogote) to the breccia dykes at La Carolina and La Rica, but are intensely silicified (Figure 13). They may be either true hydrothermal breccias or phreatomagmatic (diatreme-related?) breccias that have been overprinted by intense hydrothermal alteration and mineralisation which was focussed on these permeable zones. Other, apparently stratiform, breccias with

similar compositions and fabrics to the breccia dykes are also overprinted by argillic and sericitic alteration (Figure 14).

Precious and base metal mineralisation consists of free gold and/or electrum associated with pyrite, sphalerite, galena, marcasite, chalcopyrite, wurtzite, tennantite-tetrahedrite, arsenopyrite, pyrrhotite, and pearcite-polybasite (Bassi, 1992; Malvicini & Urbina, 1995; Urbina and others, 1995). Trace enargite was reported at La Rica by Malvicini and Urbina (1995). The precious and base metal minerals at La Estancia, La Rica and Cerro Mogote occur in subvertical, massive to finely banded and brecciated, fine-grained, quartz-pyrite-clay replacement zones of a few centimetres to metres in width. Common vughy domains are filled with fine grained euhedral quartz and sulfides. Contacts of siliceous mineralised zones with less silicified, argillic-sericite altered breccia and metamorphic rocks are gradational. According to Bassi (1992) gold at the La Carolina deposit occurs in a "vein-like body in the west wall of a lenticular quartzite horizon". Observations in the present study suggest that intense argillic and sericite-pyrite alteration is associated with a 10 m wide breccia dyke (Figure 12); 'quartzite' and a 'vein-like' mineralised zone were not identified in surface workings. The altered breccia dyke contains disseminated Cu sulfate (7525 ppm Cu) and anomalous Au, Zn and Pb (A95RS084B).

Genesis: The paleogeographic-paleohydrological setting of the mineralised district is one of low to moderate relief volcanic edifices (lava domes and small stratovolcanoes) that have undergone slight to moderate erosion in a cordilleran-like terrane. Several lines of evidence suggest the hypogene Au-Ag mineralisation of the La Carolina district formed contemporaneously with Mio-Pliocene volcanism:

- Known mineralisation and alteration is spatially associated with, and occurs partially within, the volcanic rocks;
- The K-Ar age of altered and least altered equivalent volcanics is similar (Urbina and others, 1995);
- Alteration and mineralisation are spatially associated with breccia dykes and with other breccias interpreted to be of phreatomagmatic origin; hydrothermal breccias also may be present.

The predominace of sericitic alteration and presence of adularia in some mineralised zones led Malvicini and Urbina (1995), Urbina and others (1995) and Sruoga and others (1996) to conclude that the epithermal mineralisation was of the sericite-adularia or low sulfidation type. However, in recognition of the (minor) alunite and enargite in some deposits, and reported 'sinter', these authors suggested a hot spring

environment of mineralisation. The disseminated style of Au mineralisation in narrow siliceous pyritic replacement zones and presence of pyrophyllite (Table 1) are also indicative of extremely acid, relatively high temperature conditions (probably >270°C). These mineral assemblages, including enargite, are similar to those of high sulfidation epithermal systems, and it is probable they are the product of reaction of magmatic volatiles (e.g. SO_2, CO_2) with groundwaters (Sillitoe, 1993). Influx of such magmatic fluids is supported by oxygen and sulfur isotopic compositions of quartz and sulfides in the mineralised zones (Figures 15, 16). Low sulfidation epithermal veins, by contrast, are conventionally interpreted to have formed from fluids of meteoric origin (e.g. Field & Fifarek, 1985). These observations may be reconciled in an alternative genetic model involving:

1. early, relatively deep epithermal, high temperature, high sulfidation style alteration (and Au, Ag mineralisation?) in narrow zones associated with phreatomagmatic activity,
2. erosion of the upper parts of the hydrothermal systems,
3. overprinting by broad zones of lower temperature, adularia-calcite bearing alteration (and Pb-Zn±Au, Ag mineralisation?) in a shallower epithermal setting.

2.3.3 PORPHYRY-STYLE CU (-AU) MINERALISATION OF THE DIENTE VERDE AREA

Quartz vein stockworks containing chalcopyrite, pyrite, pyrrhotite, magnetite, electrum, bornite, tennantite and supergene oxidation products occur in 9.5±0.5 Ma andesitic monolithic volcanic breccia at Diente Verde (Figure 17; Brogioni, 1990; Urbina and others, 1995; Sruoga and others, 1996). The occurrence has been worked

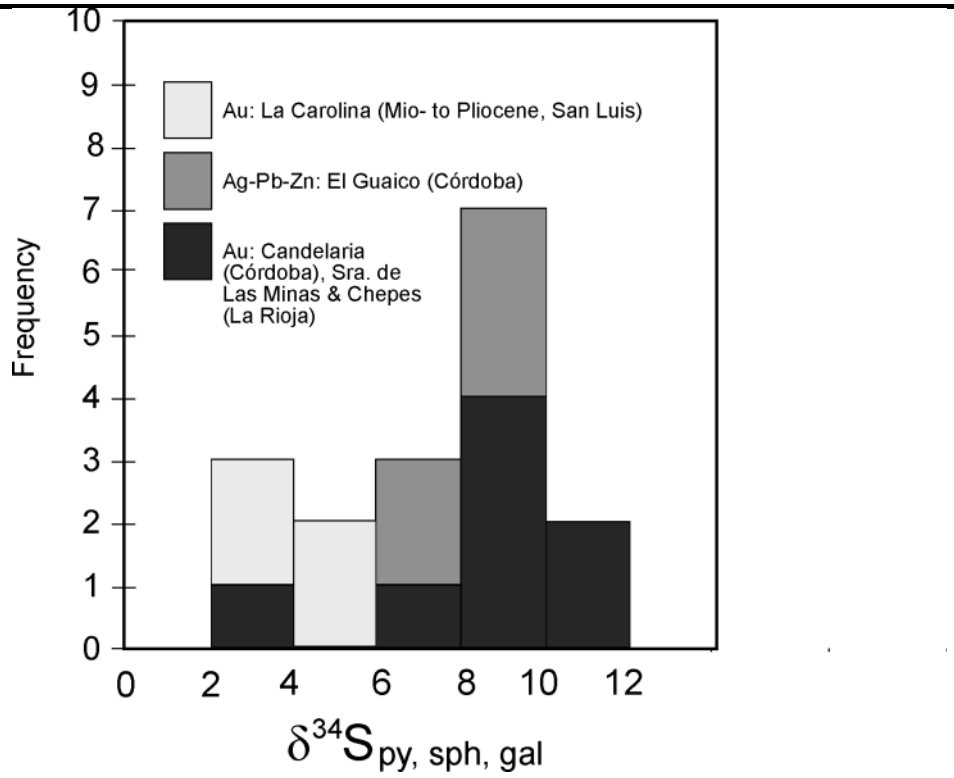

Figure 16. Sulfur isotope compositions of sulfides in Au±Cu, Ag-Pb-Zn and W deposits of the southern Sierras Pampeanas.

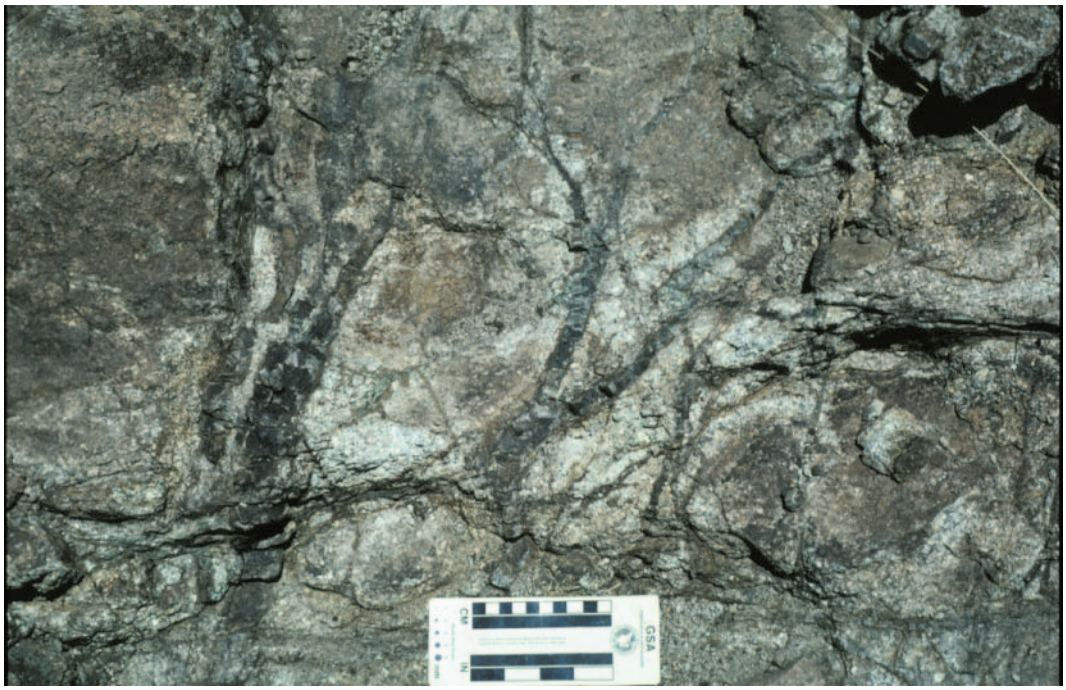

Figure 17. Quartz-chalcopyrite-pyrite vein stockwork in bleached, altered, monolithic breccia of amphibole andesite, Diente Verde, La Carolina - Cañada Honda

district. The stockwork zone is exposed in a small area of a few tens of metres diameter in the centre of a volcanic crater. Veins are limonitic/goethitic after sulfides, and also contain secondary copper sulfides and carbonates. Site A95RS111, scale total length 10cm.

for Cu from several small pits, but there is little evidence of recent exploration. The stockwork is exposed over an area of a few tens of metres diameter centrally within a cone-like volcanic edifice. Hydrothermal alteration is limited in the crater but an extensive zone of bleached argillic/sericitic altered volcanic breccia and lapilli tuff encompasses the volcanic edifice.

2.3.4 ALLUVIAL AU OF THE LA CAROLINA DISTRICT

The La Carolina district and particularly the Cañada Honda area, is well known for its alluvial gold deposits, some of which are currently being exploited. The deposits were described by Bassi (1948, 1992), Rossello and Barboso (1988), and Rossello and Castro (1995), amongst others. Rosello and Castro (1995) proposed two types of gold placer deposits: Pleistocene-Holocene colluvial-alluvial deposits, and modern alluvial deposits that formed by reworking of the earlier placer deposits. The source of gold is presumed to be epithermal mineralisation associated with Miocene-Pliocene volcanism.

2.4 PEGMATITE-HOSTED DEPOSITS OF BE, LI, TA, NB, SN, REE, U, TH

Introduction and classification: Argentina has been a globally significant producer of rare metals, and since 1930 pegmatites of the Sierras Pampeanas have produced more than 25 000 t of beryl, 45 t of Nb-Ta ore and 1000 t of Li minerals (Galliski, 1993). The Provincia de San Luis accounted for about half of the national Be output between 1945 and 1979 (Angelelli, 1984). Pegmatites in the San Luis map area also represent important sources of industrial minerals (e.g. feldspar, quartz, mica, etc.), and minor resources of Sn, Bi, REE, U and Th are also known from pegmatites of the region.

Multiple generations of a variety of pegmatite types were emplaced through the Paleozoic tectonic evolution of the San Luis area. Although pegmatites of the region have been described by many workers (including reviews by Herrera, 1963; 1965, 1968; Angelelli & Rinaldi, 1965; Galliski, 1993, 1994), their relative and absolute timing relationships in the tectonic and magmatic evolution of the region are less well

understood. An improved assessment of the potential of the region for new resources of rare elements such as Ta, Nb, Be, Li and REE will require better knowledge of the temporal and spatial relationships of pegmatites to regional structure, metamorphism and magmatism.

The earliest pegmatites in the region are interpreted to represent the melt products of the leucosome-forming reactions during high grade (upper amphibolite and granulite facies) metamorphism in both the Pampean and Famatinian cycles (see Sims and others, this Report). These generally small unmineralised garnet-bearing quartz-K-feldspar±plagioclase±biotite pegmatites are common in the Monte Guazú and Pringles Metamorphic Complexes. Cordierite-bearing pegmatites are present in higher grade areas of the Pringles Metamorphic Complex. These synmetamorphic pegmatites correspond to the abyssal type of Cerný (1991a), and may be equivalent to the type 1 pegmatites of Herrera (1968).

Herrera (1968) and Galliski (1993, 1993) described muscovite-rich K-feldspar-quartz pegmatites from other regions of the Sierras Pampeanas (type 2 of Herrera, 1968; transitional between muscovite and rare element classes of Cerný, 1991a, according to Galliski, 1993, 1994). These are a major economic source of muscovite, and relatively small examples may be present in San Luis (e.g. López, 1984) but their tectonic-magmatic setting and genetic relationships to other pegmatite types within the map area are not well constrained. The minor quantities of beryl, structural setting and K-Ar age dates for some of these deposits near Tilisarao (López, 1984; Rinaldi & Linares, 1973) suggest they may be members of either the muscovite class or primitive variants (beryl subclass) of the rare element class that formed during the Famatinian extensional tectonism (see below).

Pegmatites of the rare element class of Cerný (1991a) (types 3 and 4 of Herrera, 1968) are widely represented in the San Luis region. The deposits have been described by many workers including Herrera (1963, 1965, 1968), Angelelli and Rinaldi (1965), Arcidiácono (1974), Ortíz Suárez and Sosa (1991), Sosa (1990, 1991, 1993), Oyarzábal and Galliski (1993), and Galliski (1993, 1994). Examples of the beryl, complex (spodumene subtype) and albite-spodumene types of Cerný (1991a) have been recognised (Galliski, 1993), including cassiterite-bearing pegmatites (Sosa, 1990, 1991, 1993; Ortíz Suárez & Sosa, 1991). Internal zoning, dimensions, geometry and parageneses are described in the cited references. Galliski (1993, 1994) defined three rare metal pegmatite districts in San Luis: La Estanzuela, Totoral (extending north from La Florida) and Conlara, which includes the Renca-

Tilisarao region. The rare element pegmatites of the LCT (Li, Cs, Ta>Nb, Rb, Be, Sn, Ga) petrogenetic family of Cerný (1991a, b), were recognised in all of these districts. In addition, Galliski (1993) suggested that some REE-mineralised pegmatites in the Conlara district are of the hybrid LCT-NYF (Nb>Ta, Y, F, Ti, Sc, REE, Zr, U, Th) family. These REE-U bearing pegmatites occur mainly to the north of the map area (Rinaldi, 1968; Gay & Lira, 1985), and appear to be spatially associated with granites of the Achalian cycle.

Timing and tectonic setting: Based on compilation of K-Ar age data for pegmatites of the Sierras Pampeanas and correlation with other igneous events, two principal periods of rare element pegmatite emplacement were suggested by Galliski (1994): an orogenic Cambrian-Ordovician stage, and a post-orogenic Devonian-Carboniferous phase. Rapela and others (1990), on the other hand suggested that Li, Be, Nb and Ta mineralised pegmatites were related to 'post-D2' (late Ordovician to early Devonian) granites such as the Achala batholith. A re-evaluation of the timing and tectonic setting of the rare element pegmatites in light of the results of the current mapping project broadly corroborates the interpretation of Galliski (1994) of two periods of rare metal mineralisation, with some added temporal and spatial constraints, as discussed below.

High-grade metamorphism during the early Ordovician compressive tectonism was closely followed by extensional tectonism late in the Famatinian cycle under greenschist-facies conditions, accompanied by emplacement of peraluminous S-type granites, leucogranites and voluminous pegmatites that are spatially associated with the granites (Undifferentiated Ordovician Granitoids; Sims and others, this Report). Extensional tectonism and granite-pegmatite emplacement was restriced to discrete belts and resulted in pervasive retrogression within those belts of the high-grade metamorphic assemblages. These are shown as Cambro-Ordovician schist units of the Pringles complex in 1:100,000 geology maps of the Sierras de San Luis. Abundant unmineralised K-feldspar-quartz-plagioclase-muscovite pegmatites associated with the Paso del Rey suite typically contain black tourmaline with minor garnet and apatite. Many of the rare metal mineralised pegmatites in the Sierra de San Luis also occur within the retrograde parts of the Pringles complex, spatially associated with the Paso del Rey suite. No district-scale zonation of pematite types has been identified, possibly as a result of multiple episodes of superimposed granite-pegmatite systems obscuring these relationships. Sosa (1990, 1991, 1993) and Ortíz Suárez and Sosa (1991) recognised a regional pattern of Sn-bearing rare element (Be, Li, Nb, Ta) pegmatites in schists in the eastern parts of the Sierras de San Luis, and

relatively Nb-Ta-rich Be-Li-Bi-bearing pegmatites in an eastern belt of the sierras. Given the location of the Sn-bearing pegmatites in schists that may correlate with the San Luis formation (Sims and others, this Report), it is possible the Sn-bearing pegmatites were emplaced and deformed during the Achalian tectonic cycle.

A summary of available radiometric age dates for pegmatites of San Luis (Table 2) indicates that the pegmatites cooled to the blocking temperature of 350±50°C for Ar in muscovite (McDougall & Harrison, 1988) during two main periods: ~440 to ~470 Ma, and ~415 to ~340 Ma. The U-Pb uraninite age of ~460 Ma for the Santa Ana Be-Ta-Nb-bearing pegmatite in the Totoral district may be close to the age of crystallisation. K-Ar age determinations on K-feldspars in the same pegmatites as the muscovite age determinations are younger than the muscovite ages and are consistent with the lower blocking temperature of K-feldspar (McDougall & Harrison, 1988). The ~440 to ~470 Ma muscovite ages are interpreted to represent cooling ages of pegmatites emplaced during the late-Famatinian extensional tectonism in San Luis, some in association with 'fertile' granites of the Paso del Rey suite.

Table 2. Geochronology of pegmatites from San Luis. Data from: 1. Rinaldi and Linares (1973) and 2. Linares and Gonzales (1990), 3. Llambías and Malvicini (1982), 4. Linares (1959).

Metals	Age (Ma)	Ref	Method	Comment
	305 ± 20	1	K/Ar K-feldspar	Yac. Cholita - Sa. de La Estenzuela
Be, Ta, Nb	310 ± 20	1	K/Ar K-feldspar	Yac. Rona - Sa. de La Estenzuela
Be	325 ± 20	1	K/Ar K-feldspar	Yac. Don Paco - Sa. d. La Estenzuela
Be	328 ± 15	1	K/Ar K-feldspar	Yac. María - Sa. de La Estenzuela
Be	340 ± 10	1	K/Ar K-feldspar	Yac. Renquina - Sa. de Tilisarao
Be, Ta, Nb	343 ± 10	1	K/Ar Muscovite	Yac. Rona - Sa. de La Estenzuela
Be	343 ± 20	1	K/Ar K-feldspar	Yac. Los Duraznos - west of Tilisarao
Be	347 ± 15	1	K/Ar Muscovite	Yac. Don Paco - Sa. de La Estenzuela
Be	360 ± 15	1	K/Ar Muscovite	Yac. Renquina - Sa. de Tilisarao
Be	368 ± 15	1	K/Ar K-feldspar	Yac. Flamingo - 7 km west of Tilisarao
Be	371 ± 20	1	K/Ar K-feldspar	Yac. Don Paco - Sa. de La Estenzuela
	375 ± 16	2	K/Ar Muscovite	Sierra de Yulto
Be	415 ± 20	1	K/Ar Muscovite	Yac. María - Sa. de La Estenzuela
Be	430 ± 15	1	K/Ar Muscovite	Yac. Don Paco - Sa. de La Estenzuela
	438 ± 15	1	K/Ar Muscovite	Yac. Cholita - Sa. de La Estenzuela
W	455 ± 15	3	K/Ar Muscovite	Mina Don José - Sa. Los Morillos, with scheelite
Be-Nb-Ta	455 ± 25	4	U-Pb chem. uraninite	Yac. Santa Ana - Paso del Rey
Be-Nb-Ta	459 ± 1	4	U-Pb isot. uraninite	Yac. Santa Ana - Paso del Rey. Pb^{206}/U^{238} age, without correction for common lead.
Be-Nb-	460 ± 1	4	U-Pb isot.	Yac. Santa Ana - Paso del Rey.

Pegmatite swarms spatially associated with early Devonian granites in the San Luis map area and elsewhere in the Sierras Pampeanas occur both within and external to the granites. REE, U and Th enriched pegmatites of the NYF petrogenetic family occur within the Las Chacras granite (Gay & Lira, 1985; Galliski, 1993, 1994), and Be-Nb-Ta-F-U-bearing pegmatites occur within the Achala batholith (e.g. Morteani and others, 1995). Granites of the Achalian cycle are fractionated, peraluminous to borderline-metaluminous (Rapela and others, 1990), oxidised to weakly reduced, magnetic to non-magnetic S- and I-types and form zoned ovoid plutons that were emplaced at relatively high crustal levels synchronous with compressive deformation (Sims and others, this Report). U-Pb zircon dating in the current study indicates that magmatism during the Achalian cycle was mainly during the period ~403 to ~382 Ma (Camacho & Ireland, 1997). The ~415 to ~340 Ma muscovite ages of some Be and Be-Ta-Nb pegmatites in the Sierras de Estanzuela and Tilisarao (Table 2) are consistent with emplacement of these LCT(?) pegmatites during the Achalian cycle, although the possibility of complete resetting of older muscovite during the Achalian cannot be ruled out. This period therefore likely represents the focus of a second rare metal pegmatite event that included both LCT and NYF petrogenetic types, in association with 'fertile' Achalian granites.

3. NON-METALLIC MINERAL OCCURRENCES

3.1 MICA, QUARTZ, FELDSPAR

Numerous pegmatite bodies have been worked for muscovite, quartz and feldspar and occur widely in the map area. As noted above, most of those mined for muscovite probably are members of the muscovite or primitive rare element classes of pegmatites, and formed during the early Famatinian extensional tectonism.

3.2 MARBLE, TRAVERTINE AND ONYX

A large number of deposits of marble are present in the map area. These deposits occur in the Conlara and Monte Guazú Metamorphic Complexes, particularly in the sierras de Comechingones, La Estanzuela, Los Morillos and Yulto.

Travertine and calcareous onyx (calcite) and aragonite deposits (e.g. Cantera Santa Isabel) occur near Cerro Tiporco, 18 km NW of La Toma. The onyx occurs as mantos and veins hosted by Miocene to Pliocene epiclastic sediments and volcanics (Lacreu,

1990, 1992, 1995). An epigenetic (Pliocene) hydrothermal origin for the onyx was proposed by Lacreu (1990, 1992, 1995). Oxygen and carbon isotope analyses of carbonates from Santa Isabel and travertines were reported by Lacreu (1995).

Pliocene to Pleistocene travertine occurs in ten mapped bodies within 5 km of Cerro Tiporco, and represent low temperature hydrothermal activity associated with Miocene-Pliocene volcanism (Lacreu, 1990, 1992, 1995).

3.3 GRANITE ORNAMENTAL STONE

The San Luis region including the map area is well known for its production of ornamental stone, including several types of granite.

4. METALLOGENIC EVOLUTION OF THE REGION

The southern Sierras Pampeanas comprise a basement terrane dominated by Paleozoic tectonics (Stuart-Smith and others, 1996). The eastern part of the region which includes part of the San Luis map area was metamorphosed at medium-high grade, intruded by I- and S-type granitoids and deformed during the Cambrian (Pampean cycle). Low to high grade metamorphism and compressive deformation of the western part of the region including the Sierra de San Luis peaked in the early Ordovician, and was closely followed by extensional tectonism, retrograde metamorphism and emplacement of granitoids and pegmatites (Famatinian cycle). The post-Ordovician history was dominated by the emplacement of fractionated granites in a compressive tectonic setting synchronous with folding and shearing of the terrane during the early Devonian (Achalian cycle; Sims and others, this Report). These shallow intrusions crystallised from relatively oxidised magmas and have ASI values ranging from those typical of S-type granites to values transitional between I- and S-type granites. Following graben formation in the Cretaceous and basaltic volcanism in the Sierras de Córdoba, intermediate to felsic high-K calcalkaline volcanic rocks were erupted in the Neogene and are associated with Andean tectonics.

Determination of relative and absolute timing relationships in conjunction with regional geological and stable isotope studies has led to significant improvement in the resolution of Paleozoic metallogenic phases in the southern Sierras Pampeanas. The three principal Paleozoic stages and one Neogene stage recognised in the project areas each exhibit distinctive metal associations and deposit styles. The earliest

metallogenic stage investigated includes magmatic Ni-Cu-Co sulfide deposits with anomalous PGE-Au hosted by mafic-ultramafic intrusions, in the Sierras de San Luis. Differentiates of the mafic parent magma crystallised during the early Ordovician, approximately coeval with Famatinian high grade metamorphism and compressive deformation. The whole rock geochemistry of the mafic-ultramafic rocks and metasediments from the Sierras de San Luis is similar to those of rocks emplaced in back-arc basin tectonic settings (Brogioni & Ribot, 1994; Sims and others, this Report). It is proposed that the mafic-ultramafic rocks were emplaced within a back-arc basin as it underwent compression in a collisional tectonic setting.

No metallic manifestations of the Pampean cycle have been recognised in the present study in the Córdoba, La Rioja or San Luis map areas, although such mineralisation has been suggested by many authors as discussed above.

The second metallogenic phase in the map areas is spatially and temporally related to extensional deformation in the final stages of Famatinian tectonism in the early Ordovician. This tectonism is well developed in the San Luis map area, during which granites and voluminous pegmatites were emplaced that contain important deposits of Li, Be, Nb, Ta, Sn, and industrial minerals. Although subordinate W mineralisation may have formed as early as the Ordovician in the Sierras de San Luis, the majority of the W deposits in the map areas are proposed to have formed during the Devonian (below).

The third phase of metallogenic evolution in the southern Sierras Pampeanas occurred in the Devonian and is characterised by diverse deposits of Au, W, Ag, Pb, Zn, Cu, and a second period of pegmatite-related mineralisation including Be, Li, Nb, Ta, U, REE, Th and F. New $^{40}Ar/^{39}Ar$ dating of white mica hydrothermal alteration associated with Au±Cu, W and Ag-Pb-Zn veins suggests mineralisation occurred from ~390 to ~360 Ma in the southern Sierras Pampeanas including some W deposits of the San Luis map area (Figure 11). Based on this and U-Pb zircon dating this metallogenic phase commenced during the period of Devonian magmatism (~403 to ~382 Ma, Camacho & Ireland, 1997), and may have continued for at least 25 Ma after granite emplacement (Figure 11). However, Rb-Sr and K-Ar age data for these granites extend to as young as 300 Ma (Rapela and others, 1990). Malvicini and others (1991) proposed that some deposits of W, Pb, Zn Cu and Bi in the Sierras de San Luis formed in association with Carboniferous granites. A clearer understanding of the significance of this Rb-Sr and K-Ar data in the magmatic and thermal history of

the region is required before it is possible to define the full extent of temporal overlap of mineralisation with the period of Achalian granite emplacement.

Mesothermal shear-hosted Au±Cu quartz vein deposits in the Sierra de las Minas (Prov. de La Rioja), shear-related Au in the Candelaria district and high-level Ag-Pb-Zn quartz veins in the El Guaico district (both Prov. de Córdoba) are now recognised to have formed during the Devonian metallogenic phase from fluids of similar stable isotopic composition. It is probable that Pb-Zn-Cu quartz veins of the Las Aguadas district in the northern Sierras de San Luis also formed during the Achalian cycle (Malvicini and others, 1991). Our oxygen and hydrogen isotope results are compatible with input of evolved meteoric fluids with or without a minor component of magmatic or metamorphic waters in the formation of these Au±Cu and Ag-Pb-Zn deposits (Figures 10 & 15). Sulfur was probably derived from the host metasedimentary rocks. Hydrothermal muscovite from the Loma Blanca W deposit in the Sierra del Morro has oxygen and hydrogen isotopic compositions and a $^{40}Ar/^{39}Ar$ age broadly similar to those of the other Devonian deposits investigated. Epigenetic tungsten deposits hosted mainly by calcsilicate rocks in the Sierras del Morro, Yulto and Estanzuela (Prov. de San Luis) and W±Cu in the Punilla region of the Sierras de Córdoba are proposed to have formed during the Devonian metallogenic phase. Localisation of quartz-scheelite vein deposits and possibly some Au±W quartz vein deposits in the Sierras de San Luis in structures characteristic of the Achalian tectonism suggests these deposits also formed during the Devonian metallogenic stage.

In the final main metallogenic stage, Au (-Ag-Pb-Zn) mineralisation in the La Carolina district of the Sierra de San Luis formed in association with Miocene-Pliocene volcanism. Alteration, geochemical and geological characteristics indicate metal deposition in the upper levels of low sulfidation epithermal systems. Andesitic volcanics in the Pocho district of Provincia de Córdoba also were erupted in the Miocene (Gordillo & Linares, 1981).

The significance of a possible Cretaceous metallogenic event associated with basaltic volcanism (e.g. fluorite deposits in the Cerro Aspero batholith, Sierra de Comechingones, Galindo and others, 1996) and a Tertiary U event (e.g. in Valle de Punilla, Provincia de Córdoba) has yet to be determined.

5. PROSPECTIVITY AND METALLOGENIC MODELS

5.1 METHODOLOGY

A qualitative appraisal of metallic mineral prospectivity for the map area has been carried out using the 'Mineral Systems' approach and the concepts of 'essential ingredients' and 'mappable criteria' developed in AGSO (Wyborn and others, 1994). In this methodology a number of 'essential ingredients' in a genetic model for a particular style of mineralisation in an ore-forming hydrothermal system are chosen. These geological factors have been selected on the basis of multi-disciplinary ore deposit and regional geological studies, as discussed in preceding sections for specific deposit styles. In general, an ore-forming system requires: (1) a source of hydrothermal fluid components and metals, (2) energy to drive fluid flow, (3) fluid transport pathways linking the source regions with depositional sites, and (4) depositional 'traps' for ore deposition. An outflow pathway must also exist.

The 'essential ingredients' are manifested in some cases by observable features, or 'mappable criteria', which may be represented as domains in geoscientific maps and in a GIS. By combining the domains of 'mappable criteria' a map representation of a metallogenic model can be constructed for particular ore-forming systems and deposit styles. The final results of this procedure are metallogenic or prospectivity maps showing areas where critical geological factors in ore formation are similar to those existing at the known deposits (1:250 000 Metallogenic Map, Córdoba). In theory the methodology also allows prediction of areas for mineralisation styles not previously known to exist in a region.

Set out below are proposed metallogenic models for the principal mineral deposit styles recognised in the Córdoba map area, based on the methodology described above. These models were used in production of the 1:250 000 Metallogenic Map for the Córdoba area. Also shown are several hypothetical mineralisation styles not known in the map area but which are considered to have potential within and close to the area investigated. The model ingredients and criteria are based on deposit models described in the literature together with local geological constraints in the map area.

It should be noted that the methodology is qualitative and interpretive in nature, and should be considered a preliminary stage in assessment of prospectivity. Further work (research and exploration) is required to validate the proposed 'essential ingredients'

in the models, and test their related 'mappable criteria', so that the prospectivity evaluations can be refined.

5.2 METALLOGENIC MODELS

5.2.1 Ni-Cu (Co, PGE, Au) hosted by mafic-ultramafic plutonic bodies

Essential ingredients	Mappable criteria
Sulfur-undersaturated Ni-Cu (Co, PGE, Au) rich parent magma; differentiates that reached sulfur saturation	Mafic-ultramafic intrusions, especially those with melagabbro or ultramafic parts; 1 km buffer
Mafic-ultramafic host rocks	Magnetic highs representing mafic-ultramafics and/or high grade metamorphics
Magma pathways? and/or zones facilitating contamination of magma	Famatinian mylonites, esp. intersections with mafic-ultramafics; 1 km buffer
Thermal anomaly associated with mafic-ultramafic intrusions	High grade metamorphic rocks of Pringles complex
Cumulate sulfide zone	Ultramafic base of intrusive bodies

5.2.2 Pegmatite-hosted Be, Li, Ta, Nb, Sn

Further geochemical and petrogenetic work is required to distinguish between different granite types; nevertheless, some possible 'essential ingredients' and 'mappable criteria' are given below as a preliminary guide to prospectivity.

Essential ingredients	Mappable criteria
'fertile' granite source of LCT-type magma: peraluminous, fractionated S or I type	Paso del Rey suite and equivalent aged late-Famatinian granites; Achalian granites

synorogenic to late-orogenic tectonic zones	Famatinian extensional zones: retrograde metamorphic zones with abundant pegmatites, e.g. in Pringles complex
synorogenic to late-orogenic tectonic zones	Achalian compressive zones
highly fractionated magmas	Leucogranites
zonation from granite outwards to most fractionated pegmatites	Li, Rb, Cs, Be, Sn, Ga, Ta, Nb, B, P, F anomalies external to 'fertile' granites

5.2.3 PEGMATITE-HOSTED REE, U, TH, NB, TA, F

As for deposits of Be, Li, Ta, Nb and Sn further geochemical and petrogenetic work is required to distinguish between different granite types; some possible 'essential ingredients' and 'mappable criteria' are given below as a preliminary guide to prospectivity.

Essential ingredients	Mappable criteria
'fertile' granite source of NYF-type magma: subaluminous to metaluminous, fractionated A or I type	Achalian granites, especially those less peraluminous, more magnetic?
synorogenic to late orogenic tectonic zones (but commonly post-orogenic)	Achalian compressive zones (?)
highly fractionated magmas	Leucogranites
granite host	REE, U, Th, F, Nb, Ta, Ti, Y, Sc, Zr anomalies in or near Achalian granite

5.2.4 SHEAR-RELATED LODE AU±W (E.G. SANTO DOMINGO TYPE)

Essential ingredients	Mappable criteria
Source of energy for hydrothermal system and/or source of fluid components and/or metals; related to Devonian magmatism	Devonian granites - 5 km buffer on outcrops and magnetic lows interpreted as Dev. granite
Extensive fluid flow paths that were active in the Devonian	Devonian shear/mylonite zones trending NE to NW; also older shears reactivated in Devonian; 1 km buffer

Hydrothermal fluids out of equilibrium with feldspathic host rocks; changing physico-chemical conditions for ore deposition	Quartz veins; sericite-pyrite alteration; later hematite-chlorite alteration; represented by magnetic lows
Structural 'trap' for ore deposition - dilational zones	Flexures/jogs in shears, lineaments; contacts between rocks of differing competancy, e.g. gneiss and schist or mylonite
Chemical 'trap' for ore deposition; reductants	Presence of abundant graphite or Fe^{2+}-rich phases, e.g. magnetite (magnetic highs)

5.2.5 W (SCHEELITE) QUARTZ VEINLET DEPOSITS (LA FLORIDA - SANTO DOMINGO STYLE)

Essential ingredients	Mappable criteria
Source of energy for hydrothermal system and/or source of fluid components and/or metals; related to Devonian magmatism	Devonian granites - 5 km buffer on outcrops and magnetic lows interpreted as Dev. granite
Extensive fluid flow paths that were active in the Devonian	Devonian shear/mylonite zones trending NE to NW; also older shears reactivated in Devonian; 1 km buffer
Hydrothermal fluids out of equilibrium with feldspathic host rocks; changing physico-chemical conditions for ore deposition	Quartz veinlets; sericite-tourmaline ±calcsilicate or biotite-tourmaline alteration
Structural 'trap' for ore deposition - dilational zones	Rocks of differing competancy: e.g. felsic dykes in phyllite; flexures/jogs in shears, lineaments
Chemical 'trap' for ore deposition; pH change & source of Ca	Presence of abundant Ca-bearing minerals, e.g. plagioclase in felsic dykes

5.2.6 W (WOLFRAMITE) VEIN DEPOSITS (SAN ROMÁN STYLE)

Essential ingredients	Mappable criteria
Source of energy for hydrothermal system	Devonian granites - 2 km buffer on

and/or source of fluid components and/or metals; related to Devonian magmatism	outcrops and magnetic lows interpreted as Dev. granite
Hydrothermal fluids out of equilibrium with feldspathic host rocks	Muscovite-pyrite alteration
Extensive fluid flow paths that were active in the Devonian	Devonian shear/mylonite zones trending N to NW - ?? km buffer
Structural 'trap' for ore deposition - dilational zones	Contacts between rocks of differing competancy, e.g. granite - schist/gneiss, 1 km buffer

5.2.7 W CALC-SILICATE ASSOCIATED OR SKARN DEPOSITS (LOMA BLANCA STYLE)

Essential ingredients	Mappable criteria
Source of energy for hydrothermal system and/or source of fluid components and/or metals; related to Devonian magmatism	Devonian granites - 5 km buffer on outcrops and magnetic lows interpreted as Dev. granite; extensive zones of Devonian pegmatites
Hydrothermal fluids out of equilibrium with carbonate and/or Ca-rich host rocks; changing physico-chemical conditions for ore deposition	Calcsilicate alteration (skarn assemblages) - may include magnetite, hence magnetic highs
Fluid flow paths that were active in the Devonian	Devonian shear/mylonite zones and lineaments trending N to NW; 1 km buffer
Chemical 'trap' for ore deposition - pH change; carbonate and/or Ca-rich rock	Pre-Devonian marble and other carbonate-bearing units; amphibolite

5.2.8 EPITHERMAL AU-AG (ZN-PB) - LOW OR HIGH SULFIDATION STYLES

Essential ingredients	Mappable criteria
Source of energy for hydrothermal system and/or source of fluid components and/or metals; related to Tertiary magmatism	Tertiary volcanics - 3 km buffer on outcrops
Hydrothermal fluids out of equilibrium	Hydrothermal alteration typical of

with volcanic, or metamorphic or other pre-Tertiary host rocks	epithermal mineralisation; K-rich alteration signature in radiometrics, Landsat-TM, etc.
Meteoric hydrothermal fluid with associated Au-Ag	Proximity to known mineralisation of La Carolina district
Extensive fluid flow paths that were active in the Tertiary, syn- or post-volcanic	Tertiary fault zones, 1 km buffer
Structural 'trap' for ore deposition - dilational zones	Intersections of Tertiary stuctures (e.g. NW to WNW faults/lineaments or 'diatreme' ring fractures(with older N to NE mylonites; 1 km buffer
Physical-chemical 'trap' environment for ore deposition - near-surface (<1km depth) at time of volcanism and shortly afterwards	Travertine, onyx & volcanics - 3 km buffer

5.2.9 PORPHYRY CU-AU

Essential ingredients	Mappable criteria
Source of energy for hydrothermal system and/or source of fluid components and/or metals; related to Tertiary magmatism	Tertiary volcanics - 10 km buffer on outcrops & volcanics inferred from aeromagnetics
Hydrothermal fluids out of equilibrium with volcanics, or metamorphic or other pre-Tertiary host rocks	Hydrothermal alteration typical of porphyry mineralisation; K-rich alteration signature in radiometrics, Landsat-TM, etc.
Magmatic-hydrothermal hydrothermal fluid with associated Au-Ag	Proximity to known mineralisation of La Carolina district (e.g. Diente Verde)
Extensive fluid flow paths that were active in the Tertiary, syn- or post-volcanic	Tertiary fault zones
Structural 'trap' for ore deposition - dilational zones	Intersections of Tertiary stuctures (e.g. NW to WNW faults/lineaments or 'diatreme' ring fractures with older N to NE mylonites)
Physical-chemical 'trap' environment for ore deposition - subvolcanic environment	Exposed subvolcanic rocks

5.3 OTHER POTENTIAL DEPOSIT STYLES

5.3.1 CU, AU, FE SKARNS

Essential ingredients and mappable criteria will be similar to those for calc-silicate associated W±Cu mineralisation, above.

BIBLIOGRAPHY

ACENOLAZA, F.G., y TOSELLI, A.J., 1976. Consideraciones estratigraficas y tectonicas sobre el Paleozoico inferior del Noroeste Argentino. Memoria, II Congreso Latinoamericano de Geología, 2, 755-764.

ACENOLAZA, F.G., y TOSELLI, A.J., 1981. Geología de Noroeste Argentino. Publicacíon especial Fac. Ci. Nat. UNT, Tucumán, 1287, 212 p

AMBROSINI, G.L., GONZALEZ, R., QUARTINO, B.J. y RINALDI, C.A., 1981. Mineralización de wolfram en el faldeo oriental de la Sierra de San Luis. VIII Congreso Geológico Argentino, Actas, IV: 623-630.

ANGELELLI, V., 1984. Yacimientos Metalíferos de la República Argentina I, II. Comisión de Investigaciones Científicas, Provincia de Buenos Aires.

ANGELELLI, V., y RINALDI, C.A., 1965. Reseña acerca de la estructura, mineralización y aprovechamiento de nuestras pegmatitas

ARCIDIACONO, E.C., 1974. Contribución al conocimiento de columbita-tantalitas de las provincias de Córdoba y San Luis. Asoc. Geol. Argent., Rev., 29(2): 171-184.

ASTINI, R.A., 1996. Las fases diastroficas del Paleozoico medio en La Precordillera del oeste Argentino - evidencias estratigraficas. XIII Congreso Geológico Argentino y III Congreso de Exploración de Hidrocarburos, Actas V: 509-526.

ASTINI, R.A., RAMOS, V.A., BENEDETTO, J.L., VACCARI, N.E., y CANAS, F.L., 1996. La Precordillera: Un terreno exotico a Gondwana. XIII Congreso Geológico Argentino y III Congreso de Exploración de Hidrocarburos, Actas V: 293-324.

BALDO, E., and CASQUET, C., 1996. Garnet zoning in migmatites, and regional metamorphism, in the Sierra Chica de Córdoba (Sierras Pampeanas, Argentina). XIII Congreso Geológico Argentino y III Congreso de Exploración de Hidrocarburos, Actas V: 507.

BASSI, H.G.L., 1948. Los aluviones auríferos de la zona 'La Carolina-Rio de la Carpa' (Provincia de San Luis), Soc. Geol. Argentina, Rev., 3:1.

BASSI, H.G.L., 1992. The Sierra Alta de San Luis; a case of regmagenic control of gold mineralization. In: RICKARD, M. J., HARRINGTON, H. J., and WILLIAMS, P. R. (eds.): Basement tectonics 9, Australia and Other Regions; Proceedings of the Ninth

BENINATO, M.A., GARAY, C.H, ESPINOSA, A., REILE, E. y CAÑADAS, A., 1994. San Luis potencial minero. Gobierno de la Provincia de San Luis, Fondo Editorial SanLuiseño, Colección Investigación 24-4, 99p.

BRODTKORB, M.K. DE y BRODTKORB, A., 1975 (published in 1980). Especulaciones sobre un origen singenético-sedimentario de la scheelita presente en las metamorfitas del nordeste de la Provincia de San Luis. VI Congreso Geológico Argentino, Bahia Blanca, 1975, Actas 3: 37-50.

BRODTKORB, M.K. DE y BRODTKORB, A., 1977. Strata-bound scheelite deposits in the Precambrian basement of San Luis (Argentina). In: KLEMM,

BRODTKORB, M.K. DE y BRODTKORB, A., 1979. Consideraciones genéticas de la scheelita presente en las metamorfitas de la provincia de San Luis. Asociación Geológica Argentina, Revista, 34(2): 131-140.

BRODTKORB, M.K. DE, DONNARI, E. y VILLAR, L.M., 1976. Estudio petrocalcográfico de la perforación VI del básico de Las Aguilas, Provincia de San Luis. Servicio Minero Nacional, Informe 1126, Buenos Aires.

BRODTKORB, M.K. y PEZZUTTI, N., 1991. Yacimientos scheeliticos en rocas calcosilicaticas asociadas a anfibolitas, Provincias de San Luis y Córdoba. In: BRODTKORB, M.K. (ed.), Geología de yacimientos de wolfamio de las provincias de San Luis y Córdoba, Argentina. Publicación del Instituto de Recursos Minerales, Universidad Nacional de La Plata, 1, 169-184.

BRODTKORB, M.K., DE, PEZZUTTI, N., y BRODTKORB, A., 1985. La franja con mineralización scheelitica entre el dique La Florida y Paso del Rey, Provincia de San Luis. Asociación Geológica Argentina, Revista, XL (1-2): 51-59.

BRODTKORB, M.K., DE, PEZZUTTI, N.E., y DALLA SALDA, L.H., 1984. Presencia de vulcanismo acido en el Precámbrico de la Provincia de San Luis. Noveno Congreso Geológico Argentino, Actas, 2: 181-190.

BROGIONI, N. y RIBOT, A., 1994. Petrología de los cuerpos La Melada y La Gruta, faja máfica-ultramáfica del borde oriental de la Sierra de San Luis. Asociación Geológica Argentina, Revista, 49: 269-283.

BROGIONI, N., 1987a. El Batolito de Las Chacras-Piedras Coloradas, Provincia de San Luis. Geologia y edad. X Congreso Geológico Argentina, 4, 115-118.

BROGIONI, N., 1987b. Petrologia del vulanismo Mio-Plioceno de la Provincia de San Luis. Revista del Museo de La Plata, Tomo 10 (83), 71-100.

BROGIONI, N., 1988. Caracteres geológicos y clasificación de los domos volcanicos Mio-Pliocenos de San Luis. Revista del Museo de La Plata, Tomo 10 (84): 101-112.

BROGIONI, N., 1990. Geología y petrografia del vulcanismo Mio-Plioceno de la Provincia de San Luis. Revista del Museo de La Plata, Tomo 10 (90): 197-214.

BROGIONI, N., 1991. Caracterización pertográfica y geoquímica del Batolito de Las Chacras-Piedras Coloradas, San Luis, Argentina. VI Congreso Geológico Chileno, Resúmen Expandidos, 766-770.

BROGIONI, N., 1992. El cuerpo máfico-ultramáfico de Las Aguilas, Provincia de San Luis. Mineralogía de los silicatos. Primero Reunión de Mineralogía y Metalogenía y Primero Jornada de Mineralogía, Petrografía y Metalogénesis de rocas ultrabásicas, Actas: 379-392. La Plata.

BUTROVSKI, D., 1997. Geographic Information System (GIS) for the Sierras Pampeanas Mapping Project, Argentina. Geoscientific mapping of the Sierras Pampeanas, Argentine-Australian Cooperative Project, Australian Geological Survey Organisation, unpublished report. Arc/Info GIS.

CAELLES, J.C. y McBRIDE, S.L., 1971. Potassium-argon ages of porphyry copper and associated rocks in the Farallón Negro Capillitas District, Catamarca, Argentina. Economic Geology, 66:961-964.

CAMACHO, A. and IRELAND, T.R., 1997. U-Pb Geochronology: Final report. Geoscientific mapping of the Sierras Pampeans, Argentine-Australian Cooperative Project, Australian Geological Survey Organisation, unpublished report.

CAMACHO, A., 1997. ^{40}Ar-^{39}Ar and Rb-Sr Geochronology: Final report. Geoscientific mapping of the Sierras Pampeans, Argentine-Australian Cooperative Project, Australian Geological Survey Organisation, unpublished report.

CANDIANI, J.C., y MAZA, A.E., 1982. Sierra de Comechingones, prospeccíon Geológico-minera. Mapa Geologica Preliminar, Secretaria de Mineria, Direccion Nacional de Mineria y Geologia.

CAROTTI, M., CONDE, S.A.R., MALLAVIABARRENA, M., y RINALDI, C.A., 1985. Caracteristicas de los yacimientos de scheelita de La Pampa del Tamboreo, Provincia de San Luis. Actas del Noveno Congreso Geológico Argentino, Bariloche, 1984, 9(7): 220-230.

CERNY, P., 1991a. Rare-element granitic pegmatites. Part I: Anatomy and internal evolution of pegmatite deposits. Geoscience Canada, 18 (2): 49-67.

CERNY, P., 1991b. Rare-element granitic pegmatites. Part II: Regional to global environments and petrogenesis. Geoscience Canada, 18 (2): 68-81.

CHAMBERS, P., 1996. Survey details, technical specifications and survey logistics report for airborne geophysical survey, Córdoba, La Rioja and San Luis. Report compiled by P. Chambers, and prepared by World Geoscience Corporation Limited, for the Geoscientific Mapping of the Sierras Pampeanas Argentine-Australian Cooperative Project. Australian Geological Survey Organisation, unpublished report 14.

CHAPPELL, B.W. and WHITE, A.J., 1974. Two contrasting granite types. Pacific Geology, 8: 173-174.

CONIGLIO, J.E., Y ESPARZA, A.M., 1988. Geología del sector sur del Batolito Cerro Aspero-Alpa Corral, Provincia de Córdoba, Argentina. V Congreso Chileno., II E1-15

COSTA, C.H. and VITA-FINZI, C., 1996. Late Holocene faulting in the southeast Sierras Pampeanas of Argentina. Geology, 24, 1127-1130.

COSTA, C.H., 1996. Analysis neotectonico en las sierras de San Luis y Comechingones: problemas y methods. XIII Congreso Geológico Argentino y III Congreso de Exploración de Hidrocarburos, Actas II: 285-300.

COSTA, C.H., MURILLO, M.V., VITA-FINZI, C. and GARDINI, C.E., 1994. Quarternary folding and perspectives for paleoseismological studies in the southeastern Sierras Pampeanas, Argentina. In Prentice, C. Schwartz, D. and Yeats, R. (editors), Workshop on paleoseismology, U.S. Geological Survey Open-File Report, 94-568, 39-40.

CRAIG, H., 1961. Isotopic variations in meteoric waters. Science, 133: 1702-1703.

CRIADO ROQUE, P., MOMBRU, C. y RAMOS, V.A., 1981. Estructura y interpretación tectónica. In: Geología y recursos narurales de la Provincia de San Luis (edited by Yrigoyen, M), VIII Congreso Geológico Argentino Relat., 155-192.

D. D., SCHNEIDER, H. J. (eds.): Time- and Strata-Bound Ore Deposits, Springer Verlag, Berlin, 141-149.

DAHLQUIST, J.A. Y BALDO, E.G.A., 1996. Metamorfismo y deformacion famatinianos en la Sierra de Chepes, La Rioja, Argentina. XIII Congreso Geológico Argentino y III Congreso de Exploración de Hidrocarburos, Actas V: 393-409.

DALLA SALDA, L., 1987. Basement tectonics of the southern Pampean ranges, Argentina. Tectonics, 6, 249-260

DALLA SALDA, L., LOPEZ DE LUCHI, M., CINGOLANI, C., and VARELA, R., 1996. A Laurentia-Gondwana fit: Lower Paleozoic tectonics and granitoids. XIII Congreso Geológico Argentino y III Congreso de Exploración de Hidrocarburos, Actas II: 435-440.

DALLA SALDA, L.H., CINGOLANI, C., and VARELA, R., 1992. Early Paleozoic orogenic belt of the Andes in southwestern South america: result of Laurentia-Gondwana collision? Geology, 20, 617-620.

DALLA SALDA, L.H., CINGOLANI, C., VARELA, R., and LOPEZ DE LUCHI, M., 1995. The Famatinian Orogenic Belt in South-western South America: granites and metamorphism: an Appalachian similitude?. IX Congreso Latinoamericano de Geología, Caracas, Resumenes.

DALZIEL, I.W.D., 1991. Pacific margins of Laurentia and East Antarctica-Australia as a conjugate rift pair: Evidence and implications for an Eocambrian supercontinent. Geology, 19, 598-601.

DELAKOWITZ, B., HULL, R., BRODTKORB, M.K. DE y BRODTKORB, A., 1991. Geología génesis de yacimientos scheelíticos en la Sierra del Morro Oeste, Provincia de San Luis. En: BRODTKORB, M.K. de (Ed.), Geología de yacimientos de wolframio de las Provincias de San Luis y Córdoba. Publicación del Instituto de Recursos Minerales, Universidad Nacional de La Plata, 1: 49-96.

DEMANGE, M., BALDO, E.G., and MARTINO, R.D., 1993. Structural evolution of the Sierras de Córdoba (Argentina). Second ISAG, Oxford (UK), 21, 513-516.

DEMICHELIS, A.H., CONGLIO, J.E., OTAMENDI, J.E., y RABBIA, O.M., 1996. Geology, Petrology and geochemistry of the Sol de Mayo-Inti Yaco Metagabbro, sierra de Comechingones, Córdoba. XIII Congreso Geológico Argentino y III Congreso de Exploración de Hidrocarburos, Actas V: 413.

ESCAYOLA, M., VILLAR, L.M., y PAGE, N.J., 1993. Elementos do grupo da platina no cinturao central de rochas ultramáficas nas Sierras Pampeanas, Córdoba, Argentina. Encontro Brasileiro de EGP, 59.

ESCAYOLA, M.P., RAME, G.A., Y KRAEMER, P.E., 1996. Caracterizacion y significado geotectonico de las fajas ultramaficas de las Sierras Pampeans de Córdoba. XIII Congreso Geológico Argentino y III Congreso de Exploración de Hidrocarburos, Actas III: 421-438.

ESPARZA, A.M., y FAGIANO, M., 1995. Estudio Geológico de las rocas de caja del sector sur de la Sierra de Comechingones (entre los 32˚ 40' y 32˚ 55' LS y los 64˚ 45' y 64˚ 55' de LO) 6th Simposio Sul-Brasileiro de Geología, 1st Encontrode Geología do Cone Sul. Pg.. 175-177.

FAGIANO, M., OTAMENDI, J., NULLO, F.E., y BRIEN, C., 1992. Geologia y petrografia del Granito Los Nogales, Achiras, Provincia de Córdoba. XII Congreso Geológico Argentino y II Congreso de Exploración de Hidrocarburos, Actas IV: 33-41.

FERNANDEZ, R.R., PEZZUTTI, N., y BRODTKORB, M.K. DE, 1991. Geología, petrografía y yacimientos entre Pampa de Tamboreo - Paso del Rey - Santo Domingo, Provincia de San Luis. Publication del Instituto de Recursos Minerales, Universidad de La Plata, 1: 153-170.

FIELD, C.W. and FIFAREK, R.H., 1985. Light stable-isotope systematics in the epithermal environment. In: BERGER, B.R. and BETHKE, P.M. (eds.), Geology and geochemistry of epithermal systems, Reviews in Economic Geology, 2: 99-128.

GALINDO, C., PANKHURST, R.J., CASQUET, C., CONIGLO, J., BALDO, E., RAPELA, C.W., and SAAVEDRA, J., 1996. Two fluorite lodes located in the Achala Batholith and the Cerro Aspero Batholith (Sierras Pampeanas, Córdoba, Argentina) based on Nd- and Sr- isotope geochemistry. XIII Congreso Geológico Argentino y III Congreso de Exploración de Hidrocarburos, Actas V: 331.

GALLISKI, M.A., 1993. La Provincia Pegmatítica Pampeana. II: Metalogénesis de sus distritos económicos. Asociación Geológica Argentina, Revista, 49: 113-122.

GALLISKI, M.A., 1994. La Provincia Pegmatítica Pampeana. I: Tipología y distribución de sus distritos económicos. Asociación Geológica Argentina, Revista, 49: 99-112.

GAY, H.D. y LIRA, R., 1985. Mineralización thorífera y de tierras raras en el extremo septentrional del batolito de las Chacras, San Luis. Actas del Congreso Geológico Argentino, 9(7): 342-356.

GERVILLA, F., SANCHEZ-AGUILA, A., ACEVEDO, R.D., y FENOLL HACH-ALI, P., 1995. Mineralogía de los elementos del grupo del platino del yacimiento Ni-Cu de Las Aguilas, Provincia de San Luis. Congreso Nacional de Geología Económica, San Juan, Secretaría de Minería de la Nación.

GONZALE, R.R. y ACENOLAZA, F.G. 1972. La cuenca de deposición neopaleozóica-mesozóica del oeste argentino. Fundación e Instituto Miguel Lillo, Tucamán, Miscelánea. 40: 629-643.

GONZALEZ BONORINO, F., 1961. Petrología de algunos cuerpos básicos de San Luis y las granulitas asociadas. Asociación Geológica Argentina, Revista, XVI(1-2): 61-106.

GORDILLO, C.E. y LINARES, E., 1981. Geochronología y petrografía de las vulcanitas Terciarias del Departamento Pocho. Asociación Geológica Argentina, Revista, XXXVI: 380-388.

GORDILLO, C.E., 1984. Migmatites cordieriticas de la Sierra de Córdoba; condiciones fisicas de la migmatización. Acadamia Nacional de Ciencas; Miscelánea 68, 40p, Córdoba

GRANT, J.A. 1985. Phase equilibria in low-pressure partial melting of pelitic rocks. American Journal of Science, 285, 409-435.

HACK, M., BRODTKORB, M.K. DE, HÜLL, R., y BRODTKORB, A., 1991. Geología y consideraciones genéticas de los yacimientos scheeliticos entre el dique La Florida y Pampa de Tamboreo, Provincia de San Luis. Publication del Instituto de Recursos Minerales, Universidad de La Plata, 1: 113-152.

HERRERA, A.O., 1963. Las pegmatitas de la Sierra de San Luis: Estructura interna, mineralogía y génesis. Asociación Geológica Argentina, Revista, 18(1-2): 43-71.

HERRERA, A.O., 1965. Evolución geoquímica de las pegmatitas zonales de los principales distritos Argentinos. Asociación Geológica Argentina, Revista, 20: 2.

HERRERA, A.O., 1968. Geochemical evolution of zoned pegmatites of Argentina, Economic Geology, 63: 13-29.

HOATSON, D.M., WALLACE, D.A., SUN, S-S., MACIAS, L.F., SIMPSON, C.J., and KEAYS, R.R., 1992. Petrology and platinum-group-element geochemistry of Archean layered mafic-ultramafic intrusions, west Pilbara Block, Western Australia. Australian Geological Survey Organisation, Bulletin 242.

HUNGERFORD, N. and PIETERS, P., 1996. Magnetic interpretation - Sierras de Chepes y Las Minas. Geoscientific Mapping of the Sierras Pampeanas Argentine-Australian Cooperative Project, Australian Geological Survey Organisation, unpublished report 29.

HUNGERFORD, N., LYONS, P. and STUART-SMITH, P.G., 1996a. Magnetic interpretation - Sierras Septentrionales de Córdoba. Australian Geoscientific Mapping of the Sierras Pampeanas Argentine-Australian Cooperative Project, Australian Geological Survey Organisation, unpublished report 28.

HUNGERFORD, N., SIMS, J.P. and STUART-SMITH, P.G., 1996b. Magnetic interpretation - Sierras de San Luis y Comechingones. Geoscientific Mapping of the Sierras Pampeanas Argentine-Australian Cooperative Project, Australian Geological Survey Organisation, unpublished report 30.

JORDAN, T.E. and ALLMENDINGER, R.W. 1986. The Sierras Pampeanas of Argentina: A modern analogue of Rocky Mountain foreland deformation. American Journal of Science, 286: 737-764.

KAY, S. MAHLBURG, and GORDILLO, C.E., 1985. Expiration of volcanism over the Andean flat slab: the 5-7 m.y. Pocho volcanic field, central Argentina. Geological Society of America Abstracts with Programs,17: 624.

KAY, S. MAHLBURG, MAKSAEV, V., MOSCOSO, R., MPODOZIS, C., NASI, C. y GORDILLO, C.E., 1988. Tertiary Andean magmatism in Chile and Argentina betweeen 28S and 33S: Correlation of magmatic chemistry with a changing Benioff zone. Journal of South American Earth Sciences, 1(1):21-38.

KELLER, M., and DICKERSON, P.W., 1996. The missing continent of Llanoria - was it the Argentine Precordillera? XIII Congreso Geológico Argentino y III Congreso de Exploración de Hidrocarburos, Actas V: 355-367

KILMURRAY, J. y VILLAR, L., 1981. El basamento de la Sierra de San Luis y su petrología. VIII Congreso Geológico Argentino, San Luis, Relatorio, I: 33-55.

KRAEMER, P., ESCAYOLA, M.P., y MARTINO, R.D., 1995. Hipótesis sobre la evolucíon tectónica neoproterozoica de las Sierras Pampeanas de Córdoba (30˚40' - 32˚40'), Argentina. Revista de la Asociacíon Geológica Argentina, 50, 47-59.

KRAEMER, P., ESCAYOLA, M.P., y SFRAGULLA, J., 1996. Dominios tectonicos y mineralizacion en el basamento de las Sierras Pampeanas de Córdoba. XIII Congreso Geológico Argentino y III Congreso de Exploración de Hidrocarburos, Actas II: 239-248.

LACREU, H.L., 1990. Control estructural de los depósitos calcareos geotermales, proximos al Cerro Tiporco, Pcia. de San Luis. Decimo Primer Congreso Geológico Argentino, San Juan, 1990, Actas, 1: 328-331.

LACREU, H.L., 1992. Secuencias epiclasticas y volcaniclasticas Cenozoicas en la Cantera Santa Isabel y alrededores, Dpto. Cnel. Pringles, Pcia. de San Luis. Cuarta Reunión Argentina de Sedimentología, I: 219-226.

LACREU, H.L., 1995. Origen de las soluciones mineralizadoras del onice calcareo 'Santa Isabel', Pcia. de San Luis, República Argentina. V Congreso Nacional de Geología Económica, San Juan, 1995, 190-200.

LEMA, H. 1980. Geología de los afloramientos del arroyo Peñas Blancas, sierra de Yulto, Provincia de San Luis. Revista de la Asociacíon Geológica Argentina, 35, 147-150.

LEVERATO, M.A. y MALVICINI, L., 1982. Geología y génesis del yacimiento de wolframio El Duraznito, San Luis. Asociación Geológica Argentina, Revista, 37: 369-383.

LINARES, E. y GONZALES, R.R., 1990. Catalogo de edades radimtricas de la Republica Argentina. Años 1957 - 1987. Publicaciones especiales de la Asociacion Geologica Argentina, Serie "B" (Didáctica y Complementaria). N° 19. 627pp.

LINARES, E., 1959. Los métodos geochronológicos y algunas edades de minerales de la Argentina, obtenidas por medio de la relación plomo-uranio. Asociacion Geológica Argentina, Revista, 14: 181-217.

LLAMBIAS, E. y BROGIONI, N., 1981. Magmatismo Mesozoico y Cenozoico. Relatorio VIII Congreso Geológico Argentino, 101-115.

LLAMBIAS, E.J. y MALVICINI, L., 1982. Geología y génesis de los yacimientos de tungsteno de las Sierras del Morro, Los Morrillos y Yulto, Provincia de San Luis. Asociación Geológica Argentina, Revista, 37: 100-143.

LLAMBIAS, E.J., CINGOLANI, C., VARELA, R., PROZZI, C., ORTIZ SUAREZ, A., TOSELLI, A. y SAAVEDRA, J., 1991. Leucogranodioritas sin-cinemáticas ordovícicas en la Sierra de San Luis. VI Congreso Geológico Chileno Resúmenes Expandidos. 187-191.

LLAMBIAS, E.J., QUENARDELLE, S., SUAREZ, A.O., y PROZZI, C., 1996a. Granitoides sin-cinematicos de la Sierra Central de San Luis. XIII Congreso Geológico Argentino y III Congreso de Exploración de Hidrocarburos, Actas III: 487-496.

LLAMBIAS, E.J., SATO, A.M., PROZZI, C. y SANCHEZ, V., 1996b. Los pendants de gneises en el plutón Gasparillo: Evidencia de un metamorfismo pre-Famatiniano en las Sierras de San Luis. XIII Congreso Geológico Argentino y III Congreso de Exploración de Hidrocarburos, Actas V: 369-376.

LOPEZ, M.G., 1984. Relaciones petrológicas entre pegmatitas y sus cajas en la región de Tilisarao-Renca, Provincia de San Luis. Asociación Geológica Argentina, Revista, 39(1-2): 131-143.

LYONS, P. and SKIRROW, R.G., 1996. Whole rock and stable isotope geochemistry - Final Report. Geoscientific mapping of the Sierras Pampeanas, Argentine-Australian Cooperative Project, Australian Geological Survey Organisation, unpublished report.

LYONS, P., STUART-SMITH, P.G., SIMS, J.P., PIETERS, P., SKIRROW, R.G. and CAMACHO, A., 1996. Whole Rock Geochemistry Report Geoscientific mapping of the Sierras Pampeanas, Argentine-Australian Cooperative Project, Australian Geological Survey Organisation, unpublished report.

MALVICINI, L. y BROGIONI, N., 1993. Petrología y génesis del yacimiento de sulfuros de Ni, Cu y platinoideos 'Las Aguilas Este', Provincia de San Luis. Asociación Geológica Argentina, Revista, 48: 3-20.

MALVICINI, L. y URBINA, N.E., 1995(?). Mina La Rica, un depósito epitermal de tipo sericite-adularia asociado a rocas volcanicas Terciarias de la Sierras de San Luis, República Argentina. Congreso abstract?, 2p.

MALVICINI, L., ORTIZ SUAREZ, A., SOSA, G.M., ULACCO, H. y RAMOS, G., 1991. El ciclo metalogenético Precambrico-Paleozoico de la Sierra de San Luis, República Argentina. 6 Congreso Geológico Chileno, Resumenes Ampliados, 101-105.

MARTINO, R., KRAEMER, P., ESCAYOLA, M., and GUERESCHI, A., 1994. Thermobarometry at 32 00'S in the Pampean Ranges near Córdoba, Argentina. Geological Society of America, Seattle, Abstracts.

MARTINO, R., KRAEMER, P., ESCAYOLA, M., GIAMBASTIANI, M., y ARNOSIO, M., 1995. Transect de Las Sierras Pampeanas de Córdoba a los 32˚ S. Revista de la Asociacíon Geológica Argentina, 50, 60-77.

MARTINO, R.D., 1993. Taconic- (Ocloyic-) afged west-directed ductile thrusts in basement rocks of the sierras Pampeanas, Argentina. Geological Society of America, 1993 Annual Meeting, Boston, Abstracts, 233.

MARTINO, R.D., and SIMPSON, C., 1993. Taconic- (Ocloyic-) aged west-directed ductile thrusts in basement rocks of the Sierras Pampeanas, Argentina. Geological Society of America, Annual general Meeting, Boston, Abstracts A-233

MARTINO, R.D., SIMPSON, C., and LAW, R.D., 1994. Ductile thrusting in Pampean ranges: its relationships with the Ocloyic deformation and tectonic significance. IGCP Projects 319/376, Novia Scotia, Abstracts.

MATSUHISA, Y., GOLDSMITH, J.R. and CLAYTON, R.N., 1979. Oxygen isotope fractionation in the system quartz-albite-anorthite-water. Geochimica et Cosmochimica Acta, 43: 1131-1140.

McDOUGALL, I. y HARRISON, T.M., 1988. Geochronology and thermochronology by the $^{40}Ar/^{39}Ar$ method. Oxford University Press, New York.

MEINERT, L.D., 1993. Igneous petrogenesis and skarn deposits. In: KIRKHAM, R.V., SINCLAIR, W.D., THORPE, R.I. and DUKE, J.M. (eds), Mineral Deposit Modeling. Geological Association of Canada Special Paper 40, 569-584.

MIRANDA, S., y INTROCASO, A., 1996. Cartas gravimetricas y comportamiento isostatico areal de las Sierras de Córdoba - Rep. Argentina. XIII Congreso Geológico Argentino y III Congreso de Exploración de Hidrocarburos, Actas II: 405-417.

MONCHABLON, A., 1956. Yacimientos de wolframio de la Provincia de San Luis, Dirección Nacional de Geología y Minería, Buenos Aires, inedito.

MORTEANI, G., PREINFALK, C., SPIEGEL, W. and BONALUMI, A.A., 1995. The Achala granitic complex and the pegmatites of the Sierras Pampeanas (northwest Argentina): A study of differentiation. Economic Geology, 90: 636-647.

MURRA, J.A., y BALDO, E.G., 1996. El granito de Capilla del Monte y su encajonante ígneo-metamórfico, Sierras Pampeanas de Córdoba. XIII Congreso Geológico Argentino y III Congreso de Exploración de Hidrocarburos, Actas III: 499-505.

MUTTI, E. and RICCHI LUCCHI, F., 1978. Turbidites of the Northern Apennines: introduction to facies analysis. International Geological Review, 20, 125-166.

NALDRETT, A.T., 1989. Magmatic sulfide deposits. Clarendon Press - Oxford University Press, New York - Oxford.

NULLO, F.E., FAGIANO, M.R., y OTAMENDI, J.E., 1992. Geologia y Petrologia de los granitoides del sur de la Sierra de Comechingones, Córdoba, Argentina. Estudios Geol., 48, 221-227

O'NEIL, J.R. and TAYLOR, H.P.J., 1969. Oxygen isotope equilibrium between muscovite and water. Journal of Geophysical Research, 74: 6012-6022.

ORTIZ SUAREZ, A., PROZZI, C. y LLAMBIAS, E.J., 1992. Geología de la parte sur de la Sierra de San Luis y granitoides asociados, Argentina. Estudios Geológicos, España, 48(5-6): 269-277.

ORTIZ SUAREZ, A.E. y SOSA, G.M., 1991. Relaciones genéticas entre las pegmatitas portadores de estaño y metamorfitas asociadas en la zona de La Carolina / San Francisco del Monte de Oro, Provincia de San Luis. Asociación Geológica Argentina, Revista, XLVI(3-4): 339-343.

OTAMENDI, J.E., NULLO, F.E., FAGIANO, M. y ARAGON, E., 1996. Dos Terrenos Metamorficos y estructurales en el extremo sur de la Sierra de Comechingones, Córdoba-San Luis: Algunas implicacias tectonicas. XIII Congreso Geológico Argentino y III Congreso de Exploración de Hidrocarburos, Actas II: 249-266.

OYARZABAL, J.C. y GALLISKI, M.A., 1993. Geología del yacimiento San Luis: Un caso de yuxtaposición de tipologías diferentes en pegmatitas de clase elementos raras. XII Congreso Geológico Argentino, Actas, V: 167-174.

PASTORE, F. y GONZALES, R.L., 1954. Descripcíon geológica de la Hoja 23g, San Francisco (San Luis). Dirreccíon Nacional de Mineria, Republica Argentina, 80, 62p.

PASTORE, F. y RUIZ HUIDOBRO, O.J., 1952. Descripcíon geológica de la Hoja 24g, Saladillo (San Luis). Dirreccíon Nacional de Minería, República Argentina, 78, 63p.

PEREZ, M.B., RAPELA, C.W., y BALDO, E.G., 1996. Geología de los granitoides del sector septentrional de la Sierra Chica de Córdoba. XIII Congreso Geológico Argentino y III Congreso de Exploración de Hidrocarburos, Actas V: 493-505.

PIETERS, P. and SKIRROW, R.G., 1996. Regional geology, mineral deposits and prospectivity of the Sierra de Chepes and Sierra de Las Minas, La Rioja Province: Preliminary results of the DNSG-AGSO Mapping Project. Geoscientific Mapping of the Sierras Pampeanas Argentine-Australian Cooperative Project, Australian Geological Survey Organisation, unpublished report.

PINOTTI, L.P., CONIGLIO, J.E., y LLAMBIAS, E.J., 1996. Características geológico-estructurales del Plutón Alpa-Corral, 32∞ 38' - 32∞ 47'S y 64∞ 55' - 64∞ 45'W., Sierras Pampeanas de Córdoba, Argentina. XIII Congreso Geológico Argentino y III Congreso de Exploración de Hidrocarburos, Actas III: 477-486.

PINOTTI, L.P., ESPARZA, A., y CONIGLIO, J.E., 1992. Formacion de megacristales de feldespato potasico en el sector sur del batolito Cerro Aspero-Alpa Corral (32∞ 40' y 64∞ 50'W), Sierras Pampeanas, Córdoba, Argentina. Estudios geol. 48, 211-219.

PROZZI, C.R. y RAMOS, G. 1988. La Formación San Luis. I Jornadas de trabajo de Sierras Pampeanas, San Luis.

RABBIA, O., DEMICHELIS, A., HERNÁNDEZ, L., OTAMENDI, J., and CONIGLO, J., 1996. Evidence ofpre-metamorphic within-plate magmatism in the Sierras de Córdoba, eastern Sierras Pampeanas, Argentina. XIII Congreso Geológico Argentino y III Congreso de Exploración de Hidrocarburos, Actas V: 441.

RAMOS, G., 1990. Estudios preliminares sobre el control estructural en la mina de scheelita 'La Teodolina', Provincia de San Luis, Argentina. Decimo Primer Congreso Geológico Argentino, San Juan, 1990, Actas, 1: 357-360.

RAMOS, G.A., 1992. Caracteres estructurales de algunas manifestaciones de scheelita en la zona de la Mina 'La Teodolina', San Luis, Argentina. In: BRODTKORB, M.K. DE y SCHALAMUK, I.B. (eds.), I Reunión de mineralogía y metalogenía, La Plata, 1991. Instituto de Recursos Minerales, Universidad Nacional de La Plata, No. 2: 237-247.

RAMOS, V., MUNIZAGA, F. y KAY, S. MAHLBERG, 1991. El magmatismo Cenozoico a los 33S de latitud: Geocronología y relaciones tectónicas. 6 Congreso Geológico Chileno, 1: 892-896.

RAMOS, V.A., 1996. Late Proterozoic - Early Paleozoic of South America - a collisional histrory. Episodes, 11, 168-174.

RAMOS, V.A., JORDAN, T.E., ALLMENDINGER, R.W., MPODOZIS, C., KAY, S., CORTES, J.M., and PALMA, M.A., 1986. Paleozoic terranes of the Central Argentine-Chilean Andes. Tectonics, 5, 855-880.

RAMOS, V.A., VUJOVICH, G.I., Y DALLMEYER, R.D., 1996. Los Klippes y ventanas tectonicas preandicas de La Sierra de pie de Plao (San Juan): edad e implicacaciones tectonicas. XIII Congreso Geológico Argentino y III Congreso de Exploración de Hidrocarburos, Actas V: 377-391.

RAPELA, C.W., SAAVEDRA, J., TOSELLI, A., Y PELLITERO, E, 1996. Eventos magmaticos fuertemente peraluminosos en las Sierras Pampeanas. XIII Congreso Geológico Argentino y III Congreso de Exploración de Hidrocarburos, Actas V: 337-353.

RAPELA, C.W., and PANKHURST, R.J., 1996. The Cambrian plutonism of the Sierras de Cordoba: pre-Famatinian subduction? and crustal melting. XIII Congreso Geológico Argentino y III Congreso de Exploración de Hidrocarburos, Actas V: 491.

RAPELA, C.W., TOSELLI, A., HEAMAN, L. y SAAVEDRA, J., 1990. Granite plutonism of the Sierras Pampeanas: An inner cordilleran Paleozoic arc in the southern Andes. Geological Society of America Special Paper 241: 77-90.

RICCI, S.M., 1971. Provincia de San Luis - Mapa Minero, Escala 1:750 000, Ministero de Indústria y Minería, Subsecretería de Minería, Dirección Nacional de Promoción Minera.

RINALDI, C. A., 1968. Estudio de las pegmatitas uraniferas de las Sierras de Comechingones, Provincia de Córdoba. Asociacion Geológica Argentina, Revista, 23: 161-195.

RINALDI, C.A. y LINARES, E., 1973. Edades potasio-argón de pegmatitas de la provincia de San Luis. V Congreso Geológico Argentino, Actas I: 411-418.

ROEDER, P.L. y EMSLIE, R.F., 1970. Olivine-liquid equilibrium. Contributions to Mineralogy and Petrology, 29: 275-289.

ROLLINSON, H.R. 1993. Using Geochemical Data: Evaluation, Presentation, Interpretation. Longman Scientific and Technical. New York 352 pp.

ROSSELLO, E.A. y BARBOSA, C.E., 1988. Tantalatos y otros minerales detríticos con interes económico en el aluvión aurífero de Cañada Honda, San Luis. Asociación Geológica Argentina, Revista, 43(3): 296-303.

ROSSELLO, E.A. y CASTRO, L.N., 1995. Consideraciones genéticas del oro detrítico de Cañada Honda, Carolina, San Luis, Argentina. V Congreso de Geología Económico, San Juan, Actas, 1: 95-108.

ROSSELLO, E.A., 1987. Primera manifestación antimonífera en la Provincia de San Luis y aportes sobre su control estructural. Asociacion Geológica Argentina, Revista, XLII: 196-200.

SABALUA, J., CHABERT, M., y SANTAMARIA, G., 1981. Mineralización de sulfuros de hierro, cobre y niquel, en el cuerpo basico de Las Aguilas, Provincia de San Luis. VIII Congreso Geológico Argentino, San Luis, Actas, IV: 497-507.

SABALUA, J.C., 1986. Yacimiento Las Aguilas: Mineralización Ni-Cu-Co, Departamento Pringles, Provincia de San Luis, República Argentina, Dirección General de Fabricaciones Militares, Subdirección de Desarrollo Minero, Centro de Exploración Geológico Minera, 29p.

SANCHEZ, V., SAUREZ, A.O. y PROZZI, C. 1996. Geologia y petrografia de la tonalita bemberg, Provincia de San Luis. XIII Congreso Geológico Argentino y III Congreso de Exploración de Hidrocarburos, Actas III: 669-677.

SATO, A.M., SUAREZ, A.O., LLAMBIAS, E.J., CAVAROZZI, C.E., SANCHEZ, V., VARELA, R., y PROZZI C., 1996. Los plutones pre-Ocloyicos del sur de la Sierra de San Luis: Arco magmatico al inicio del ciclo Famatiniano. XIII Congreso Geológico Argentino y III Congreso de Exploración de Hidrocarburos, Actas V: 259-272.

SCHMIDT, C., 1993. Neogene inversion of two Cretaceous basins, Sierrras Pampeanas, Argentina. Geological Society of America, 1993 Annual Meeting, Boston, Abstracts, 233.

SHEPPARD, S.M.F., 1986. Characterisation and isotopic variations in natural waters. In: Valley, J.W., Taylor, H.P.J. and O'Neil, J.R. (eds), Stable isotope in high temperature geological processes, Reviews in Mineralogy, Mineralogical Society of America, 16: 165-184.

SILLITOE, R.H., 1993. Epithermal models: Genetic types, geometrical controls and shallow features. In: Mineral deposit modeling, R.V. Kirkham, W.D. Sinclair, R.I. Thorpe and J.M. Duke, eds., Geological Association of Canada Special Paper 40, p. 403-417.

SIMKIN, T. and SMITH, J.V., 1970. Minor element distribution in olivine. Journal of Geology, 78:304-325.

SIMS, J.P., STUART-SMITH, P.G., LYONS, P., PIETERS, P., SKIRROW, R.G. and CAMACHO, A., 1996. Petrography Report. Geoscientific mapping of the Sierras Pampeanas, Argentine-Australian Cooperative Project, Australian Geological Survey Organisation, unpublished report.

SKIRROW, R.G. and TRUDU, A., 1997. ARGMIN: a mineral deposit database for the Sierras Pampeanas, Republic of Argentina. Geoscientific mapping of the Sierras Pampeanas, Argentine-Australian Cooperative Project, Australian Geological Survey Organisation, unpublished report. Database in Microsoft Access and Oracle.

SKIRROW, R.G. y JOHNSTON, A.I., 1997. Atlas Metalogenético de las Sierras Pampeanas, República Argentina. Geoscientific mapping of the Sierras Pampeanas, Argentine-Australian Cooperative Project, Australian Geological Survey Organisation, unpublished report.

SMALLEY, R. Jr., PUJOL, J., REGNEIR, M., CHIU, J.M., CHATELAIN, J.L., ISACKS, B.L., ARAUJO, M. and PUEBLA, N., 1993., Basement seismicity beneath the Andean Precordillera thin-skinned thrust belt and implications for crustal and lithospheric behaviouor. Tectonics, 12, 63-76.

SMITH, W.C. and GONZALES, E.M., 1947. Tungsten investigations in the Republic of Argentina, 1942-43, U.S. Geological Survey Bulletin, 954-A:1-37.

SOSA, G.M, 1991. Pegmatitas portadoras de estaño de la Provincia de San Luis: Su geología, mineralogía y génesis. Primero Reunión de Mineralogía y Metalogenía, La Plata, Instituto de Recursos Minerales, Universidad Nacional de La Plata, Actas, (2): 379-392.

SOSA, G.M., 1990. Relaciones entre las pegmatitas portadores de estaño y las portadoras de niobio-tantalo de la Provincia de San Luis. Decimo Primer Congreso Geológico Argentino, San Juan, 1990, Actas, 1: 366-368.

SOSA, G.M., 1993. Pegmatita estannifera compleja mina 'Victor Hugo', Provincia de San Luis. XII Congreso Geológico Argentino, Actas, V: 159-166.

SOSIC, M., 1964. Descripcíon geológica de la Hoja 24 h - Sierra del Morro, San Luis-Córdoba. Dirreccíon Nacional Geologia y Mineria, Buenos Aires, 95, 44p

SPEAR, F.S., 1981. An experimental study of hornblende stability and compositional variability in amphibolite. AmericanJournal of Science, 281, 697-734.

SPEAR, F.S., 1993. Metamorphic phase equilibria and pressure-temperature-time paths. Mineralogical Society of America, Monograph. 799pp.

SRUOGA, P., URBINA, N. y MALVICINI, L., 1996. El volcanismo Terciario y los depósitos hidrotermales (Au, Cu) asociados en La Carolina y Diente Verde, San Luis, Argentina. XIII Congreso Geológico Argentino, Actas I: 89-100.

STOLL, W.C., 1963a. Los yacimientos de scheelita de Cerro Los Cocos (Provincia de San Luis), Asociación Geológica Argentina, Revista, 18(3-4): 116-120.

STOLL, W.C., 1963b. La geología del tungsteno en Argentina. Asociación Geológica Argentina, Revista, 18(1-2): 96-106.

STRASSER, E.N., TOGNELLI, G.C., CHIESA, J.O. y PRADO, J.L., 1996. Estratigrafia y sedimentologia de los depositos eolicos del pleistoceno tardio y Holoceno en el sector sur de la sierra de San Luis. XIII Congreso Geológico Argentino y III Congreso de Exploración de Hidrocarburos, Actas IV: 73-83.

STUART-SMITH, P.G. and LYONS, P., 1995. Reconnaissance Field Survey - Progress Report. Geoscientific Mapping of the Sierras Pampeanas Argentine-Australian Cooperative Project, Australian Geological Survey Organisation, unpublished report 11.

STUART-SMITH, P.G., MIRO, R.C., PIETERS, P.E., LYONS, P., SIMS, J.P. and CAMACHO, A., 1996. Tectonic framework of the southern Sierras Pampeanas, Argentina. XIII Congreso Geológico Argentino, Actas II: 147.

STUART-SMITH, P.G., PIETERS, P., SKIRROW, R.G., SIMS, J.P., CAMACHO, A. and LYONS, P., 1996. Field Program 2 - Progress Report. Geoscientific Mapping of the Sierras Pampeanas Argentine-Australian Cooperative Project, Australian Geological Survey Organisation, unpublished report 19.

STUART-SMITH, P.G., PIETERS, P., SIMS, J.P. and LYONS, P., 1996. Field Program 3 - Progress Report. Geoscientific Mapping of the Sierras Pampeanas Argentine-Australian Cooperative Project, Australian Geological Survey Organisation, unpublished report 25.

SUAREZ, A.O., PROZZI, C. y LLAMBIAS, E.J., 1992. Geologia de la parte sur de la Sierra de San Luis y granitoides asociados, Argentina. Estudios Geologicos, 48, 269-277.

THOMPSON, J.F.H. and NALDRETT, A.J., 1984. Sulfide-silicate reactions as a guide to Ni-Cu-Co mineralization in central Maine. In: BUCHANAN, D.L and JONES, M.J. (eds.), Sulfide deposits in mafic and ultramafic rocks, Institute of Mining and Metallurgy Special Publication, 103-113.

TOSELLI, A.J., DALLA SALDA, L., y CAMINOS, R., 1992. Evolucíon metamórfica del Paleozoic Inferior de Argentina. In J.G. Gutiérrez Marco, J Saavedra y I. Rábano (Eds), Paleozoico Inferior de Ibero-América. Universidad de Extremadura.

TOSELLI, A.J., DURAND, F.R., ROSSI DE TOSELLI, J.N., y SAAVEDRA, J., 1996. Esquema de evolucion geotectonica y magmatica eopaleozoica del Sistema de Famatina y sectores de Sierras Pampeanas. XIII Congreso Geológico Argentino y III Congreso de Exploración de Hidrocarburos, Actas V: 443-462.

URBINA, N., SRUOGA, P. y MALVICINI, L., 1995. El volcanismo Mioceno y la mineralización aurífera asociada en La Carolina y Diente Verde, Provincia de San Luis, Argentina, Set de diskettes del IX Congreso Latinoamericano de Geología, Caracas, Venezuela.

VENNEMANN, T.W. and O'NEIL, J.R., 1996. Hydrogen isotope exchange reactions between hydrous minerals and molecular hydrogen: I. A new approach for the determination of hydrogen isotope fractionation at moderate temperatures. Geochimica et Cosmochimica Acta, 60: 2437-2451.

VON GOSEN, W. and PROZZI, C., 1996. Geology, structure and metamorphism in the area south of La Carolina (Sierra de San Luis, Argentina). XIII Congreso Geológico Argentino y III Congreso de Exploración de Hidrocarburos, Actas II: 301-314.

VUJOVICH, G., MILLER, H., and RAMOS, V.A., 1994. Proterozoic metavolcanics from western Sierras Pampeanas terrane, Argentina. Journal of South American Earth Sciences, 7: 309-323.

WILLNER, A.P., and MILLER, H., 1986. Structural division and evolution of the lower Paleozoic basement in the NW Argentine Andes. Zentralblat fur Geologie und Paläontologie, I, 1245-1255.

WINKLER, H.G.F., 1979. Petrogenesis of metamorphic rocks. Springer-Verlag, 5th Edition, New York.

WYBORN, L.A.I., HEINRICH, C.A. and JAQUES, A.L., 1994. Australian Proterozoic Mineral Systems: Essential ingredients and mappable criteria. In: Australian Institute of Mining and Metallurgy Conference, Proceedings, Darwin, 5-9 August 1994: 109-115.

ZARDINI, R., 1966. Composición, estructura y origen de la Pampa del Tamboreo (provincia de San Luis). Acta Geológica Lilloana, 8, 50- 73.

APPENDIX A

Sierras de San Luis and Comechingones
Field observation locations, lithologies and geophysical rock properties

Site ID	Observation site identification number
Latitude	Decimal degrees
Longitude	Decimal degrees
Sample No	Field sample identification number
Rock Type	Brief lithological description
Min	Minimum magnetic susceptibility (SI units x 10^{-5})
Max	Maximum magnetic susceptibility (SI units x 10^{-5})
Mean	Mean magnetic susceptibility (SI units x 10^{-5})
K	Spectometric response, counts per second Potassium
Th	Spectometric response, counts per second Thorium
U	Spectometric response, counts per second Uranium
Tc	Spectometric response, total counts per second
Pet	Number of samples thin sectioned for petrographic analysis
Chem	Sample collected for whole rock geochemical analysis
Chron	Sample collected for geochronological analysis
	U-Pb: zircon SHRIMP analysis
	Ar-Ar: muscovite or biotite ^{40}Ar-^{39}Ar analysis

Site ID	Latitude	Longitude	Sample No	Rock type	Min	Max	Mean	K	Th	U	Tc	Pet	Chem	Chron
A95JS001	-32.852361	-66.105949	A95JS001	biotite-muscovite-k-feldspar granite										
A95JS002	-33.071430	-66.067810	A95JS002	biotite-sillimanite-garnet schist			23							
A95JS003	-33.077744	-66.108898	A95JS003A	amphibolite			86					1	x	
			A95JS003B	amphibolite										
A95JS004	-33.059870	-66.141879	A95JS004	muscovite-biotite schist			2							
A95JS005	-33.054640	-66.142230	A95JS005	muscovite-biotite schist										
A95JS006	-33.050497	-66.139667	A95JS006	muscovite-quartz schist			1							
A95JS007	-33.047973	-66.128680	A95JS007	biotite-sillimanite-muscovite schist			2							

Site ID	Latitude	Longitude	Sample No	Rock type	Min	Max	Mean	K	Th	U	Tc	Pet	Chem	Chron
A95JS008	-33.051322	-66.128464	A95JS008	foliated granite			3							
A95JS009	-33.055713	-66.120699	A95JS009	garnet-bearing mylonite			7							
A95JS010	-33.073639	-66.129794	A95JS010	pegmatite			0							
A95JS011	-33.074955	-66.125511	A95JS011A	garnet-bearing mylonite			1680					1	x	
			A95JS011B	sillimanite-bearing mylonite										
			A95JS011C	garnet-sillimanite bearing mylonite										
			A95JS011D	sillimanite-bearing mylonite								1	x	
			A95JS011E	metabasic rock										
A95JS012	-33.094239	-66.118093	A95JS012	amphibolite			137							
A95JS013	-33.110557	-66.107994	A95JS013	garnet-sillimanite-biotite-cordierite gneiss			1191							
A95JS014	-33.108075	-66.001505	A95JS014A	biotite-muscovite schist			13						x	
			A95JS014B	tourmaline-bearing mylonite										
A95JS015	-33.108439	-66.000560	A95JS015	metaquartzite			1							
A95JS016	-33.109242	-65.995696	A95JS016	muscovite-garnet schist			22					1	x	
A95JS017	-33.102452	-65.936309	A95JS017	muscovite-biotite schist			20					1	x	
A95JS018	-33.104275	-65.930521	A95JS018	muscovite-biotite schist			20							
A95JS019	-33.110926	-65.921004	A95JS019	muscovite-biotite-(aluminosilicate) schist			13					1	x	
A95JS020	-33.120953	-65.908588	A95JS020	muscovite-biotite schist			14							
A95JS021	-33.037553	-66.088273	A95JS021	muscovite-biotite schist			7							
A95JS022	-33.063167	-66.151225	A95JS022	quartz-feldspar gneiss			6							
A95JS023	-33.067689	-66.155961	A95JS023	biotite-muscovite schist			19							
A95JS024	-33.068569	-66.164689	A95JS024	muscovite-andalusite schist			3					1	x	
A95JS025	-33.065667	-66.168895	A95JS025	interbedded phyllite and quartzite			16					1	x	
A95JS026	-33.063929	-66.173648	A95JS026	mylonitic granite			18							
A95JS027	-33.110985	-66.110401	A95JS027A	biotite-sillimanite-garnet-cordierite gneiss			2622							
			A95JS027B	garnet cordierite gneiss										
			A95JS027C	spinel-bearing gneiss										
			A95JS027D	pyroxene hornblende plagioclase gneiss										
			A95JS027E	cordierite bearing pegmatite										
A95JS028	-33.113330	-66.114848	A95JS028A	composite layered gneiss (para- & ortho-gneiss)			9905							
			A95JS028B	garnet-bearing metapsammitic gneiss										
			A95JS028C	pelitic gneiss										
			A95JS028D	sillimanite-bearing gneiss								1	x	
A95JS029	-33.066470	-66.179483	A95JS029A	medium-grained, foliated granite			10					1	x	
			A95JS029B	mylonitic granite								1	x	Ar-Ar
A95JS030	-33.205399	-66.176577	A95JS030	quartz-feldspar-biotite schist			3					1	x	
A95JS031	-33.206767	-66.184645	A95JS031	mylonitic granite			2							
A95JS032	-33.197116	-66.199740	A95JS032	muscovite-quartz schist			6							
A95JS033	-33.196017	-66.251201	A95JS033	k-feldspar-quartz-biotite granite			9					1	x	U-Pb
A95JS034	-33.212502	-66.220426	A95JS034A	biotite-quartz-feldspar granodiorite			20					1	x	
			A95JS034B	granite								1	x	

Site ID	Latitude	Longitude	Sample No	Rock type	Min	Max	Mean	K	Th	U	Tc	Pet	Chem	Chron
A95JS035	-33.207400	-66.213253	A95JS035A	biotite-muscovite mylonite			16							Ar-Ar
			A95JS035B	mylonite								1	x	
			A95JS035C	mylonitic pegmatite										
A95JS036	-33.199101	-66.217609	A95JS036	mylonitic granite			12							
A95JS037	-33.190212	-66.211397	A95JS037	foliated k-feldspar porphyritic granite			9					1	x	
A95JS038	-33.188984	-66.207894	A95JS038	muscovite-biotite schist			23							
A95JS039	-33.187133	-66.204660	A95JS039	mylonitic k-feldspar porphyritic granite			15						x	
A95JS040	-33.115078	-66.122793	A95JS040A	pelitic gneiss			3749					1	x	
			A95JS040B	cordierite-bearing leucosome										
A95JS041	-33.116570	-66.127728	A95JS041	garnet cordierite gneiss			2962					1	x	
A95JS042	-33.118769	-66.132610	A95JS042	sillimanite-garnet-cordierite gneiss			1012							
A95JS043	-33.249366	-66.181603	A95JS043	muscovite-quartz-biotite schist			2							
A95JS044	-33.237634	-66.174554	A95JS044	mylonitic pegmatite			1							
A95JS045	-33.228766	-66.172360	A95JS045	pegmatite			5							
A95JS046	-33.205517	-66.203394	A95JS046	mylonitic granite			6					1	x	
A95JS047	-33.205147	-66.206349	A95JS047	mylonitic pegmatite			17							
A95JS048	-33.082023	-66.033406	A95JS048A	muscovite-biotite-quartz-tourmaline schist			20					1	x	
			A95JS048B	?andalusite schist								1		
A95JS049	-33.089683	-66.041871	A95JS049	quartz-feldspar-muscovite granite			1							
A95JS050	-33.123940	-66.038202	A95JS050	quartz-feldspar-muscovite granite			2					1	x	
A95JS051	-33.115765	-65.995367	A95JS051	muscovite-quartz-chlorite schist			34					1	x	
A95JS052	-33.083874	-66.053893	A95JS052	k-feldspar-quartz-biotite granite			24							Ar-Ar
A95JS053	-33.080875	-66.043652	A95JS053	quartz-feldspar-biotite-garnet granite			7					1	x	
A95JS054	-33.105492	-66.002083	A95JS054	muscovite-biotite-garnet-staurolite schist			232					1	x	
A95JS055	-33.091512	-66.145458	A95JS055	garnet-sillimanite-biotite schist			11							
A95JS056	-33.088836	-66.161063	A95JS056	garnet-sillimanite-biotite schist			33							
A95JS057	-33.101533	-66.143505	A95JS057	garnet-k-feldspar-sillimanite mylonite			253							
A95JS058	-33.106222	-66.137615	A95JS058	hornblende plagioclase pyroxene amphibolite			130							
A95JS059	-33.052229	-65.955745	A95JS059	meta conglomerate			34					1	x	
A95JS060	-33.067373	-65.958352	A95JS060	metaquartzite			13.6					1	x	
A95JS061	-33.066965	-65.960959	A95JS061	meta conglomerate			24							
A95JS062	-33.178223	-66.187032	A95JS062	quartz-feldspar-biotite gneiss			34							
A95JS063	-33.173384	-66.187890	A95JS063	quartz-biotite-sillimanite gneiss			5							
A95JS064	-33.169195	-66.193695	A95JS064	retrogressed amphibolite			188					1	x	
A95JS065	-33.182348	-66.196704	A95JS065	quartz-feldspar-biotite gneiss			3							
A95JS066	-33.194295	-66.191190	A95JS066	quartz-feldspar-biotite mylonite			12							
A95JS067	-33.261361	-66.265497	A95JS067	foliated quartz-feldspar-biotite granite			37					1	x	
A95JS068	-33.276832	-66.235451	A95JS068	foliated granodiorite			12							
A95JS069	-33.284138	-66.262794	A95JS069	poorly consolidated sandstone/conglomerate			1							
A95JS070	-33.288961	-66.272241	A95JS070	quartz-feldspar-biotite granodiorite			6							
A95JS071	-33.251962	-66.185053	A95JS071	quartz-muscovite-biotite schist			4							

Site ID	Latitude	Longitude	Sample No	Rock type	Min	Max	Mean	K	Th	U	Tc	Pet	Chem	Chron
A95JS072	-33.161411	-66.266753	A95JS072	foliated quartz-feldspar-biotite granite			49							
A95JS073	-33.137555	-66.250552	A95JS073	foliated porphyritic k-feldspar granite			12					1	x	
A95JS074	-33.016180	-66.276146	A95JS074	foliated quartz-feldspar-biotite granite			13							
A95JS075	-32.896414	-66.244110	A95JS075	mafic mylonite			232					1	x	
A95JS076	-32.910453	-66.255616	A95JS076	k-feldspar-quartz-biotite-hornblende granite dyke			369							
A95JS077	-32.919175	-66.258974	A95JS077A	hornblende-bearing granite			51					1	x	
			A95JS077B	hornblende-bearing granodiorite								1	x	
A95JS078	-32.924679	-66.276334	A95JS078	quartz-biotite-hornblende-feldspar granodiorite			28							
A95JS079	-33.121838	-66.135249	A95JS079A	high-grade mylonite (para- & ortho-gneiss)			6947							
			A95JS079B	high-grade mylonite (para- & ortho-gneiss)										
			A95JS079C	high-grade mylonite (para- & ortho-gneiss)										
			A95JS079D	high-grade mylonite (para- & ortho-gneiss)										
			A95JS079E	felsic gneiss								1	x	U-Pb
A95JS080	-33.123061	-66.136451	A95JS080A	dunite								1	x	
			A95JS080B	pyroxenite								1	x	
			A95JS080C	pyroxenite								1	x	
			A95JS080D	meta-pyroxenite								1	x	
			A95JS080E	pegmatite								2	x	U-Pb
			A95JS080F	?pyroxenite								1	x	
A95JS081	-33.058478	-65.994160	A95JS081	foliated granite (quartz-feldspar-biotite)			15					1	x	U-Pb
A95JS082	-33.057738	-66.000458	A95JS082	foliated felsite			4					1	x	U-Pb
A95JS083	-33.057159	-66.001568	A95JS083	muscovite quartz biotite tourmaline schist			22							
A95JS084	-33.056402	-65.982154	A95JS084	foliated granite (quartz-feldspar-biotite)			16					1	x	
A95JS085	-33.050764	-65.969693	A95JS085	chlorite-quartz phyllite			11							
A95JS086	-33.261725	-66.170590	A95JS086	sheared pegmatite			2					1	x	Ar-Ar
A95JS087	-32.959006	-65.666882	A95JS087A	intermediate volcanic			687					1	x	
			A95JS087B	intermediate volcanic								1	x	
A95JS088	-32.947076	-65.807870	A95JS088	onyx and volcanic tuff										
A95JS089	-32.811120	-66.076144	A95JS089	intermediate volcanic								1	x	Ar-Ar
A95JS090	-32.841547	-65.890739	A95JS090	intermediate volcanic			964					1	x	
A95JS091	-33.095573	-65.713987	A95JS091	massive biotite granite			972					1	x	
A95JS092	-33.058446	-65.659576	A95JS092	conglomerate (reworked volcanic)			757							
A95JS093	-33.155998	-65.722710	A95JS093	massive biotite granite			721					1	x	
A95JS094	-33.094227	-65.682090	A95JS094	quartz-biotite-k-feldspar schist			4							
A95JS095	-33.046655	-65.662242	A95JS095	biotite-andalusite-quartz schist			25						x	
A95JS096	-33.118329	-65.189508	A95JS096	biotite-muscovite-quartz schist			14					1	x	
A95JS097	-33.178454	-65.216357	A95JS097	foliated granite (k-feldspar-quartz-muscovite)			5							
A95JS098	-33.196419	-65.289458	A95JS098	volcanic tuff			392							
A95JS099	-33.205780	-65.300761	A95JS099	volcanic tuff			657							
A95JS100	-32.959939	-65.669173	A95JS100	volcaniclastic breccia (volcanic rich)			684							
A95JS101	-32.953239	-65.778521	A95JS101	intermediate volcanic			786					1	x	

Site ID	Latitude	Longitude	Sample No	Rock type	Min	Max	Mean	K	Th	U	Tc	Pet	Chem	Chron
A95JS102	-32.957660	-65.786793	A95JS102	volcaniclastic breccia (basement rich)			134							
A95JS103	-33.220441	-65.516362	A95JS103	biotite granite			710							
A95JS104	-33.227618	-65.519049	A95JS104	foliated biotite granite			431							
A95JS105	-33.261044	-65.545045	A95JS105	cataclasite			7							
A95JS106	-33.211150	-65.492195	A95JS106	biotite-quartz-feldspar schist			29							
A95JS107	-33.225145	-65.430440	A95JS107	conglomerate (reworked volcanic)			761							
A95JS108	-33.349514	-65.512682	A95JS108	quartz-biotite-sillimanite schist			22							
A95JS109	-33.190652	-65.472449	A95JS109	quartz-biotite-sillimanite schist			34					1	x	
A95JS110	-33.169259	-65.511695	A95JS110	quartz-biotite-sillimanite schist			16							
A95JS111	-33.160515	-65.489867	A95JS111	quartz-biotite-sillimanite schist			12							
A95JS112	-33.122669	-65.474192	A95JS112	quartz-biotite-sillimanite-garnet schist			19					1	x	
A95JS113	-33.135715	-65.438047	A95JS113	quartz-biotite-tourmaline schist			16							
A95JS114	-33.196993	-65.418032	A95JS114	quartz-feldspar-biotite schist			10							
A95JS115	-33.176657	-65.416390	A95JS115	intermediate volcanic			1485							
A95JS116	-33.171759	-65.420028	A95JS116	subvolcanic breccia dyke			2199							
A95JS117	-33.171759	-65.420028	A95JS117	intermediate volcanic			1727					1	x	
A95JS118	-33.168149	-65.425290	A95JS118	intermediate volcanic			2710						x	Ar-Ar
A95JS119	-33.356853	-65.490741	A95JS119A	quartz-biotite-sillimanite schist			33					1	x	
			A95JS119B	garnet spinel schist										
A95JS120	-33.312628	-65.494545	A95JS120	foliated breccia			19					1	x	
A95JS121	-33.284932	-65.490580	A95JS121	granite (quartz-feldspar-biotite)			46							
A95JS122	-33.242532	-65.895862	A95JS122	quartz-biotite-muscovite schist			14							
A95JS123	-33.027837	-65.949646	A95JS123	meta conglomerate			27							
A95JS124	-33.021754	-65.931326	A95JS124	mylonitic phyllite			23							
A95JS125	-33.035551	-65.956673	A95JS125A	slaty phyllite			591					1	x	
			A95JS125B	quartzite								1	x	U-Pb
A95JS126	-33.121237	-66.080484	A95JS126	quartz-sillimanite-garnet gneiss			15					1	x	
A95JS127	-33.106876	-66.069305	A95JS127	quartz-biotite-sillimanite schist			144							
A95JS128	-33.011604	-66.066075	A95JS128	sheared biotite-sillimanite-garnet schist			19							
A95JS129	-32.981011	-66.073076	A95JS129A	biotite-sillimanite-garnet gneiss			39					1	x	
			A95JS129B	biotite sillimanite cordierite gneiss										
			A95JS129C	garnet sillimanite biotite cordierite gneiss										
			A95JS129D	metabasic rock										
A95JS130	-33.027944	-65.932051	A95JS130	muscovite-chlorite schist			79					1	x	Ar-Ar
A95JS131	-33.042000	-65.914000	A95JS131	muscovite-biotite-quartz schist			13							
A95JS132	-33.035851	-65.872591	A95JS132	muscovite-biotite-quartz schist			25							
A95JS133	-33.156400	-65.891066	A95JS133	quartzite			69					1	x	
A95JS134	-33.112546	-65.946213	A95JS134	muscovite-biotite-garnet schist			21					1	x	
A95JS135	-33.120727	-66.005511	A95JS135	muscovite-chlorite-biotite schist			31							
A95JS136	-32.933664	-65.165100	A95JS136	megacrystic muscovite granite			2							
A95JS137	-32.945075	-65.138229	A95JS137	calcsilicate rock			3							

Site ID	Latitude	Longitude	Sample No	Rock type	Min	Max	Mean	K	Th	U	Tc	Pet	Chem	Chron
A95JS138	-32.810819	-65.217333	A95JS138	muscovite granite			5							
A95JS139	-33.123061	-66.136451	A95JS139.1	pyroxenite cumulate										
			A95JS139.2	pyroxenite cumulate								1		
			A95JS139.3	pyroxenite cumulate										
			A95JS139.4	pyroxenite cumulate								1		
			A95JS139.5	pyroxenite cumulate										
			A95JS139.6	mylonite								1		
			A95JS139.7	mylonite								2		
			A95JS139.8	mylonite										
			A95JS139.9	mylonite								1		
			A95JS139.10	mineralised biotite pyroxenite										
			A95JS139.11	olivine pyroxenite								1		
			A95JS139.12	chloritised olivine pyroxenite								1		
			A95JS139.13	mineralised dunite								1		
			A95JS139.14	mineralised dunite										
			A95JS139.15	mineralised dunite								1		
			A95JS139.16	dunite/pyroxenite contact								1		
			A95JS139.17	pyroxenite										
			A95JS139.18	cordierite sillimanite sulphide vein								1		
			A95JS139.19	mineralised pyroxenite								1		
			A95JS139.20	gneiss										
			A95JS139.21	garnet orthopyroxene gneiss								1		
			A95JS139.22	orthopyroxene plagioclase vein										
			A95JS139.23	orthopyroxene plagioclase vein										
			A95JS139.24	gneiss										
			A95JS139.25	two pyroxene gneiss								2		
			A95JS139.26	gneiss								1		
			A95JS139.27	biotite rich mafic rock										
			A95JS139.28	biotite rich mafic rock								1		
			A95JS139.29	garnet cordierite graphite vein								1		
			A95JS139.30	mineralised pyroxenite								1		
			A95JS139.31	veined mineralised pyroxenite								1		
			A95JS139.32	veined mineralised pyroxenite										
			A95JS139.33	mineralised pyroxenite										
			A95JS139.34	two pyroxene gneiss										
A95PS095	-32.750240	-64.753857	A95PS095	mylonitic biotite gneiss			13	6.4	1.9	1.7	80.5			
A95PS096	-32.750087	-64.756437	A95PS096	coarse-grained pink biotite granite			83	9.3	4.3	1.3	113.9	1	x	
A95PS097	-32.904747	-64.778824	A95PS097	mylonitic garnet sillimanite biotite plagioclase gneiss			12	5.7	4.3	0.5	63.2	1	x	
A95PS098	-32.902159	-64.783861	A95PS098	mylonitic garnet sillimanite biotite plagioclase gneiss			10	6.2	4.3	1.4	56.4			
A95PS099	-32.897446	-64.838979	A95PS099	mylonitic mica schist			341	7.9	3.1	1.4	82.8	1		
A95PS100	-32.898637	-64.854205	A95PS100	mylonitic garnet sillimanite biotite plagioclase gneiss			40	6.6	1.8	1.1	65.5			

Site ID	Latitude	Longitude	Sample No	Rock type	Min	Max	Mean	K	Th	U	Tc	Pet	Chem	Chron
A95PS101	-32.897597	-64.858652	A95PS101	mylonitic garnet sillimanite biotite plagioclase gneiss			5	5.8	0.9	1.1	63.8			
A95PS102	-32.891395	-64.868174	A95PS102	mylonitic garnet sillimanite biotite plagioclase gneiss			31	5.5	1.5	0.5	71.3	1	x	
A95PS103	-32.887394	-64.873381	A95PS103	mylonitic garnet sillimanite biotite plagioclase gneiss			13	6.3	1.1	1.4	79.6			
A95PS104	-32.886125	-64.881595	A95PS104	amphibolite			33	1.2	0.4	0.2	15.8	1	x	
A95PS105	-32.703507	-64.751129	A95PS105	coarse-grained pink equigranular biotite granite			102	9.1	1.8	1.6	95			
A95PS106	-32.694014	-64.769512	A95PS106	pink biotite microgranite			1	14.3	6.7	4.1	180.1	1	x	
A95PS107	-32.696733	-64.762110	A95PS107	coarse-grained pink biotite granite			27	5.4	5.7	1.3	89.1	1	x	
A95PS108	-32.681209	-64.816714	A95PS108	coarse-grained pink biotite granite			211	11.1	9.2	4.3	148.1	1	x	
A95PS109	-32.671623	-64.837654	A95PS109	coarse-grained pink biotite granite			816	12.8	8.6	4.3	180.4	1	x	
A95PS110	-32.877297	-64.882734	A95PS110A	tonalitic ortho gneiss			21	2.2	1.5	0.5	22	1	x	
			A95PS110B	ortho amphibolite			47	1	1	0.4	25.3	1	x	
A95PS111	-32.876477	-64.877287	A95PS111	meta gabbro			343	1.4	1.7	0.3	22.4	1	x	
A95PS112	-32.871658	-64.885949	A95PS112	mylonitic biotite muscovite gneiss			19	4.3	5.4	1.6	76.2			
A95PS113	-32.861534	-64.888085	A95PS113	biotite muscovite sillimanite gneiss			9	6.3	4.1	1.6	90.4			
A95PS114	-32.854829	-64.887142	A95PS114	muscovite biotite gneiss			20	7.4	8.6	1.6	112			
A95PS115	-32.850222	-64.891852	A95PS115	mylonitic biotite gneiss			20	6.5	7.8	2.2	112.2			
A95PS116	-32.845301	-64.896395	A95PS116	biotite gneiss			9	4.7	4.2	1.2	75.8			
A95PS117	-32.838034	-64.899829	A95PS117	migmatitic biotite quartz feldspar gneiss			32	4.8	4.4	1.4	69.9			
A95PS118	-32.835279	-64.909011	A95PS118	mylonitic biotite quartz feldspar gneiss			29	4.8	4.1	0.7	59.8			
A95PS119	-32.831736	-64.915472	A95PS119	biotite quartz feldspar gneiss			19	4	3.5	1.6	76.8			
A95PS120	-32.824351	-64.921252	A95PS120	biotite quartz feldspar gneiss			6	5.8	6.9	1.5	72.5			
A95PS121	-32.822665	-64.925958	A95PS121	biotite quartz feldspar gneiss			7	4	3.7	1.4	59.7			
A95PS122	-32.805113	-64.929573	A95PS122	biotite feldspar gneiss			20	3.6	4.6	0.5	68.3			
A95PS123	-32.801365	-64.939849	A95PS123	biotite feldspar gneiss			17	3.4	4.1	0.8	62			
A95PS124	-32.795345	-64.943061	A95PS124	mylonitic gneiss			10	3.8	5.1	0.6	62.5			
A95PS125	-32.793351	-64.953555	A95PS125	mylonitic gneiss			8	6.4	6.4	1.8	93.7			
A95PS126	-32.792926	-64.959995	A95PS126	mylonitic biotite quartz feldspar gneiss			9	7.5	6.6	1.7	93			
A95PS127	-32.791171	-64.964355	A95PS127	biotite quartz feldspar gneiss			13	5.4	5.5	1	69.2			
A95PS128	-32.847874	-64.812860	A95PS128	mylonite			26	6.6	6.8	1.3	91.6	1		
A95PS129	-32.840325	-64.820986	A95PS129	mylonitic biotite gneiss			7	6.2	7.5	1.6	95.4			
A95PS130	-32.835344	-64.829857	A95PS130	mylonitic gneiss			13	5.8	4.6	1.3	67.2			
A95PS131	-32.834024	-64.839284	A95PS131	mylonitic gneiss			16	7.5	5.8	1.9	87.6			
A95PS132	-32.831158	-64.849586	A95PS132	mylonitic biotite quartz feldspar gneiss			22	4.7	2.8	1	64			
A95PS133	-32.828445	-64.857402	A95PS133	tonalitic ortho gneiss			17	3.5	3	0.6	40.3	1	x	
A95PS134	-32.829368	-64.867451	A95PS134	mylonitic biotite quartz feldspar gneiss			26	7.5	6.7	1.9	87.7			
A95PS135	-32.823088	-64.875512	A95PS135	biotite quartz feldspar gneiss			11	3.5	3.3	1	62.7			
A95PS136	-32.818057	-64.883256	A95PS136	biotite quartz feldspar gneiss			15	3.5	3.6	0.8	53.9			
A95PS137	-33.103296	-64.960901	A95PS137A	medium-grained. equigranular pink syenite			39	5.9	6.2	2.9	101.1	1	x	
			A95PS137B	mylonitic granite			6	5.9	5.4	1.8	79.2	1	x	
			A95PS137C	my gneiss			27	3.5	3.8	0.6	51.3	1	x	
			A95PS137D	mylonitic aplo pegmatite			1	5.9	5	0.9	54	1	x	

Site ID	Latitude	Longitude	Sample No	Rock type	Min	Max	Mean	K	Th	U	Tc	Pet	Chem	Chron
A95PS138	-33.103944	-64.966690	A95PS138	mylonitic chlorite muscovite quartz gneiss			21	5.6	4.3	1.1	68.5	1		
A95PS139	-33.038653	-64.788235	A95PS139	coarse-grained equigranular biotite leucogranite			258	6.9	8.5	2.4	123.4	1	x	
A95PS140	-33.106136	-64.969493	A95PS140	mylonitic amphibolite			22	0.3	0.5	0.1	9.3	1		
A95PS141	-33.099871	-64.980185	A95PS141	mylonitic granite				7.2	5.8	1.1	97.4	1		
A95PS142	-33.097568	-64.977508	A95PS142A	mylonitic gneiss			13	6.1	3.9	0.9	70.7			
			A95PS142B	mylonitic tour pegmatite			5	7.2	2.4	0.3	51.1			
A95PS143	-33.106809	-64.952493	A95PS143	mylonitic ortho gneiss			3	6.5	3	1.5	64.3			
A95PS144	-33.104293	-64.945580	A95PS144	mylonitic gneiss				4.8	2.1	0.4	53.1			
A95PS145	-33.100678	-64.939768	A95PS145	mylonitic gneiss			14	5.3	2.5	0.8	59.4			
A95PS146	-33.048647	-64.985430	A95PS146	mylonitic fine-grained. equigranular biotite granite			7	5.7	4.8	0.8	84	1	x	
A95PS147	-33.046951	-64.978635	A95PS147A	banded gneiss			12	5.1	2.5	1	52.3			
			A95PS147B	mylonitic granite			6	5.1	3.9	0.9	57			
			A95PS147C	pegmatite			7	4.1	3.2	0.7	41.6			
A95PS148	-33.096959	-64.932401	A95PS148A	mylonitic biotite feldspar quartz gneiss			20	6.9	3.3	1.3	77.2			
			A95PS148B	mylonitic equigranular granite			15	5.4	1.7	1.3	52.3			
A95PS149	-33.084625	-64.921784	A95PS149A	mylonitic equigranular fine-grained. tonalite			189	5.4	1.3	0.6	38.8			
			A95PS149B	mylonitic banded biotite gneiss			69	4.3	1.2	0.6	37.8			
A95PS150	-33.076857	-64.921400	A95PS150	mylonitic banded biotite gneiss			29	3.6	1.4	1	56.8			
A95PS151	-33.071620	-64.921276	A95PS151	mylonitic chlorite gneiss			16	6	2.2	0.6	51.9	1	x	
A95PS152	-33.061907	-64.920701	A95PS152	mylonitic tonalite			511	1.7	0.4	0	20.3	1	x	
A95PS153	-33.051821	-64.922099	A95PS153	mylonitic tonalitic gneiss			418	5	2.2	0.7	48.6			
A95PS154	-33.042305	-64.924601	A95PS154	mylonitic tonalitic gneiss			10	8	2.7	0.9	66.8			
A95PS155	-33.026523	-64.912878	A95PS155	mylonitic tonalitic gneiss			144	2.9	2.2	0.2	32.6			
A95PS156	-33.027540	-64.925329	A95PS156A	banded amphibolite quartz gneiss			50	1.8	2	0.9	43.9	1	x	
			A95PS156B	mylonitic chlorite biotite feldspar quartz gneiss			44	6.4	4.2	2.8	83			
A95PS157	-33.026964	-64.939822	A95PS157	medium-grained. tonalite			150	2.6	2.3	0.3	39.3			
A95PS158	-33.028409	-64.946662	A95PS158	mylonitic feldspar quartz biotite gneiss			13	7.6	6.1	1.1	93			
A95PS159	-33.034246	-64.951105	A95PS159	mylonitic feldspar quartz biotite gneiss			7	4.7	3.8	1	58.8			
A95PS160	-33.152851	-64.976712	A95PS160A	banded garnet biotite quartz gneiss			25	4.1	4.3	1.1	63.1			
			A95PS160B	fol medium-grained. biotite granite			5	9.8	8.1	3	113.8			
A95PS161	-33.145860	-64.977434	A95PS161A	banded garnet biotite quartz gneiss			20	5.1	4.7	1.2	81.3			
			A95PS161B	pegmatite			13	6.8	5.8	0.3	60.5			
A95PS162	-33.142788	-64.976657	A95PS162	banded calcsilicate gneiss			45	3.6	2.4	0.9	49.6	1		
A95PS163	-33.139846	-64.973408	A95PS163	banded biotite quartz gneiss			26	5.5	2.5	0.7	49.6			
A95PS164	-33.137801	-64.965859	A95PS164	banded biotite quartz gneiss			60	5.7	3.3	0.8	67.2	1	x	
A95PS165	-33.159558	-64.980818	A95PS165	gneissic pegmatitic biotite granite			18	9.1	5.7	0.6	81.5			
A95PS166	-33.144489	-64.925060	A95PS166A	banded garnet biotite quartz gneiss			31	5.3	3	1.6	60.2			
			A95PS166B	gneissic tonalite			21	4.7	2.7	1.1	63.2			
A95PS167	-33.170954	-65.048937	A95PS167	coarse-grained seriate biotite granite			475	8.8	8.4	1.4	104.1	1	x	U-Pb
A95PS168	-33.182434	-65.009065	A95PS168	tonalitic ortho gneiss			322	4.6	3.2	1.1	49.4	1		
A95PS169	-33.184163	-65.003099	A95PS169A	banded plagioclase biotite quartz gneiss			24	8.7	4.3	3.2	89.6			

Site ID	Latitude	Longitude	Sample No	Rock type	Min	Max	Mean	K	Th	U	Tc	Pet	Chem	Chron
			A95PS169B	coarse-grained seriate biotite granite			68	7.9	3.7	0.8	73.8			
A95PS170	-33.173712	-65.035308	A95PS170	banded garnet plagioclase biotite quartz gneiss			42	8	5.7	1.3	86.7			
A95PS171	-33.161535	-65.054132	A95PS171	coarse-grained por biotite granite			5	11.4	9.6	1	119.5			
A95PS172	-33.094895	-65.049195	A95PS172	banded garnet biotite quartz gneiss			20	4.7	4.8	0.9	64.9			
A95PS173	-33.095158	-65.040330	A95PS173	banded biotite quartz gneiss			10	4.3	4.5	0.8	65.7			
A95PS174	-33.093873	-65.036754	A95PS174	peg. biotite granite			7	7.4	8.4	1.1	110.4			
A95PS175	-33.094391	-65.030939	A95PS175	banded feldspar biotite quartz gneiss			13	4.3	5	1.1	69.6			
A95PS176	-33.094061	-65.021846	A95PS176	peg biotite granite			7	4.9	6.2	1.5	81.6			
A95PS177	-33.110679	-65.055583	A95PS177	banded biotite feldspar quartz gneiss			15	4.7	6	1.7	75.9			
A95PS178	-33.116685	-65.066460	A95PS178	medium-grained. equigranular biotite granite			3	8	8.1	1.8	98.4			
A95PS179	-33.172159	-64.958402	A95PS179	equigranular biotite granite			5					1	x	
A95PS180	-32.470056	-64.310989	A95PS180	granodioritic ortho gneiss			556					1	x	
A95PS181	-33.005628	-64.991283	A95PS181A	equigranular muscovite leucogranite			21	4.5	5.6	0.7	61.6			
			A95PS181B	grey equigranular biotite granite			13	3.2	3.2	0.8	42.6	1	x	
A95PS182	-33.006227	-64.982006	A95PS182	banded ortho amphibolite			48	0.7	0.7	0.3	11.4			
A95PS183	-33.007860	-64.977987	A95PS183	mylonitic equigranular tonalite			311	5.6	2.7	1.1	47.2	1		
A95PS184	-33.006956	-64.972390	A95PS184A	banded feldspar quartz biotite gneiss			207	3.8	4	1	51.2			
			A95PS184B	tonalite			515	5.3	4.5	1.5	59.4	1	x	
A95PS185	-33.008479	-64.969609	A95PS185	granitic cataclasite			11	4.3	4.5	1.4	70.4	1		
A95PS186	-33.008199	-64.968522	A95PS186	mylonitic medium-grained. equigranular tonalite			263	3.2	2.8	0.9	41.5			
A95PS187	-33.010178	-64.961973	A95PS187	mylonitic gneiss			65	5.6	5	1.5	70.7			
A95PS188	-33.013982	-64.951129	A95PS188	mylonitic tonalite			6	3.6	2.4	1.1	47.6			
A95PS189	-33.015155	-64.945300	A95PS189	mylonitic banded biotite quartz feldspar gneiss			22	4.5	2.3	1.9	56.5			
A95PS190	-33.035587	-64.991207	A95PS190	mylonitic biotite quartz feldspar gneiss			4	5.8	4.8	1.9	77.5			
A95PS191	-33.030941	-64.899987	A95PS191	biotite quartz feldspar gneiss			30	5.6	2.1	0.6	67			
A95PS192	-33.032952	-64.898799	A95PS192	leucogranite			21	9.4	4.3	1.7	97.7	1	x	
A95PS193	-33.025210	-64.871014	A95PS193	mylonitic equigranular biotite granite			14	2	1.7	0.6	22.2			
A95PS194	-33.029822	-64.868371	A95PS194	mylonitic gneiss			18	6.1	1.5	1.5	61.2			
A95PS195	-33.037541	-64.868448	A95PS195	mylonitic sillimanite biotite quartz feldspar gneiss			247	5.2	2.2	0.9	60.3			
A95PS196	-33.046260	-64.873933	A95PS196	mylonitic muscovite biotite quartz feldspar gneiss			28	4.8	2.4	0.5	60.7			
A95PS197	-33.052183	-64.871660	A95PS197	mylonitic biotite quartz feldspar gneiss			26	3	0.9	0.6	33			
A95PS198	-33.055804	-64.858661	A95PS198	equigranular biotite tonalite			729	2.6	0.6	0.8	31.3			
A95PS199	-33.063874	-64.844180	A95PS199	coarse-grained leucogranite			26	8	7.5	0.7	83.9	1		
A95PS200	-33.078976	-65.073343	A95PS200	mylonitic sillimanite biotite quartz feldspar gneiss			25	4.2	2.4	1	68			
A95PS201	-33.081788	-65.049983	A95PS201A	leucogranite			6	11.4	7.62.6		127.1			
			A95PS201B	biotite quartz feldspar quartz banded gneiss			11	5.8	2.9	1.1	72.2			
A95PS202	-33.081144	-65.056234	A95PS202A	coarse-grained equigranular garnet biotite granite			8	9.1	7.6	0.9	110.7			
			A95PS202B	banded quartz biotite feldspar gneiss			10	5.6	3.9	1.5	65.9			
A95PS203	-33.083625	-65.061680	A95PS203	mylonitic banded biotite quartz feldspar gneiss			22	4.9	4.3	1.4	76.9			
A95PS204	-33.075095	-65.064330	A95PS204	banded biotite quartz feldspar gneiss			11	6.9	3.3	0.2	70.7			
A95PS205	-32.980619	-65.048315	A95PS205A	coarse-grained por biotite granite			19	4.5	4.4	0.7	60.4	1		

Site ID	Latitude	Longitude	Sample No	Rock type	Min	Max	Mean	K	Th	U	Tc	Pet	Chem	Chron
			A95PS205B	aplite			46	6.6	8.5	0.6	82.4	1	x	
A95PS206	-32.989518	-65.052212	A95PS206	banded biotite feldspar quartz gneiss			26	3.2	4.4	1	57			
A95PS207	-33.170916	-65.037549	A95PS207	coarse-grained seriate biotite granite			1445	7.5	6.9	2.7	100.1			
A95PS208	-33.019238	-65.031429	A95PS208	mylonitic feldspar biotite quartz gneiss			20	4.6	4.8	0.8	71.9			
A95PS209	-33.017441	-65.027695	A95PS209A	serpentinite			2678	0.7	0.3	0.2	6.9	1	x	
			A95PS209B	serpentinite			4343	0.8	0.4	1.3	8.2	1		
A95PS210	-33.019073	-65.019929	A95PS210	mylonitic feldspar biotite quartz gneiss			22	4.8	3.5	1.1	62.3			
A95PS211	-33.018655	-65.012887	A95PS211	mylonitic biotite quartz feldspar gneiss			35	4.2	3	1.3	54.5			
A95PS212	-33.017502	-65.014477	A95PS212	fine-grained banded para amphibolite			35	1	0.3	0	10.9			
A95PS213	-33.016795	-65.020294	A95PS213	mylonitic marble			1	1.6	0.7	0	14.8			
A95AC001	-32.847260	-66.104910	A95AC001	biotite granite (mylonitic muscovite overprint)			13.4							
A95AC002	-32.846220	-66.086270	A95AC002A	biotite muscovite schist			7.2							
			A95AC002B	biotite granite (mylonitic muscovite overprint)			14.3							
A95AC003	-32.821220	-65.939450	A95AC003A	Sillimanite garnet biotite gneiss			23.3							
			A95AC003B	Muscovite biotite pegmatite										
A95AC004	-32.812940	-65.941900	A95AC004A	Sillimanite garnet biotite gneiss			10.1							
			A95AC004B	Amphibolite			1042.3							
A95AC005	-32.811390	-66.086010	A95AC005A	Biotite muscovite schist			18.5							
			A95AC005B	Granite			36.2							
A95AC006	-32.832950	-66.101450	A95AC006	Biotite muscovite schist										
A95AC007	-32.832720	-66.025800	A95AC007A	Garnet granite										
			A95AC007B	Amphibolite										
			A95AC007C	Sillimanite garnet biotite gneiss										
			A95AC007D	Hornblende biotite granite (dacite)										
A95AC008	-32.923470	-66.055930	A95AC008	Sillimanite garnet biotite gneiss			146.4							
A95AC009	-32.935480	-66.068280	A95AC009	Garnet biotite gneiss			12.4							
A95AC010	-32.952560	-66.070600	A95AC010	Sillimanite garnet biotite gneiss			17.4							
A95AC011	-32.881540	-66.085970	A95AC011A	Garnet muscovite schist			38							
			A95AC011B	Kyanite staurolite muscovite pegmatite			13							
			A95AC011C	Metabasite/ Calcsilicate?			53.2							
A95AC012	-32.800580	-66.077340	A95AC012A	Biotite muscovite schist			12.6							
			A95AC012B	Kyanite staurolite muscovite schist										
A95AC013	-32.928230	-66.047800	A95AC013A	Sillimanite garnet biotite gneiss			53.2							
			A95AC013B	Amphibolite			1245.4							
			A95AC013C	Sillimanite biotite mylonite			19.6							
A95AC014	-32.929450	-66.040540	A95AC014A	Sillimanite garnet biotite gneiss			19.2							
			A95AC014B	Garnet biotite granite			12.6							
			A95AC014C	Amphibolite			92							
A95AC015	-32.941040	-66.030530	A95AC015A	Sillimanite garnet biotite gneiss			15.6							
			A95AC015B	Garnet pegmatite										
A95AC016	-32.945560	-66.024010	A95AC016A	Sillimanite garnet biotite gneiss			41.2							

Site ID	Latitude	Longitude	Sample No	Rock type	Min	Max	Mean	K	Th	U	Tc	Pet	Chem	Chron
			A95AC016B	Muscovite tourmaline pegmatite			6							
A95AC017	-32.953150	-66.012130	A95AC017	Biotite garnet muscovite granite			14							
A95AC018	-32.951490	-66.002190	A95AC018A	Biotite garnet muscovite granite			53.6							
			A95AC018B	Muscovite tourmaline pyrite pegmatite			19.2							
A95AC019	-32.941620	-65.994930	A95AC019A	Biotite garnet granite			10.8							
			A95AC019B	Biotite garnet granite (more mafic)										
A95AC020	-32.937880	-65.985600	A95AC020	Garnet biotite muscovite schist			17.8							
A95AC021	-32.934240	-65.977620	A95AC021A	Garnet biotite muscovite schist			18.6							
			A95AC021B	Biotite muscovite tourmaline pegmatite			15.6							
A95AC022	-32.928560	-65.962100	A95AC022A	Garnet biotite muscovite schist			163.2							
			A95AC022B	Garnet muscovite pegmatite			7.6							
A95AC023	-32.930140	-65.954600	A95AC023	Garnet biotite muscovite schist			19.6							
A95AC024	-32.947970	-65.954320	A95AC024A	Muscovite tourmaline pegmatite										
			A95AC024B	Biotite schist			9.8							
			A95AC024C	Garnet biotite muscovite schist			1034.2							
A95AC025	-32.929720	-65.937580	A95AC025	Garnet biotite muscovite schist			25.8							
A95AC026	-32.929720	-65.935610	A95AC026	Biotite muscovite phyllite										
A95AC027	-32.831490	-66.119400	A95AC027	Muscovite phyllite			7.6							
A95AC028	-32.832710	-66.123330	A95AC028A	Conglomerate (dolerite)			126.2							
			A95AC028B	Conglomerate (gabbro)			2622.7							
			A95AC028C	Cordierite biotite schist			18.4							
A95AC029	-32.825200	-66.130550	A95AC029A	Muscovite tourmaline pegmatite										
			A95AC029B	Biotite muscovite schist			6.6							
A95AC030	-32.826550	-66.135000	A95AC030A	Biotite garnet granodiorite/tonalite			11.6							
			A95AC030B	Biotite garnet xenolith										
			A95AC030C	Muscovite tourmaline pegmatite										
A95AC031	-32.925190	-65.987780	A95AC031A	Biotite plagioclase quartz schist			27.8							
			A95AC031B	Biotite plagioclase K-feldspar pegmatite			4.8							
A95AC032	-32.920870	-65.977800	A95AC032	Garnet Biotite plagioclase schist			32							
A95AC033	-32.933620	-65.932750	A95AC033	Biotite muscovite phyllite			22.4							
A95AC034	-32.940540	-65.924650	A95AC034	Slate/Phyllite			26.2							
A95AC035	-32.827280	-66.128650	A95AC035	Muscovite schist			3.8							
A95AC036	-32.823540	-66.135830	A95AC036A	Biotite gneiss			24							
			A95AC036B	Hornblende clinopyroxene - amphibolite			41.3							
			A95AC036C	Hornblende clinopyroxene - gabbro			40.7							
A95AC037	-32.815750	-66.147080	A95AC037A	Garnet muscovite pegmatite			0							
			A95AC037B	Hornblende biotite - amphibolite			3033.8							
			A95AC037C	Biotite garnet granite			8.6							
A95AC038	-32.948000	-66.156000	A95AC038	Biotite muscovite schist			29							
A95AC039	-32.949260	-66.156000	A95AC039	Hornblende biotite quartz tonalite			23							
A95AC040	-32.971100	-66.171240	A95AC040	Hornblende biotite diorite			40.3							

Site ID	Latitude	Longitude	Sample No	Rock type	Min	Max	Mean	K	Th	U	Tc	Pet	Chem	Chron
A95AC041	-32.987220	-66.170120	A95AC041	Sillimanite biotite gneiss			1166.7							
A95AC042	-32.894280	-66.091490	A95AC042A	Biotite muscovite mylonite			14.9							
			A95AC042B	Garnet biotite muscovite schist			13.6							
A95AC043	-32.893640	-66.085850	A95AC043	Biotite muscovite schist			11.4							
A95AC044	-32.783170	-66.085230	A95AC044	Muscovite phyllite			15.6							
A95AC045	-32.764220	-66.119250	A95AC045A	Biotite muscovite gneiss			233							
			A95AC045B	Garnet muscovite tourmaline pegmatite										
			A95AC045C	Muscovite granite			15.2							
A95AC046	-32.760480	-66.131170	A95AC046	Muscovite granite (mylonitised)			167.9							
A95AC047	-32.836950	-66.184380	A95AC047A	Garnet muscovite pegmatite										
			A95AC047B	Biotite granite. Mylonitic muscovite overprint			5.1							
			A95AC047C	Amphibolite			2222.3							
			A95AC047D	Amphibolite										
A95AC048	-32.906800	-66.098970	A95AC048	Biotite granite. Mylonitic muscovite overprint										
A95AC049	-32.909990	-66.093350	A95AC049A	Biotite granite. Mylonitic muscovite overprint										
			A95AC049B	Biotite muscovite schist										
A95AC050	-32.936290	-66.085370	A95AC050A	Garnet biotite muscovite schist										
			A95AC050B	Amphibolite										
			A95AC050C	Garnet biotite muscovite pegmatite										
A95AC051	-32.789630	-65.450120	A95AC051	Biotite muscovite granite										
A95AC052	-32.702110	-65.558120	A95AC052A	Biotite muscovite gneiss										
			A95AC052B	Muscovite tourmaline pegmatite										
A95AC053	-32.673160	-65.551620	A95AC053	Muscovite beryl tourmaline pegmatite										
A95AC054	-32.768760	-65.387410	A95AC054	Hornblende biotite allanite granite										
A95AC055	-32.664860	-65.690510	A95AC055	Biotite granite										
A95AC056	-32.673410	-65.668670	A95AC056	Biotite chlorite granite										
A95AC057	-32.728540	-65.617840	A95AC057	Biotite muscovite gneiss										
A95AC058	-32.833230	-65.304690	A95AC058	Muscovite tourmaline apatite pegmatite										
A95AC059	-33.108700	-65.983290	A95AC059	Aplite? metavolcanic?										
A95AC060	-32.728540	-65.617840	A95AC060	Chlorite phyllite										
A95AC061	-32.833230	-65.304690	A95AC061											
A95AC062	-33.108700	-65.983290	A95AC062											
A95RS082	-33.123847	-66.135735	A95RS082A	pyroxenite								1	x	
			A95RS082B	pyroxenite										
			A95RS082C	pyroxenite										
A95RS083	-33.094975	-66.117940	A95RS083A	pyroxenite								1		
			A95RS083B	pyroxenite										
A95RS084	-32.800690	-66.084050	A95RS084A	quartz vein										
			A95RS084B	volcanic breccia dyke									x	
			A95RS084C	sericitic, faulted schist										
			A95RS084D	sericitised, pyritised volcanic breccia dyke								1		

Site ID	Latitude	Longitude	Sample No	Rock type	Min	Max	Mean	K	Th	U	Tc	Pet	Chem	Chron
A95RS085	-32.811970	-66.073600	A95RS085A	moderately clay & propylitic altered dacite								1		
			A95RS085B	strongly clay & pyrite altered dacite										
			A95RS085C	intensely clay altered dacite										
A95RS088	-32.811790	-66.078950	A95RS088A	propylitic altered dacite										
			A95RS088B	propylitic altered dacite										
			A95RS088C	polymict breccia dyke										
			A95RS088D	clay & propylitic altered dacite								1		
A95RS089	-32.974334	-65.980519	A95RS089	rhyolite										
A95RS090	-32.962385	-65.967445	A95RS090A	quartz-biotite-garnet schist										
			A95RS090B	scheelite-bearing quartz-biotite schist								1		
			A95RS090C	quartz-biotite schist										
			A95RS090D	quartz-biotite schist										
A95RS091	-32.974569	-65.971404	A95RS091	meta-quartzite								1		
A95RS092	-33.119647	-65.994506	A95RS092A	pyrite-quartz vein								1		
			A95RS092B	muscovite-biotite-quartz-tourmaline schist										
A95RS093	-33.070166	-66.014259	A95RS093	schist										
A95RS095	-33.072543	-65.999022	A95RS095	meta-rhyolite										
A95RS096	-33.041551	-65.997831	A95RS096A	muscovite-biotite-quartz-tourmaline schist										
			A95RS096B	muscovite-biotite-quartz-tourmaline schist										
A95RS097	-33.064598	-65.984096	A95RS097A	phyllite										
			A95RS097B	meta-rhyolite										
A95RS098	-32.824781	-66.095794	A95RS098A	muscovite-biotite-quartz schist										
			A95RS098B	quartz-chalcopyrite-tourmaline vein										
A95RS099	-32.828404	-66.096893	A95RS099A	schist										
			A95RS099B	volcanic breccia dyke										
			A95RS099C	muscovite schist										
A95RS101	-33.155753	-65.509277	A95RS101A	quartz-feldspar-muscovite-fluorite pegmatite										Ar-Ar
			A95RS101B	banded quartz-biotite-feldspar-muscovite gneiss										
			A95RS101C	partly skarn altered marble										
			A95RS101D	banded quartz-biotite-cordierite-muscovite gneiss										
			A95RS101E	partly skarn altered amphibolite										
A95RS102	-33.148569	-65.510508	A95RS102	quartz biotite feldspar gneiss										
A95RS103	-33.148820	-65.509680	A95RS103	marble										
A95RS104	-32.795847	-66.053634	A95RS104A	migmatitic gneiss										
A95RS105	-32.793484	-66.054768	A95RS105	pyrite-illite altered volcanic breccia								1	x	
A95RS106	-32.822529	-66.027565	A95RS106	feldspar-amphibole-biotite-quartz porphytitic andesite	141	2935	1900							
A95RS107	-32.819956	-66.026263	A95RS107A	clay altered, garnetiferous gneiss										
			A95RS107B	clay altered, garnetiferous gneiss										
			A95RS107C	clay altered, garnetiferous gneiss										
A95RS108	-32.818917	-66.026938	A95RS108	silica-clay-pyrite altered breccia dyke?								1	x	
A95RS109	-32.771180	-66.072076	A95RS109	schist										

Site ID	Latitude	Longitude	Sample No	Rock type	Min	Max	Mean	K	Th	U	Tc	Pet	Chem	Chron
A95RS110	-32.772810	-66.072880	A95RS110	volcanic breccia										
A95RS111	-32.836460	-65.999884	A95RS111A	monolithic andesite breccia										
			A95RS111B	quartz-chalcopyrite veined sericitised andesite								1	x	
			A95RS111C	andesite										
A95RS112	-32.839574	-65.997126	A95RS112	clay altered monolithic andesite breccia										
A95RS113	-32.806103	-66.063063	A95RS113	silicified, basement-derived breccia									x	
A95RS114	-32.932590	-65.932689	A95RS114	rhyolite										
A95RS115	-32.945395	-65.920634	A95RS115	phyllite										
A95RS116	-32.945271	-65.917476	A95RS116	phyllite										
A96JS001	33.043810	66.073580	A96JS001A	layered orthogneiss	8	35	21							
			A96JS001B	granite	7	13	9							
A96JS002	33.043240	66.075190	A96JS002A	intermediate gneiss	502	946	759							
			A96JS002B	porphyritic granite	3	26	11							
A96JS003	33.040680	66.079700	A96JS003	mylonitic paragneiss	10	19	13							
A96JS004	33.041440	66.081770	A96JS004	layered paragneiss	38	220	103							
A96JS005	32.900530	66.232810	A96JS005A	metabasite	0	8	3							
			A96JS005B	porphyritic monzogranite	0	15	7							
			A96JS005C	orthogneiss	0	0	0							
A96JS006	32.907070	66.227010	A96JS006A	felsic orthogneiss	24	179	91							
			A96JS006B	amphibolite	41	1619	566							
A96JS007	32.759310	66.210650	A96JS007	orthogneiss	24	97	58							
A96JS008	32.762140	66.207500	A96JS008	pelitic gneiss	20	54	42							
A96JS009	32.768970	66.201280	A96JS009	high-grade mylonite	4	43	21							
A96JS010	32.772190	66.200530	A96JS010	high-grade mylonite	13	41	25							
A96JS011	32.783650	66.084760	A96JS011	bedded phyllite	0	3	1							
A96JS012	32.769410	66.109560	A96JS012A	bedded schist	0	0	0							
			A96JS012B	foliated tonalite	0	350	123							
A96JS013	32.746440	66.154420	A96JS013A	felsic orthogneiss	0	5	3							
			A96JS013B	amphibolite	17	58	30							
A96JS014	32.736590	66.167450	A96JS014A	felsic orthogneiss	8	13	11	4	1	7	58			
			A96JS014B	paragneiss	107	457	314	7	2	6	90			
A96JS015	32.719870	66.162240	A96JS015	mylonitic paragneiss	144	253	187							
A96JS016	32.741250	66.165010	A96JS016A	foliated granodiorite	0	0	0							
			A96JS016B	amphibolite	36	98	57							
			A96JS016C	paragneiss	1	20	9							
A96JS017	32.741720	66.163410	A96JS017	fine-grained amphibolite	42	60	52							
A96JS018	32.754780	66.141290	A96JS018	amphibolite	44	61	53							
A96JS019	32.764260	66.119490	A96JS019	paragneiss										
A96JS020	32.960520	66.106810	A96JS020	low-grade mylonite	0	6	4							

Site ID	Latitude	Longitude	Sample No	Rock type	Min	Max	Mean	K	Th	U	Tc	Pet	Chem	Chron
A96JS021	32.956640	66.103740	A96JS021	bedded phyllite	3	10	6							
A96JS022	32.959170	66.103350	A96JS022	bedded quartzite	0	12	4							
A96JS023	32.960440	66.101130	A96JS023	high-pressure schist	7	11	8							
A96JS024	32.960090	66.102240	A96JS024	schist	6	19	14							
A96JS025	32.911630	66.126260	A96JS025	bedded phyllite	1	9	3							
A96JS026	32.982620	66.204380	A96JS026A	paragneiss	0	9	2							
			A96JS026B	sheared pegmatite	0	0	0							
A96JS027	32.984760	66.197970	A96JS027	ultramafic metabasite	416	2627	1582							
A96JS028	32.956320	66.148420	A96JS028	foliated tonalite	13	42	28							
A96JS029	32.944100	66.153000	A96JS029	bedded phyllite	5	15	9							
A96JS030	32.921920	65.622870	A96JS030A	mylonitic schist	8	27	15							
			A96JS030B	mylonitic pegmatite	0	2	1							
			A96JS030C	bedded sandstone										
A96JS031	32.841190	65.673240	A96JS031A	granite	0	0	0							
			A96JS031B	paragneiss	7	13	9							
A96JS032	32.813960	65.716780	A96JS032	quartz-tourmaline vein										
A96JS033	32.815110	65.795130	A96JS033	schist	2	21	7							
A96JS034	32.809710	65.832480	A96JS034	high-pressure schist	3	19	9					1		
A96JS035	32.806070	65.843110	A96JS035	chloritic mylonite	0	23	5							
A96JS036	32.734800	65.752910	A96JS036	pegmatitic gneiss	10	37	22							
A96JS037	32.728220	65.828070	A96JS037	bedded quartzites & phyllites	0	3	1							
A96JS038	32.863980	65.868350	A96JS038A	intermediate tuff	112	215	162							
			A96JS038B	chloritic mylonite	4	25	13							
A96JS039	32.668390	65.827120	A96JS039	retrograde schist	256	1505	710							
A96JS040	32.668220	65.946980	A96JS040	foliated granite	3	12	8							
A96JS041	32.706980	65.950000	A96JS041	foliated granite	3	13	9							
A96JS042	32.934480	65.893950	A96JS042A	chloritic mylonite	11	31	19							
			A96JS042B	lamprophyre dyke	44	72	55							
A96JS043	32.941350	65.923470	A96JS043	phyllite	0	0	0							
A96JS044	33.302810	65.863370	A96JS044	foliated leucocratic granite	0	3	1							
A96JS045	33.332320	65.875750	A96JS045	calcrete	27	54	42							
A96JS046	33.208440	65.827510	A96JS046	pegmatitic schist	10	33	21							
A96JS047	33.185130	65.867280	A96JS047	foliated leucocratic granite	13	51	28							
A96JS048	33.144600	65.507650	A96JS048A	retrograde schist	0	15	9							
			A96JS048B	calc-silicate gneiss	1	1231	346							
A96JS049	33.158920	65.440240	A96JS049A	andesite plug	763	5416	2329							
			A96JS049B	retrogressed gneiss	7	15	9							
A96JS050	33.308790	65.519280	A96JS050	foliated granite	14	24	19							
A96JS051	33.314400	65.508080	A96JS051	psammitic gneiss	5	20	13							
A96JS052	33.317050	65.485420	A96JS052A	calc-silicate gneiss & marble	31	3883	1373							
			A96JS052B	epidote-amphibole vein	151	3512	1284							

Site ID	Latitude	Longitude	Sample No	Rock type	Min	Max	Mean	K	Th	U	Tc	Pet	Chem	Chron
A96JS053	33.195000	65.376600	A96JS053	bedded intermediate tuff	564	952	693							
A96JS054	33.166390	65.365760	A96JS054	porphyritic andesite	11	155	60							
A96PL006	32.788270	65.469330	A96PL006	granite	5	10	8							
A96PL007	32.790760	65.450790	A96PL007	granite	0	2	1	7.3	1.3	8.4	101.3			
A96PL008	32.683470	65.667130	A96PL008	phyric granite	3	13	8							
A96PL009	32.725660	65.505920	A96PL009	phyric granite	510	1104	1014							
A96PL010	32.692230	65.440300	A96PL010	pegmatite										
A96PL011	32.692390	65.444090	A96PL011	biotite gneiss	4	13	8							
A96PL012	32.773380	65.381890	A96PL012	phyric granite	430	1262	666	7.4	1.3	8.5	105.2			
A96PL013	32.877850	65.399600	A96PL013	biotite gneiss	6	20	14							
A96PL014	32.843900	65.405060	A96PL014	phyric granite	193	284	205							
A96PL015	32.829530	65.422880	A96PL015	phyric granite	229	592	302	6.4	2.2	7.2	113.3			
A96PL016	32.806860	65.445440	A96PL016A	phyric granite	24	311	92							
			A96PL016B	granite	0	2	1	6.3	1.2	5.9	87.5			
A96PL017	32.804880	65.461850	A96PL017	granite (oxidised)	0	1	0	7.5	1.4	7.3	98.9			
A96PL018	32.892980	65.465620	A96PL018	biotite gneiss	4	12	8							
A96PL019	32.775830	65.175350	A96PL019	granite	1	11	5							
A96PL020	32.811340	65.216150	A96PL020	granite	0	3	1							
A96PL021	32.797150	65.221010	A96PL021	granite	1	13	4							
A96PL022	32.707710	65.163510	A96PL022	granite	0	14	4							
A96PL023	32.826840	65.295830	A96PL023	garnet granite	5	16	12							
A96PL024	32.953470	65.216740	A96PL024A	biotite schist	20	26	22							
			A96PL024B	marble	0	3	1							
A96PL025	32.948200	65.195940	A96PL025A	biotite muscovite schist	1	11	4							
			A96PL025B	pegmatite										
A96PL026	32.874060	65.140680	A96PL026	biotite muscovite schist	16	49	26							
A96PL027	32.942870	65.137510	A96PL027	marble-calc silicate	0	0	0							
A96PL028	32.833480	65.030820	A96PL028	biotite schist	1	6	4							
A96PL029	32.745340	64.999060	A96PL029	muscovite granite	1	2	1							
A96PL030	32.690940	65.379400	A96PL030	biotite gneiss	6	26	13							
A96PL031	32.844110	65.885190	A96PL031	conglomerate	267	301	278							
A96PL032	32.834740	65.904640	A96PL032	muscovite biotite schist	2	9	6							
A96PL033	32.830260	65.929920	A96PL033	biotite sillimanite schist	6	28	15							
A96PL034	32.829120	65.936170	A96PL034	rhyolite	97	199	136							
A96PL035	32.814510	65.944550	A96PL035A	micaceous quartzite	0	1	3							
			A96PL035B	amphibolite	36	186	71							
A96PS008	33.177490	64.874860	A96PS008	mylonitic granite	1	17	7							
A96PS009	33.347000	64.882120	A96PS009	quartz arenite	3	10	6							
A96PS010	33.317280	64.823620	A96PS010A	muscovite biotite leucogranite	5	12	10							
			A96PS010B	schist	16	29	23							
A96PS011	33.258620	64.856210	A96PS011	biotite muscovite leucogranite	3	27	11							

Site ID	Latitude	Longitude	Sample No	Rock type	Min	Max	Mean	K	Th	U	Tc	Pet	Chem	Chron
A96PS012	32.951870	64.844900	A96PS012	gneiss	2	11	5							
A96PS013	32.956880	64.856330	A96PS013	biotite granite	72	523	261							
A96PS014	32.959320	64.863180	A96PS014A	banded gneiss	7	24	16							
			A96PS014B	meta tonalite	452	898	704							
A96PS015	32.960720	64.867850	A96PS015	mylonite	16	213	54							
A96PS016	32.963850	64.871250	A96PS016	mylonitic gneiss	2	14	7							
A96PS017	32.963050	64.878480	A96PS017	amphibolite	38	78	61							
A96PS018	32.961400	64.884600	A96PS018	mylonitic gneiss	13	32	20							
A96PS019	32.958850	64.893040	A96PS019	banded gneiss	10	26	18							
A96PS020	32.955860	64.902530	A96PS020A	meta tonalite	15	900	246							
			A96PS020B	banded gneiss	52	340	123							
			A96PS020C	amphibolite	52	146	97							
A96PS021	33.322250	65.064430	A96PS021	biotite granite	2	10	7							
A96PS022	32.723580	64.974720	A96PS022	brecciated granite	1	10	6							
A96PS023	32.680480	64.967730	A96PS023	porphyritic granite	0	4	1							
A96PS024	32.684550	64.956990	A96PS024A	tonalitic orthogneiss	730	1055	908							
			A96PS024B	porphyritic biotite granite	146	480	293							
A96PS025	32.740120	64.999980	A96PS025	biotite granite	0	10	4					1		
A96PS026	32.785570	64.973490	A96PS026	mylonitic gneiss	10	20	14							
A96PS027	32.821210	65.030090	A96PS027	banded gneiss	6	74	21							
A96PS028	32.832270	65.031760	A96PS028	banded gneiss	13	21	15							
A96PS029	32.916790	65.003600	A96PS029	muscovite biotite granite	9	14	10							
A96PS030	32.915150	64.994680	A96PS030	banded gneiss	18	30	22							
A96PS031	32.922880	65.006290	A96PS031	banded gneiss	15	19	18							

SAMPLE	A95JS003A	A95JS011A	A95JS011D	A95JS014A	A95JS016	A95JS017	A95JS019	A95JS024
LITH	amphibolite	mylonite	mylonite	schist	schist	schist	schist	calc-silicate
LAT	-33,07774	-33,07496	-33,07496	-33,10807	-33,10924	-33,10245	-33,11093	-33,06857
LONG	-66,10890	-66,12551	-66,12551	-66,00150	-65,99570	-65,93631	-65,92100	-66,16469
SIO2	48,32	73,14	69,04	63,99	43,13	60,98	71,45	71,04
TIO2	0,30	0,70	0,91	0,77	1,20	0,87	0,66	0,43
AL2O3	16,64	11,12	12,28	16,59	28,14	17,37	13,08	10,36
FE2O3	2,55	2,22	2,18	1,84	3,54	1,86	1,35	0,45
FEO	5,95	3,12	3,95	4,28	6,09	5,27	2,70	1,74
MNO	0,17	0,13	0,10	0,18	0,21	0,13	0,08	0,40
MGO	10,84	2,55	3,31	2,63	3,84	3,49	1,80	0,74
CAO	13,08	2,34	2,27	0,57	0,30	0,91	1,90	10,71
NA2O	0,89	1,66	1,84	1,64	1,27	1,55	2,38	0,22
K2O	0,21	1,96	2,63	4,45	6,74	4,00	2,63	0,08
P2O5	0,01	0,01	0,02	0,15	0,09	0,15	0,20	0,15
LOI	18,00	0,00	0,00	0,00	0,00	0,00	0,00	0,04
Rest	0,15	0,18	0,21	0,20	0,31	0,20	0,18	0,11
TOTAL	**99,29**	**99,13**	**98,74**	**97,29**	**94,86**	**96,78**	**98,41**	**96,47**
BA	10	360	435	520	1020	475	520	35
RB	2	90	128	242	260	171	119	5
SR	180	122	118	102	117	102	155	306
PB	2	8	10	22	34	20	18	2
TH	<1	3	10	16	23	13	11	15
U	<1	<1	1	3	3	5	2	4
ZR	20	394	432	170	248	158	234	250
NB	<2	12	16	16	28	14	10	14
Y	8	30	13	31	38	27	29	44
LA	4	14	22	34	34	26	24	34
CE	10	30	50	70	85	55	60	80
SC	58	20	20	20	36	22	12	6
V	190	98	122	102	174	120	74	24
MN	1220	900	690	1190	1150	895	590	2830
CR	292	68	90	74	114	88	50	20
NI	84	36	44	36	58	42	20	16
CU	136	32	38	10	<2	46	2	4
ZN	66	84	108	122	196	154	72	44
GA	15	16	18	23	43	27	17	13
AS	<1	<1	1	<1	2	<1	1	<1
SN	<5	<5	5	5	10	5	5	<5
AU	0,001	<0.001	<0.001	0,001	<0.001	0,003	0,001	0,001
AG								
MO								
CD								
SB								
TE								
RH								
RU								
OS								
PD								
PT								
IR								

SAMPLE	A95JS025	A95JS028D	A95JS029A	A95JS029B	A95JS030	A95JS033	A95JS034A	A95JS034B
LITH	quartzite	mylonite	granite	granite	granite	monzogranite	granite	granite
LAT	-33,06567	-33,11333	-33,06647	-33,06647	-33,20540	-33,19602	-33,21250	-33,21250
LONG	-66,16890	-66,11485	-66,17948	-66,17948	-66,17658	-66,25120	-66,22043	-66,22043
SIO2	69,27	74,81	77,16	78,13	79,35	69,92	66,10	72,32
TIO2	0,58	0,62	0,05	0,37	0,38	0,42	0,60	0,14
AL2O3	14,39	12,35	12,74	11,63	10,56	14,83	15,75	15,25
FE2O3	1,79	1,83	0,44	0,90	0,65	1,03	1,52	0,42
FEO	1,14	1,95	0,18	1,20	1,19	1,55	2,88	0,50
MNO	0,04	0,04	0,06	0,04	0,03	0,07	0,11	0,02
MGO	1,35	1,49	0,05	0,78	0,71	0,96	1,81	0,31
CAO	2,08	0,81	0,41	0,90	1,27	1,96	3,84	1,75
NA2O	3,78	1,53	3,81	2,10	2,83	3,62	2,88	4,17
K2O	2,83	3,04	4,57	2,35	2,12	4,19	3,22	3,93
P2O5	0,12	0,05	0,00	0,10	0,08	0,21	0,16	0,04
LOI	0,13	0,00	0,00	0,00	0,00	0,00	0,00	0,00
Rest	0,18	0,17	0,11	0,13	0,12	0,37	0,19	0,38
TOTAL	**97,68**	**98,69**	**99,58**	**98,63**	**99,29**	**99,12**	**99,06**	**99,24**
BA	275	535	15	325	245	1300	700	2170
RB	144	100	655	111	90	189	152	112
SR	231	100	6	109	91	830	183	770
PB	28	20	52	24	24	30	26	44
TH	19	18	25	19	20	37	18	11
U	4	1	9	4	4	3	2	2
ZR	198	242	38	236	278	254	158	102
NB	16	10	20	10	10	18	10	4
Y	25	21	47	29	34	29	14	7
LA	36	28	4	28	28	94	34	22
CE	85	65	20	65	70	200	55	50
SC	16	10	6	6	8	6	14	2
V	150	66	<2	26	30	38	90	14
MN	360	235	385	290	250	520	870	170
CR	48	38	<2	18	16	6	14	<2
NI	4	22	<2	8	6	4	8	<2
CU	24	<2	<2	6	6	<2	14	2
ZN	82	84	24	44	42	58	72	24
GA	18	17	17	13	12	20	18	23
AS	4	<1	<1	<1	<1	<1	<1	2
SN	<5	5	20	<5	<5	5	<5	<5
AU	<0.001		0,001		0,001	0,001	<0.001	<0.001
AG								
MO								
CD								
SB								
TE								
RH								
RU								
OS								
PD								
PT								
IR								

SAMPLE	A95JS035B	A95JS037	A95JS039	A95JS040A	A95JS041	A95JS046	A95JS048A	A95JS048B
LITH	mylonite	granite	granite	gneiss	gneiss	granite	schist	schist
LAT	-33,20740	-33,19021	-33,18713	-33,11508	-33,11657	-33,20552	-33,08202	-33,08202
LONG	-66,21325	-66,21140	-66,20466	-66,12279	-66,12773	-66,20339	-66,03341	-66,03341
SIO2	70,32	67,01	67,32	61,22	74,68	66,30	73,56	77,27
TIO2	0,53	0,56	0,52	1,03	0,57	0,55	0,63	0,46
AL2O3	15,38	15,78	16,01	17,63	12,09	15,93	12,38	11,86
FE2O3	1,73	1,10	0,59	4,58	1,84	1,36	1,73	0,79
FEO	1,44	1,99	2,18	5,23	1,89	1,61	2,65	1,50
MNO	0,05	0,05	0,07	0,13	0,08	0,05	0,05	0,04
MGO	1,27	1,38	1,23	3,90	1,58	1,07	1,68	0,98
CAO	0,67	2,45	2,34	0,78	1,37	2,05	0,03	0,33
NA2O	1,27	3,85	3,94	1,18	1,92	3,84	0,48	0,97
K2O	4,62	3,84	3,65	2,39	2,94	5,10	4,02	3,87
P2O5	0,09	0,25	0,30	0,05	0,05	0,25	0,05	0,10
LOI	0,00	0,00	0,03	0,00	0,00	0,00	0,04	0,00
Rest	0,18	0,44	0,37	0,20	0,19	0,46	0,16	0,16
TOTAL	**97,55**	**98,70**	**98,54**	**98,32**	**99,20**	**98,57**	**97,46**	**98,33**
BA	550	1850	1390	405	635	1810	275	550
RB	211	131	181	109	90	159	211	154
SR	80	950	810	91	146	1110	44	87
PB	18	26	30	14	20	36	14	22
TH	20	28	22	31	17	31	17	14
U	6	2	2	<1	<1	4	5	3
ZR	212	280	262	232	280	306	242	222
NB	18	14	14	16	8	10	16	14
Y	35	15	11	18	21	15	35	25
LA	34	92	70	48	34	110	34	26
CE	80	185	150	120	80	200	80	60
SC	12	6	6	10	12	6	16	8
V	60	52	42	126	54	44	68	40
MN	400	435	560	875	525	400	435	305
CR	32	16	10	102	42	<2	46	26
NI	6	6	4	52	20	4	4	12
CU	24	2	2	<2	2	4	10	6
ZN	82	88	72	194	70	72	100	56
GA	20	24	20	34	16	22	21	16
AS	3	1	1	<1	<1	<1	2	4
SN	5	<5	10	10	<5	<5	5	<5
AU	<0.001	<0.001	0,001	0,002	0,002	<0.001		0,001
AG								
MO								
CD								
SB								
TE								
RH								
RU								
OS								
PD								
PT								
IR								

SAMPLE	A95JS050	A95JS051	A95JS053	A95JS054	A95JS059	A95JS060	A95JS064	A95JS067
LITH	granite	schist	granite	schist	conglomerate	phyllite	amphibolite	granite
LAT	-33,12394	-33,11576	-33,08087	-33,10549	-33,05223	-33,06737	-33,16919	-33,16919
LONG	-66,03820	-65,99537	-66,04365	-66,00208	-65,95575	-65,95835	-66,19369	-66,19369
SIO2	74,12	61,73	75,13	63,02	73,49	77,86	47,47	70,71
TIO2	0,11	0,81	0,09	0,76	0,59	0,47	0,92	0,30
AL2O3	14,35	17,62	13,70	17,56	12,94	10,69	15,62	14,53
FE2O3	0,31	2,31	0,37	2,21	4,24	2,53	1,98	0,99
FEO	0,93	4,12	0,55	4,00	0,57	0,63	7,38	1,17
MNO	0,10	0,16	0,08	0,13	0,05	0,02	0,17	0,05
MGO	0,26	2,89	0,31	2,72	1,26	1,03	10,61	0,64
CAO	1,18	0,54	0,70	0,51	0,23	0,52	10,34	1,72
NA2O	3,44	1,55	2,63	1,60	1,06	1,58	0,96	2,25
K2O	4,46	4,77	5,34	4,35	2,97	2,58	1,34	6,67
P2O5	0,07	0,18	0,24	0,14	0,16	0,13	0,10	0,15
LOI	0,00	0,00	0,00	0,00	0,00	0,00	0,18	0,00
Rest	0,10	0,21	0,08	0,19	0,14	0,13	0,17	0,18
TOTAL	**99,42**	**96,89**	**99,22**	**97,20**	**97,70**	**98,17**	**97,24**	**99,36**
BA	295	570	205	560	335	335	135	625
RB	202	224	212	199	128	110	59	212
SR	93	70	67	80	60	55	170	130
PB	36	22	44	24	18	16	6	44
TH	12	19	4	16	13	13	5	36
U	3	3	2	4	2	1	1	4
ZR	64	182	36	148	184	186	34	200
NB	10	16	8	16	12	12	<2	8
Y	22	29	17	27	26	24	16	21
LA	14	38	6	28	26	26	10	40
CE	35	95	10	60	55	55	25	100
SC	6	24	6	24	16	10	64	8
V	6	106	8	112	74	48	364	28
MN	715	1190	515	735	405	110	1310	425
CR	<2	80	4	76	54	30	158	4
NI	<2	40	<2	38	26	18	18	<2
CU	<2	18	<2	24	<2	10	50	<2
ZN	36	134	26	90	88	86	74	38
GA	16	25	12	25	17	13	14	14
AS	<1	<1	<1	<1	<1	3	<1	1
SN	<5	5	<5	5	<5	<5	<5	<5
AU	<0.001	<0.001	<0.001	<0.001	0,001	0,001	0,002	<0.001
AG								
MO								
CD								
SB								
TE								
RH								
RU								
OS								
PD								
PT								
IR								

SAMPLE	A95JS073	A95JS075	A95JS077A	A95JS077B	A95JS079E	A95JS080A	A95JS080B	A95JS080C
LITH	monzogranite	mylonite	QZM	MZT	gneiss	pyroxenite	pyroxenite	pyroxenite
LAT	-33,13756	-32,89641	-32,91918	-32,91918	-33,12184	-33,12306	-33,12306	-33,12306
LONG	-66,25055	-66,24411	-66,25897	-66,25897	-66,13525	-66,13645	-66,13645	-66,13645
SIO2	68,72	61,62	61,04	50,60	67,61	40,31	52,41	53,71
TIO2	0,44	0,75	0,47	1,28	0,50	0,09	0,17	0,18
AL2O3	14,97	16,22	17,67	15,65	16,85	2,20	3,52	3,99
FE2O3	0,81	1,50	1,65	2,13	0,95	8,69	7,32	2,12
FEO	2,20	4,55	2,12	5,31	2,99	6,51	6,72	9,67
MNO	0,07	0,11	0,07	0,11	0,09	0,21	0,26	0,24
MGO	1,03	3,51	1,73	7,72	1,50	33,60	25,95	25,56
CAO	2,62	5,09	3,20	7,22	4,77	1,11	2,70	2,80
NA2O	2,88	1,90	4,64	3,22	3,00	0,13	0,22	0,33
K2O	5,00	2,65	5,18	3,21	1,19	0,08	0,13	0,37
P2O5	0,14	0,20	0,34	0,69	0,15	0,01	0,01	0,01
LOI	0,02	0,01	0,00	0,03	0,02	0,30	0,24	0,10
Rest	0,18	0,16	0,79	0,63	0,15	0,98	0,61	0,51
TOTAL	**99,08**	**98,27**	**98,90**	**97,80**	**99,76**	**94,21**	**100,26**	**99,60**
BA	595	315	3000	1780	280	10	10	30
RB	214	129	92	98	54	3	6	15
SR	143	226	2400	1720	253	16	7	15
PB	26	12	42	18	18	<2	<2	<2
TH	30	5	39	30	22	1	<1	1
U	3	2	4	2	<1	<1	<1	<1
ZR	186	92	382	318	248	6	12	18
NB	12	8	8	16	8	<2	<2	<2
Y	22	17	18	31	23	1	4	6
LA	50	18	180	160	46	<2	4	6
CE	115	35	360	340	100	<5	<5	10
SC	8	22	6	28	8	18	58	58
V	50	164	66	170	40	76	162	150
MN	515	835	495	890	585	1530	1940	1860
CR	8	48	18	272	6	4190	2510	2470
NI	4	16	10	66	2	1680	960	510
CU	6	28	14	26	6	965	494	216
ZN	48	82	68	136	76	84	104	102
GA	16	18	22	25	17	4	6	7
AS	1	<1	<1	<1	<1	2	1	<1
SN	<5	<5	<5	<5	<5	<5	5	<5
AU	0,001	<0.001	0,001	0,002	0,001	36*		6*
AG								
MO								
CD								
SB								
TE								
RH						2		<0.5
RU						2		<0.5
OS						2		<0.5
PD						30		2
PT						32		4
IR						2		<0.5

SAMPLE	A95JS080D	A95JS080E1	A95JS080E2	A95JS080F	A95JS081	A95JS082	A95JS084	A95JS086
LITH	pyroxenite	pyroxenite	pegmatite	pyroxenite	monzogranite	aplite	granite	pegmatite
LAT	-33,12306	-33,12306	-33,12306	-33,12306	-33,05848	-33,05774	-33,05640	-33,26173
LONG	-66,13645	-66,13645	-66,13645	-66,13645	-65,99416	-66,00046	-65,98215	-66,17059
SIO2	49,42	48,75	51,43	45,65	64,13	74,45	64,37	74,88
TIO2	0,29	0,31	0,37	1,09	0,58	0,03	0,57	0,07
AL2O3	8,78	5,08	25,32	17,94	16,81	14,76	16,88	14,47
FE2O3	2,99	5,33	1,77	1,86	1,52	0,50	1,49	0,21
FEO	7,37	9,10	1,78	8,56	3,03	0,34	2,88	0,24
MNO	0,18	0,24	0,02	0,19	0,13	0,14	0,12	0,05
MGO	16,40	18,48	3,13	8,69	1,81	0,10	1,69	0,15
CAO	12,22	9,72	9,00	11,97	3,99	0,87	3,90	0,84
NA2O	0,39	0,31	3,33	1,12	3,01	3,70	2,91	3,95
K2O	0,11	0,17	1,51	0,87	3,30	4,39	2,83	3,91
P2O5	0,00	0,01	0,06	0,36	0,20	0,10	0,20	0,26
LOI	0,58	1,17	0,43	0,10	0,00	0,00	0,00	0,00
Rest	0,31	0,53	0,40	0,19	0,17	0,06	0,18	0,05
TOTAL	**99,04**	**99,20**	**98,55**	**98,58**	**98,69**	**99,45**	**98,02**	**99,08**
BA	10	10	190	205	470	80	545	30
RB	4	5	69	27	145	220	137	233
SR	72	29	229	205	232	37	254	33
PB	<2	<2	12	4	20	34	22	24
TH	<1	1	7	3	17	7	19	1
U	<1	<1	2	<1	3	3	1	1
ZR	14	16	38	62	162	36	164	18
NB	<2	<2	6	6	12	18	12	14
Y	10	16	7	29	26	21	27	9
LA	4	4	16	24	38	4	36	6
CE	5	10	35	60	85	10	80	5
SC	72	76	6	54	14	6	14	8
V	240	248	58	316	82	2	82	<2
MN	1430	1810	185	1420	1020	770	935	300
CR	620	1150	550	102	14	<2	12	<2
NI	535	1080	910	66	8	<2	6	<2
CU	615	1160	905	78	8	<2	6	<2
ZN	72	112	14	100	76	36	70	24
GA	9	8	26	20	19	16	19	18
AS	<1	<1	<1	<1	2	17	1	2
SN	<5	<5	<5	5	<5	<5	<5	10
AU	7*	11*	8*	1*	<0.001	<0.001	<0.001	0,001
AG								
MO								
CD								
SB								
TE								
RH	1	1	1	<0.5				
RU	<0.5	<0.5	<0.5	<0.5				
OS	<0.5	<0.5	<0.5	<0.5				
PD	20	34	18	<0.5				
PT	10	8	46	<0.5				
IR	<0.5	<0.5	<0.5	<0.5				

SAMPLE	A95JS087A	A95JS087B	A95JS089	A95JS090	A95JS091	A95JS093	A95JS095	A95JS096
LITH	BAD	BAD	andesite	dacite	granite	granite	schist	schist
LAT	-32,95901	-32,95901	-32,81112	-32,84155	-33,09557	-33,15600	-33,04666	-33,11833
LONG	-65,66688	-65,66688	-66,07614	-65,89074	-65,71399	-65,72271	-65,66224	-65,18951
SIO2	64,65	64,36	61,82	57,56	73,34	71,03	70,68	62,43
TIO2	0,39	0,38	0,48	0,81	0,31	0,34	0,66	0,84
AL2O3	17,50	17,35	16,16	17,15	13,27	14,73	13,25	16,68
FE2O3	2,20	2,28	1,76	4,40	0,90	1,03	1,08	1,24
FEO	1,02	0,96	1,96	1,83	0,93	1,17	3,37	4,75
MNO	0,12	0,13	0,13	0,12	0,04	0,04	0,10	0,12
MGO	0,76	0,82	1,04	2,39	0,59	0,65	2,20	3,25
CAO	4,04	4,37	4,59	5,81	1,37	1,69	1,59	1,60
NA2O	5,19	5,24	4,38	3,81	3,38	3,86	2,28	2,69
K2O	2,80	2,76	3,64	2,69	5,03	4,69	3,09	4,00
P2O5	0,15	0,16	0,22	0,46	0,09	0,12	0,18	0,21
LOI	0,01	0,00	0,04	0,00	0,00	0,00	0,00	0,00
Rest	0,38	0,37	0,26	0,31	0,15	0,19	0,19	0,22
TOTAL	**99,20**	**99,19**	**96,48**	**97,33**	**99,40**	**99,54**	**98,68**	**98,03**
BA	1070	1040	530	640	365	620	650	580
RB	52	53	116	74	143	212	122	170
SR	1570	1590	1020	1080	224	219	159	168
PB	10	8	14	10	22	26	22	26
TH	5	5	5	5	33	21	9	16
U	1	2	2	<1	4	6	2	4
ZR	230	218	180	180	184	238	194	234
NB	12	12	6	8	20	14	12	14
Y	21	22	18	24	30	17	25	30
LA	24	34	22	28	54	42	22	30
CE	55	55	50	65	115	95	55	70
SC	6	4	8	16	4	4	14	22
V	46	46	92	206	18	22	78	122
MN	885	965	1030	780	275	295	790	920
CR	2	<2	2	12	8	8	58	98
NI	<2	<2	<2	6	4	4	28	42
CU	6	4	24	44	4	6	16	6
ZN	60	60	66	74	28	64	86	124
GA	21	21	21	21	18	22	17	22
AS	1	1	5	<1	<1	1	1	1
SN	<5	<5	<5	<5	<5	<5	<5	5
AU	<0.001	<0.001	0,001	<0.001	<0.001	0,001	0,001	0,002
AG								
MO								
CD								
SB								
TE								
RH								
RU								
OS								
PD								
PT								
IR								

SAMPLE	A95JS101	A95JS109	A95JS112	A95JS117	A95JS118	A95JS119A	A95JS120	A95JS125A
LITH	BAD	schist	schist	BAD	BAD	schist	calc-silicate	slate
LAT	-32,95324	-33,19065	-33,12267	-33,17176	-33,16815	-33,35685	-33,31263	-33,03555
LONG	-65,77852	-65,47245	-65,47419	-65,42003	-65,42529	-65,49074	-65,49454	-65,95667
SIO2	61,61	53,89	51,38	56,42	57,20	61,27	43,74	61,38
TIO2	0,45	1,07	1,19	0,42	0,50	0,92	1,88	0,80
AL2O3	17,35	20,19	20,22	19,80	19,30	17,46	15,61	18,08
FE2O3	2,98	2,83	3,01	2,21	2,59	1,50	5,75	3,21
FEO	1,05	5,39	7,18	1,21	1,37	5,18	3,24	3,51
MNO	0,18	0,12	0,22	0,16	0,15	0,12	0,16	0,18
MGO	1,11	4,26	5,10	0,64	0,89	3,44	5,12	2,60
CAO	3,94	0,98	0,81	4,84	4,77	1,30	22,73	0,28
NA2O	6,03	1,83	1,48	5,39	4,98	2,00	0,22	1,92
K2O	3,87	5,76	5,29	5,37	5,53	3,62	0,12	4,11
P2O5	0,27	0,13	0,15	0,15	0,13	0,20	0,32	0,15
LOI	0,00	0,00	0,00	0,03	0,01	0,00	0,00	0,00
Rest	0,51	0,27	0,29	0,69	0,54	0,22	0,13	0,19
TOTAL	**99,35**	**96,72**	**96,32**	**97,32**	**97,96**	**97,23**	**99,02**	**96,41**
BA	1170	900	870	1420	1120	620	45	475
RB	76	207	218	109	131	141	9	191
SR	2430	110	86	3590	2620	132	413	81
PB	20	22	20	18	18	18	14	14
TH	10	16	18	13	13	12	10	19
U	5	2	4	4	3	3	<1	3
ZR	188	174	190	224	230	214	108	168
NB	20	18	22	14	16	14	14	18
Y	17	27	33	20	19	25	20	33
LA	42	30	28	46	40	24	12	32
CE	80	60	65	105	90	70	25	80
SC	6	28	36	4	4	26	16	24
V	106	172	196	106	114	134	144	108
MN	1270	875	1500	1180	1080	890	1100	1330
CR	<2	122	142	<2	<2	106	54	76
NI	<2	56	70	<2	<2	42	40	42
CU	18	16	96	38	54	8	<2	28
ZN	76	162	188	72	68	124	58	138
GA	26	31	33	24	23	24	26	25
AS	1	1	2	2	2	1	3	2
SN	<5	5	10	<5	<5	5	5	5
AU	0,001	0,001	0,001	<0.001	0,001	<0.001	<0.001	0,001
AG								
MO								
CD								
SB								
TE								
RH								
RU								
OS								
PD								
PT								
IR								

SAMPLE	A95JS125B	A95JS126	A95JS129A	A95JS130	A95JS133	A95JS134	A95AC011C	A95AC023
LITH	quartzite	gneiss	gneiss	mylonite	quartzite	schist	calc-silicate	schist
LAT	-33,03555	-33,12124	-32,98101	-33,02794	-33,15640	-33,11255	-32,88154	-32,93014
LONG	-65,95667	-66,08048	-66,07308	-65,93205	-65,89107	-65,94621	-66,08597	-65,95460
SIO2	53,62	71,97	65,75	64,44	68,74	72,62	55,49	64,45
TIO2	0,66	0,75	0,84	0,72	0,64	0,72	0,43	0,79
AL2O3	16,12	12,34	15,54	15,76	12,07	12,82	12,30	16,27
FE2O3	1,87	1,10	1,56	4,58	1,46	1,09	1,57	1,48
FEO	4,71	3,16	4,63	1,83	2,33	2,79	3,07	4,55
MNO	0,30	0,06	0,07	0,07	0,07	0,08	1,08	0,23
MGO	4,34	1,92	2,73	2,80	2,44	1,82	1,14	2,81
CAO	4,62	2,05	1,23	0,31	3,68	1,75	21,20	1,18
NA2O	3,11	2,12	2,39	1,66	2,53	2,52	-0,01	2,48
K2O	2,20	2,67	4,23	4,30	2,80	2,24	0,01	2,98
P2O5	0,11	0,07	0,09	0,14	0,19	0,19	0,16	0,19
LOI	0,00	0,00	0,00	0,00	0,00	0,00	0,00	0,00
Rest	0,19	0,18	0,21	0,17	0,19	0,16	0,08	0,18
TOTAL	**91,84**	**98,39**	**99,28**	**96,77**	**97,14**	**98,80**	**96,52**	**97,59**
BA	240	460	605	390	585	325	<5	390
RB	103	109	169	178	103	98	<1	145
SR	352	142	114	71	167	151	86	150
PB	26	16	22	16	18	24	<2	32
TH	6	16	18	16	12	14	10	16
U	2	2	2	1	2	4	3	6
ZR	110	286	216	132	236	304	148	158
NB	6	12	14	16	12	10	10	16
Y	14	28	36	26	26	31	29	31
LA	18	32	36	34	30	26	30	30
CE	35	75	90	75	70	65	60	70
SC	28	12	18	22	10	12	<2	20
V	156	80	102	94	68	56	46	94
MN	2290	405	500	520	600	520	8070	1480
CR	120	58	76	74	50	50	24	74
NI	52	24	36	38	20	20	16	32
CU	12	10	12	12	22	8	<2	<2
ZN	146	84	128	124	72	76	78	120
GA	17	17	23	23	15	13	17	21
AS	2	1	<1	2	<1	1	11	9
SN	<5	<5	<5	5	<5	<5	50	<5
AU	0,001	0,001	0,002	<0.001	0,001	0,001	<0.001	0,002
AG								
MO								
CD								
SB								
TE								
RH								
RU								
OS								
PD								
PT								
IR								

SAMPLE	A95AC030A	A95AC036B	A95AC047C	A95AC047D	A95AC051	A95AC054	A95AC055	A95AC056
LITH	granodiorite	amphibolite	amphibolite	amphibolite	granite	granite	granite	granite
LAT	-32,82655	-32,82354	-32,83695	-32,83695	-32,78963	-32,76876	-32,66486	-32,67341
LONG	-66,13500	-66,13583	-66,18438	-66,18438	-65,45012	-65,38741	-65,69051	-65,66867
SIO2	65,26	52,04	59,38	52,00	73,21	69,09	72,17	75,71
TIO2	0,78	0,79	1,43	0,59	0,21	0,53	0,32	0,12
AL2O3	15,11	15,21	13,55	16,05	14,24	14,57	14,05	13,14
FE2O3	1,30	1,87	6,18	1,82	0,49	1,18	0,66	0,54
FEO	4,62	6,84	5,98	5,83	0,89	1,67	1,19	0,27
MNO	0,10	0,16	0,19	0,16	0,03	0,05	0,06	0,06
MGO	2,41	8,34	2,11	8,27	0,33	1,23	0,66	0,13
CAO	3,01	12,01	6,84	11,77	1,20	2,48	1,61	0,81
NA2O	2,29	1,10	2,61	1,65	3,60	3,44	3,30	3,60
K2O	3,15	0,12	0,58	0,43	4,86	4,47	5,16	4,72
P2O5	0,04	0,07	0,25	0,06	0,08	0,16	0,11	0,02
LOI	0,01	0,04	0,00	0,02	0,00	0,00	0,01	0,00
Rest	0,20	0,19	0,13	0,14	0,14	0,23	0,20	0,11
TOTAL	**98,27**	**98,77**	**99,23**	**98,79**	**99,28**	**99,11**	**99,50**	**99,23**
BA	445	50	65	80	410	805	555	75
RB	168	3	14	15	235	161	197	386
SR	136	127	189	102	125	419	325	41
PB	18	4	6	4	24	22	32	44
TH	27	1	10	2	20	24	25	32
U	3	<1	2	<1	3	6	5	10
ZR	246	62	218	54	136	194	170	80
NB	14	2	10	<2	14	12	18	50
Y	17	17	51	15	12	19	16	62
LA	50	8	22	6	30	50	74	34
CE	125	15	60	20	75	110	165	80
SC	22	50	42	46	2	6	10	14
V	120	234	168	194	12	46	24	4
MN	800	1220	1330	1180	215	410	410	475
CR	46	436	<2	222	2	16	8	<2
NI	20	116	<2	108	<2	8	4	<2
CU	14	104	4	70	2	2	4	<2
ZN	92	64	72	68	44	44	30	20
GA	19	15	21	14	25	20	18	22
AS	2	<1	<1	<1	1	<1	2	1
SN	<5	<5	<5	<5	5	<5	<5	10
AU		0,003	<0.001	0,002	<0.001	<0.001	<0.001	
AG								
MO								
CD								
SB								
TE								
RH								
RU								
OS								
PD								
PT								
IR								

SAMPLE	A95AC058	A95AC059A	A95AC059B	A95PS096	A95PS097	A95PS102	A95PS104	A95PS106
LITH	granite	aplite	phyllite	granite	gneiss	gneiss	amphibolite	granite
LAT	-32,83323	-33,10870	-33,10870	-32,75009	-32,90475	-32,89139	-32,88613	-32,69401
LONG	-65,30469	-65,98329	-65,98329	-64,75644	-64,77882	-64,86817	-64,88159	-64,76951
SIO2	68,00	73,88	69,72	71,20	67,76	64,49	47,08	74,99
TIO2	0,57	0,02	0,52	0,27	0,79	0,77	0,99	0,15
AL2O3	14,98	15,56	14,69	15,00	14,15	16,37	16,11	13,99
FE2O3	1,03	0,55	1,17	0,69	1,09	1,25	2,86	0,72
FEO	2,04	0,07	1,73	0,89	4,29	4,41	6,80	0,27
MNO	0,06	0,08	0,05	0,04	0,14	0,08	0,18	0,01
MGO	1,60	0,09	1,28	0,57	2,68	2,72	5,60	0,27
CAO	2,69	0,84	2,94	1,17	1,72	1,16	16,24	0,19
NA2O	3,56	5,84	3,86	3,58	2,44	2,47	2,28	3,56
K2O	4,17	1,78	3,12	5,34	2,98	3,68	0,36	4,86
P2O5	0,18	0,04	0,16	0,12	0,19	0,17	0,08	0,11
LOI	0,00	0,00	0,00	0,00	0,00	0,00	0,00	0,00
Rest	0,23	0,09	0,20	0,20	0,20	0,16	0,16	0,12
TOTAL	**99,11**	**98,84**	**99,43**	**99,07**	**98,43**	**97,73**	**98,74**	**99,24**
BA	775	280	520	820	595	320	85	350
RB	175	65	132	252	114	143	5	276
SR	381	219	434	252	169	100	142	106
PB	28	20	18	34	20	18	<2	32
TH	18	5	20	22	11	13	<1	24
U	11	3	7	5	2	2	<1	2
ZR	170	40	194	126	214	174	44	84
NB	14	16	12	14	12	14	<2	12
Y	20	20	17	19	30	25	20	3
LA	44	10	42	32	26	24	<2	18
CE	90	25	90	75	65	55	<5	65
SC	10	2	6	6	20	20	42	2
V	52	2	48	20	90	96	240	16
MN	500	590	410	325	1030	650	1330	120
CR	26	<2	14	6	70	72	378	<2
NI	12	<2	8	6	30	30	78	<2
CU	8	<2	4	4	18	26	12	8
ZN	60	22	46	40	94	106	78	42
GA	21	14	21	20	17	21	15	22
AS	<1	1	<1	<1	<1	<1	<1	<1
SN	5	<5	<5	<5	<5	<5	<5	<5
AU	<0.001	<0.001		<0.001		<0.001	<0.001	<0.001
AG								
MO								
CD								
SB								
TE								
RH								
RU								
OS								
PD								
PT								
IR								

SAMPLE	A95PS107	A95PS108	A95PS109	A95PS110A	A95PS110B	A95PS111	A95PS133	A95PS137B
LITH	granite	granite	granite	gneiss	amphibolite	gabbro	gneiss	mylonite
LAT	-32,69673	-32,68121	-32,67162	-32,87730	-32,87730	-32,87648	-32,82844	-33,10330
LONG	-64,76211	-64,81671	-64,83765	-64,88273	-64,88273	-64,87729	-64,85740	-64,96090
SIO2	70,77	74,89	70,58	59,95	56,21	56,44	66,19	74,91
TIO2	0,31	0,19	0,48	0,68	0,48	0,51	0,64	0,03
AL2O3	15,16	13,41	14,41	17,37	7,04	10,50	15,99	14,47
FE2O3	0,77	0,61	1,06	1,78	2,44	1,10	1,12	0,31
FEO	0,96	0,49	1,45	3,99	6,70	9,21	3,19	0,06
MNO	0,05	0,02	0,06	0,11	0,19	0,19	0,10	0,01
MGO	0,63	0,25	0,98	3,58	13,65	15,65	2,02	0,11
CAO	1,68	0,58	1,61	6,61	10,28	1,16	4,25	0,64
NA2O	3,69	2,83	3,54	3,27	0,78	0,74	3,23	3,15
K2O	5,08	6,01	4,68	1,56	0,38	1,82	2,02	5,85
P2O5	0,12	0,03	0,17	0,13	0,06	0,06	0,24	0,07
LOI	0,00	0,00	0,00	0,00	0,00	0,04	0,00	0,00
Rest	0,19	0,11	0,21	0,14	0,17	0,36	0,13	0,07
TOTAL	**99,41**	**99,41**	**99,22**	**99,16**	**98,39**	**97,78**	**99,12**	**99,68**
BA	665	205	665	225	40	180	265	200
RB	237	202	261	58	8	80	89	157
SR	289	88	251	213	17	55	187	94
PB	32	36	28	10	4	8	10	36
TH	19	78	24	5	4	7	5	3
U	2	4	7	<1	<1	<1	<1	1
ZR	132	108	184	100	72	90	160	22
NB	12	8	22	6	<2	6	8	6
Y	16	7	30	16	20	17	12	12
LA	36	40	32	16	6	14	14	6
CE	75	90	75	40	25	30	30	10
SC	8	4	8	22	92	48	8	4
V	28	10	38	136	268	188	76	<2
MN	340	160	460	795	1440	1450	690	75
CR	8	2	10	46	348	1370	30	<2
NI	4	2	6	20	156	290	10	<2
CU	4	<2	8	68	36	24	36	6
ZN	38	26	62	76	100	140	66	6
GA	20	16	21	18	10	17	17	15
AS	<1	<1	<1	<1	<1	<1	<1	<1
SN	<5	<5	5	<5	<5	<5	<5	<5
AU	<0.001	0,002	0,001	0,001	0,001	<0.001	<0.001	<0.001
AG								
MO								
CD								
SB								
TE								
RH								
RU								
OS								
PD								
PT								
IR								

SAMPLE	A95PS137C	A95PS137D	A95PS139	A95PS146	A95PS151	A95PS152	A95PS156A	A95PS164
LITH	gneiss	granite	granite	granite	gneiss	tonalite	gneiss	gneiss
LAT	-33,10330	-33,10330	-33,03865	-33,04865	-33,07162	-33,06191	-33,02754	-33,13780
LONG	-64,96090	-64,96090	-64,78824	-64,98543	-64,92128	-64,92070	-64,92533	-64,96586
SIO2	70,93	75,19	75,70	70,41	68,45	68,84	67,73	70,52
TIO2	0,91	0,05	0,11	0,45	0,83	0,45	0,60	0,79
AL2O3	12,42	14,73	13,42	14,91	14,27	15,76	12,54	12,88
FE2O3	1,52	0,39	0,45	0,76	1,48	1,07	2,69	0,64
FEO	3,64	0,13	0,29	1,97	4,22	2,09	1,64	4,30
MNO	0,08	0,03	0,04	0,06	0,09	0,05	0,10	0,09
MGO	2,28	0,12	0,18	0,90	2,69	1,68	1,85	2,59
CAO	1,49	0,91	0,86	1,87	0,83	3,85	11,23	2,17
NA2O	2,18	3,30	3,92	3,46	1,80	3,71	0,24	2,26
K2O	2,55	4,55	4,81	4,12	2,73	1,39	0,06	2,62
P2O5	0,18	0,09	0,03	0,16	0,11	0,06	0,18	0,18
LOI	0,00	0,00	0,00	0,00	0,00	0,00	0,00	0,00
Rest	0,17	0,05	0,10	0,15	0,18	0,19	0,16	0,17
TOTAL	**98,36**	**99,53**	**99,91**	**99,22**	**97,68**	**99,14**	**99,02**	**99,21**
BA	430	95	215	415	370	310	30	470
RB	107	119	285	207	114	53	2	106
SR	109	57	94	108	130	359	565	125
PB	20	38	46	26	24	10	4	18
TH	10	4	25	12	16	1	13	8
U	2	2	5	2	2	<1	3	3
ZR	240	20	70	178	264	118	226	194
NB	12	10	14	14	14	4	12	12
Y	25	15	9	23	22	2	27	29
LA	16	4	18	24	26	2	30	18
CE	65	10	40	55	80	<5	70	45
SC	18	4	4	10	22	4	10	18
V	102	2	8	36	106	76	68	110
MN	550	130	270	450	625	370	740	710
CR	70	<2	<2	12	78	24	46	70
NI	26	<2	<2	6	32	10	20	28
CU	12	<2	<2	12	<2	515	54	8
ZN	90	14	24	60	100	54	62	92
GA	15	16	20	19	17	17	18	15
AS	<1	<1	<1	<1	<1	<1	1	<1
SN	5	<5	<5	10	<5	<5	5	<5
AU	0,001	<0.001	0,002	0,001	<0.001	<0.001	<0.001	<0.001
AG								
MO								
CD								
SB								
TE								
RH								
RU								
OS								
PD								
PT								
IR								

SAMPLE	A95PS167	A95PS179	A95PS180	A95PS181B	A95PS184B	A95PS192	A95PS205B	A95PS209A
LITH	granite							
LAT	-33,17095	-33,17216	-32,47006	-33,00563	-33,00696	-33,03295	-32,98062	-33,01744
LONG	-65,04894	-64,95840	-64,31099	-64,99128	-64,97239	-64,89880	-65,04832	-65,02769
SIO2	65,87	72,70	61,91	72,04	69,64	73,54	73,58	41,13
TIO2	0,60	0,30	0,71	0,28	0,41	0,17	0,05	0,01
AL2O3	16,74	14,41	17,30	15,13	15,73	14,12	14,21	0,71
FE2O3	1,38	0,44	2,05	0,53	0,93	0,99	0,46	5,34
FEO	1,42	1,13	3,23	1,44	1,78	0,07	0,21	1,83
MNO	0,04	0,02	0,12	0,06	0,06	0,05	0,03	0,07
MGO	0,79	0,44	2,19	0,89	0,92	0,24	0,13	34,98
CAO	2,10	1,30	5,23	2,34	3,29	0,76	0,47	3,53
NA2O	3,70	3,28	4,34	4,69	3,71	3,70	4,26	0,03
K2O	6,02	5,31	1,61	1,74	2,93	5,04	6,04	0,01
P2O5	0,19	0,14	0,18	0,10	0,14	0,07	0,25	0,01
LOI	0,01	0,00	0,02	0,00	0,00	0,00	0,00	0,03
Rest	0,40	0,16	0,15	0,11	0,15	0,17	0,07	0,56
TOTAL	**99,26**	**99,64**	**99,04**	**99,35**	**99,69**	**98,92**	**99,76**	**88,23**
BA	2010	535	140	285	390	715	145	10
RB	152	172	87	151	125	209	270	<1
SR	550	147	274	155	195	155	34	21
PB	26	34	12	22	18	42	30	<2
TH	11	30	15	10	17	14	5	<1
U	<1	4	2	3	1	3	3	<1
ZR	348	204	184	126	186	108	34	<1
NB	10	10	14	8	10	10	20	<2
Y	11	10	38	11	12	11	13	<1
LA	76	46	32	16	32	16	12	<2
CE	165	100	70	30	85	30	20	<5
SC	6	4	16	6	6	2	4	10
V	28	14	96	28	44	10	6	26
MN	275	125	940	420	455	425	205	555
CR	<2	2	12	16	4	2	<2	2170
NI	<2	<2	8	8	4	<2	<2	1770
CU	2	<2	18	8	16	60	<2	2
ZN	52	48	118	50	58	52	12	38
GA	20	19	21	17	18	19	21	1
AS	<1	<1	<1	<1	<1	1	1	5
SN	<5	<5	<5	<5	<5	<5	10	<5
AU	<0.001	0,001	<0.001		<0.001	<0.001	0,003	
AG								
MO								
CD								
SB								
TE								
RH								
RU								
OS								
PD								1,5
PT								4
IR								

SAMPLE	A95RS069C	A95RS070B1	A95RS070B2	A95RS072A	A95RS081	A95RS082	A95RS084B	A95RS105
LITH	vein	gneiss	gneiss	vein	schist	pyroxenite	breccia	gneiss
LAT	-30,95309	-30,96441	-30,96441	-30,98422	-31,22242	-33,12385	-32,80069	-32,79348
LONG	-65,21918	-65,21976	-65,21976	-65,21749	-65,30422	-66,13574	-65,08405	-66,05477
SIO2	92,65	74,33	76,64	60,46	87,68	46,47	69,36	81,98
TIO2	0,01	0,67	0,53	0,00	0,01	0,19	0,36	0,27
AL2O3	0,85	12,06	8,39	0,26	0,25	4,44	12,24	8,58
FE2O3	0,71	0,93	5,94	0,24	3,47	11,76	3,37	2,68
FEO	1,33	2,53	0,08	1,24	0,39	8,21	0,24	0,28
MNO	0,55	0,05	0,00	0,01	0,00	0,28	0,04	0,05
MGO	0,31	1,53	0,35	0,01	0,01	22,04	0,44	0,36
CAO	0,04	1,69	0,13	0,01	0,01	2,86	0,04	0,02
NA2O	0,00	3,24	0,00	0,00	0,01	0,25	0,06	0,04
K2O	0,23	1,91	2,66	0,06	0,21	0,25	3,78	2,60
P2O5	0,01	0,20	0,09	0,01	0,00	0,01	0,10	0,03
LOI	0,24	0,01	2,35	5,60	0,69	2,13	1,56	1,09
Rest	1,18	0,17	0,53	30,93	4,65	1,38	1,69	0,39
TOTAL	**98,11**	**99,31**	**97,69**	**98,83**	**97,37**	**100,27**	**93,28**	**98,37**
BA	0	365	25			25	195	110
RB	14	89	163			8	224	159
SR	1	200	13			12	24	14
PB	292	30	2020	21217	36070	4	410	2370
TH		12	4			<1	18	
U		2	3			<1	6	
ZR	2	266	244			8	184	110
NB	0	10	6			<2	12	8
Y	0	24	4			4	18	9
LA	46	26	22			2	20	22
CE	10	60	60			<5	50	50
SC	<2	15	10			53	10	12
V	4	78	50			194	38	36
MN	4600	440	50			2010	340	410
CR	<2	52	46			3470	18	24
NI	<2	18	16			4210	20	4
CU	34	12	6	1470	570	2180	7525	6
ZN	7490	60	246	226683	2230	130	4710	66
GA	<1	13	9			8	14	10
AS	1310	3	1080			2	56	201
SN	10	<5	5			5	10	<5
AU	704*	1*	151*	98*	1098*	11*	83*	889*
AG	1,5	0,2	4,5	302	375		2,3	21,1
MO	0,6	0,3	0,5	8,9	0,9		3,9	0,7
CD	76,6	0,5	0,8	1440	22,4		11,5	1,0
SB	10,4	0,2	15,6	619	92,6		6,2	10,8
TE	<0.2	<0.2	0,2	<0.2	<0.2		0,4	<0.2
RH						6		
RU						2		
OS						2		
PD						125		
PT						18		
IR						4		

SAMPLE	A95RS108	A95RS111B	A95RS113
LITH	breccia	andesite	breccia
LAT	-32,81892	-32,83646	-32,80610
LONG	-66,02694	-65,99988	-66,06306
SIO2	82,38	75,59	93,85
TIO2	0,28	0,21	0,58
AL2O3	5,68	5,45	2,59
FE2O3	5,54	8,55	0,86
FEO	0,09	0,23	0,06
MNO	0,02	0,16	0,00
MGO	0,31	0,17	0,06
CAO	0,07	0,16	0,02
NA2O	0,01	0,49	0,04
K2O	1,64	2,70	0,64
P2O5	0,03	0,08	0,05
LOI	2,24	0,15	0,07
Rest	0,19	2,73	0,15
TOTAL	**98,48**	**96,67**	**98,97**
BA	60	370	30
RB	92	76	37
SR	19	85	14
PB	955	16	840
TH	<1	4	6
U	<1	2	3
ZR	42	62	162
NB	2	4	16
Y	<1	8	<1
LA	4	8	8
CE	10	16	20
SC	10	4	2
V	70	58	18
MN	230	330	55
CR	12	2	10
NI	4	<2	<2
CU	8	20870	28
ZN	184	226	14
GA	7	12	2
AS	84	4	28
SN	<5	<5	<5
AU	416*	1612*	>2
AG	11,6	25,9	15,7
MO	0,2	7,9	1,2
CD	1,6	1,3	0,3
SB	4,1	0,3	19,4
TE	1,8	1,0	2,7
RH			
RU			
OS			
PD			
PT			
IR			